THE UNIVERSITY OF CALGARY

DYNAMIC MODELING AND OPTIMAL CONTROL OF FLEXIBLE MANIPULATORS

by

MEHRDAD FARID

A DISSERTATION

SUBMITTED TO THE FACULTY OF GRADUATE STUDIES

IN PARTIAL FULFILLMENT OF THE REQUIREMENTS FOR THE

DEGREE OF DOCTOR OF PHILOSOPHY

DEPARTMENT OF MECHANICAL ENGINEERING

CALGARY, ALBERTA

JULY, 1997

0-612-24537-3

ABSTRACT

Current industrial robots are made very heavy to achieve high stiffness which increases the accuracy of their motion. However, this heaviness limits the robot speed and increases the required energy to move the system. The requirement for higher speed and better system performance makes it necessary to consider a new generation of lightweight manipulators as an alternative to today's massive inefficient ones. Lightweight manipulators require less energy to move and they have larger payload abilities and more maneuverability. However, due to the dynamic effects of structural flexibility, their control is much more difficult. Therefore, there is a need to develop accurate dynamic models for design and control of such systems.

There are two types of control problems for such manipulators, namely, trajectory control and time-optimal control (TOC) problems. In the first one, the position of the payload is given versus time while in the second one the path and the joint torque constraints are known. Since feedback control systems are non-collocated and position commands contain high frequency components, they may cause these systems to become unstable. This is why inverse dynamic methods have been recently used by many authors to determine the joint torques such that the end-point of the flexible manipulator follows a given trajectory. Due to the flexibility, a complete model consisting of the kinematic and dynamic equations should be solved simultaneously. But the difficulty is so called non-causality of the inverse dynamics of flexible manipulators. In other words, since the point, for which the prescribed motion is specified, is connected to the application points of control torques by elastic bodies, the joint torques should be applied from negative time to future time in order to control the position of the end-point according to the desired trajectory. The reason for this phenomenon is the fact that elastic waves propagate with finite speeds.

In this dissertation three topics, dynamic modeling, trajectory control, and time-optimal control of multi-link flexible manipulators are studied.

First an efficient finite element/Lagrangian approach is developed for dynamic modeling of planar and spatial manipulators with flexible links and joints. For planar case, the nonlinear and coupled equations of motion of multi-link manipulators are derived using minimum number of coordinates by considering joint or relative coordinates. In the case of spatial manipulators, the equations of motion are obtained using a mixed set of differential equations and algebraic constraints.

Then a technique based on numerical optimization is proposed to solve trajectory control and time optimal control of multi-link flexible manipulators. The proposed technique finds the joint torques required to move the end point from rest to rest along a specified path. The "non-causality" of the inverse dynamics of such systems is taken into account via considering pre-actuation and post-actuation in the solution procedure. The proposed technique is complete and effective and can be used to find joint torques as feedforward controls in order to minimize the work of the feedback controllers.

ACKNOWLEDGMENTS

I would like to express my sincere gratitude and appreciation to Dr. Stanislaw A. Lukasiewicz, my supervisor, for his guidance, support, and encouragement through the course of this work. He gave me the most valuable gift - freedom. His encouragement allowed me to pursue my own idea, to make mistakes and to learn.

I also highly appreciate Dr. Marcelo Epstein for his invaluable helps and suggestions.

My special thanks goes to the fellow students of the Department of Mechanical Engineering, Reza Babaei and Krzystof Palka, for their advice and constant exchange of ideas.

I wish to express my deepest appreciation to my wife for her patient, understanding, and steadfast support during this endeavor.

The financial support in the form of scholarship provided by Shiraz University and Ministry of Culture and Higher Education of Iran is appreciated and acknowledged.

This thesis is dedicated to

My wife and two sons: Fereshteh, Nima, and Navid

My parents, sister, and two brothers

All my teachers

TABLE OF CONTENTS

Chapter 3 Dynamics of Deformable Multibody Systems

Chapter 4 Dynamic Modeling of Planar Manipulators with Flexible Links and Joints

Chapter 5 Dynamic Modeling of Spatial Manipulators with Flexible Links and Joints

Chapter 6 Optimal Control through Optimum Design Theory

Chapter 7 Trajectory Control of Multi-Link Manipulators with Flexible Links and Joints

---

Chapter 8 Time Optimal Control of Multi-Link Flexible Manipulators Along Specified Path

---

Chapter 9 Concluding Remarks

LIST OF FIGURES

NOMENCLATURE

A_k	Cross sectional area of link k
A_y, A_z, A_Θ	Rotation matrices about y, z, and x axes
$A_{yz\Theta}$	Rotation matrix due to elastic deformation of end point of each link
A_γ	Rotation matrix due to large rotation at each joint
B	Inverse Hessian matrix
b_k	Viscous damping of the k-th joint
b_b	Viscous damping of the base joint in spatial case
C	Vector of constraint equations
C_q	Constraint Jacobean matrix
$e_k^{(1)}$, $e_k^{(2)}$	Unit vectors along x_k and y_k axes in planar case
E_k	Young modules of link k
fE	External load vector in planar case
fS	Quadratic load vector in planar case
G_k	Shear modules of link k
g	Gravity acceleration
G	Gradient vector
h_k	Length of each element of link k
H	Hessian matrix
I, J, K	Base unit vectors of the global coordinate system in spatial case
$\underline{i}_k$, $\underline{j}_k$, $\underline{k}_k$	Base unit vectors of the local coordinate system in spatial case
I_k	Cross sectional area moment of inertia about neutral axis of link k in planar case
I_y^k, I_z^k	Cross sectioanl area moment of inertia about y_k and z_k axes of link k in spatial case
Ir_k	Moment of inertia of the k-th rotor in planar case
Is_k	Moment of inertia of the k-th stator in planar case
Ir_b	Moment of inertia of the rotor of the base actuator in spatial case

Irx_k, Iry_k, Irz_k	Moments of inertia of the k-th rotor about x_k, y_k, and z_k axes in spatial case
Isx_k, Isy_k, Isz_k	Moments of inertia of the k-th stator about x_k, y_k, and z_k axes in spatial case
IP	Mass moments of inertia of the payload in planar case
IPx_n, IPy_n, Ipz_n	Mass moments of inertia of the payload about x_n, y_n, and z_n axes in spatial
J_k	Cross sectional polar moment of inertia of link k
K_{ff}	Stiffness of the deformable system
KE	Kinetic energy
K_b	Joint stiffness of the base actuator
Kj_k	Stiffness of the k-th joint
k_1, k_2	Two enough large numbers
L	Lagrangian
L_k	Length of the k-th link
$l^{(k)}$, $m^{(k)}$, $n^{(k)}$	Direction cosines of unit vector $\underline{i}_k$ along x_k-axis
$ls^{(k)}$, $ms^{(k)}$, $ns^{(k)}$	Direction cosines of unit vector $\underline{i}_k^*$ along x_k^*-axis
M_p	Payload mass
ms_k	Mass of the stator of the k-th actuator
mr_k	Mass of the rotor of the k-th actuator
MS	System mass matrix
KS	System stiffness matrix
BS	System damping matrix
n	Number of links of the manipulator
N_l^{ek}	l-th Hermite shape function of the e-th element of the k-th link
NL	Linear shape functions
N_1, N_2	Number of torque intervals in the pre-actuation and post-actuation times
NM	Number of torque intervals in the main time domain
n_1, n_2	Number of time steps in the pre-actuation and post-actuation times

nm	Number of time steps in the main time domain
OXY	Inertial frame coordinate system in planar case
$o_kx_ky_k$	Pinned-pinned rotating local frame in planar case
OXYZ	Inertial frame coordinate system in spatial case
$o_kx_ky_kz_k$	Clamped-free coordinate system whose x_k and y_k axes are tangent to link k at o_k and parallel to the horizontal plane (XY plane), respectively
PE	Potential energy
$\mathbf{Q}_e$	Vector of generalized externally applied torques
$\mathbf{Q}_v$	Load vector including the velocity terms due to Coriolis and centrifugal effects, and gravity terms
$\mathbf{Q}_c$	Vector consisting of nonlinear terms resulting from twice time differentiation of the constraints
$\mathbf{q}$	Vector of dependent and independent degrees of freedom of spatial manipulator
q_b	Rotation angle of the base rotor
q_k	Rotation angle of the rotor of actuator k relative to the line tangent to link k-1 at its end
$\mathbf{r}_k$	Position vector of an arbitrary point of link k
$\mathbf{r}^k$	Position vector of each point of link k in the global system
$\mathbf{R}^k$	Position vector of the origin of link k in the global system
$\mathbf{r}_{rel}$	Position vector of each point of link k in local coordinate system o_k-$x_ky_kz_k$
R_x^k, R_y^k, Rz^k	Components of vector $\mathbf{R}^k$ along three axes of the global coordinate system
r_0	A positive constant
r_i	Large penalty coefficient
$\mathbf{S}^{(i)}$	Search direction
$\mathbf{T}_a$	Vector of unknown actuator torques
T_b	Torque applied by the base actuator in spatial case
T_k	Torque applied by the k-th actuator

$\mathbf{T_1}$, $\mathbf{T_2}$	Arrays of discretized joint torques as design variables
t_1	Pre-actuation time
t_f	Main time domain
t_2	Post-actuation time
T_{min}, T_{max}	Bounds on the actuator torques
U	State vector
$\mathbf{u}_f^j$	Deformation vector
$\mathbf{u}_0^j$	Position vector in the undeformed state
v^k	Elastic deflection of the k-th link in planar case
v_{2e-1}, v_{2e+1}	Nodal displacements of the e-th element in y_k direction
v_{2e}, v_{2e+2}	Nodal flexural slopes of the e-th element about z_k axis
v'_e, w'_e, Θ_e	Angular deformation of link k at point o_{k+1} about z_k, y_k, and x_k-axes, respectively
v_p, v'_p	Flexural displacement and slope of the end point of the last link in y_n direction
w_{2e-1}, w_{2e+1}	Nodal displacements of the e-th element along z axis
w_{2e}, w_{2e+2}	Nodal flexural slopes of the e-th element in xz plane
w_p, w'_p	Flexural displacement and slope of the end point of the last link in z_n direction
x^k	x coordinate of the points of the k-th link in planar case
x_k^*	Axis which is associated with x_k-axis, but different from it because of the joint flexibility
x_i , y_i	Discretized end point coordinates in planar case
$y(x_i)$	Given exact y coordinate of the end point for time optimal problem

Greek Symbols

δw	Virtual work of nonconservative loads
∇	Gradient operator

Γ_b	Gear ratio of the base actuator
Γ_k	Gear ratio of the k-th joint
$\gamma^{(k)}$	Angle between tangent lines to links k-1 and k at point o_k
Φ_k	Angular position of the k-th pinned-pinned coordinate system in planar case
$\Phi_1^{(k)}$	Angle between the projection of the x_k-axis on the horizontal (XY) plane and the X-axis in spatial case
$\Phi_2^{(k)}$	Angle between x_k-axis and Z-axis in spatial case
λ	Vector of Lagrange multipliers
μ	A non-square matrix which maps the joint torque vector from a space whose dimension is equal to the number of joints to a vector with the dimension of all degrees of freedom of the system
η_j, η_f, η_r	Vectors of motor coordinates, joint coordinates, and elastic coordinates of the system
$\xi^{(1)}$, $\xi^{(2)}$	Transformed unbounded variables used instead of bounded joint torques in optimization procedure
ρ_k	Mass density of link k
$\Psi_1^{(k)}$	Angle between the projection of the x_k^*-axis on the horizontal (XY) plane and the X-axis
$\Psi_2^{(k)}$	Angle between x_k^*-axis and Z-axis
Θ_e, Θ_{e+1}	Nodal torsional deformation of the e-th element along x axis in spatial case
$\Theta_0^{(k)}$	Rotation of link k at its origin (o_k) about x_k-axis resulting from the absolute rotation of end point (o_k) of link k-1 about x_{k-1} axis
$\Theta^{(k)}$	Rotational deformation of various sections of link k about x_k-axis relative to the cross section of link k at point o_k.
Θ_p	Elastic rotation of the end point of the last link

CHAPTER 1

INTRODUCTION

1.1 Prologue

As primitive man became aware of his environment he started to increase his physical and territorial capability by creating tools such as lever, hammer, and pince gripper. The lever increased the effect of the physical force that he was able to apply directly. The hammer helped him to accomplish tasks which previously were not possible. And the pince gripper enabled him to manipulate objects from a distance.

Much later, man invented machine tools with some degrees of autonomy which allowed him merely to start, stop, and observe machines at work. With the introduction of automation his role was reduced to starting the machine by pressing a button which concurrently switched on sophisticated systems of controls. Finally, machines were invented which not only had degrees of autonomy but also were able to cause action from a distance. These machines, called robots, were powerful, autonomous, and flexible in their application.

The word robot is Slav in origin, related to the words for work and workers. This word was introduced by Karel Capek, a Czech playwright, in his play "Rossum's Universal Robots" in 1920. In that play an engineer made machines that were modeled on human beings but had none of their weaknesses. Those small artificial and anthropomorphic creatures strictly obeyed their master's command.

Probably the first occurrence of mechanical arms was in the prosthetic devices to replace lost limbs. These arms were designed to grasp objects. The second field in which robot arms had found application was remote manipulation. The need to work with hazardous materials or environment, led to the design of teleoperator systems. These devices permit a user to perform simple manipulations from a safe distant place. Applications in space, nuclear, and underwater environments are the typical use of teleoperators. Also robots are now to be found in various applications such as spot welding, arc welding, material handling, and assembly. Mainly, they are used to reduce labor cost and material wastage, to increase output rate, and to improve production quality.

Robots are so new that there is no standard definition for them. However, an industrial robot is defined by US Robot International Association (RIA) as: "a programmable, multifunctional manipulator designed to move materials, parts, tools, or specified devices through variable programmed motions for the performance of a variety tasks".

Industrial robots are built of the following basic systems:

1) The mechanical structure consisting of mechanical linkage and joints.
2) The control system.
3) The power input(s) which can be hydraulic, pneumatic, electrical, or their combination.

Most of the contemporary robotic manipulators are very massive and inefficient. Their payload-to-weight ratio is about 1:20 to 1:15, which is very low when compared with the capability of the human arm. By considering a human being as a manipulator, it is a very effective and efficient one. With total mass of 70-90 kg and its linkages (lower and upper arms and wrist) 4.5-9 kg, this manipulator can precisely carry loads up to 4.5-9 kg with fairly high speed. It can handle loads up to 15-25 kg with slightly lower speed, while it is able to make simple movement with loads up to 90-135 kg. Therefore, a typical manipulator is more than 10 times less efficient than a human being.

Robots are very different from any other structures. Their structure consists of active linkages which differ from passive ones such as crank mechanisms. In active linkages each link has its own power supply, while in passive linkages all the links receive motion from a single driving motor. As it was mentioned earlier, the load carrying capacity of most of the existing industrial manipulators is very low. This low weight efficiency is mainly due to control design which is usually based on rigid body dynamics. The excessive mass of the arms limits their speed and increases the energy requirements and the size of actuators. Moreover, manipulator systems with large workspace volumes and large payloads, such as long-reach manipulators for nuclear waste remediation or the outer space arms with extreme penalty on the mass carried into orbit, should be as light as possible. Therefore, many benefits can be received from manipulators with low weight-to-payload ratio and high stiffness. This is why a new generation of light robots which are able to handle heavy payloads is required to replace the inefficient and massive ones. Lighter manipulators need less energy and can operate at higher speeds. Therefore, they save manufacturing time and increase productivity. Due to the flexibility of the links, the assumption of rigid body dynamics and kinematics is no longer valid and the problem of position control resulting from link flexibility needs to be resolved.

It goes without saying that accurate dynamic modeling is the first step for design and control of lightweight, heavy payload, and high speed manipulator systems. Due to the distributed flexibility of the links, they should be regarded as deformable bodies with an infinite number of degrees of freedom. These degrees of freedom are used to define the location of each point of the system. Mathematical modeling of multi-link flexible manipulators as multi-deformable-body systems is a challenging research topic. The rigid body or nominal motion of the system changes the geometry of the system. This results in varying system parameters which influence the elastic deformations of the links. In turn the elastic deformations influence the rigid body motion. In other words, since the interconnected bodies of the manipulator system undergo large translational and rotational displacements, the dynamic equations governing the motion of the system are highly nonlinear and coupled. The dynamic formulation of multi-deformable-body systems leads to a set of partial differential equations. Since these space- and time-dependent equations can not be solved analytically, approximate techniques such as Rayleigh-Ritz and finite element methods are used to change them to a set of ordinary differential equations by reducing the number of coordinates to a finite set.

In multibody systems, the motion of each body is constrained because of the mechanical joints which connect the adjacent bodies. The configuration of a multibody system can be described by vector quantities such as displacement and velocity. These quantities should be measured with respect to an appropriate coordinate system. The dynamics of such systems can be formulated by means of either minimal or redundant coordinate methods. In general, two kinds of coordinates are required. The first one is an inertial or global frame of reference which is fixed in time and the second one is a body reference coordinate for each component of the system. This reference frame translates and rotates with the body; therefore, its location and orientation change with time with respect to the inertial frame. In rigid body analysis, the set of coordinates defining the location and orientation of the body references is enough for defining the location of an arbitrary point of the rigid body. However, the configuration of deformable bodies must be identified not only by a complete set of coordinates defining the location and orientation of a selected body reference, but also the elastic coordinates describing the deformation of the body with respect to the body reference. In redundant methods, connectivity between different bodies can be introduced to the dynamic formulation by using a set of nonlinear algebraic constraint equations. Therefore, by using the redundant approach, the dynamic formulation of motion of multibody systems leads to a mixed set of differential and algebraic constraint equations (DAE) which have to be solved simultaneously.

Instead of using connectivity constraints, it is possible to use joint or relative coordinates to find dynamic equations of the system expressed in terms of the system degrees of freedom. Using this approach, the number of dynamic equations is minimum because extra variables including the Cartesian coordinates presenting the location of the origins of the body reference frames and the Lagrange multipliers resulting from connectivity constraints are not used in the formulation. However, this minimal approach leads to a complex recursive formulation in many applications.

Another way for dynamic modeling of flexible manipulators is to find the dynamic response of the system directly with reference to a fixed global coordinate frame. This approach eliminates the nonlinear Coriolis and centrifugal terms from the dynamic equations; however, it requires the use of finite strains, large displacements, and large rotations. Therefore, this approach is somehow complicated and not suitable for the control design specially for chains of flexible links.

One of the major open problems related to flexible manipulators is controlling the position of their end-point. There are two types of control problems for such manipulators, namely, trajectory control and time-optimal control (TOC) problems. In the first one the position of the payload is given versus time, while in the second one the path and the joint torque constraints are known. Various feedback control strategies are proposed in the literature for trajectory control of flexible manipulators. Because such control systems are non-collocated and position commands contain high frequency components, the feedback control may cause these systems to become unstable. This is why inverse dynamic methods have been recently proposed by many authors to determine the joint torques such that the end-point of the flexible manipulator follows a given trajectory. Due to the flexibility, a complete model consisting of the kinematic and dynamic equations should be solved simultaneously. The main difficulty is the non-causality of the inverse dynamics of flexible manipulators. Because the point for which the prescribed motion is specified and the application points of control torques are connected by elastic bodies, the joint torques should be applied from negative time to the future time in order to control the position of the end-point according to the desired trajectory. The reason for this phenomenon is the fact that elastic waves propagate with finite velocity. Little work has been done on the non-causal inverse dynamics of multi-link manipulators with flexible links. To the best knowledge of the author, no work has been done in the field of non-causal inverse dynamics of multi-link robots with both flexible links and joints.

Although various approaches have been developed for time-optimal control of rigid manipulators, little work has been devoted in the literature to the time-optimal control of flexible manipulators. The exact minimal time solution is not available at present because of the highly nonlinear structure of the equations of motion as well as the non-causality of such systems. In the previous studies the non-causality of such systems was not taken into account for time optimal control problem of flexible manipulators.

1.2 Scope and Outline of This Dissertation

In this dissertation three aforementioned topics: dynamic modeling, trajectory control, and time-optimal control of multi-link flexible manipulators are studied. At the beginning, two efficient finite element/Lagrangian approaches are developed for dynamic modeling of such manipulators. In the first approach the nonlinear and coupled equations of motion of multi-link planar manipulators with flexible links and joints are derived using minimum number of coordinates by considering joint or relative coordinates. In the second approach, equations of motion of spatial multi-link manipulators with flexible links and joints are obtained using a mixed set of differential and algebraic constraints.

Two techniques based on numerical optimization are proposed to solve trajectory control and time optimal control of multi-link flexible manipulators. The proposed techniques find the joint torques required to move the end point from rest to rest along a specified path. The non-causality of the inverse dynamics of such systems is taken into account via considering pre-actuation and post-actuation in the solution procedure. In the trajectory control problem, the mimnimized objective function is the summation of squares of tracking errors at the integration time points from zero time to the end of the post-actuation time. The proposed technique for time minimization is based on transforming the optimal control problem into an equivalent unconstrained optimum design problem using penalty function methods.

It will be shown that these techniques are complete and effective and can be used to find joint torques as feedforward controls in order to minimize the work of the feedback controllers.

1.3 Organization of The Text

Chapter 2 is a review of the literature relating to the dynamic modeling, trajectory control, and time optimal control of flexible manipulators.

In chapter 3, a general overview of dynamics of multi-deformable-body systems is presented and the governing equations including equations of motion of the system and constrained equations are obtained and various solution procedures are described.

Chapter 4 presents an efficient finite element/Lagrangian approach developed for dynamic modeling of lightweight planar multi-link manipulators with both flexible joints and links. The dynamic elastic response of each flexible link is formulated relative to a floating frame called pinned-pinned or virtual link coordinate system. Using this coordinate system, the link deformation is measured relative to the line connecting the end points of the link. The finite element method is used to discretize the continuos elastic deformation of links. Both the rigid degrees of freedom and the elastic degrees of freedom of the system are treated as generalized coordinates. Using virtual work of external loads as well as kinetic and potential energies of flexible links and actuated flexible joints, the equations of motion of the system are derived in terms of the generalized coordinates through a Lagrangian approach. Therefore, the dynamic model derived in this study is free from the assumption of nominal motion and takes into account not only the coupling effects between rigid body motion and elastic motion but also the interaction between flexible links and actuated flexible joints. The main advantage of the proposed model is its compactness and completeness.

In chapter 5, dynamic modeling of multi-link spatial manipulators with flexible links and joints is developed based on using tangential (clamped free) local coordinate systems. The links are assumed to be deformable due to bending and torsion and the finite element method is used to discretize the elastic deflections of the links. In this modeling the connectivity of the links is taken into account by introducing the Cartesian coordinates of origin of each local coordinate system as extra unknown variables. By using the finite element method and employing Lagrange multipliers, a mixed set consisting of nonlinear ordinary differential equations and nonlinear algebraic constraint equations is obtained. These equations are solved simultaneously by means of numerical integration in order to predict the dynamic behavior of the system.

A short review of numerical optimization techniques such as quasi-Newton methods and penalty functions is presented in chapter 6. These methods are used in chapters 7 and 8 to solve trajectory and time optimal control of flexible manipulators,

Chapter 7 describes the non-causal nature of the inverse dynamics of flexible manipulators and proposes a simple but efficient approach based on numerical optimization to solve such difficult problem.

In chapter 8, an approach utilizing nonlinear programming is proposed to solve the control problem of flexible manipulators for a rest to rest motion in minimum time. For such systems, the proposed technique is simpler and more effective than optimal control methods. Moreover, the non-causality of the inverse dynamics of the flexible manipulators is taken into account in the proposed approach.

Finally, chapter 9 presents the conclusion of this work.

CHAPTER 2

LITERATURE REVIEW

2.1 Introduction

Robots, mechanisms, teleoperators, spacecrafts, and walking machines share common kinematical, dynamical, and control problems. In the age of high productivity, it is required to design these mechanical systems in such a way that they can operate at higher speeds with less energy consumption. In order to increase the operating speed of a mechanical system, the mass of its moving parts must be reduced. However, the lighter members are more likely to deform due to their flexibility. Therefore, the control problem of lighter mechanical systems is much more complicated than that of massive, rigid ones.

The demand for designing light mechanical systems has prompted researchers to develop comprehensive mathematical methods to model their dynamic behavior as well as to control their motion. The literature on lightweight flexible multibody systems began in the early 1970s. Three main subject areas discussed in the literature have included modeling and control of mechanisms, spacecrafts, and robotic manipulators.

This chapter starts with an overview of the literature dealing with dynamic modeling of flexible multibody systems including manipulators and mechanisms. Then a literature review on trajectory and time optimal control of flexible manipulators is presented.

2.2 Modeling

Many works in the past have been done in the formulation of the equations of motion of rigid multibody systems. The kinematics of rigid multibody systems has been completely described using symbolic notation of Hertenberg-Denavit Matrix [1]. Uicker [2] and Paul and Rong [3] employed this 4X4 transformation matrix approach to model the kinematics of spatial linkages and manipulators.

The dynamic modeling of rigid mechanisms and robots was approached by several techniques. Greenwood [4] and Luh et.al [5] used the Newton-Euler method, while Asada and Soltine [6] and Hollerbach [7] made use of Lagrangian approach. Kane's method also was used by Kane and Levinson [8].

During the past 20 years there has been an increasing interest in formulation of the equations of motion of large flexible multibody systems. Mathematical modeling of multi-deformable-body systems is a challenging task. Since the nominal or rigid body motion of the system changes the geometry of the system, system parameters vary with time and subsequently influence the elastic deformations of the bodies. On the other hand, the elastic deformations influence the rigid body motion of the interconnected bodies of the system. This is why the dynamic equations governing the motion of such systems are highly nonlinear and coupled.

In the literature a number of formulations and solution algorithms have been proposed which differ in the techniques used to develop the equations of motion, the approaches utilized to model the elastic deformation of the bodies, and the assumptions regarding coupling of rigid body motion and elastic deformations.

2.2.1 Techniques for Deriving Equations of Motions

Three main techniques were used by researchers to develop the dynamic equations of motion of flexible multibody systems, namely: Newton-Euler approach, Lagrangian approach, and Hamiltonian approach. While vector quantities are used in Newtonian mechanics, scalar quantities such as kinetic energy, potential energy, and work are used in Lagrangian dynamics which greatly simplify the problem. Moreover, the Lagrangian formulation eliminates the forces of constraints from the dynamic equations. This is why most of the researchers [9-12] have used the Lagrangian approach to formulate the dynamic equations of flexible multibody systems, while only a few [13,14] have used the Newton-Euler approach. Meanwhile, some other researchers applied directly the Hamiltonian principle to obtain dynamic model for flexible single-body or multibody systems [15,16].

2.2.2 Selection of Coordinates

Regarding the systems of coordinates, two fundamentally different approaches have been proposed in the literature to describe the motion of flexible bodies of a multi-deformable-body system. They are: the floating reference frame method and the inertial reference frame method. Floating reference frames, which translate and rotate with flexible bodies of the systems, have long been used in spacecraft dynamics [17]. The deformation of each body is described with respect to its floating or body reference frame. The introduction of this type of frame was motivated by the assumption of small deformations in flexible bodies. Most of the researchers in the field of flexible mechanisms and robots have used this system of coordinates [10,18,19,20,21]. Usoro et. al [10], Hasting and Book [18], and Wang and Vidyasagar [19] defined the floating frame to be attached at the base of a beam to model flexible manipulators, while Cannon and Schmit [20] used the floating frame passed through the center of the mass. Asada et al [21] let the floating frame pass through the end points. By using the latter approach, the resulting equations of motion, although restricted to small deformations, are nonlinear and highly coupled in the inertia terms such as Coriolis and centrifugal effects.

The inertial reference frame method was proposed by Simo and Vu-Quoc [22] to model the dynamics of moving beams. In this method the displacement vector is described in an absolute coordinate system. Therefore, the rigid body motion and the elastic deformations are expressed together. This leads to a formulation whose inertia matrix becomes simple, but the stiffness matrix becomes highly nonlinear. This approach also was used by Yang and Sadler [23], Jonker [24], Crisfield [25], and Hsia and Jang [26] to model dynamics of flexible mechanisms. It is worth noting that these inertia reference frame models incorporate geometric stiffening via various routes. For example, Simo and Vu-Quoc [22] used the finite strain beam theory developed by Reissner [27] for finding appropriate finite strain measures, while Hsia and Jang [26] proposed a finite element approach based on co-rotational formulation and small deflection beam theory with inclusion of axial forces. In this model, the nodal coordinates, velocities, accelerations, incremental displacements and rotations, and equations of motion of the system were defined in terms of fixed global coordinates, while the strains in beam elements are measured with respect to a set of element coordinates associated with each element. However, since these methods require the definition of finite strains, large displacements and rotations, they are somehow complicated and, therefore, not suitable for the control design especially for chains of flexible links.

2.2.3 Minimal and Redundant Methods

Since a system is a collection of bodies connected with various mechanical joints, each body of the system has a constrained motion. The dynamics of such systems can be formulated by means of either redundant or minimal coordinate methods.

In redundant methods, connectivity between different bodies is introduced to the dynamic formulation by using a set of nonlinear algebraic constraint equations. This approach has the advantage that the governing equations of motion of the system can be found in a straightforward manner. However, the dynamic formulation of motion of multibody systems based on this approach, leads to a mixed set of differential and algebraic constraint equations which have to be solved simultaneously. Moreover, this procedure increases the dimension of the problem by considering dependent coordinates at joints and Lagrange multipliers as additional unknowns. Many researchers such as Shabana [11], Song and Haug [28], and Avello et al. [29] have used this type of formulation. Song and Haug [28] developed a finite element formulation in which kinematic constrains and equations of motion were combined to obtain a coupled system of equations presenting the behavior of the planar flexible mechanisms. Avello et al.[29] used a general non-linear finite element formulation to establish the equations of motion of flexible multibody systems. Even though their model was based on the redundant method, they did not use Lagrange multipliers, but they introduced the constrain equation into equations of motions through a penalty formulation.

In the minimal method, the appended constraints are eliminated by using independent coordinates. In other words, joint or relative coordinates are used to find dynamic equations of the system expressed in terms of the system degrees of freedom. This leads to a formulation with a minimum number of dynamic equations because extra unknown variables including dependent coordinates used to represent connectivity of the bodies and the Lagrange multipliers resulting from connectivity constraints are not considered. However, this approach leads to a complex recursive formulation in many applications. This approach was used by many researchers such as Book [9], Usoro et al [10], Naganathan and Soni [14], and Nagarajan and Turcic [30].

2.2.4 Approximate Methods

The dynamic formulation of flexible multibody systems leads to a set of complicated partial differential equations. Since these equations are space and time dependent, they can not be solved analytically. This is why many approximate techniques were proposed to change these partial differential equations to a set of ordinary differential equations. Mainly three methods have been used in the literature, namely: lumped parameter methods, assumed mode methods, and finite element methods.

2.2.4.1 Lumped Methods

The lumping approximation is the oldest method to model continuos systems in all engineering fields. This technique was used widely in vibration analysis of mechanical systems with distributed inertia and elasticity. Inertia and compliance effects were lumped to obtain ordinary differential equations as approximations for partial differential equations governing the dynamic behavior of the continuos systems.

Mirro [31] in his pioneering work considered both the modeling and control of a single flexible link via a lumped parameter approximation technique. Book [32] derived the linear dynamics of spatial flexible arms represented as lumped mass and spring components via 4X4 homogenous transformation matrices used in rigid multibody dynamics. He neglected nonlinear and coupling terms such as Coriolis, centrifugal, and gravity effects in his model. Later Book et al [33] directly approximated a two-link flexible manipulator with a linear model derived from a nonlinear distributed parameter model by using impedance methods. Also a generalized lumped parameter method was proposed by Sadler and Sandor [34] and Sadler [35] to present a finite set of submasses of an elastic member for simulating planar motion of flexible mechanisms. They considered the components of the mechanisms as simply supported beams subject to planar bending. A finite difference formulation was used to solve the equations of motion numerically. In 1979 Book [36] utilized 4X4 transformation matrices to model a spatial manipulator which was light and operated at low speed. By neglecting the mass of the manipulator compared to the mass of the payload and assuming that the links bent in their first mode of vibration, he developed the linear equations of manipulator as two rigid masses connected by a chain of massless beam segments.

As mentioned earlier, in lumped parameter methods, it is necessary to approximate the physical system with distributed mass and elasticity as a system of rigid bodies connected with massless elements. This idealization is difficult in many practical problems. This is why more advanced approximate methods such as assumed mode methods and finite element methods, have been developed. These methods can be used to discretize continuous systems in an easier and more systematic way.

2.2.4.2 Assumed Mode Method

The assumed mode method is mainly presented by Book [9] for modeling the dynamics of flexible manipulator systems consisting of rotary joints that connect pairs of flexible links. In fact he extended the recursive Lagrangian dynamics proposed by Hollerbach [7] to flexible manipulator systems by using the assumed mode method introduced by Meirovich [37]. In his model, 4X4 transformation matrices were used to describe the kinematics of both the rotary-joint motions and the link deformations. Therefore, hybrid coordinates including the joint motions and elastic deformations described by a series of vibration modes were employed to describe the system behavior.

Judd and Falkenberg [38] and Singh and Schy [39] used a similar modal analysis approach to model flexible robot arms. Since they neglected the kinetic energy due to the link deformation, their models were not accurate. Also Yuan, Book, and Huggins [40] used a Lagrangian assumed mode method for dynamic modeling and control of flexible manipulators. They used the finite element method to derive suitable mode shapes.

An assumed mode method based on Kane's method was also used in the literature by Singh et.al [41] who proposed a recursive formulation for flexible multibody systems. The formulation was restricted to clamped-free mode shape shapes. In this work the assumed modes were obtained by a prior finite element analysis.

Generally, floating reference coordinates are used in the assumed mode methods. Depending on the choice of these rigid body coordinates, different mode shapes functions have to be used. Some authors have used the rigid body coordinates attached at the base with the clamped free boundary condition [19,42], while the others have used rigid-body coordinates passing through the end-point [21] or through the center of mass of the beam [20].

The main drawback of these methods is the difficulty in finding modes for links with non-regular cross sections and for multi-link manipulators. Benati and Morro [43] proposed an assumed mode method for dynamic modeling of the chain of flexible links. They described the flexibility of each link by the first two eigenmodes of clamped beams. In their work the first two eigenmodes of the links were found by treating the mass of distal links as a lumped effect at the extremity of the link under consideration. This method of finding modes for links is only an approximation because the mode shapes of the links are configuration dependent especially when the effect of gravity is taken into account.

On the other hand, the use of transformation matrices makes the modeling rather complicated. This is why the solution of models based on assumed mode method (Book's method) especially for spatial manipulators are computationally inefficient and time consuming. To improve Book's method, a more efficient method which uses the Newton-Euler formulation was proposed by Hasting and Book [13]. Also a Lagrangian formulation by using angular velocities instead of transformation matrices was presented by King et.al [44]. Meanwhile, Li and Sanker [45] improved Book's by using Lagrange assumed mode method via using a 3X3 matrix and a 3X1 vector to present link kinematics.

It is worth mentioning that some of the researchers such as Asada et.al [21] have used Raylieght Ritz functions instead of mode shapes in their formulation. However, choosing Ritz functions specially for non-uniform links is a difficult task.

2.2.4.3 Finite Element Method

In one of the early works on flexible mechanism Neubauer et.al [46] derived a nonlinear partial differential equation by force and momentum balance of a link section for investigating the transverse vibrations of the connecting rod of a planar slider-crank mechanism. They remove all nonlinearity by assuming the independency of end reactions from elastic vibrations. Chu and Pan [47] transform the governing partial differential equations of motion derived by [46] to ordinary differential equations by using Kantrovich method and the method of weighted residuals. Other researchers such as Jasinski et.al [48], Badlani and Midha [49], and Tadjbakhsh [50] also modeled the elastic links as continuos systems with infinite degrees of freedom. These analyses were so limited and complicated that they were used exclusively for simple slider-crank mechanisms with only one flexible member.

Later finite element method was used to develop approximate models for flexible mechanisms with more than one flexible links. In early use of finite element procedure, only specific structures were analyzed mainly in the aerospace and civil engineering. However, at the present time, finite element method is widely used in most of the engineering analysis. This method is quite general and can be applied to the flexible multibody systems with complex shaped components. Using finite element method, flexible bodies are presented as discrete systems with finite degrees of freedom.

Finite element method was used to model flexible mechanisms by many authors. Winfery [51,52] was the first to introduce the finite element concept for analysis of mechanisms using stiffness technique of structural analysis. He used the assumption of uncoupled rigid body motion and small deformation in his model. The idea of kineto-elasodynamics, which is the study of motion of mechanisms consisting of flexible links, was introduced by Erdman et.al [53,54]. They employed the finite element method based on flexibility method of structural analysis to study flexible mechanisms. Their model was based on the assumption that small elastic deformations are caused by inertia forces arising from rigid body motion of the system which was assumed to be independent of elastic deformations.

Midha et.al [55] used a displacement finite element method to model an entirely elastic four-bar mechanism. By assuming that the rigid body velocity and acceleration are small as compared to the velocity and acceleration of the elastic nodal deformations, they obtained the linear differential equations of motion via Lagrange's equations. Later Turcic and Midha [12] used finite elements to derive the equation of motion of elastic mechanisms by preserving tangential and Coriolis acceleration terms which leads to the presence of nonlinear coupling terms. However, they assumed that the elastic motions did not have any effect on the large rigid body motion.

Bahgat and Willmert [56] presented a finite element approach for vibration analysis of general flexible planar mechanisms. All moving links are assumed to be elastic. Lagrange equation was used to obtain the equation of motion. Similar to the previous authors, they assumed that the gross motion is determined by traditional rigid body kinematic analysis and the elastic response is driven by inertial forces arising in the rigid body motion. Khan and Willmert [57] adapted the vibration analysis method first introduced by Bahgat and Willmert [56] to quasi-static analysis of elastic deformations of a slider-crank mechanism and a four-bar linkage.

In the field of robotics Sunada and Dubowsky [58] presented a general Lagrangian/finite element approach to model industrial manipulators with elastic members, They utilized NASTRAN (a large general-purpose FE program) to generate the lumped mass and stiffness matrices of the individual links. In their method the effect of the system deformations on the kinematics of succeeding links was ignored.

All the aforementioned finite element method approaches were based on linear superposition theory, in which elastic deformations were found by assuming known rigid body motion and later superposing the elastic deformations to the rigid body motion. Therefore, they did not consider the coupling effects between rigid body motion and elastic deformations.

There are some works in literature which consider rigid body motion and elastic motion coupling terms, but only those which represent the effect of the rigid body motion on the elastic motion [14,59,60,61]. Therefore, these works neglected the effect of elastic motion on the rigid body motion. Natagathan and Soni [14] included coupling effects and presented a nonlinear finite element based model for flexible manipulators. Utilizing a finite element method and Timoshenko beam theory, Nath and Ghosh [59,60] developed the differential equations of motion of flexible mechanisms by considering coupling terms. Kalra and Sharan [61] proposed a Galerkin approach for dynamic modeling of planar multi-link flexible manipulators. They considered axial deformations and coupling terms between rigid and elastic motions. However, similar to the previous finite element models, in this model the nominal motion of the system was assumed to be independent of elastic deformations.

The effect of elastic deformations on the rigid body motion of the system was taken into consideration by few researchers. Nagarajan and Turcic [30] developed a Lagrangian finite element dynamic model for spatial flexible mechanisms. They treated both the rigid body degrees of freedom and the elastic degrees of freedom as generalized coordinates. Although they considered the mutual dependence between the rigid body and elastic motions, they ignored the effect of elastic deformation on the transformation matrix between the link coordinates and the global coordinates. Usoro et.al [10] presented a finite element/Lagrangian approach for modeling of lightweight flexible planar manipulators. They introduced a model in which the system configuration at any time is described by a combination of gross motion and elastic coordinates. The tangent coordinate systems, which are attached at the base of the links, were utilized. This model was based on small deformation theory and neglected axial deformations. Although most of the coupling terms were taken into account, this model can not be easily used for manipulators with more than two links due to its computational complexity.

Avello et al. [29] established a general non-linear finite element formulation for dynamics of flexible multibody systems using large displacement theory and redundant method based on penalty functions. Even though most of the coupling terms were taken into consideration, the complexity of the method for control design is its main disadvantage.

2.2.5 Joint Flexibility

All of the above studies neglected the joint flexibility and the actuator dynamics. Unfortunately, joint elasticity exists in most of today's manipulators and must be considered in modeling for many cases. Most industrial robots are equipped with gear boxes such as DC motors with harmonic drive transmissions that introduce joint flexibility. In addition to gears, motor shafts and bearings can cause joint flexibility. The small angular deviation due to joint compliance will influence the end effector position accuracy especially as the arms length get longer. Neglecting this effect may be acceptable when the operator speed is low, but may be quite devastating when the speed becomes high. Because of the high complexity of the dynamical equations for multi-link manipulators with both joint and link flexibility, most of the literature on the control of flexible manipulators have discussed arms with joint flexibility and with link flexibility separately.

The problem of joint elasticity has been addressed in recent years. Spong [62] investigated the modeling and control problem for flexible joint manipulators. He developed a simple model to represent the elastic joint manipulator by assuming that the motion of the rotor is purely rotation with respect to an inertial frame and the rotor velocity and the gravitational potential of the system are both independent of the rotor position. Also Good et al [63], Soni and Dado [64], and Readman and Belanger [65] and many others studied the dynamic response and control properties of manipulators with elastic joints. Generally, in the proposed models, the dynamic model of the elastic joint has been modeled as a torsional spring in parallel with a viscous damper.

Though a lot of work has been done in the modeling and control of joint flexibility and link flexibility, little work has been devoted to the problem of combined link and joint flexibilites. The problem of controlling manipulators and mechanisms with flexible links and joints has received widespread attention in the past decade. When the link flexibility and joint flexibility are comparable, the corresponding subsystems are strongly coupled due to significant interactions between link and joint flexibility. The link flexibility by its own complicates the manipulator dynamics, therefore, it is obvious that the inclusion of the joint flexibility causes greater complication in the dynamic model of the system.

Gebler [66] modeled a flexible link planar robot with two revolute joints using Ritz approximation considering joint flexibility. The two static deflection bending lines of a cantilever beam with only one concentrated force or one concentrated torque acting on the outer end of the beam were used as Ritz-functions. He neglected the dynamic forces resulting from deviations from the nominal position and linearized the equations of motion of the system with regards to the nominal trajectory. Jonker [67] presented a finite element dynamic model of multi-link manipulators with link and joint flexibility by considering both links and joints as specific finite elements. In his model the actuators were chosen linear and their dynamics was not taken into account. Besides, he neglected the effects of damping and gravity. Huang and Wang [68] developed the equations of motion of robotic manipulators with both flexible links and flexible joints by combining the finite element model of flexible links using Timoshenko beam theory with multi-degree of freedom models of elastic joints. But they assumed that the rigid body motion was known in advance. Yang and Donath [69] and Yang and Fu [70] investigated the combination effect of link flexibility and joint compliance by combining a simple assumed mode shapes model of beams with spring-damper models. Similarly Gogate and Lin [71] formulated the manipulator dynamics by a superposition of two models, namely, an assumed modes of vibration model for links and a torsional spring model for joints. Based on this model they proposed a two step control which found the total control torque as simply the superposition of the first-step and the second-step control torque. Xi *et al* [72] studied a manipulator consisting of only one flexible link and one flexible joint. They assumed that the link was constrained to move only in a horizontal plane, therefore; they didn't take into account the gravity in their model. Also they neglected the component of centripetal acceleration based on the assumption of small angular velocity of the link. Recently Lieh [73] investigated the dynamic behavior of a slider crank mechanism with flexible coupler and joint by using a virtual work formulation. The slider was assumed to move on a horizontal plane and angular velocity was applied to the flexible joint. They used first two modes of vibration to approximate the link flexibility.

2.3 Trajectory Control of Flexible Manipulators

Robotic applications can be divided into two major tasks: (1) point-to-point motions, as in spot welding and parts handling, and (2) specified path motions, as in arc welding, laser cutting, painting, and glue dispensing. Controlling the position of the end-point of flexible manipulators to track a desired trajectory with specified speed is a very difficult task due to the structural flexibility coupled with noncolocated sensors and actuators. This is why advanced techniques, which are significantly different from those for rigid arm control, have been developed for control of nonminimum phase flexible arms.

A number of feed-back control strategies have been proposed in the literature by the control community for the problem of end-point trajectory tracking in flexible multibody systems. Hasting and Book [18], Cannon and Schmitz [20], Book [33], and Sakawa et. al. [74] employed linear control theory, while Singh and Schy [39], De Luca et al [81], and De Luca and Siciliano [82] made use of nonlinear decoupling.

To control flexible systems, the early studies obtained linear models from nonlinear equations of motion, and then they utilized linear control theory. For example Hasting and Book [18] used joint and strain feedback to damp structural vibration of a flexible manipulator. However, their experiments showed overshoot and vibration to step position command. Book et al [33] addressed the control of two-link flexible manipulator by linearizing the manipulator dynamics and using linear feedback control schemes. They neglected nonlinear effects of Coriolis, centrifugal, and gravity forces. Cannon and Schmitz [20] developed a specific linear model for a single-link flexible manipulator moving on a horizontal plane. Gravity and Coriolis forces were neglected. With the linear model, collocated and noncollocated control systems were developed utilizing linear control theory. They recognized that a multi-link arm could not be controlled based on their approach because of nonlinearities in the dynamics of a multi-link arm. Sakwa et al. [74] introduced a similar closed-loop approach but with a more detailed analytical model of the link and a different sensor system. Their algorithm was used to suppress arm vibrations by measuring strains over the arm links.

As mentioned earlier the aforementioned authors have used linearized equations of motion of flexible manipulators. The linearized models can only work in the neighborhood of operating points about which linearization has been taken. Therefore, the motion of manipulators is confined to a small range, and the linearization has to be affected frequently due to nonlinear and time varying nature of the system. We see that the control design based on linearized models is not adequate for high speed manipulators. Moreover, since control systems for flexible manipulators are non-collocated and position commands contain high frequency components, the feedback control may cause these systems to become unstable.

Siciliano et al. [75], Siciliano and Book [76], and Khorrami and Ozguner [77] proposed singular perturbation approaches based on two-time scale model of the flexible arm to control flexible link manipulators. These approaches allowed the definition of a slow subsystem corresponding to the rigid body motion, and a fast subsystem describing the flexible motion. Then a composite control strategy was applied. First a slow control was designed for the slow subsystem as it would be done for an equivalent rigid arm, then a fast control stabilized the fast subsystem. However, the separation of time scales between the rigid and flexible subsystems can not be realized for many systems.

An approach proposed in the literature is the feedforward compensation which is based on inverse dynamics of models of flexible structures. A key issue in feedforward compensation is the computation of actuator torques required for flexible manipulators to track a specified trajectory with a specified speed. Feedforward compensation has been used to reduce tracking errors and residual vibrations [66,78,79]. The inverse dynamic problems were usually simplified by decoupling the kinematic and dynamic equations based on the concept of nominal joint motions, which were determined using the kinematic equations for the rigid link counterpart of a flexible link manipulator by neglecting the effect of link deflections. Pfeiffer [80] suggested a control scheme consisting of a feedforward computed joint torque based on rigid body inverse dynamics and a linear stabilizing feedback on the linearized system around the given rigid trajectory. In Singh and Schy paper [39], a generalization of the computed torque method, which had the end effector actuation for vibration damping in addition to joint actuation, was presented. It proposed a joint space closed-loop control for elastic robots based on nonlinear inversion and modal damping. Also De Luca et .al [81,82] proposed a closed-loop control strategy consisting of a linearized model-based feedforward term and a linear feedback control on joint angles. However, De Luca et. al [81] showed that numerical inversion techniques for a flexible manipulator lead to an unstable behavior.

Wang et al [83] presented a new method for synthesis of open-loop control inputs to move a flexible system along a given trajectory. Their approach was based on the closed-loop simulation to generate the open-loop control input. This method was applied to a linear problem. It was claimed that the proposed method could be extended to nonlinear systems, but such extension has not yet been done.

To avoid the aforementioned problems, inverse dynamic methods have been recently proposed by many authors to determine the joint torques such that the end-point of the flexible manipulator follows a given trajectory. Since the system is redundant due to its flexibility, a complete model consisting of the kinematic and dynamic equations should be solved simultaneously. But the main difficulty is the non-causality of the inverse dynamics of flexible manipulators. In other words, since the point for which the prescribed motion is specified and the application points of control torques are connected by elastic bodies, the joint torques should be applied from negative time to the future time in order to control the position of the end-point according to the desired trajectory. The delay is due to the fact that elastic waves propagate with finite velocity. This is the reason why standard causal time domain integration schemes are unstable in solving the inverse dynamics of flexible manipulators.

Asada et al. [21] derived an inverse dynamic equation by using Ritz-functions as assumed modes. However, they did not solve the inverse dynamic equations completely.

Idler [84] formulated the inverse dynamics of flexible multibody systems by utilizing higher order derivative information. However, he obtained a causal solution for the inverse problem. This is why one of the links was assumed to be rigid. Moreover, backward Euler method, which is only a first order method and not accurate enough, was used in numerical integration.

Xi [85] recently proposed a new method to solve the inverse dynamics of flexible manipulators. He used a Lagrangian assumed mode method to derive the equations of motion of the system. Even though this study mentioned the noncausality of the inverse dynamics of flexible manipulators, it was basically based on causal solution of such problems. For this reason an initial velocity was assumed for the system in order to be able to solve the problem.

Noncausal solutions for inverse dynamic problems have been developed by Bayo [86] and Kwon and Book [87]. Moulin and Bayo [88] showed that the causal integration of the inverse dynamics of the flexible multibody systems leads to unstable results. Bayo [86] developed a new approach to calculate the required torque to produce a desired end effector motion for a single-link arm by solving the inverse dynamic equation in the frequency-domain with inverse fast Fourier transform. This method took into consideration the noncausal nature of the inverse dynamics of flexible manipulators. Since the necessary torques are provided by the solution of the inverse dynamics, the reduction of vibration in positioning of the tip is no longer required for input shaping. Later Bayo and Mouline [89] introduced the convolution integral method to solve the inverse dynamic equation in the time-domain. This technique was computationally much more efficient than the approach developed in frequency domain. Ledesma and Bayo [90,91] extend the noncausal integration method to the inverse dynamics of multi-link closed-loop and open-loop flexible multibody systems. However, this approach was limited to systems with flexible links only.

Kwon and Book [87] introduced another new solution for the inverse problem for a single-link arm. They decoupled the inverse dynamics of the manipulator into causal and anti-causal parts, then these two parts were solved forward and backward in time, respectively. The limitation of this approach is that it can be used only for linear single-link systems in which the effects of gravity, Coriolis and centrifugal accelerations are neglected.

It is important to note that when the dynamic effects of the elastic modes are small (quasi-rigid), causal inverse solution may be obtained by regularizing the problem with the addition of artificial damping either through the damping matrix or the numerical integration scheme. However, these ad hoc processes change the nature of the problem and do not yield the desired time delay effect [90].

All of the above studies did not take into account the joint flexibility and actuator dynamics. Only a few works were reported in the literature which addressed control of manipulators with both link and joint flexibility. Gebler [66] proposed a feedforward control strategy to control an industrial robot with elastic links and joints. As it was mentioned in section 2.2.5, his model was based on Ritz approximation and linearization with regard to a nominal trajectory. The desired joint angles calculated under the assumption of rigid joints and links were modified by taking into account nominal deflections. A two step control law which found the total control torque as the superposition of the first-step and the second-step control torque was developed by Gogate and Lin [71]. By assuming that only joints are elastic, the first control torque was found using a singular perturbation approach. Then by treating the effects due to link flexibility as nonlinear disturbances to the manipulator system the feedback control law yields a second control torque. Also Yang and Fu [70] used singular perturbation approaches to control manipulators with both joint and link flexibility. They decomposed the full-order nonlinear system into slow subsystem, mid-speed subsystem and fast subsystem, and then they proposed a composite control law using optimal control theory.

None of the aforementioned works have taken into consideration the noncausal nature of the inverse dynamic problem.

2.4 Time Optimal Control of Flexible Manipulators

For high productivity, it is desirable that the motion of the robotic manipulators be time-optimal so as to reduce the motion time. Therefore, another type of problems related to the flexible manipulators is controlling the position of their end-point for a rest to rest motion in minimum time along a specified path, while actuator torques are not exceeding the limits due to physical capabilities of actuators or bending strengths of links.

Time optimal control problems lead to two-point boundary value problems with fixed initial and final states and free final time. These problems, even in the case of rigid manipulators, have no closed form solutions except in the simplest cases. Further, numerical approaches used for time-optimal problems have yielded acceptable results only when certain restrictions were placed on the problems. For example, for the unconstrained motion of linear single-degree of freedom systems with only one controller, the solution is characterized by saturated controls for the entire motion with one switch at the mid-point as shown in figure 2.1. This type of solution is known as bang-bang profile in optimal control control theory. Nevertheless a general multi-degree of freedom nonlinear time optimal control algorithm has not yet been developed. This is why most of the papers dealing with computational algorithms for the time-optimal control problems assumed a bang-bang control profile and found the number of switches and the switch times for each controller.

Work on minimum-time control problems begun as early as the late 1960s and most commonly, the researchers have linearized the dynamics in order to apply standard techniques of linear optimal control theory to the time optimal solution. A survey of the literature shows that two types of problems are commonly considered: a point to point

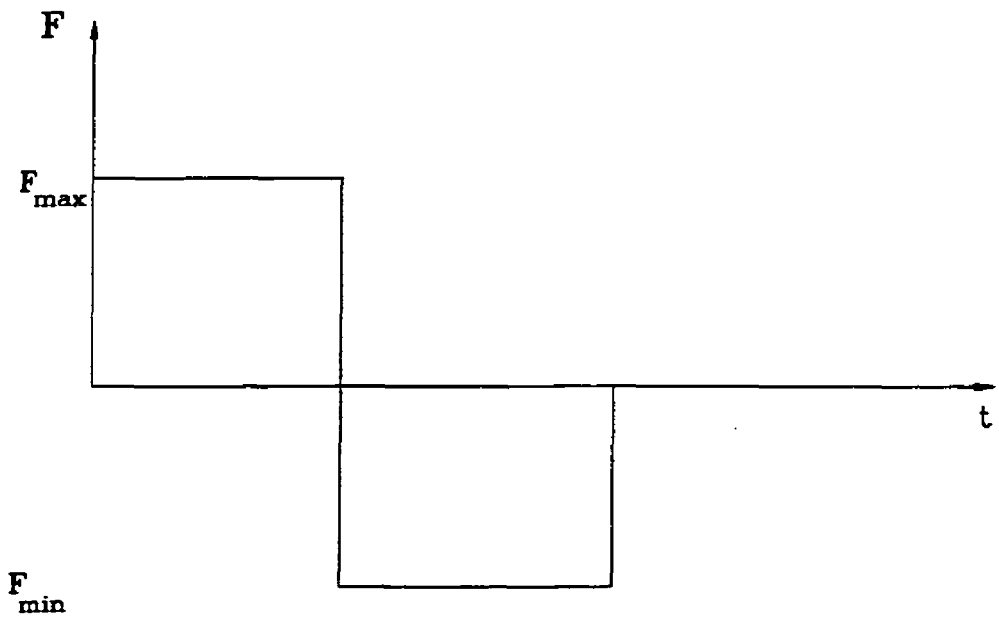

Figure 2.1 Bang-bang profile for a single degree of freedom system

motion without constraints on the path and a point to point motion along a specified or constrained path.

Although various approaches have been developed for the time-optimal control of rigid manipulators without path constraints [92-95] and with path constraint [96-98], little work has been devoted in the literature to the time-optimal control of flexible manipulators.

Many algorithms were proposed for solving unconstrained path minimum problems. In the earliest attempts, Khan and Roth [92] derived the expected bang-bang solution with multiple switching points. They addressed the time-optimal control of a system of rigid bodies in series by rigid joints. A suboptimal feedback control in terms of switching curves for each of the system controls was developed. These curves were obtained from linearized equations of motion of the system, then approximations were made for the effects of nonlinear terms consisting gravity loads and angular velocity terms. Luh and Lin [93] and Lin et al. [94] used purely kinematical approaches to find the sequence of time intervals that minimize the total time spent on moving between two points. They assumed that the path consisted of a sequence of straight line segments and the constant limits on Cartesian velocity and acceleration were known *a priori* along each path segment. It is almost impossible to select such limits without knowing the dynamic properties and the actuator characteristics of the manipulator. However, it is often difficult and tedious to determine these limits.

Sahar and Hollerbach [95] presented a general solution by using a dynamic time-scaling algorithm and a graph search. They did not pre-assume a bang-bang solution and their algorithm took into account a full dynamic model for the manipulator and actuator constraints.

Although unconstrained path minimum time approaches are suitable for some appllications, it is often necessary to specify the manipulator trajectory in order to avoid obstacles. Niv and Auslander [96] used a parameter optimization technique on the joint actuator switching times to solve a constrained path minimum time problem. They assumed that during the motion, each actuator exerts maximum control torque (bang-bang), while the manipulator followed the desired path and reached to its final destination. Shiller and Dubowsky [97] and Bobrow et al. [98] solved a minimum-time problem for a rigid manipulator case when the path is specified and the actuator torque limitations are known. The solution was given in the form of an algorithm for determining linear acceleration of the end effector along its path. At each position and velocity on the path the constraints on linear acceleration of the end effector corresponding to the actuator torques limits were determined. On the other hand, Bobrow et al. [98] found that the standard optimal control methods (in particular Pontryagin's maximum principle) even in simple cases did not converge to a solution.

There are a few work on time-optimal control of flexible link manipulators. Pao and Franklin [99] developed a bang-bang solution with at most 3 switches for the time-optimal control of a single flexible link manipulator. They neglected all nonlinear terms and used a one-bending mode model of the flexible link. Hetch and Junkins [100] proposed a near-minimum-time solution for a flexible robot by smoothing the classical bang-bang solution. Using an optimization algorithm, first they found the switch times of the bang-bang solution of the rigid counter-part manipulator. Then to avoid large vibrations in the flexible manipulator due to abrupt transitions (bangs), they smoothed the changes in the control torques by using smoothing functions. Szyszkowski and Youck [101] derived the control rule based on rigid body dynamics (using Pontryagin's principle for linearized system) for a single flexible arm moving in a horizontal plane. Then they tried to improve the rule by examining its effectiveness through finite element analysis of the fully nonlinear dynamics of the system. Eisler et al [102] presented an algorithm in which the method of recursive quadratic programming was used to generate approximate minimum-time trajectory for two-link flexible manipulator movements in the horizontal plane. Hwang and Eltimsahy [103] studied the effects of link flexibility on an unconstrained point to point near-time-optimal control using the method of average dynamics and the bang-bang control theory. They used only one vibration mode in their assumed mode method to approximate the link flexibility. First, they obtained the near-time optimal reference trajectory based on linearized equations of motion of a counter-part rigid link manipulator. Then they proposed a closed-loop controller with the effects of link flexibility as a disturbance on the system.

All of the aforementioned studies dealt with link flexibility and neglected joint flexibility. Also they did not take into account the non-causality of inverse dynamics of flexible systems. Because of the highly nonlinear structure of the equations of motion as well as the non-causality of such systems, the exact minimal time solution is not available at the present time. In this dissertation near-time-optimal control problem of manipulator systems with both link and joint flexibility are solved using nonlinear programming by taking into consideration the noncausal nature of their inverse dynamics via considering pre-actuation and post-actuation in the solution procedure. The proposed technique is based on transforming the optimal control problem into an equivalent unconstrained optimum design problem using penalty function methods.

CHAPTER 3

DYNAMICS OF DEFORMABLE MULTIBODY SYSTEMS

3.1 Introduction

Many mechanical systems such as machines, mechanisms, manipulators, space structures, and aircrafts can be modeled as multibody systems. Figure 1 shows some examples of this type of systems. Each multibody system consists of a set of interconnected bodies which undergo large rotational and translational displacements. This is why the dynamic equations are highly nonlinear and coupled even for systems with rigid components.

In this dissertation, mathematical models incorporated into the numerical simulation of multi-deformable-body systems are based on the Lagrangian principle. This chapter presents a general overview of dynamics of multi-deformable-body systems. The general form of governing equations, which includes equations of motion of the system and constraint equations, is developed and various solution procedures are described.

3.2 Kinematics of Deformable Bodies

The distance between two points of a rigid body remains constant during the motion of the body; therefore, there is no difference between the kinematics of the body and the kinematics of its reference coordinate. However, this is not the case when deformable bodies are considered.

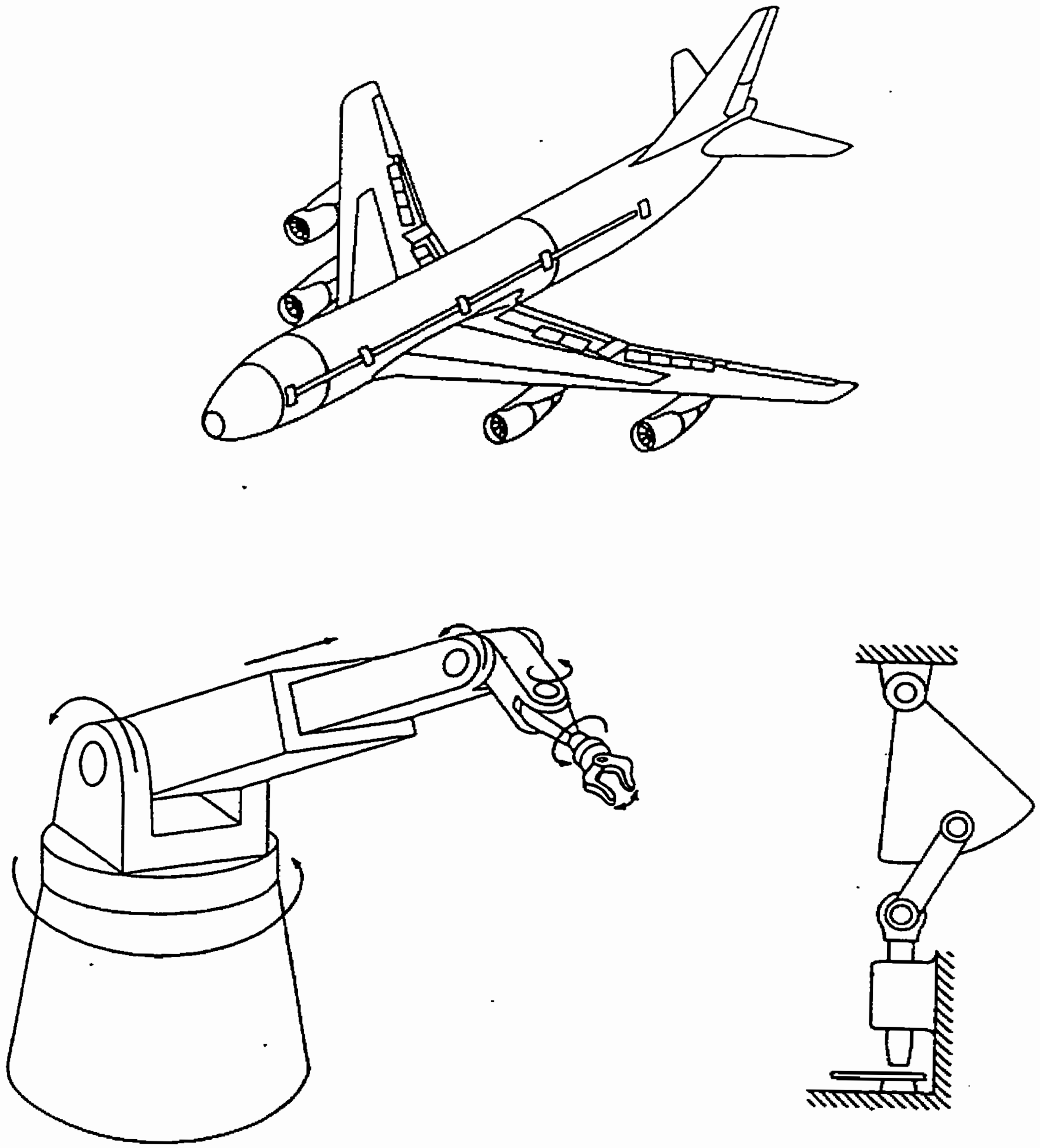

Figure 3.1 Multibody systems

Consider the floating coordinate system O^i-$X_1^iX_2^iX_3^i$ shown in figure 3.2, which translates and rotates with the body. This coordinate system called body coordinate system is assigned to a deformable body whose origin is rigidly attached to point O^i. Vector $\mathbf{u}_0^{ji}$ represents the position vector of point P^i in the undeformed state. Assume that this vector ($\mathbf{u}_0^i$) has no translational and rotational displacement with respect to the body coordinate system. It means that the components of vector $\mathbf{u}_0^i$ are constant in the local coordinate system during the motion of the deformable body.

Referring to figure 3.3, position vector of P^i after deformation can be written as

$$\boldsymbol{r}^i = \boldsymbol{R}^i + \boldsymbol{u}_o^i + \boldsymbol{u}_f^i \tag{3.1}$$

where $\mathbf{R}^i=[R_1^i,R_2^i,R_3^i]$ is the position vector of point O^i, $\mathbf{u}_0^i$ is the undeformed local position of point P^i, and $\mathbf{u}_f^i$ presents the deformation vector at this point. The components of $\mathbf{u}_f^i$ in the body coordinate system are time and space dependent. Therefore, the dynamic formulation of the system leads to a set of nonlinear time varying partial differential equations with an infinite number of degrees of freedom. To reduce the number of coordinates to a finite set, approximate techniques such as finite element method can be employed. By using these techniques, the governing partial differential equations are transformed to ordinary differential equations which can be solved with well known numerical methods such as Runge-Kutta, Newmark, and Wilson theta methods.

3.2.1 Constrained Motion

The motion of each body of a multibody system is constrained because of the mechanical joints connecting adjacent bodies. The constraint equations represent the mathematical or kinematical relationship among the coordinates. As it was mentioned in previous chapters, there are two basic methods to handle the constraints. The first method called minimal method is based on solving constraint equations for the dependent

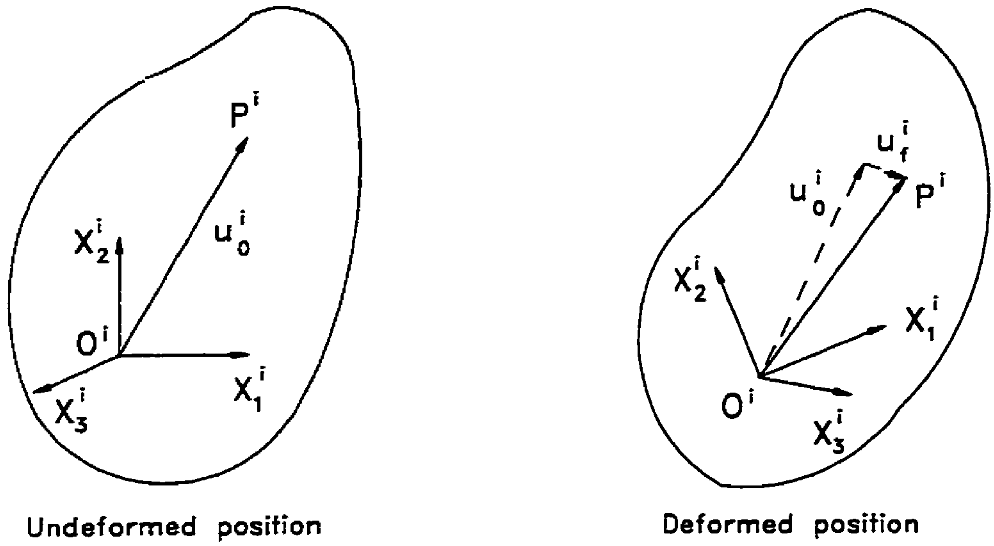

Figure 3.2 Deformation of a deformable body

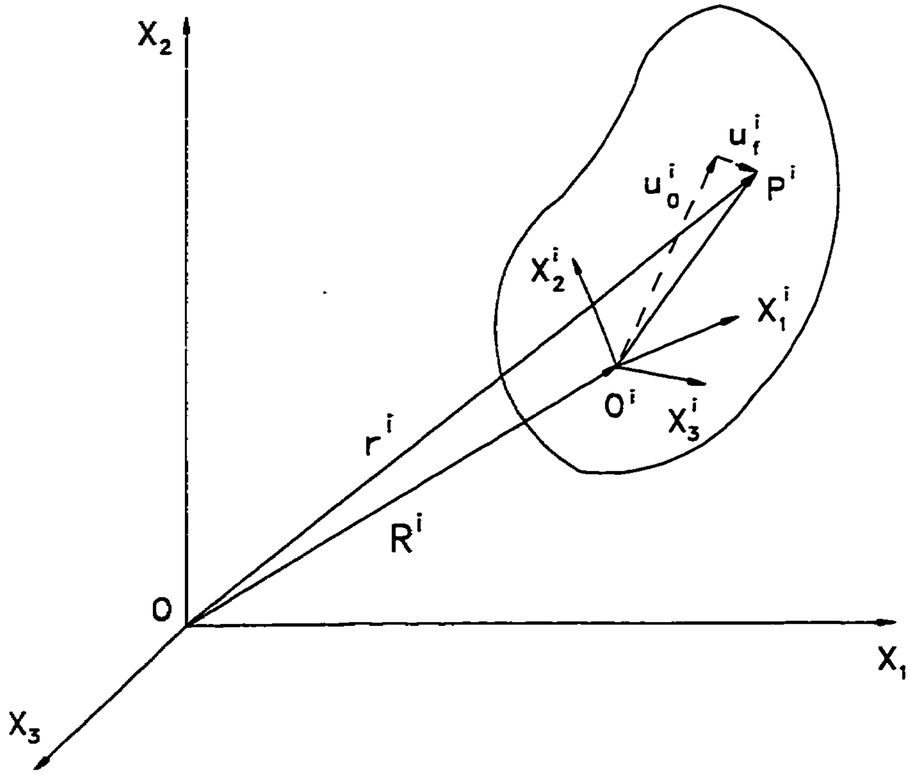

Figure 3.3 Global position of an arbitrary point on a deformable body

coordinates explicitly in terms of independent coordinates. The condition for using such a method is that the constraint equations are holonomic or integrable. Since the algebraic equations are eliminated, the minimal method leads to the smallest set of equations. But this method is not very feasible especially for large systems because the equations are highly nonlinear and complex.

In the second approach called redundant method, the constraint equations are added to the dynamic formulation by making use of Lagrange multipliers. This method leads to a set of differential and algebraic equations (DAE's) with the coordinates and the Lagrange multipliers as unknowns. The most direct approach is converting the system of DAE's to a set of differential equations by appending the double derivatives of the constraint equations with respect to time. Although the redundant method provides much more convenient means of handling the constraint equations, it increases the number of unknowns and subsequently the size of the problem.

3.3 Dynamic Equations

Several techniques can be used to develop the dynamic equations governing the motion of material bodies. Among them two basic techniques: Lagrangian and Newtonian approaches are the most popular ones in dynamic modeling of multibody systems. The former has established itself as the primary approach in multibody systems. This is mainly due to this fact that it is a scalar rather than vector approach. In the following, Lagrangian dynamics is briefly discussed.

3.3.1 Lagrangian Dynamics

Unlike Newtonian mechanics, Lagrangian mechanics makes use of scalar quantities: kinetic and potential energies and work done by the forces acting on the system. In Lagrangian dynamics, the system of equations of the motion are expressed in terms of a set of generalized coordinates and associated generalized forces. However, Lagrangian and Newtonian approaches are equivalent.

Lagrangian equations can be derived from D'Alembert's principle or Hamilton's principle. The first approach starts from a consideration of the instantaneous state of the system and small virtual displacements about the instantaneous state, while in the second approach Lagrange's equations are obtained from a principle which considers the entire motion of the system between times t_1 and t_2 and small virtual variations of the entire motion from the actual motion. This approach involves only physical quantities that can be defined without reference to a particular set of generalized coordinates, namely, kinetic and potential energies. Only the second approach (Hamilton's principle) is shortly described here.

3.3.1.1 Hamilton's Principle

This principle is one of the most basic and important principles in mathematical physics. Originally, it is formulated in terms of the dynamics of systems of particles, but it can readily extended by analogy to other cases.

First we consider a single particle of mass m subject a force field **f**. If **r** denotes the vector from a fixed origin to the particle at time t, then according to Newton's laws of motion, the path of the particle is governed by the equation

$$m\frac{d^2\boldsymbol{r}}{dt^2}-\boldsymbol{f}=0 \tag{3.2}$$

Let consider any other path **r+δr**. The true path and the virtual path coincide at two distinct instants $t=t_1$ and $t=t_2$; therefore, the variation **δr** vanishes at these two instants.

$$\delta\boldsymbol{r}\big|_{t_1}=\delta\boldsymbol{r}\big|_{t_2}=0 \tag{3.3}$$

Now by taking the scalar product of the variation $\delta \mathbf{r}$ into equation (3.2) and integrating the result with respect to time over (t_1, t_2), we have

$$\int_{t_1}^{t_2} \left(m \frac{d^2 r}{dt^2} . \delta r - f . \delta r\right) dt = 0 \tag{3.4}$$

After integration by parts and using equation (3.3), the first term of equation (3.4) takes the form

$$\delta\left[\frac{1}{2} m \left(\frac{dr}{dt}\right)^2\right] = \delta(KE) \tag{3.5}$$

where KE is the kinetic energy of the particle. Therefore, equation (3.4) can be written as

$$\int_{t_1}^{t_2} (\delta KE + f . \delta r) dt = 0 \tag{3.6}$$

This is Hamilton's principle in its most general form for a single particle [104]. The above derivation can be extended to a system of particles by summation, and to a continuous system by integration.

For a system of N particles, the virtual work δW done by the force system can be expressed in terms of virtual displacements δq_i in the form

$$\delta W = \sum_{k=1}^{N} f_k . \delta r_i = \sum_{i=1}^{n} Q_i \delta q_i \tag{3.7}$$

where n presents the number of degrees of freedom of the system. Now Hamilton's principle (equation 3.6) states that

$$\delta \int_{t_1}^{t_2} KE dt + \int_{t_1}^{t_2} \left(\sum_{i=1}^{n} Q_i \delta q_i\right) dt = 0 \tag{3.8}$$

This result is valid for both conservative or nonconservative systems [104]. By calculating the variation of the first integral of equation (3.8) in the usual way, we obtain the condition

$$\int_{t_1}^{t_2} \{ \sum_{i=1}^{n} [\frac{\partial KE}{\partial q_i} - \frac{d}{dt}(\frac{\partial KE}{\partial \dot{q}_i}) + Q_i] \delta q_i \} dt = 0 \tag{3.9}$$

The vanishing of the coefficients of the independent variations leads to Lagrange's equations in the following forms:

$$\frac{d}{dt}(\frac{\partial KE}{\partial \dot{q}_i}) - \frac{\partial KE}{\partial q_i} = Q_i, \qquad i = 1, \ldots, n \tag{3.10}$$

if the coordinates q_i are independent. This result is valid for both conservative and nonconservative systems [104].

If the force system is conservative, the generalized forces Q_i are derivable from a potential energy function (PE) in the following way:

$$Q_i = - \frac{\partial (PE)}{\partial q_i} \tag{3.11}$$

By introducing the Lagrangian of the system as L=KE-PE, equation (3.10) can be rewritten in the following form

$$\frac{d}{dt}(\frac{\partial L}{\partial \dot{q}_i}) - \frac{\partial L}{\partial q_i} = 0, \qquad i = 1, \ldots\ldots n \tag{3.12}$$

which can also be found from Hamilton's principle expressed in the form:

$$\delta \int_{t_1}^{t_2} (KE - PE) dt = \delta \int_{t_1}^{t_2} L dt = 0 \tag{3.13}$$

If the force system consists of both conservative and nonconservative parts, the Hamilton's principle leads to the Lagrange's equations:

$$\frac{d}{dt}\left(\frac{\partial L}{\partial \dot{q}_i}\right)-\frac{\partial L}{\partial q_i}=Q_i^{(nc)}, \qquad i=1,\ldots\ldots n \qquad (3.14)$$

where $Q_i^{(nc)}$ are the generalized forces resulting from the nonconservative loads.

Hamilton's principle can be extended to cover constrained systems. For problems with dependent coordinates which are interrelated through certain constraints equations (holonomic), it is possible to use the method of Lagrange multipliers to obtain the equations of motion. When the connection between bodies are of the holonomic type, the constrains can be expressed mathematically in the following form:

$$c_k(q,t)=0 \qquad k=1,\ldots\ldots,m \qquad (3.15)$$

with m<n and n-m being the number of degrees of freedom. Equation (3.15) can also be shown in the following matrix form:

$$C(q,t)=0 \qquad (3.16)$$

where C is the vector of constraint functions. By using the formal way of dealing with constraint equations in the calculus of variations, we can obtain the following mixed sets of differential and algebraic equations:

$$\frac{d}{dt}\left(\frac{\partial L}{\partial \dot{q}_i}\right)-\frac{\partial L}{\partial q_i}+C_{q_i}^{T}\lambda=Q_i, \qquad i=1,\ldots\ldots,n \qquad (3.17\text{-a})$$

$$C\ (q,t)=0 \qquad (3.17\text{-b})$$

where λ is the vector of Lagrange multipliers and C_q is the constraint Jacobian matrix.

By twice differentiation of the vector of the constraint functions with respect to time we find the following equation:

$$C_q\ddot{q} = -[C_{tt} + (C_q\dot{q})_q\dot{q} + 2C_{qt}\dot{q}] \tag{3.18}$$

which can be used instead of equations (3.17-b).

As it was mentioned earlier, approximate techniques should be used to reduce the number of coordinates of the deformable multibody systems to a finite set. After proper discretization of the continuous system, the system of equations (3.17-a) and (3.18) can be written in the following forms

$$\begin{aligned} M\ddot{q} + Kq + C_q^T\lambda &= Q_g + Q_e + Q_v \\ C_q\ddot{q} &= Q_c \end{aligned} \tag{3.19}$$

where M and K are, respectively, the symmetric positive definite mass and stiffness matrices of the system. Q_g and Q_e are the gravity load vector and the vector of generalized externally applied loads, respectively. Q_v is the quadratic velocity vector containing Coriolis and centrifugal components resulting from differentiating the kinetic energy with respect to time and with respect to the generalized coordinates of the system. Q_c is a vector which presents the right hand side of equation (3.18). Matrix K can be expressed in the following partitioned form

$$K = \begin{bmatrix} 0 & 0 \\ 0 & K_{ff} \end{bmatrix} \tag{3.20}$$

in which K_{ff} is the stiffness of the deformable system.

The system of equation (3.19) can be utilized in numerical solution of the nonlinear dynamic equations of motion of multi-deformable-body systems.

3.4 Solution Procedures

The dynamics of multibody systems with deformable components has many industrial and technological applications such as robotic manipulators, vehicle systems, and space structures. Because of the finite rotation of the deformable body reference frames, the dynamic equations of such systems are highly nonlinear. Two approaches which can be used to solve these equations are introduced in the following sections.

3.4.1 Linear Theory of Elastodynamics

A solution strategy widely used in the past [51-54] is the linear theory of elastodynamics. In this approach, the total motion of the system is assumed to be the superposition of the rigid body motion of the system and the elastic deformation of the components. The multibody system is treated first as a collection of rigid components. The inertia and reaction forces are calculated by using general-purpose multi-rigid-body computer programs. Then the forces obtained from the rigid body analysis are used to solve for deflection of the bodies in multibody systems. The total motion of the system is obtained by superimposing the small elastic deformation on the rigid body motion. Therefore, the coupling effects between rigid body motion and elastic deformations are ignored in this approach. As it was mentioned earlier, these effects become significant when high-speed, lightweight mechanical systems are considered.

3.4.2 Total Lagrangian and Updated Lagrangian Approaches

There are two finite-element formulations for large displacement problems. The first one is called total (stationary) Lagrangian approach in which the global reference coordinate system remains stationary and the motion of the bodies in multibody systems are defined with respect to the fixed frame of reference. Another finite-element formulation which has been proposed for large displacement analysis of deformable bodies is called updated Lagrangian approach. In this approach, a convected coordinate system, which is sometimes called co-rotational system, is attached to each finite element. Therefore, this coordinate system shares the rigid body motion of the corresponding finite element. By using small time steps in numerical integration, the displacement of the element between two coordinate system is described using shape functions and the nodal coordinates of the element. The current deformed state is used as the new reference state prior to the next incremental step. Therefore, the equations of motion are defined in the local coordinate system and the solution of these equations is updated in order to define a new local coordinate system. Since differentiations and integrations are defined in the local coordinate systems, the equations of motion are much simpler in the updated Lagrangian approach. However, since the general constraint equations or relative velocities and accelerations between bodies are not as simple as in the total Lagrangian formulation, this approach is not convenient for multibody system dynamics. This is why in the following two chapters, the total Lagrangian approach is used to develop dynamic equations of motion of planar and spatial flexible manipulators.

3.5 Summary and Conclusion

In this chapter a general overview on dynamic modeling of deformable multibody systems is presented. A Lagrangian approach is used to obtain equations of motion of such systems. A minimal method and redundant method are introduced and the system of equations including equations of motion of the system and constraint equations is derived using Lagrange multipliers. Moreover various solution approaches are briefly described.

In the next two chapters, the total Lagrangian approach is used to model the dynamics of flexible manipulators. The continuous flexible manipulator systems are discretized by the finite element method in order to reduce the number of coordinates necessary to describe the system. Minimal and redundant methods are used respectively in chapters 4 and 5 to present the configuration of the system in applying Lagrange's approach for dynamic modeling of planar and spatial multi-link flexible manipulators.

CHAPTER 4

DYNAMIC MODELING OF PLANAR MANIPULATORS WITH BOTH FLEXIBLE LINKS AND FLEXIBLE JOINTS

4.1 Introduction

In this chapter, an efficient dynamic modeling of lightweight multi-link planar manipulators with both flexible joints and links is developed using a finite element/Lagrangian approach. The dynamic elastic response of each flexible link is formulated relative to a floating frame called pinned-pinned or virtual link [21] coordinate system. Using this coordinate system the link deformation is measured relative to the line connecting the end points of the link. Both the rigid degrees of freedom and the elastic degrees of freedom of the system are treated as generalized coordinates. Each link is divided into a finite number of elements and the elemental kinetic and potential energies of an arbitrary link are derived in a systematic way. Then by using Lagrange's equation elemental mass and stiffness matrices and load vector of the typical element are obtained. By assembling the elemental matrices and vector of each link and then assembling the resulting link matrices and vectors in a proper manner the system mass and stiffness matrices and load vector are obtained. The effects of the payload and the revolute joints on the equations of motion of the system are included by using virtual work of the external loads and the kinetic and potential energies of the actuated flexible joints and the payload through applying Lagrange's equations. The dynamic model derived in this study is free from assumption of a nominal motion and takes into account not only the coupling effects between rigid body motions and elastic motions but also the interaction between the flexible links and the actuated flexible joints. Axial deflections, shear deformations, and rotary inertia effects due to elastic deformation are neglected and Bernoulli-Euler beam theory is used in the formulation.

The resulting equations of motion of the system are highly nonlinear and coupled. They can be integrated using any standard ordinary differential equation solver such as the Newmark method. The main advantage of the proposed model is its compactness and completeness; therefore, this modeling is quite tractable for automated computer solutions.

4.2 Kinematic Modeling

The manipulator system modeled in this chapter is a chain of flexible links which are connected by revolute actuated joints (figure 4.1). Each joint is flexible in the direction of rotation of the connecting links. There is an actuator at each joint which may contain gears. The stator of each arbitrary actuator k is fixed to the end of link k-1 and the stator of actuator 1 is fixed to the ground. Each rotor k is connected to link k through a gear train and a flexible shaft which presents the joint flexibility. The manipulator is constrained to move in the vertical plane; therefore, the effect of gravity is taken into account. The links are deformable due to bending during heavy payload operations and high speed motions.

4.2.1 Kinematic Modeling of Flexible Links

In order to develop a simple and compact model, elastic deformation of link k of

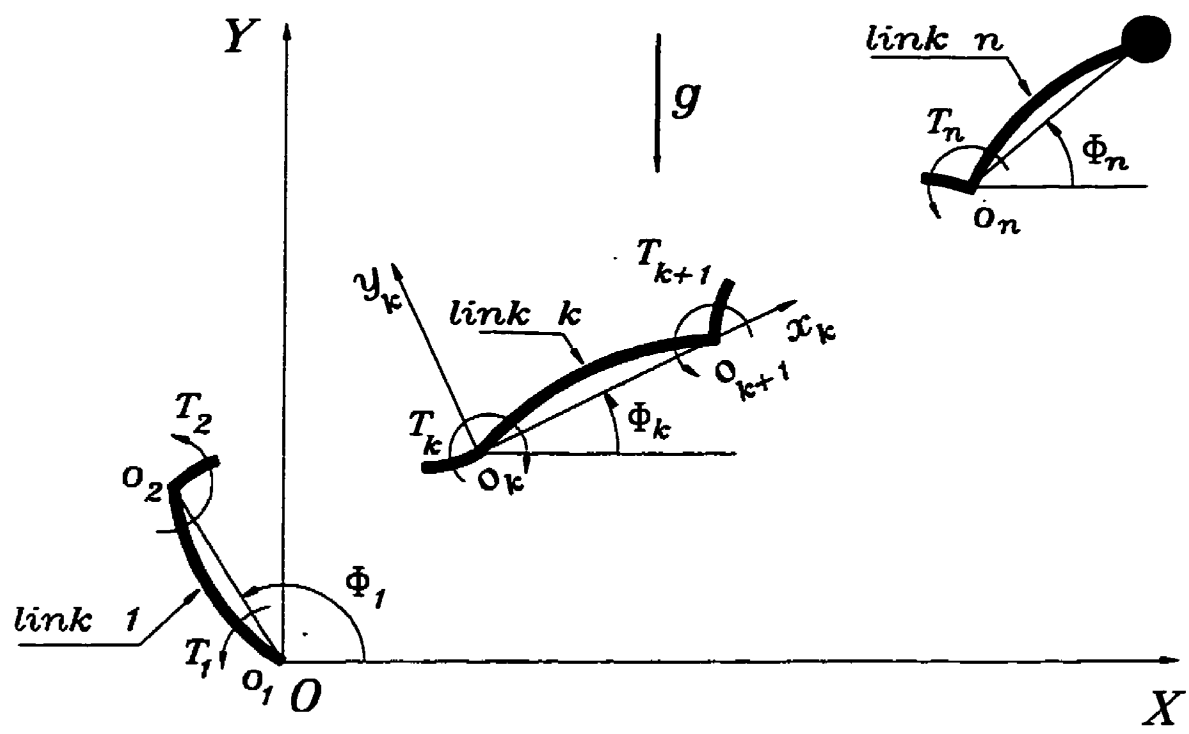

Figure 4.1 A planar multi-link flexible manipulator

the manipulator is represented relative to a floating coordinate system $o_kx_ky_k$, called pinned-pinned coordinate system. This frame describes the motion of the imaginary undeflected beam with respect to the inertial frame. As it can been seen in figures 4.1 and 4.2, OXY is the inertial frame coordinate system and $o_kx_ky_k$ is the rotating frame associated with link k of the manipulator. The axis o_kx_k of the rotating frame $o_kx_ky_k$ passes through the end points of this link whose transverse deflection $w^k(x^k)$ is expressed with respect to this rotating frame. The kinematic modeling is based on the following assumptions:

1) The manipulator is constrained to move in the vertical plane OXY; therefore, the effect of gravity is taken into account.
2) Each link is considered to be pinned at both ends in the corresponding floating frame.

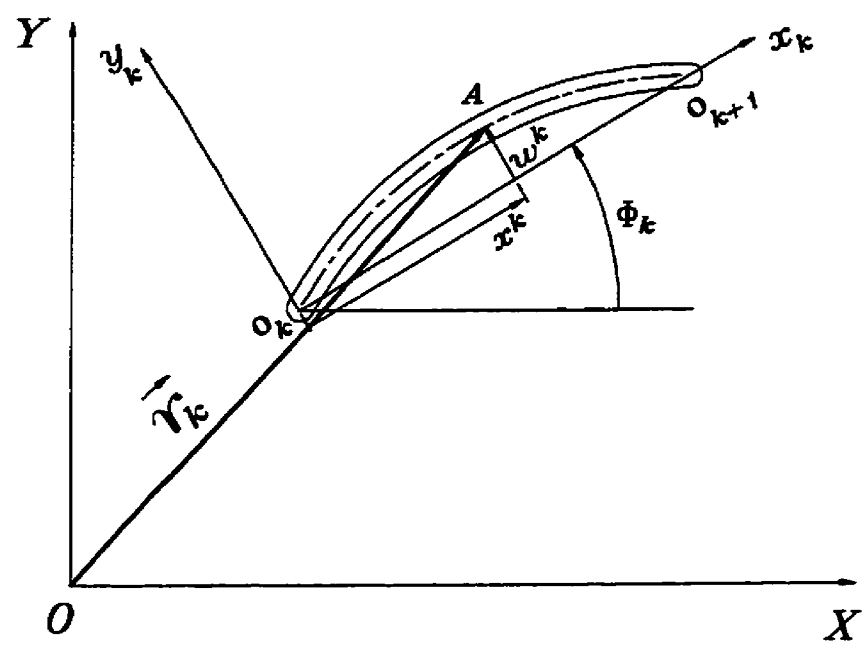

Figure 4.2 Link deformation presented in the local coordinate system

3) Axial deflections are negligible and only transverse bending deflections $w^k(x^k)$ are taken into account.

4) The links are so long and slender that shear deformations and rotary inertia effects can be neglected. This allows the use of Bernoulli-Euler beam theory.

Since x_k axis passes through both ends of link k, the origin of each local coordinate system is irrelevent to the deformation of the other links. This allows to reduce the computational complexity of the model. The equations of motion become more compact and decoupled than those derived using tangent coordinate systems [10,21].

Based on the aforementioned assumptions, the position vector of an arbitrary point A of each link k, shown in figure 4.2, can be written in the following form

$$\vec{r}_k = O\vec{A} = x^k \vec{e}_k^{(1)} + w^k(x^k)\vec{e}_k^{(2)} + \sum_{i=1}^{k-1} L_i \vec{e}_i^{(1)} \tag{4.1}$$

in which L_i, x^i, w^i, $\vec{e}_i^{(1)}$, and $\vec{e}_i^{(2)}$ are the length of link i, x and y coordinates of point A in the local coordinate system i, and the unit vectors along x_i and y_i axes of the local coordinate system i, respectively. By differentiating the position vector with respect to time, the velocity vector can be found as:

$$\dot{\vec{r}}_k = (x^k\dot{\Phi}_k + \dot{w}^k(x^k))\vec{e}_k^{(2)} - w^k(x^k)\dot{\Phi}_k\vec{e}_k^{(1)} + \sum_{i=1}^{k-1} L_i\dot{\Phi}_i\vec{e}_i^{(2)} \tag{4.2}$$

where dot over the variables indicates their time derivatives and Φ_i presents the angular position of the i-th pinned-pinned coordinate system.

4.2.1.1 Elastic Displacement Discretization

Link deflections are continuous functions of space and time. In order to reduce the system dimension from infinite to finite, it is desirable to discretize link deflections. The generalized coordinates, which are only functions of time, can be used to obtain the dynamic equations of flexible manipulator systems by using Lagrangian dynamics.

Using the finite element method, each link is divided into a number of elements and link deflections are presented in terms of shape functions and nodal values of transverse deflections and slopes of the links. The deflection $w_i^k(x^k)$ in the i-th element of link k can be described as:

$$w_i^k(x^k,t) = \sum_{l=1}^{4} N_l^{ik}(x^k)v_{2i-2+l}^k(t) \tag{4.3}$$

where v^k_{2i-1} and v^k_{2i+1} are elastic displacement, and v^k_{2i} and v^k_{2i+2} are flexural slopes at nodes i and i+1, respectively (figure 4.3). N_l^{ik} represents the l-th shape function of the i-th element of link k.

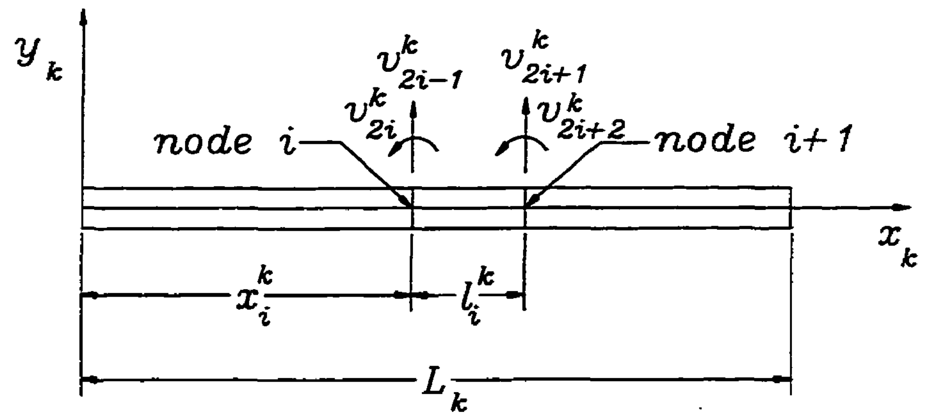

Figure 4.3 A typical element i of an arbitrary link k

Hermite polynomials, which are used as shape functions, are given by

$$N_1^{ik}(x^k)=1-3\left(\frac{x^k-x_i^k}{l_i^k}\right)^2+2\left(\frac{x^k-x_i^k}{l_i^k}\right)^3 \tag{4.4-a}$$

$$N_2^{ik}(x^k)=(x^k-x_i^k)\left(1-\frac{x^k-x_i^k}{l_i^k}\right)^2 \tag{4.4-b}$$

$$N_3^{ik}(x^k)=3\left(\frac{x^k-x_i^k}{l_i^k}\right)^2-2\left(\frac{x^k-x_i^k}{l_i^k}\right)^3 \tag{4.4-c}$$

$$N_4^{ik}(x^k)=(x^k-x_i^k)\left[\left(\frac{x^k-x_i^k}{l_i^k}\right)^2-\frac{x^k-x_i^k}{l_i^k}\right] \tag{4.4-d}$$

in which x_i^k is the x-coordinate of node i and l_i^k is the length of the i-th element with nodes i and i+1 of link k.

4.2.2 Kinematic Modeling of Flexible Joints

The arrangement of an actuated flexible joint is shown in figure 4.4. The rotations of the rotor and the link are presented by angles q_i and ψ_i, respectively. q_i is the rotation

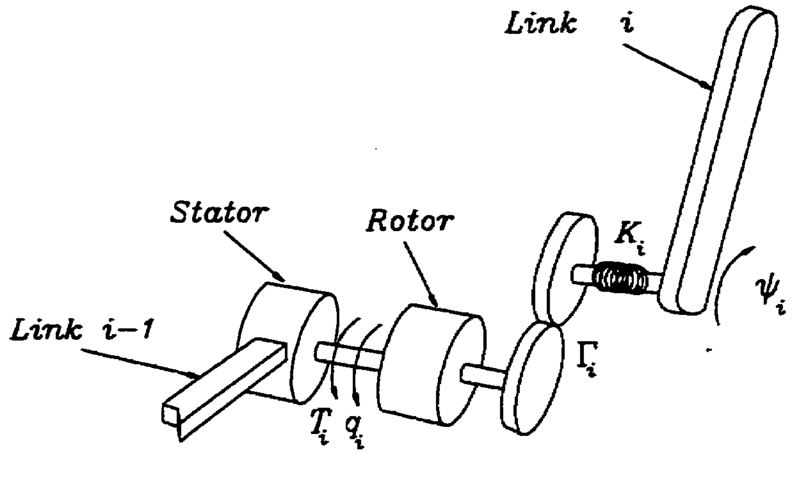

Figure 4.4 Model of an actuated flexible joint

angle of the rotor of the actuator i relative to the link I-1, while ψ_i represents the angle between tangent line of link i-1 at $x^{i-1}=L_{i-1}$ and that of link i at $x^i=0$. K_i and Γ_i are the drive shaft stiffness and the gear ratio of joint i, respectively. The difference $\psi_i - \Gamma_i q_i$ shows the joint deflection. We assume that link i, joint i, and rotor i all rotate about the same axis which can be an approximation for some arrangements of the gear train.

4.3 Dynamic Modeling

The equations of motion of the system can be found by using the standard Lagrangian approach. This can be done by computing the kinetic energy, the potential energy, and the virtual work of the nonconservative loads such as actuator torques. Then the dynamic model is obtained by satisfying the Lagrange-Euler equations:

$$\frac{d}{dt}\left(\frac{\partial(KE)}{\partial \dot{z}_i}\right)-\frac{\partial(KE)}{\partial z_i}+\frac{\partial(PE)}{\partial z_i}=Q_i\,, \qquad i=1,2,\ldots\ldots,n_{dof} \tag{4.5}$$

where z_i, KE, PE, Q_i, and n_{dof} are generalized coordinates, total kinetic energy, total potential energy, generalized forces, and the number of degrees of freedom of the system, respectively.

The total kinetic energy and total potential energy of the system can be found by summing those of various components of the system as:

$$KE = \sum_{k=1}^{n} KEL^k + \sum_{k=1}^{n} KEA^k + KEP \tag{4.6}$$

$$PE = \sum_{k=1}^{n} PEL^k + \sum_{k=1}^{n} PEA^k + PEP \tag{4.7}$$

where n is the number of links (or joints) and KEL^k, KEA^k, and KEP represent kinetic energies of link k, actuator k, and the payload. Similarly PEL^k, PEA^k, and PEP are potential energies of link k, actuator k, and the payload, respectively.

4.3.1 Kinetic and Potential Energies of an Arbitrary Link

The kinetic and potential energies of link k can be written as:

$$KEL^k = \frac{1}{2}\int_0^{L_k} \rho_k A_k \dot{\bar{r}}_k \cdot \dot{\bar{r}}_k dx^k \tag{4.8}$$

$$\begin{aligned} PEL^k = &\frac{1}{2}\int_0^{L_k} E_k I_k \left(\frac{\partial^2 w^k}{\partial x^2}\right)^2 dx^k \\ &+ \int_0^{L_k} \rho_k A_k g\left[x^k \sin\Phi_k + w^k \cos\Phi_k + \sum_{j=1}^{k-1} L_j \sin\Phi_j\right] dx^k \end{aligned} \tag{4.9}$$

where g is the gravitational acceleration. The first integral in equation (4.9) represents the strain energy stored in the link and the second one represents gravity potential energy of the link.

Using finite element discretization, equations (4.8) and (4.9) can be written in the following forms:

$$KEL^k = \sum_{e=1}^{N_k} KEE_e^k = \sum_{e=1}^{N_k} \{\frac{1}{2} \int_{x_e^k}^{x_e^k+l_e^k} \rho_k A_k \dot{\bar{r}}_k \cdot \dot{\bar{r}}_k \, dx^k\} \tag{4.10}$$

$$PEL^k = \sum_{e=1}^{N_k} PEE_e^k = \sum_{e=1}^{N_k} \{\frac{1}{2} \int_{x_e^k}^{x_e^k+l_e^k} E_k I_k (\frac{\partial^2 w^k}{\partial x^2})^2 dx^k + \int_{x_e^k}^{x_e^k+l_e^k} \rho_k A_k g[x^k \sin\Phi_k + w^k \cos\Phi_k + \sum_{j=1}^{k-1} L_j \sin\Phi_j] dx^k\} \tag{4.11}$$

where N_k, KEE_e^k, PEE_e^k, x_e^k, and l_e^k are the number of elements of link k, the kinetic and potential energies of the e-th element of link k, the x-coordinate of node 2e-1 (referring to figure 4.3), and the length of the e-th element of link k, respectively. Now by substituting equation (4.2) into equation (4.10), elemental kinetic and potential energies of the k-th link are obtained in the following forms:

$$\begin{aligned} KEE_e^k = \frac{1}{2} \int_{x_e^k}^{x_e^k+l_e^k} \rho_k A_k \{ [\sum_{i=1}^{k-1}\sum_{j=1}^{k-1} L_i L_j \dot{\Phi}_i \dot{\Phi}_j \cos(\Phi_i - \Phi_j)] + x^2 \dot{\Phi}_k^2 \\ + 2x\dot{\Phi}_k \sum_{j=1}^{k-1} L_j \dot{\Phi}_j \cos(\Phi_k - \Phi_j) + \dot{w}^2 + w^2 \dot{\Phi}_k^2 + 2x\dot{\Phi}_k \dot{w} \\ + 2\dot{w} \sum_{j=1}^{k-1} L_j \dot{\Phi}_j \cos(\Phi_k - \Phi_j) - 2w\dot{\Phi}_k \sum_{j=1}^{k-1} L_j \dot{\Phi}_j \sin(\Phi_k - \Phi_j) \} dx \end{aligned} \tag{4.12}$$

$$\begin{aligned} PEE_e^k = \int_{x_e^k}^{x_e^k+l_e^k} \rho_k A_k g[x \sin\Phi_k + w \cos\Phi_k + \sum_{j=1}^{k-1} L_j \sin\Phi_j] dx \\ + \frac{1}{2} \int_{x_e^k}^{x_e^k+l_e^k} E_k I_k (\frac{\partial^2 w}{\partial x^2})^2 dx \end{aligned} \tag{4.13}$$

in which superscript k is not shown for x and w.

Generalized coordinates used in obtaining the kinetic and potential energies of a typical element i of link k, can be represented by the following vector:

$$\{q\}^{ke} = \{\Phi_1, \Phi_2, \ldots\ldots\ldots\ldots, \Phi_k, v_{2e-1}^k, v_{2e}^k, v_{2e+1}^k, v_{2e+2}^k\}^T \tag{4.14}$$

This vector includes both rigid body motion degrees of freedom Φ_j (j=1,...k) and elastic motion degrees of freedom v_j^k (j=2e-1,2e,2e+1,2e+2). Therefore, the total number of degrees of freedom of the element is k+4.

4.3.1.1 Elemental Mass and Stiffness Matrices and Load Vector

Having the kinetic and potential energies of a typical element of an arbitrary link k, mass and stiffness matrices and load vector of the element can be found by applying Lagrange's equation. Using generalized coordinates, the kinetic energy of a generic element e of the k-th link can be written in the following form:

$$KEE_e^k = \frac{1}{2}\sum_{i=1}^{k+4}\sum_{j=1}^{k+4} M_{i,j}^{ke}\dot{q}_i^{ke}\dot{q}_j^{ke} = \frac{1}{2}\{\dot{q}^{ke}\}^T M^{ke}\{\dot{q}^{ke}\} \tag{4.15}$$

and the components $M_{i,j}^{ke}$ of mass matrix $M_{i,j}^{ke}$ can be obtained using the equation:

$$M_{i,j}^{ke} = \frac{\partial^2 KEE_e^k}{\partial \dot{q}_i^{ke}\partial \dot{q}_j^{ke}} \tag{4.16}$$

Therefore, various components of elemental mass matrix can be found in the following compact forms:

$$M_{l,m}^{ke} = \frac{\partial^2 KEE_e^k}{\partial \dot{\Phi}_l \partial \dot{\Phi}_m} = \int_{x_e^k}^{x_e^k + l_e^k} \rho_k A_k L_l L_m \cos(\Phi_l - \Phi_m) dx \qquad m, l = 1,2,\ldots\ldots k-1 \tag{4.17}$$

$$M_{l,k}^{ke} = \frac{\partial^2 KEE_e^k}{\partial \dot{\Phi}_l \partial \dot{\Phi}_k} = \int_{x_e^k}^{x_e^k + l_e^k} \rho_k A_k [x L_l \cos(\Phi_k - \Phi_l) - w L_l \sin(\Phi_k - \Phi_l)] dx \tag{4.18}$$

$$l = 1,2,\ldots,k-1$$

$$M_{l,p+k}^{ke} = \frac{\partial^2 KEE_e^k}{\partial \dot{\Phi}_l \partial \dot{v}_{2e+2-p}} = \int_{x_e^k}^{x_e^k + l_e^k} \rho_k A_k N_p^{ke} L_l \cos(\Phi_k - \Phi_l) dx \tag{4.19}$$

$$l = 1,2,\ldots k-1,\ p = 1,2,3,4$$

$$M_{k,k}^{ke} = \frac{\partial^2 KEE_e^k}{\partial \dot{\Phi}_k^2} = \int_{x_e^k}^{x_e^k + l_e^k} \rho_k A_k [x^2 + w^2] dx \tag{4.20}$$

$$M_{k,p+k}^{ke} = \frac{\partial^2 KEE_e^k}{\partial \dot{\Phi}_k \partial \dot{v}_{2e-2+p}} = \int_{x_e^k}^{x_e^k + l_e^k} \rho_k A_k x N_p^{ke} dx \qquad p = 1,2,3,4 \tag{4.21}$$

$$M_{k+p,k+r}^{ke} = \frac{\partial^2 KEE_e^k}{\partial \dot{v}_{2e-2+p} \partial \dot{v}_{2e-2+r}} = \int_{x_e^k}^{x_e^k + l_e^k} \rho_k A_k N_p^{ke} N_r^{ke} dx \qquad p, r = 1,2,3,4 \tag{4.22}$$

It is worth mentioning that $M^{ke}{}_{k+p,k+r}$ are the components of standard consistent mass matrix for a beam element.

Components of the elemental load vector can be obtained using Lagrange's equation in the following manner:

$$f_l^{ke} = \{-[\frac{d}{dt}(\frac{\partial KEE_e^k}{\partial \dot{\Phi}_l}) - STD1] + \frac{\partial KEE_e^k}{\partial \Phi_l} - \frac{\partial PEE_e^k}{\partial \Phi_l}\} \qquad l = 1,2,\ldots k-1 \tag{4.23}$$

and

$$f_k^{ke} = \{-[\frac{d}{dt}(\frac{\partial KEE_e^k}{\partial \dot{\Phi}_k}) - STD2] + \frac{\partial KEE_e^k}{\partial \Phi_k} - \frac{\partial PEE_e^k}{\partial \Phi_k}\} \tag{4.24}$$

where STD1 and STD2 are second time derivative terms obtained in finding $\frac{d}{dt}(\frac{\partial KEE_e^k}{\partial \dot{\Phi}_l})$ and $\frac{d}{dt}(\frac{\partial KEE_e^k}{\partial \dot{\Phi}_k})$, respectively.

After finding and substituting the necessary terms in equations (4.23) and (4.24) we have

$$f_l^{ke} = \int_{x_e^k}^{x_e^k+l_e^k} \rho_k A_k \{ s_1 L_l + x\dot{\Phi}_k L_l(\dot{\Phi}_k - \dot{\Phi}_l)\sin(\Phi_k - \Phi_l) + \dot{w} L_l (2\dot{\Phi}_k - \dot{\Phi}_l)\sin(\Phi_k - \Phi_l)$$
$$+ w\dot{\Phi}_k L_l(\dot{\Phi}_k - \dot{\Phi}_l)\cos(\Phi_k - \Phi_l) - s_2 L_l + x\dot{\Phi}_k L_l \dot{\Phi}_l \sin(\Phi_k - \Phi_l) \tag{4.25}$$
$$+ \dot{w} L_l \dot{\Phi}_l \sin(\Phi_k - \Phi_l) + w\dot{\Phi}_k L_l \dot{\Phi}_l \cos(\Phi_k - \Phi_l) - g L_l \cos\Phi_l \} dx, \qquad l = 1,2,\ldots,k-1$$

$$f_k^{ke} = \int_{x_e^k}^{x_e^k+l_e^k} \rho_k A_k \{ s_3 x - 2w\dot{w}\dot{\Phi}_k - x\dot{\Phi}_k s_4 - g(x\cos\Phi_k - w\sin\Phi_k) \} dx \tag{4.26}$$

in which

$$s_1 = \sum_{j=1}^{k-1} L_j \dot{\Phi}_j (\dot{\Phi}_l - \dot{\Phi}_j)\sin(\Phi_l - \Phi_j) \tag{4.27-a}$$

$$s_2 = \sum_{j=1}^{k-1} L_j \dot{\Phi}_j \sin(\Phi_l - \Phi_j) \tag{4.27-b}$$

$$s_3 = \sum_{j=1}^{k-1} L_j \dot{\Phi}_j (\dot{\Phi}_k - \dot{\Phi}_j)\sin(\Phi_k - \Phi_j) \tag{4.27-c}$$

$$s_4 = \sum_{j=1}^{k-1} L_j \dot{\Phi}_j \sin(\Phi_k - \Phi_j) \tag{4.27-d}$$

Let introduce new variables s_1^p, s_2^p, and s_3^p in order to simplify the expressions for the elemental stiffness matrix and remaining components of the load vector.

$$s_1^p = \frac{d}{dt}\left(\frac{\partial KEE_e^k}{\partial \dot{v}_{2e+2-p}}\right) - STD3 = -\int_{x_e^k}^{x_e^k+l_e^k} \rho_k A_k N_p^{ke} s_3 dx \tag{4.28}$$

$$s_2^p = \frac{\partial KEE_e^k}{\partial v_{2e+2-p}} = s_{21}^p + s_{22}^p \tag{4.29}$$

$$s_3^p = \frac{\partial PEE_e^k}{\partial v_{2e+2-p}} = s_{31}^p + s_{32}^p \tag{4.30}$$

in which STD3 is the set of second time derivatives obtained in the first part of equation (4.28), $p=1,2,3,4$, and

$$s_{21}^p = \dot{\Phi}_k^2 \int_{x_e^k}^{x_e^k+l_e^k} \rho_k A_k N_p^{ke} [N_1^{ke} v_{2e-1} + N_2^{ke} v_{2e} + N_3^{ke} v_{2e+1} + N_4^{ke} v_{2e+2}] dx \tag{4.31-a}$$

$$s_{22}^p = -\int_{x_e^k}^{x_e^k+l_e^k} \rho_k A_k N_p^{ke} \dot{\Phi}_k s_4 dx \tag{4.31-b}$$

$$s_{31}^p = \int_{x_e^k}^{x_e^k+l_e^k} \rho_k A_k N_p^{ke} g \cos\Phi_k dx \tag{4.31-c}$$

$$s_{32}^p = \int_{x_e^k}^{x_e^k+l_e^k} E_k I_k N_p^{''ke} [N_1^{''ke} v_{2e-1} + N_2^{''ke} v_{2e} + N_3^{ke} v_{2e+1} + N_4^{''ke} v_{2e+2}] dx \tag{4.31-d}$$

where $N_j^{''ke}$ represents the second derivative of N_j^{ke} with respect to x^k. Now f_{k+p}^{ke} can be written in the following form:

$$f_{k+p}^{ke} = -s_1^p + s_{22}^p - s_{31}^p = \{s_3 - \dot{\Phi}_k s_4 - g\cos\Phi_k\} \int_{x_e^k}^{x_e^k+l_e^k} \rho_k A_k N_p^{ke} \mathrm{d}x, \qquad p=1,2,3,4 \tag{4.32}$$

and the stiffness matrix of the e-th element of link k is obtained as:

$$K^{ke}_{k+p,k+r} = \int_{x_e^k}^{x_e^k+l_e^k} E_k I_k N''^{ke}_p N''^{ke}_r \mathbf{dx} - \dot{\Phi}_k{}^2 \int_{x_e^k}^{x_e^k+l_e^k} \rho_k A_k N^{ke}_p N^{ke}_r \mathbf{dx}, \qquad p,r = 1,2,3,4 \tag{4.33}$$

or in the matrix form

$$\left[K^{Ke}_{ff}\right] = \left[K^{ke}_{elastic}\right] - \dot{\Phi}_k{}^2 \left[M^{ke}_{consistant}\right] \tag{4.34}$$

K_{ff}^{ke} shows the non-zero part of the elemental stiffness matrix which corresponds to only flexible degrees of freedom. The dimension of the matrix K_{ff}^{ke} is 4X4, therefore, the rank of the elemental stiffness matrix is four. In other words the components associated with rigid degrees of freedom are all zero. Also, equation (4.34) shows that the non-zero part of the elemental stiffness matrix has two parts, the first part is the traditional stiffness matrix of beam elements and the second part is due to centrifugal effects during the large overall motion of the beam.

The components of elemental mass matrix, elemental stiffness matrix, and elemental load vector are functions of elastic deformations, elastic velocities, and nonlinear terms including rigid body degrees of freedom and their time derivatives. Therefore, the dynamic equations of motion of multi-link flexible manipulators are nonlinear. Centrifugal effects are included in the second part of the elemental stiffness matrix and the Coriolis effects can be seen in the expressions for the loading vector.

4.3.1.2 Assemblage of Elemental Matrices and Vectors of the k-th Link

As it was previously pointed out, one part of the elemental mass matrix is exactly the standard consistent mass matrix of beam elements. Similarly it was shown in equation (4.34) that the non-zero part of the elemental stiffness matrix consists of the standard beam element stiffness matrix and the consistent mass matrix multiplied by $-\Phi_k^2$. Therefore we can assemble these parts using the standard procedure used in linear finite element analysis. Also, because the coefficient $\{s_3-\dot{\Phi}_k s_4-g\cos\Phi_k\}$ in the expression for the elemental load vector (equation 4.32) is constant for all of the elements of the link, it is possible to construct link load vector $\mathbf{h}_1^k$ by assembling the elemental vectors $\mathbf{h}_1^{ke}$ whose components can be defined as:

$$h_{1p}^{ke} = \int_{x_e^k}^{x_e^k+l_e^k} \rho_k A_k N_p^{ke}\, dx \qquad p = 1,2,3,4 \tag{4.35}$$

The size of link matrices associated with elastic degrees of freedom which are constructed using standard assembly procedure is $2(N_k+1)$ X $2(N_k+1)$ and that of link vector is $2(N_k+1)$ X 1.

Other components of the elemental mass matrix and load vector corresponding to the rigid body degrees of freedom and coupling effects can be found by integrating all of the given integrals from 0 to L_k instead of x_e^k to $x_e^k+l_e^k$. If $\rho_k A_k$ (mass per unit length of the k-th link) is constant the results can be written as:

$$M_{l,m}^k = \rho_k A_k L_l L_m L_k \cos(\Phi_l - \Phi_m), \qquad m,l = 1,2,\ldots\ldots.k-1 \tag{4.36}$$

$$M_{l,k}^k = \rho_k A_k [\frac{L_k^2}{2} L_l \cos(\Phi_k - \Phi_l) - (\int_0^{L_k} w\,dx)\; L_l \sin(\Phi_k - \Phi_l)\;], \qquad l = 1,2,\ldots,k-1 \tag{4.37}$$

$$M_{k,k}^k = \rho_k A_k \{\frac{L_k^3}{3} + \int_0^{L_k} w^2 dx\} \tag{4.38}$$

$$M_{l,k+r}^k = L_l \cos(\Phi_k - \Phi_l) h_{1r}^k, \qquad l = 1,2,\ldots,k-1,\; r = 1,2,\ldots.2(N_k+1) \tag{4.39}$$

$$M_{k,k+r}^k = h_{2r}^k \qquad r = 1,2,3,,\ldots.2(N_k+1) \tag{4.40}$$

where h^k_{1r} is the r-th component of the $\mathbf{h}_1^k$ which is the assembled vector of elemental vectors $\mathbf{h}_1^{ke}$ with the components given in equation (4.35) and h^k_{2r} is the r-th component of the $\mathbf{h}_2^k$ which is the assembled vector of elemental vectors $\mathbf{h}_2^{ke}$ with the components calculated by the following equation:

$$h_{2p}^{ke} = \int_{x_e^k}^{x_e^k+l_e^k} \rho_k A_k x N_p^{ke} dx \qquad p=1,2,3,4 \tag{4.41}$$

The remaining components of the load vector can be written as:

$$\begin{aligned} f_l^k = {} & \rho_k A_k L_l \{ s_1 L_k + \frac{L_k^2}{2} \dot{\Phi}_k (\dot{\Phi}_k - \dot{\Phi}_l) sin(\Phi_k - \Phi_l) + (\int_0^{L_k} \dot{w} dx)(2\dot{\Phi}_k - \dot{\Phi}_l) sin(\Phi_k - \Phi_l) \\ & + (\int_0^{L_k} w dx) \dot{\Phi}_k (\dot{\Phi}_k - \dot{\Phi}_l) cos(\Phi_k - \Phi_l) - s_2 L_k \dot{\Phi}_l + (\int_0^{L_k} \dot{w} dx) \dot{\Phi}_l sin(\Phi_k - \Phi_l) \\ & + (\int_0^{L_k} w dx) \dot{\Phi}_k \dot{\Phi}_l cos(\Phi_k - \Phi_l) - g L_k \cos\Phi_l \}, \qquad l = 1,2,\ldots k-1 \end{aligned} \tag{4.42}$$

$$f_k^k = \rho_k A_k \{ s_3 \frac{L_k^2}{2} - 2(\int_0^{L_k} w \dot{w} dx) \dot{\Phi}_k - \dot{\Phi}_k s_4 \frac{L_k^2}{2} - g[\frac{L_k^2}{2} \cos\Phi_k - (\int_0^{L_k} w dx) \sin\Phi] \} \tag{4.43}$$

The above expressions include nonlinear effects of elastic degrees of freedom, therefore, they should be found by means of iterative procedures.

4.3.2 Assemblage of Link Matrices and Vectors

In order to reduce the size of resulting link matrices and vectors we can apply boundary conditions due to pinned-pinned position of the links in their local floating frames. Because transverse elastic deflections (w) at the both ends of each link are zero, it is sufficient to eliminate the first and the $2N_k+1$ -th rows and columns of the part of the mass and stiffness matrices of link k associated with elastic degrees of freedom before assembling them. Also the $2N_k+1$-th row of each link load vector corresponding to elastic degrees of freedom should be eliminated. Therefore, the sizes of the aforementioned part of the link mass matrix, stiffness matrix, and load vector of each link k are reduced to $2N_k$ X $2N_k$, $2N_k$ X $2N_k$, and $2N_k$ X 1, respectively.

Now the sub-system mass matrix **MS**$'$, the sub-system stiffness matrix **KS**$'$, and the sub-system load vector **fS**$'$ can be obtained by assembling corresponding link matrices and load vectors in a simple way which is shown schematically in figures 4.5 and 4.6. In these figures, n is the number of rigid degrees of freedom, and $\mathbf{M}_i$, $\dot{\Phi}_i$, and $\mathbf{KE}_i$ are the mass matrix, the angular velocity, and the elastic stiffness matrix of link i, respectively.

In figures 4.5 and 4.6, the first n rows and columns of the mass matrix and the first n rows of the load vector can be found easily by using equations (4.36-4.40) and (4.42-4.43). It is worth mentioning that to obtain the assembled mass matrix, $(n+\sum_{j=1}^{k-1} 2N_j)+r$ should be used instead of k+r in equations (4.39) and 4.40).

$$
MS' = \begin{bmatrix}
MS'(1,1) & MS'(1,2) & \cdots & MS'(1,n) & \cdots & MS'(1,n+\sum 2N_i) \\
 & MS'(2,2) & \cdots & MS'(2,n) & \cdots & MS'(2,n+\sum 2N_i) \\
 & & \ddots & & & \\
 & & & MS'(n,n) & \cdots & MS'(n,n+\sum 2N_i) \\
 & & & & \boxed{M_1} & \\
 & symmetric & & & & \boxed{M_2} \\
 & & & & & \ddots \\
 & & & & & \boxed{M_n}
\end{bmatrix}
$$

Figure 4.5 Schematics for construction of system link mass matrix

$$KS' = \left[\begin{array}{cccccc} 0 & 0 & 0\,.\,.\,.\,0\;\;.\,.\,.\,. & & & 0 \\ & 0 & 0\,.\,.\,.\,0\;\;.\,.\,.\,. & & & 0 \\ & & \ddots & & & \\ & & 0\,.\,.\,.\,.\,. & & & 0 \\ & & \boxed{\begin{matrix}KE_1\\ -\dot{\Phi}_1^2 M_1\end{matrix}} & & & \\ & & & \boxed{\begin{matrix}KE_2\\ -\dot{\Phi}_2^2 M_2\end{matrix}} & & \\ & \textit{Symmetric} & & & \ddots & \\ & & & & & \boxed{\begin{matrix}KE_n\\ -\dot{\Phi}_n^2 M_n\end{matrix}} \end{array}\right] \quad \begin{array}{l}\left.\begin{matrix}\\ \\ \\ \\ \end{matrix}\right\} n \ rows \\ \\ \\ \\ \end{array} \quad , fS' = \left[\begin{array}{c} fS'(1) \\ fS'(2) \\ \vdots \\ fS'(n) \\ \boxed{f_1} \\ \boxed{f_2} \\ \vdots \\ \boxed{f_n} \end{array}\right]$$

Figure 4.6 Schematics for construction of system link stiffness matrix and load vector

The resulting mass and stiffness matrices and the load vector are called the sub-system matrices and the sub-system load vector in order to emphasize that the degrees of freedom of flexible joints (q_k) have not yet been included in the derivation. The dimension of the system matrices is $[2n+\Sigma 2N_k]X[2n+\Sigma 2N_k]$ and that of the system load vector is $[2n+\Sigma 2N_k]X1$. In section 4.3.4 the elements of the system matrices and the load vector associated with flexible joint variables are found.

4.3.3 Boundary Conditions due to the Payload

Boundary conditions at the end of the last link due to the payload can be applied by using Lagrangian approach. Therefore, the first step is to find kinetic and potential energies of the payload.

Using the notations from the preceding parts of the chapter, the position and velocity vector of the payload are

$$\vec{r}_p = \sum_{i=1}^{n} L_i \vec{e}_i^{(1)} \tag{4.44}$$

$$\dot{\vec{r}}_p = \sum_{i=1}^{n} L_i \dot{\Phi}_i \vec{e}_i^{(2)} \tag{4.45}$$

The kinetic and potential energies of the payload can be written as:

$$KEP = \frac{1}{2} M_P \dot{\vec{r}}_P . \dot{\vec{r}}_P + \frac{1}{2} I_P (\dot{\Phi}_n + \dot{v}_{2(N_n+1)})^2 \tag{4.46}$$

$$PEP = M_P g \sum_{i=1}^{n} L_i \sin\Phi_i \tag{4.47}$$

where M_p and I_P are mass and moment of inertia of the payload, respectively.

Taking into account the effect of the payload kinetic and potential energies on the total Lagrangian of the system, the following corrections should be made in the components of the sub-system mass matrix and the load vector:

$$MS'(l,j) \leftarrow MS'(l,j) + M_p L_l L_j \cos(\Phi_l - \Phi_j) \qquad \mathbf{l,j = 1,....,n} \tag{4.48}$$

$$MS'(n, n + \sum_{j=1}^{n} 2N_j) \leftarrow MS'(n, n + \sum_{j=1}^{n} 2N_j) + I_p \tag{4.49}$$

$$MS'(n + \sum_{j=1}^{n} 2N_j, n + \sum_{j=1}^{n} 2N_j) \leftarrow MS'(n + \sum_{j=1}^{n} 2N_j, n + \sum_{j=1}^{n} 2N_j) + I_p \tag{4.50}$$

$$\begin{aligned} fS'(l) \leftarrow fS'(l) + M_p L_l \{ & \sum_{j=1}^{n} L_j \dot{\Phi}_j (\dot{\Phi}_l - \dot{\Phi}_j) \sin(\Phi_l - \Phi_j) \\ & - \dot{\Phi}_l \sum_{j=1}^{n} L_j \dot{\Phi}_j \sin(\Phi_l - \Phi_j) - g \cos\Phi_l \}, \qquad l = 1,....n \end{aligned} \tag{4.51}$$

In the above expressions, the sign $\leftarrow$ represents the substitution of the left hand side by the right hand side. The corrections are made on the sub-system mass matrix and the subsystyem load vector which were constructed by assembling elemental matrices and vectors and applying boundary conditions at both ends of each link. This is why the row and column numbers are shown in parentheses instead of subscripts used for elemental matrices and vectors.

4.3.4 Actuators Dynamics

The kinetic and potential energies of each actuator composed of the stator, the rotor, and the flexible joint are derived in this section. Then elements of the system mass matrix and the system stiffness matrix associated with the flexible joint variables are found and the whole system mass and stiffness matrices is built by including the corresponding sub-matrices obtained in the previous sections. Moreover, the elements of the damping matrix due to the joint damping, and the elements of the generalized forces due to the actuator torques are obtained by using the principle of virtual work.

Figure 4.7 shows the various angles which should be used in finding Ψ_k, the angle between tangent lines of adjacent links k-1 and k at common joint k. In this figure $\vartheta_k^1 = v_2^k$ and $\vartheta_{k-1}^e = v_{2N_{k-1}+2}^{k-1}$ are the slope of link k at x^k=0 and the slope of link k-1 at $x^{k-1} = L_{k-1}$ in the corresponding local floating system, respectively.

Referring to figures 4.1 and 4.7, the kinetic and potential energies of the first joint can be written as:

$$KEA^1 = \frac{1}{2} Ir_1 \dot{q}_1^2 \tag{4.52}$$

$$PEA^1 = \frac{1}{2} Kj_1 \left(\Phi_1 + \vartheta_1^1 - \Gamma_1 q_1\right)^2 \tag{4.53}$$

and those of other actuators (k=2,3,.......n) are

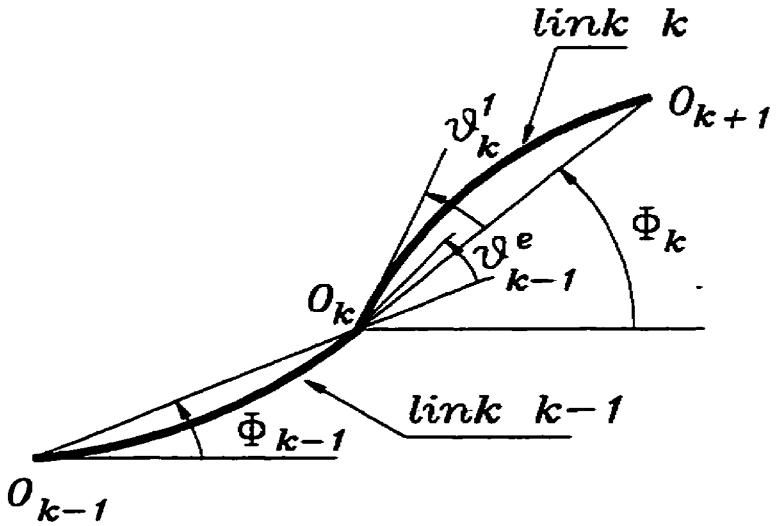

Figure 4.7 Definition of the angles at joint O_k

$$\begin{aligned} KEA^k &= \frac{1}{2} Ir_k (\dot{q}_k + \dot{\Phi}_{k-1} + \dot{\vartheta}_e^{k-1})^2 + \frac{1}{2} Is_k (\dot{\Phi}_{k-1} + \dot{\vartheta}_e^{k-1})^2 \\ &+ \frac{1}{2}(mr_k + ms_k) \sum_{i=1}^{k-1} \sum_{j=1}^{k-1} L_i L_j \dot{\Phi}_i \dot{\Phi}_j \cos(\Phi_i - \Phi_j) \end{aligned} \tag{4.54}$$

$$\begin{aligned} PEA^k &= \frac{1}{2} Kj_k [\Phi_k + \vartheta_e^k - (\Phi_{k-1} + \vartheta_e^{k-1}) - \Gamma_k q_k]^2 \\ &+ (mr_k + ms_k) g \sum_{j=1}^{k-1} L_j \sin\Phi_j \end{aligned} \tag{4.55}$$

where Ir_k, Is_k, me_k, ms_k, and Kj_k are the mass moment of inertia of rotor k, the mass moment of inertia of stator k, the mass of rotor k, the mass of stator k, and the rotational stiffness of joint k.

The system mass matrix and the stiffness matrix can be presented as:

$$MS=\begin{bmatrix} [0]_{nXn} & [0]_{nX(n+\Sigma 2N_j)} \\ [0]_{(n+\Sigma 2N_j)Xn} & [MS'] \end{bmatrix} \quad , \quad KS=\begin{bmatrix} [0]_{nXn} & [0]_{nX(n+\Sigma 2N_j)} \\ [0]_{(n+\Sigma 2N_j)Xn} & [KS'] \end{bmatrix}$$

Figure 4.8 Schematic of system mass and stiffness matrices before substituting components associated with flexible joint degrees of freedom

and the system load vector is given by

$$fS=\begin{bmatrix} [0]_{nX1} \\ [fS']_{(n+\Sigma 2N_j)X1} \end{bmatrix}$$

Figure 4.9 Schematic of system load vector before substituting components associated with flexible joint degrees of freedom

in which MS', KS', and fS' are the sub-system mass matrix, the stiffness matrix, and the load vector obtained in the previous section.

Now by using Lagrange's equation, it can be shown that the elements of the mass and the stiffness matrices and the load vector of the system can be presented as:

$$MS(1,1)=Ir_1 \tag{4.56}$$

and for k=2,3,......,n

$$MS(k,k)=Ir_k \ , \ MS(k,n+k-1)=Ir_k \ , \ MS(k,2n+\sum_{j=1}^{k-1}2N_j)=Ir_k, \tag{4.57}$$

$$MS(n+k-1,n+k-1) \leftarrow MS(n+k-1,n+k-1)+Ir_k+Is_k \tag{4.58}$$

$$MS(n+k-1,2n+\sum_{j=1}^{k-1}2N_j) \leftarrow MS(n+k-1,2n+\sum_{j=1}^{k-1}2N_j)+Ir_k+Is_k \tag{4.59}$$

$$MS(2n+\sum_{j=1}^{k-1}2N_j,2n+\sum_{j=1}^{k-1}2N_j) \leftarrow MS(2n+\sum_{j=1}^{k-1}2N_j,2n+\sum_{j=1}^{k-1}2N_j)+Ir_k+Is_k \tag{4.60}$$

$$KS(1,1)=\Gamma_1^2 Kj_1 \ , \ KS(1,n+1)=-\Gamma_1 Kj_1 \ , \ KS(1,2n+1)=-\Gamma_1 Kj_1 \tag{4.61}$$

$$KS(n+1,n+1)=Kj_1 \ , \ KS(n+1,2n+1)=Kj_1 \tag{4.62}$$

$$KS(2n+1,2n+1) \leftarrow KS(2n+1,2n+1)+Kj_1 \tag{4.63}$$

$$KS(k,k)=\Gamma_k^2 Kj_k \ , \ KS(k,n+k-1)=\Gamma_k Kj_k \ , \ KS(k,n+k)=-\Gamma_k Kj_k \tag{4.64}$$

$$KS(k,2n+\sum_{j=1}^{k-1}2N_j)=\Gamma_k Kj_k \ , \ KS(k,1+2n+\sum_{j=1}^{k-1}2N_j)=-\Gamma_k Kj_k \tag{4.65}$$

$$KS(n+k-1,n+k-1)=Kj_k \ , \ KS(n+k-1,n+k)=-Kj_k \tag{4.66}$$

$$KS(n+k-1,2n+\sum_{j=1}^{k-1}2N_j)=Kj_k \ , \ KS(n+k-1,1+2n+\sum_{j=1}^{k-1}2N_j)=-Kj_k, \tag{4.67}$$

$$KS(n+k,n+k)=Kj_k \ , \ KS(n+k,2n+\sum_{j=1}^{k-1}2N_j)=-Kj_k \tag{4.68}$$

$$KS(n+k,1+2n+\sum_{j=1}^{k-1}2N_j)=Kj_k \tag{4.69}$$

$$KS(2n+\sum_{j=1}^{k-1}2N_j,2n+\sum_{j=1}^{k-1}2N_j) \leftarrow KS(2n+\sum_{j=1}^{k-1}2N_j,2n+\sum_{j=1}^{k-1}2N_j)+Kj_k, \tag{4.70}$$

$$KS(2n+\sum_{j=1}^{k-1}2N_j,1+2n+\sum_{j=1}^{k-1}2N_j) \leftarrow KS(2n+\sum_{j=1}^{k-1}2N_j,1+2n+\sum_{j=1}^{k-1}2N_j)-Kj_k \tag{4.71}$$

$$KS(1+2n+\sum_{j=1}^{k-1}2N_j,1+2n+\sum_{j=1}^{k-1}2N_j) \leftarrow KS(1+2n+\sum_{j=1}^{k-1}2N_j,1+2n+\sum_{j=1}^{k-1}2N_j)+Kj_k, \tag{4.72}$$

Nonlinear components of the system mass matrix are not shown in the above equations. Therefore, it is necessary to correct such components in the following manner during the iterative process of solution:

$$\begin{aligned} MS(n+l,n+j) \leftarrow MS(n+l,n+j)+(mr_k+ms_k)L_lL_j\cos(\Phi_l-\Phi_j) \\ k=2,3,..n \quad \text{and} \quad l,j=1,2,....k-1 \end{aligned} \tag{4.73}$$

MS(n+l,n+j) on the right hand side is the linear part of this component shown in previous parts of this section.

By applying the Lagrange's equation, the following nonlinear components of the system load vector can be obtained.

$$\begin{aligned} fS(n+l) \leftarrow fS(n+l)+(mr_k+ms_k)L_l[\sum_{j=1}^{k-1}L_j\dot{\Phi}_j(\dot{\Phi}_l-\dot{\Phi}_j)\sin(\Phi_l-\Phi_j) \\ +\dot{\Phi}_l\sum_{j=1}^{k-1}L_j\dot{\Phi}_j\sin(\Phi_l-\Phi_j) - g\cos\Phi_l], \quad k=1,\ldots,n \text{ and } l=1,\ldots,k-1 \end{aligned} \tag{4.74}$$

In the above equations the sign $\leftarrow$ represents substitution of the left hand side by the right hand side.

4.3.4.1 Generalized Forces due to Actuator Torques and Joint Dampings

There are 2n nonconservative loads, namely, n actuator torques and n damping torques resulting from friction of the joints. The generalized forces due to the actuator torques and the damping torques in the joints can be found using the principle of virtual work. The total virtual work of these loads can be written as:

$$\delta W = \sum_{j=1}^{n} (T_j - b_j \dot{q}_j)\delta q_j \tag{4.75}$$

where b_j is the viscous damping coefficient in the j-th joint. Using equation (4.75) the generalized forces required in the right hand side of the Lagrange's equations can be obtained as:

$$Q_j = T_j - b_j \dot{q}_j \,, \qquad j = 1,2,\ldots n \tag{4.76}$$

The $(2n+\Sigma 2Nj)X(1)$ vector of generalized force Q, which is composed of the components given in equation (4.76), can be shown in the form of

$$Q = \{Q_1 \;\; . \;\; . \;\; Q_n \;\; 0 \;\; . \;\; . \;\; . \;\; . \;\; 0\}^T \tag{4.77}$$

where superscript T stands for transpose notation.

4.3.5 Equations of Motion

Using the results obtained in the preceding subsections, the system of equations can be written in the following form:

$$MS(U)\ddot{U} + KS(U,\dot{U})U = fS(U,\dot{U}) + Q \tag{4.78}$$

U is the vector of generalized coordinates of the system including all of the rigid and flexible degrees of freedom. It is worth noting that mass matrix $MS(U)$ is symmetric and positive definite. Equation (4.78) can be organized in the following partitioned form in order to represent the coupling effects between the joint motion, the large rigid body motion, and the small elastic motion of the system.

$$\begin{bmatrix} MS_{mm} & MS_{mj}(\eta_j) & MS_{mf} \\ MS_{jm}(\eta_r) & MS_{jj}(\eta_j,\eta_f) & MS_{jf}(\eta_j,\eta_f) \\ MS_{fm} & MS_{fj}(\eta_j,\eta_f) & MS_{ff}(\eta_j,\eta_f) \end{bmatrix} \begin{Bmatrix} \ddot{\eta}_m \\ \ddot{\eta}_j \\ \ddot{\eta}_f \end{Bmatrix} + \begin{bmatrix} KS_{mm} & KS_{mjr} & KS_{mf} \\ KS_{jm} & 0 & 0 \\ KS_{fm} & 0 & KS_{ff}(\dot{\eta}_f) \end{bmatrix} \begin{Bmatrix} \eta_m \\ \eta_j \\ \eta_f \end{Bmatrix} + \begin{bmatrix} CS_{mm} & 0 & 0 \\ 0 & 0 & 0 \\ 0 & 0 & 0 \end{bmatrix} \begin{Bmatrix} \dot{\eta}_m \\ \dot{\eta}_j \\ \dot{\eta}_f \end{Bmatrix} = \begin{Bmatrix} F_m(T_a) \\ F_j(\eta_j,\eta_f,\dot{\eta}_j,\dot{\eta}_f) \\ F_f(\eta_j,\eta_f,\dot{\eta}_j,\dot{\eta}_f) \end{Bmatrix} \tag{4.79}$$

In equation (4.79) η_m, η_j and η_f are vectors of flexible motor degrees of freedom (q_k ,k=1,..n), joint degrees of freedom (Φ_k , k=1,...n), and elastic degrees of freedom of the system (v_j^k, k=1,...n , j=1,...2N_k), respectively. $\boldsymbol{MS}_{mm}$, $\boldsymbol{MS}_{jj}$, and $\boldsymbol{MS}_{ff}$ represent effective inertia matrices for the motor motions, the joint motion, and the small motions, while $\boldsymbol{MS}_{mj}$, $\boldsymbol{MS}_{mf}$, and $\boldsymbol{MS}_{jf}$, are the coupled inertia matrices of the system. Due to the procedure used in the formulation, there is no static coupling between the rigid motion and the small elastic motion. As it can be seen, only $\boldsymbol{F}_m$ is function of actuator torques ($\boldsymbol{T}_a$), while other force vectors are functions of rigid and elastic displacements and velocities. Since only damping due to the joints is considered in the modeling, only sub-matrix $\boldsymbol{CS}_{mm}$ of the damping matrix is not zero. Structural damping has not been taken into account, however, it can be included in the formulation very easily.

The equation of motion will be solved in the next section using the Newmark method for some cases in order to show the validity of the model. Also, the coupling effects of joint and link flexibilities on the overall motion of the multi-link manipulators will be observed.

4.4 Simulation Results

Some simulation results are presented in this section in order to test the validity of the model and to show the effects of link and joint flexibilities on the dynamic behaviour of the system.

Consider a three-link manipulator with the following physical parameters (for i=1,2,3):

$$\begin{aligned}
&\rho_i A_i = 5 && kg/m \\
&L_i = 1 && \mathrm{m} \\
&\mathrm{M_P} = 5 && \mathrm{kg} \\
&\mathrm{I_P} = 0 && \mathrm{kg.m^2} \\
&Ir_i = 0.2 && \mathrm{kg.m^2} \\
&Is_i = 0.2 && \mathrm{kg.m^2} \\
&mr_i = 0.2 && \mathrm{kg} \\
&ms_i = 0.2 && \mathrm{kg} \\
&\Gamma_i = 1 && \\
&b_i = 0 &&
\end{aligned} \tag{4.80}$$

where $\rho_i A_i$ and L_i are mass per unit length and length of link i, M_P and I_P are mass and moment of inertia of the payload, Ir_i, Is_i, mr_i, and ms_i are moments of inertia and masses of the rotor and stator of actuator i, and Γ_i and b_i are gear ratio and damping of joint i. Different values of E_1I_1, E_2I_2, E_3I_3, Kj_1, Kj_2, and Kj_3 are used in various cases to show the effects of flexibility. Each link is divided into two elements, therefore; the total number of degrees of freedom of the system in the presented examples is 18.

4.4.1 Free Vibration of the System

In this case, the aforementioned system is released from its initial rest position

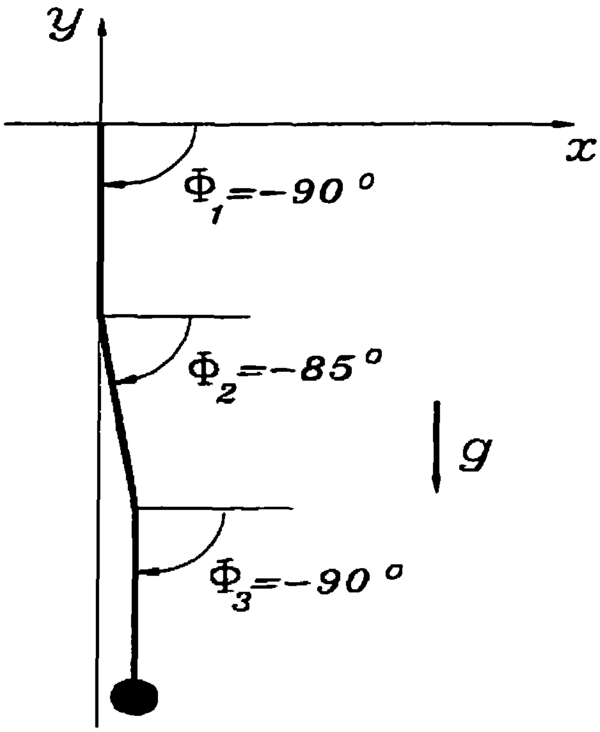

Figure 4.10 Initial position for free vibration simulation

shown in figure 4.10.

The results of joint angles Φ_1, Φ_2, and Φ_3 for such system with large values of *EI*s and *Kj*s are shown in figures 4.11 a-c. It can be seen that the response of the system is completely in agreement with the motion of a triple rigid pendulum with similar masses and inertias for the links, the payload, the stators, and the rotors. The response of the rigid counterpart was obtained by solving its system of equations of motion, which were obtained separately but not shown here.

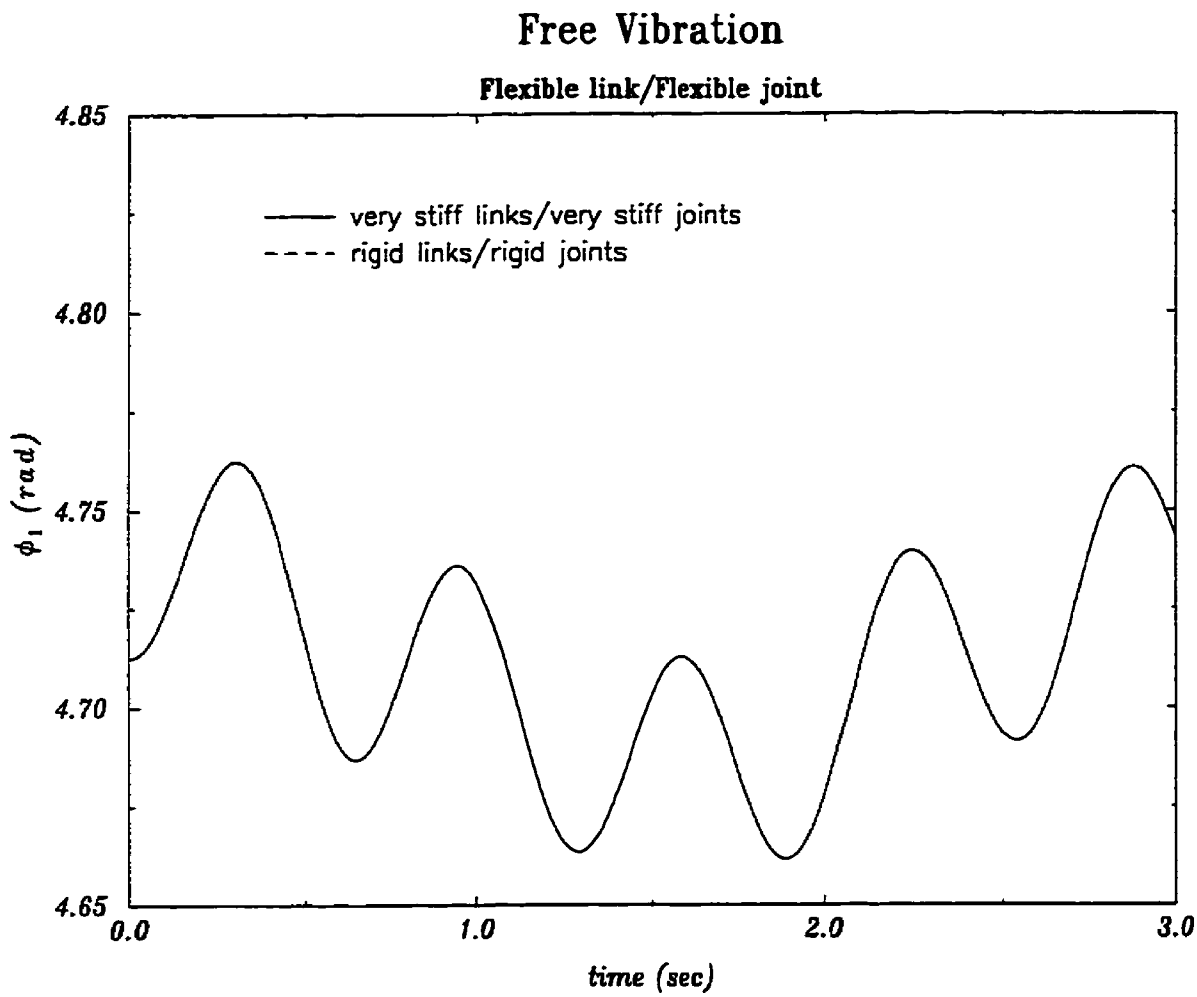

Figure 4.11-a Joint angle Φ_1 for a rigid manipulator and a manipulator with very stiff links and joints

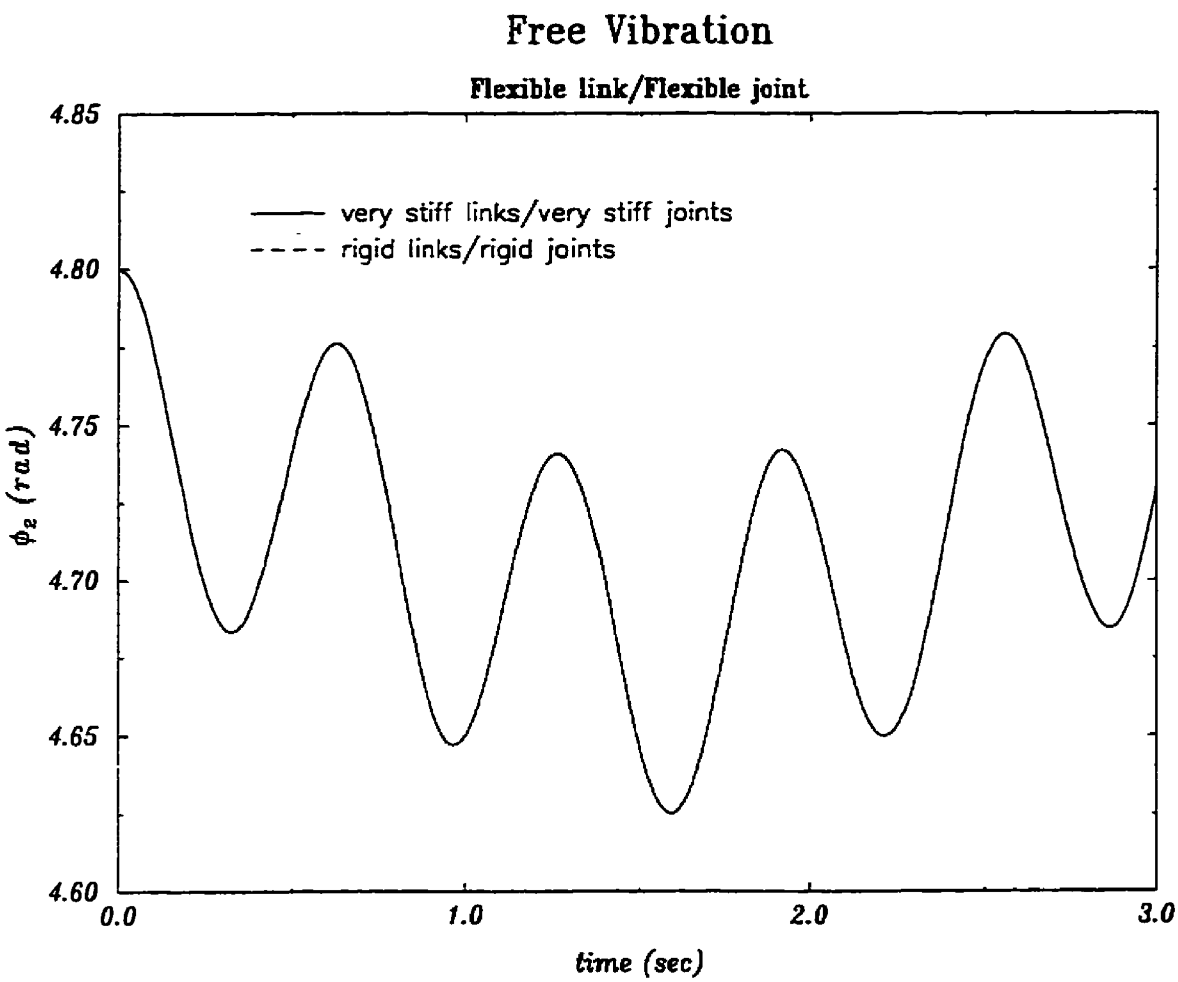

Figure 4.11-b Joint angle Φ_2 for a rigid manipulator and a manipulator with very stiff links and joints

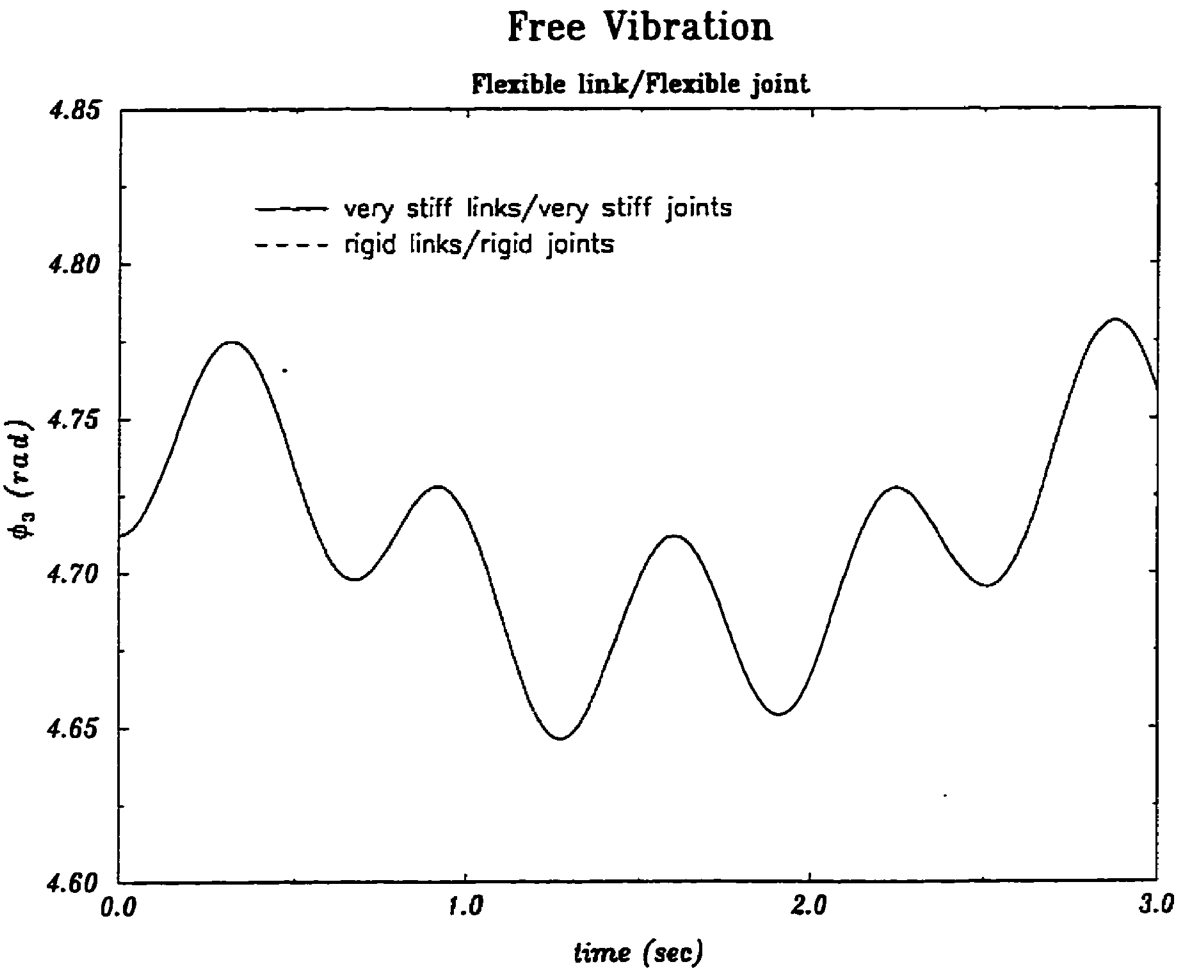

Figure 4.11-c Joint angle Φ_3 for a rigid manipulator and a manipulator with very stiff links and joints

Figures 4.12-a and 4.12-b present x and y coordinates of the end effector for various combinations of link and joint flexibility. These figures illustrate the effects of these flexibilities on the overall motion of the system. Either joint flexibilty or link flexibility changes the overall motion motion of the system from that of the rigid manipulator. But as it can be seen in figure 4.12-b, in the presence of both joint and link flexibilities, the deviation of overall motion is much larger than other cases. In other words, the interaction between joint and link flexibilities plays an important role in the dynamic behavior of the system.

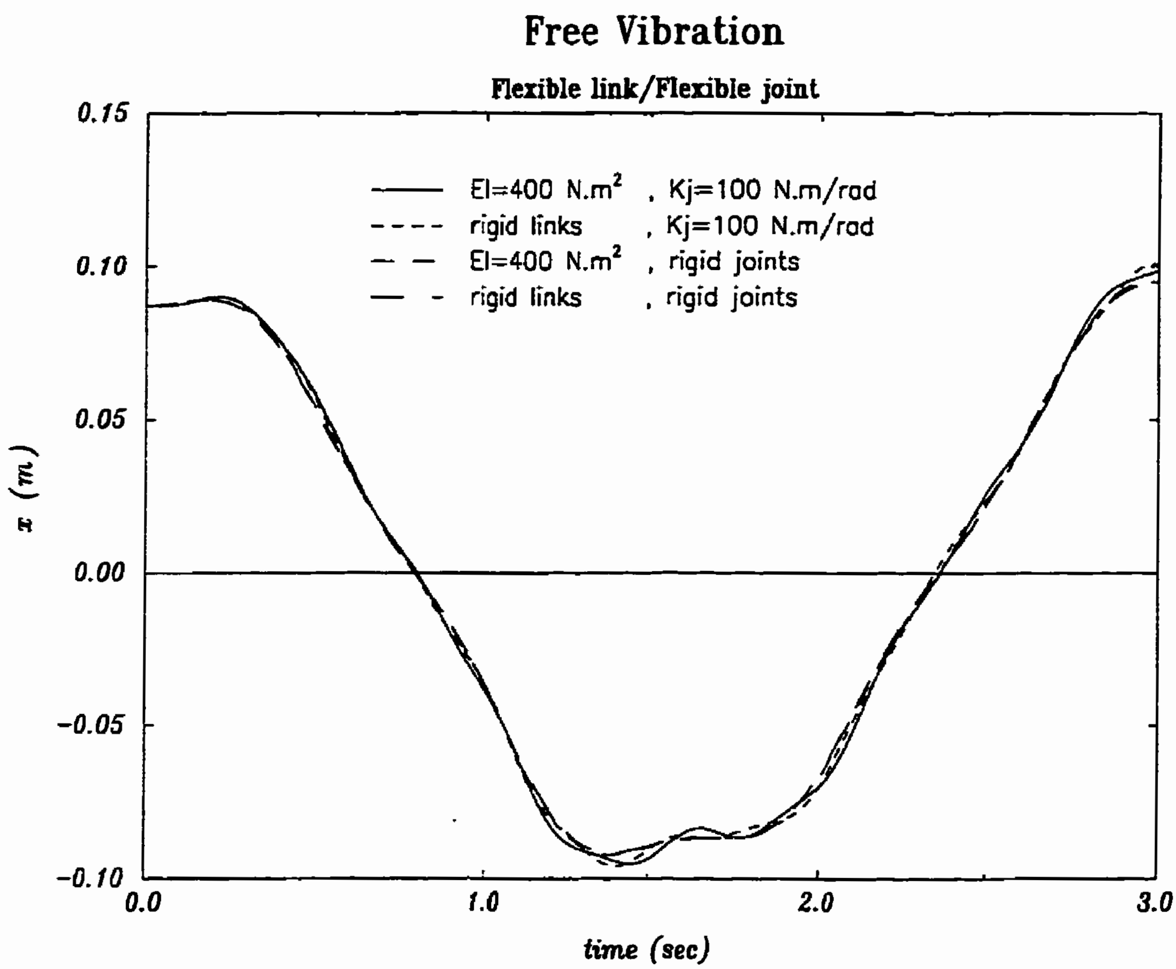

Figure. 4.12-a x-coordinate of the payload for various cases

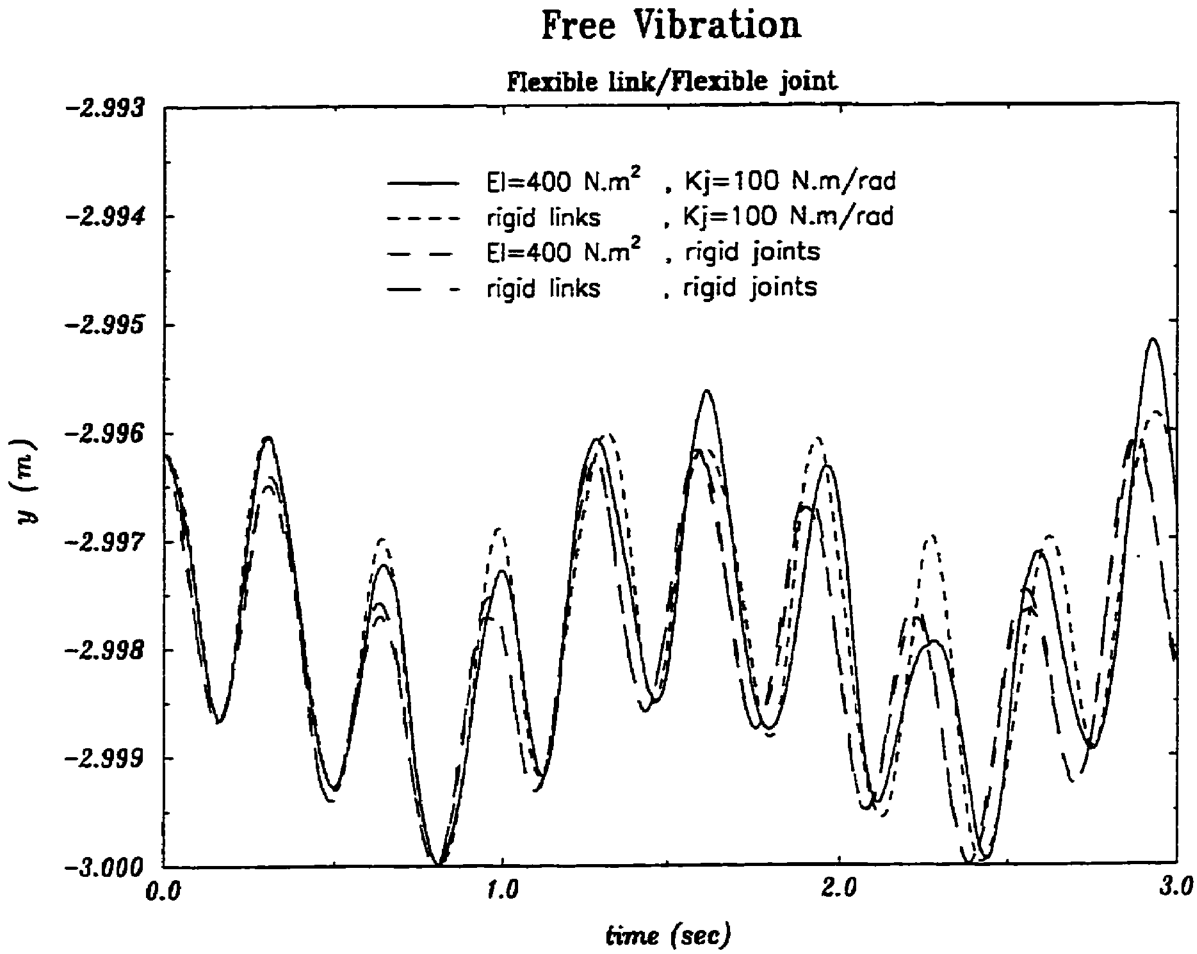

Figure. 4.12-b y-coordinate of the payload for various cases

4.4.2 Large Overall Motion of the Manipulator

In this case, the system is released from its initial rest position shown in figure 4.13. The initial x and y coordinates of the payload are chosen 3 and 0 m, respectively. The nonlinear effects are much stronger than the previous case, because the motion of the system is not limited to small vibration about its equilibrium position.

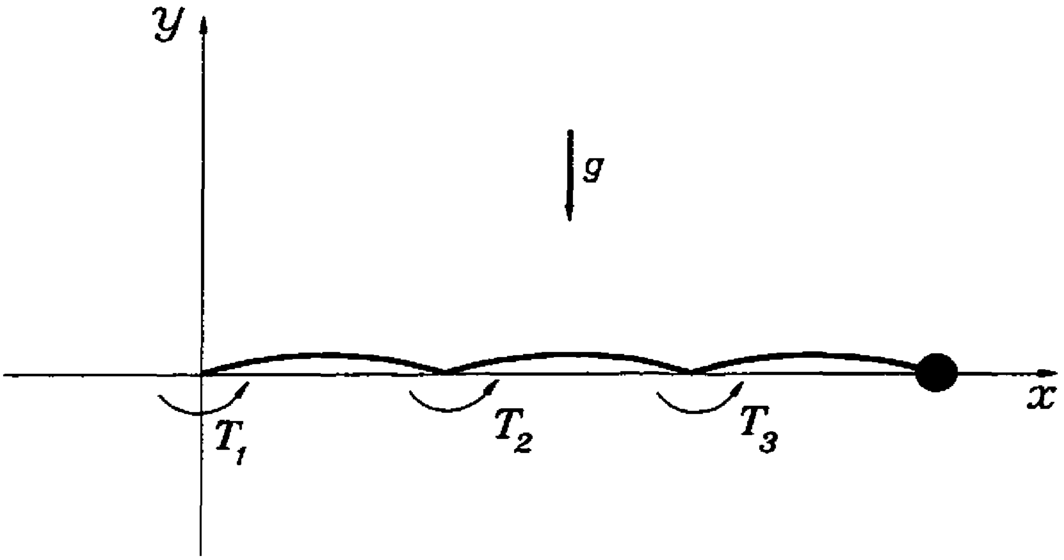

Figure 4.13 Initial position for large overall motion simulation

In figures 4.14 a-b the effect of link flexibility on the x and y coordinates of the payload is shown. As it can be seen, the difference between large overall motion of the system and that of the rigid link/flexible joint manipulator (Kj=100 N.m/rad) increases especially at the end by increasing the link flexibility. Figures 4.15 a-b show the x and y coordinates of the payload for manipulators with similar link flexibility but with various values of the joint flexibility. These figures lead to the conclusion that more flexible joints cause more deviations in large overall motion with respect to the flexible link/rigid joint counterpart. However, similar to the previous case (section 4.4.1), the interaction between joint and link flexibilities has the most significant effect on the dynamic behavior of the system. Figures 4.16 a-c represent the tip elastic transversal deflection of various links relative to the tangent lines to the corresponding link at the base for a manipulator with flexible links and joints. As it can be seen the tip points oscillate undesirably.

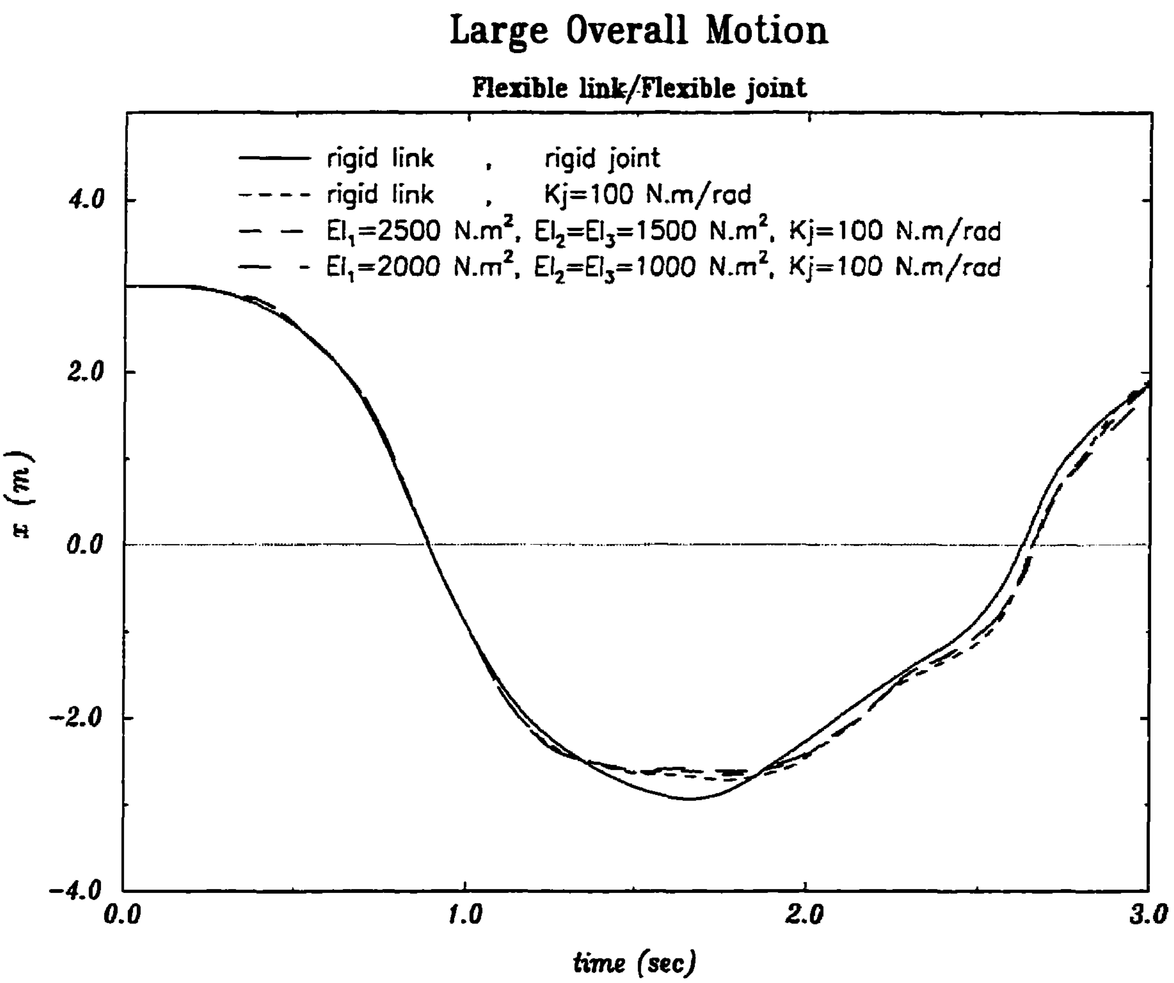

Figure 4.14-a Effect of link flexibility on the x-coordinate of the payload

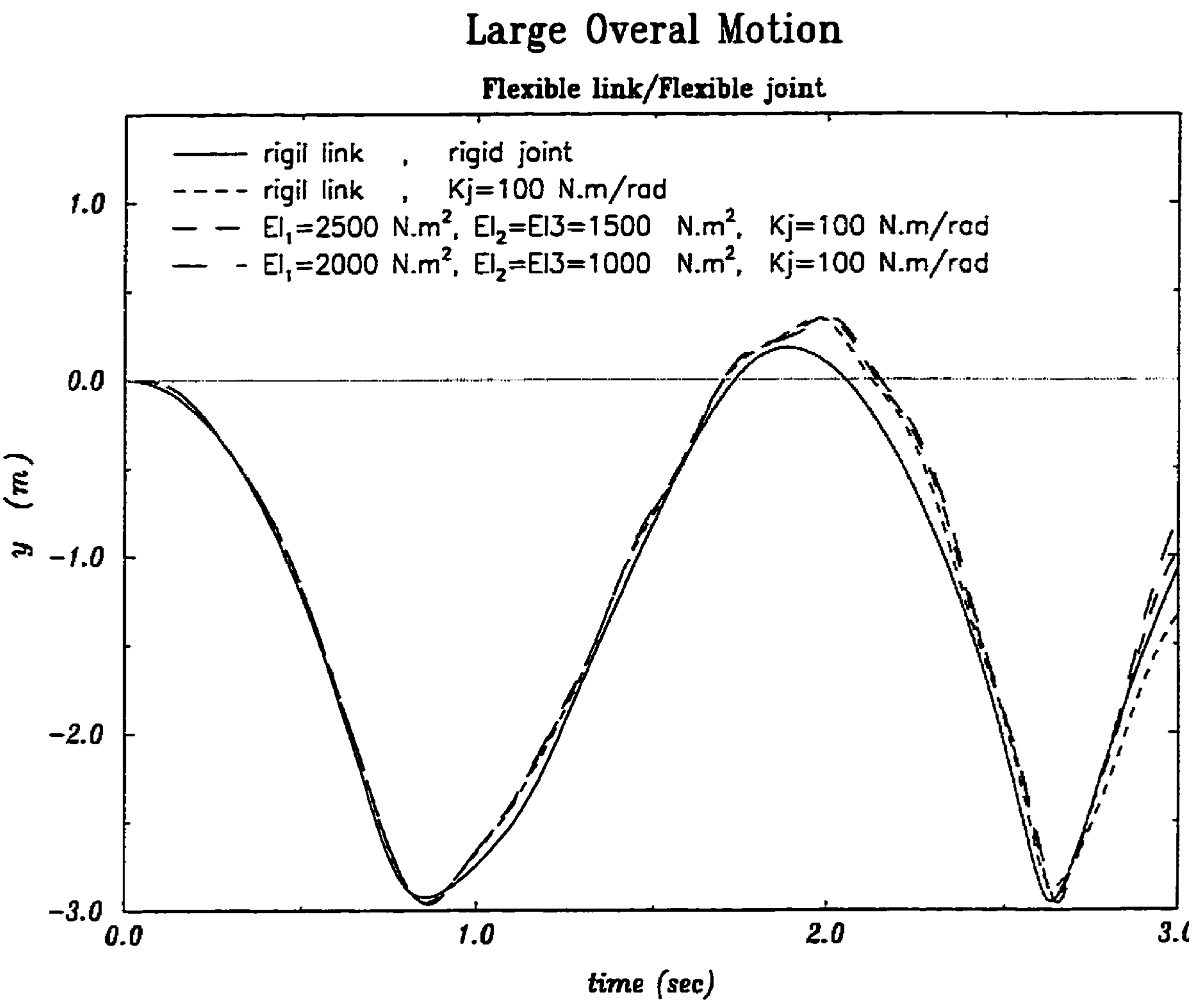

Figure 4.14-b Effect of link flexibility on the y-coordinate of the payload

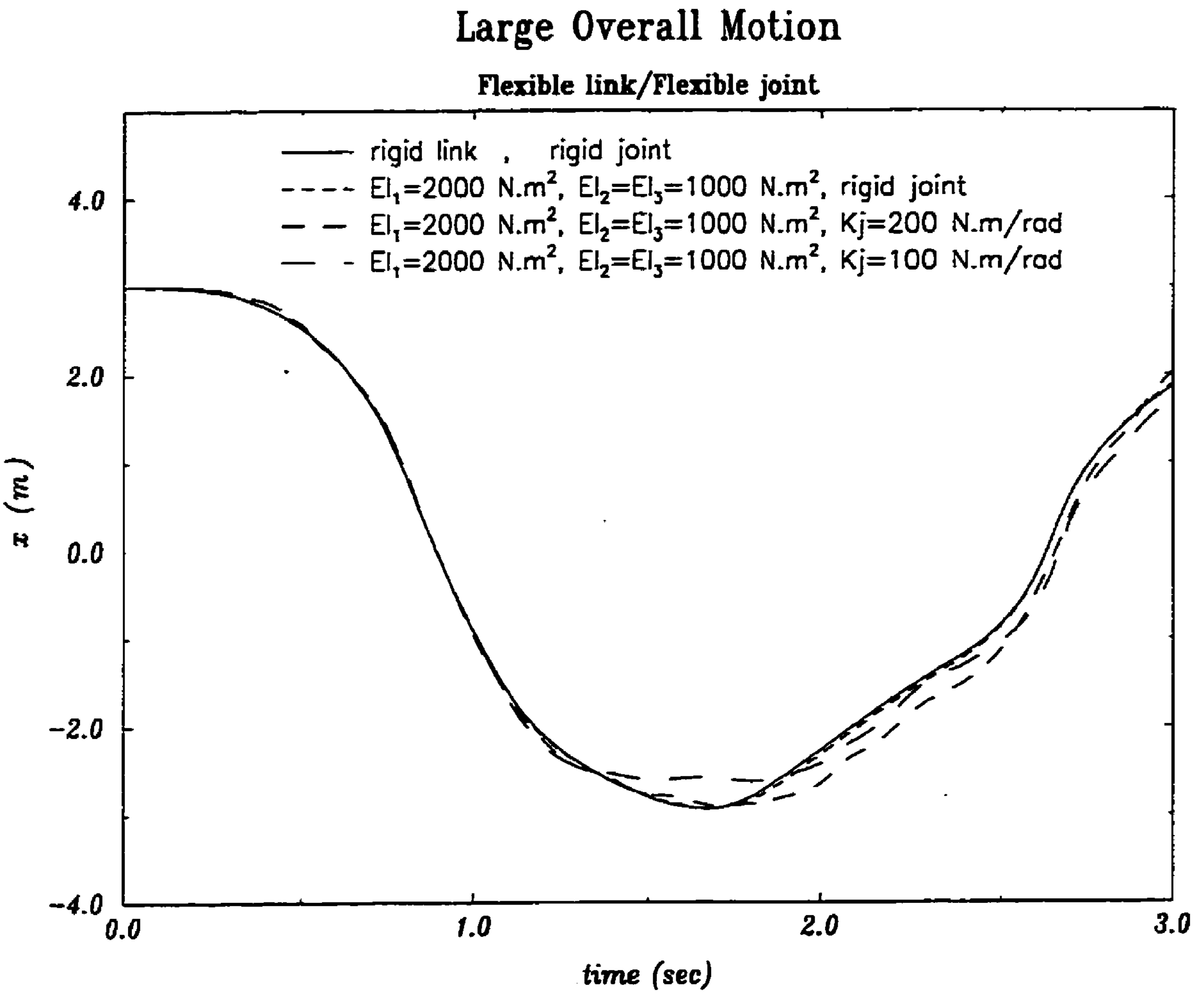

Figure 4.15-a Effect of joint flexibility on the x-coordinate of the payload

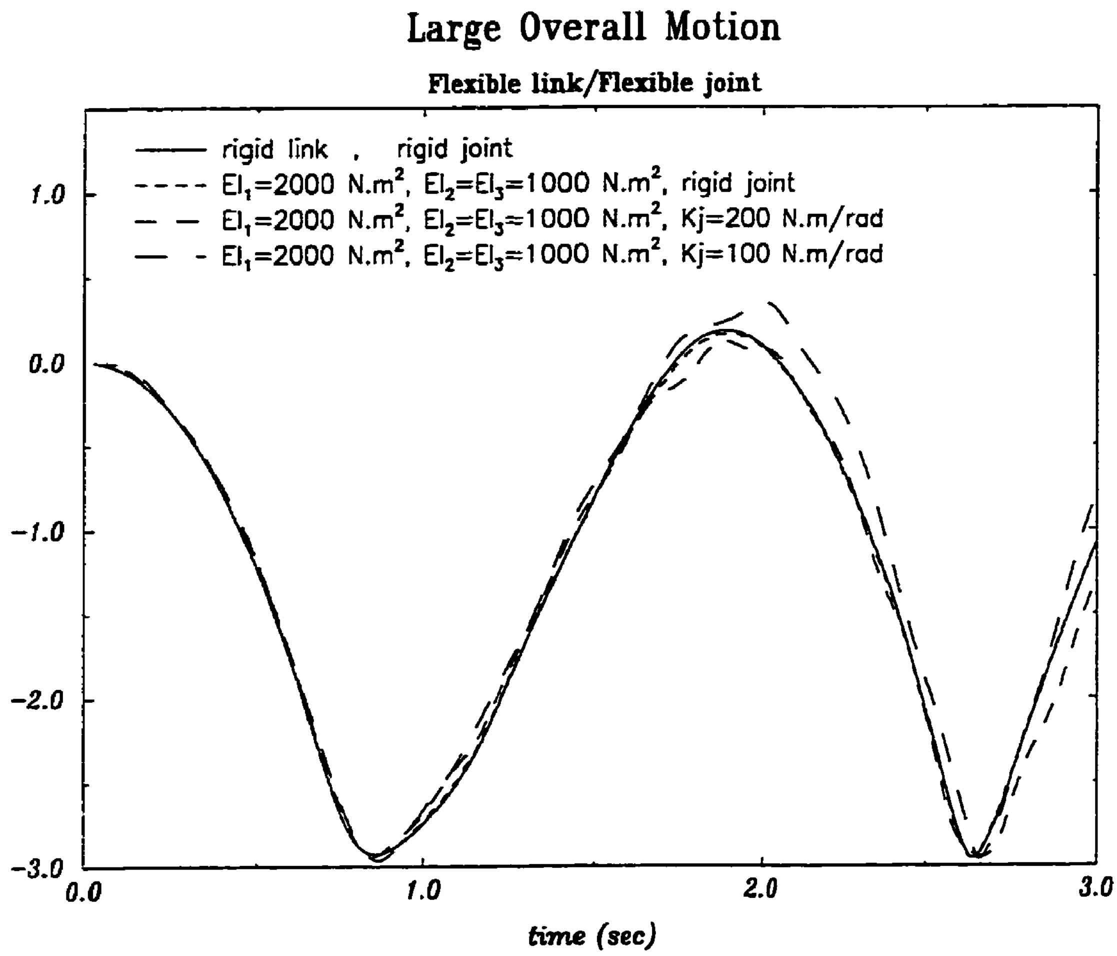

Figure 4.15-b Effect of joint flexibility on the y-coordinate of the payload

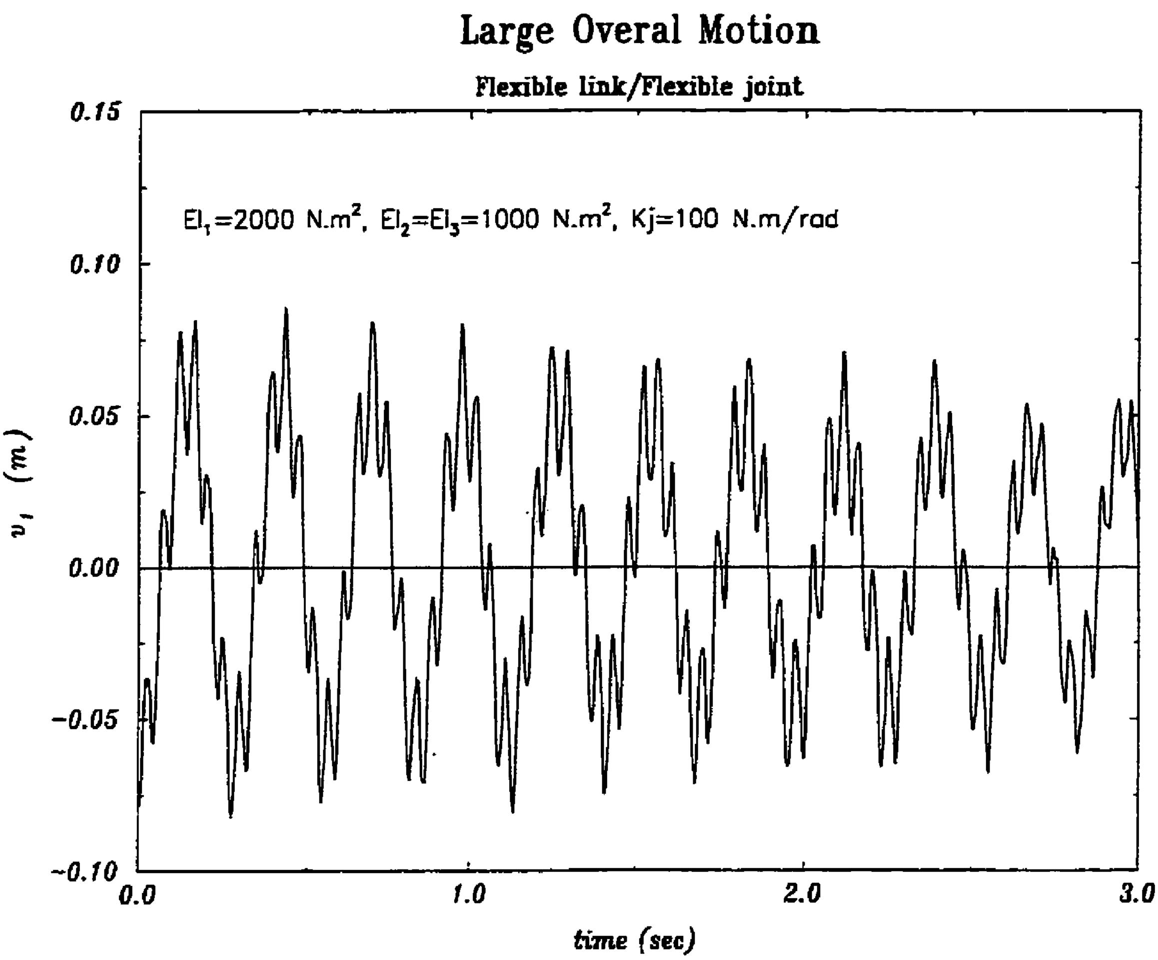

Figure 4.16-a Tip deflection of the first link with respect to its tangent line at the base

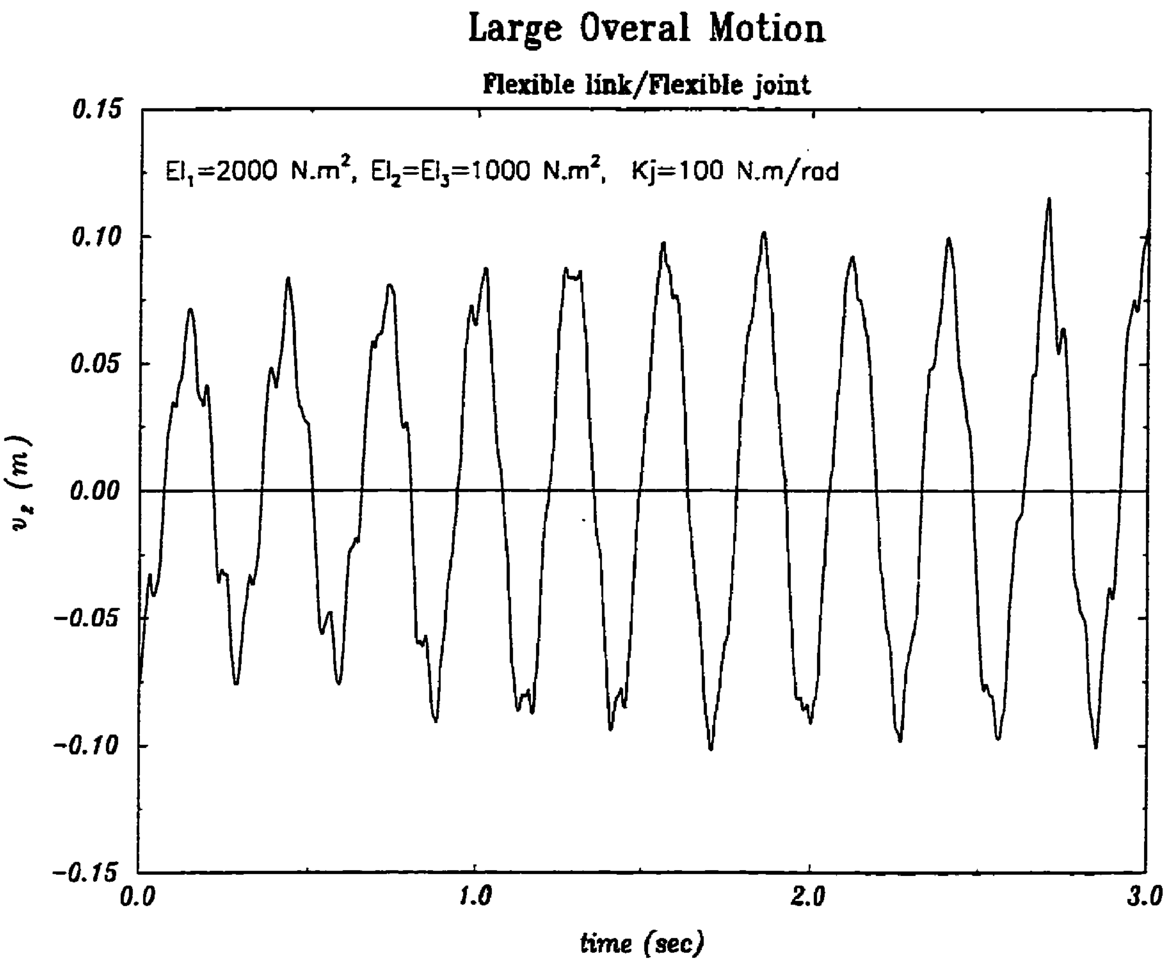

Figure 4.16-b Tip deflection of the second link with respect to its tangent line at its base

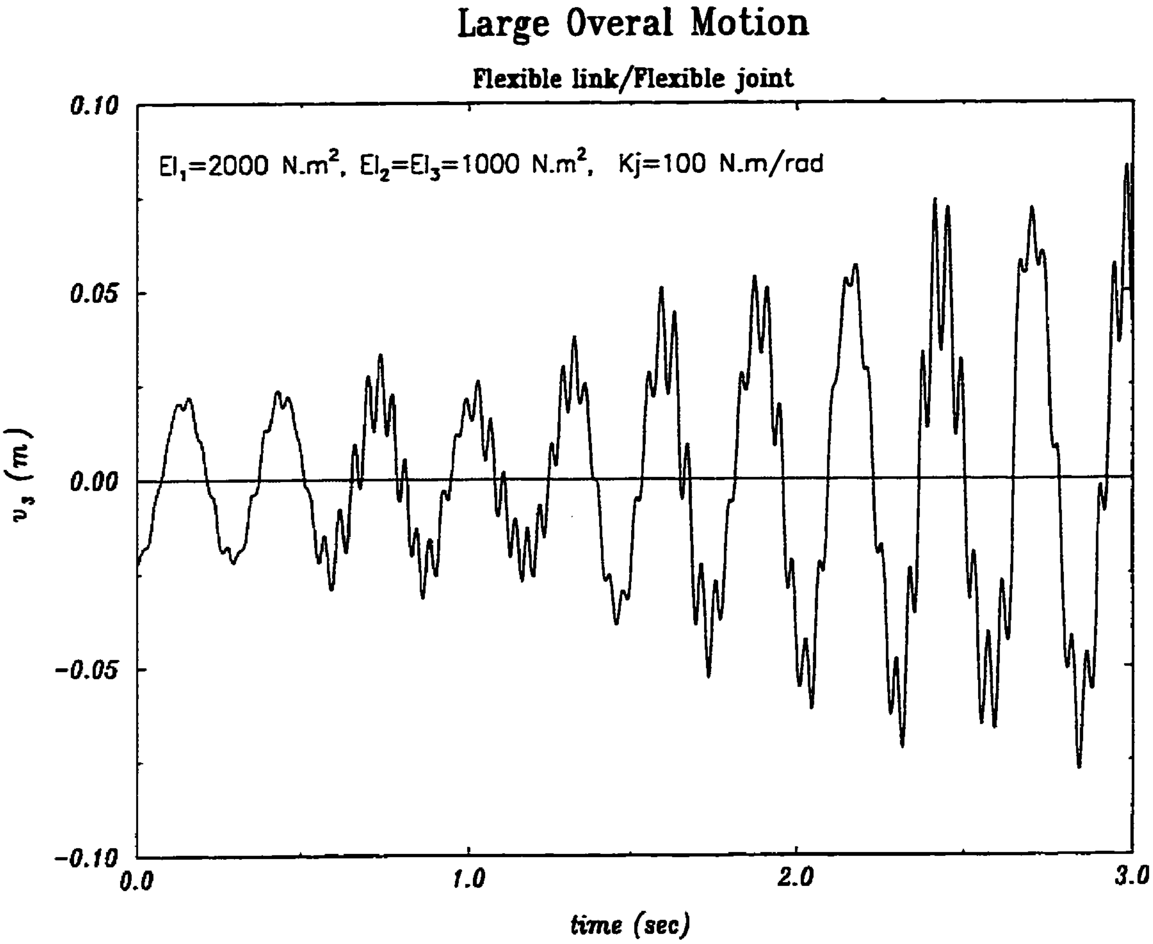

Figure 4.16-c Tip deflection of the third link with respect to its tangent line at the base

4.5 Summary and Conclusion

In this chapter an efficient finite element/Lagrangian approach for dynamic modeling of lightweight multi-link manipulators with both flexible links and flexible joints has been developed. The dynamic elastic response of each flexible link is formulated relative to a floating frame called pinned-pinned or virtual link coordinate system. Each link is divided into a finite number of elements and the elemental kinetic and potential energies of an arbitrary link are derived in a systematic way. Using virtual work of external loads and kinetic and potential energies of flexible links, actuated flexible joints, and payload, the equations of motion of the system have been found by using Lagrange's equations. The dynamic model derived in this study is free from assumption of a nominal motion and takes into account not only the coupling effects between the rigid body motion and the elastic motion but also the interaction between flexible links and actuated flexible joints. Due to the aforementioned couplings as well the variation in the effective inertia of the system as its configuration is changing with time, the model is highly nonlinear and coupled.

The validity of the model is shown and the effects of the link and joint flexibilities are illustrated by some case examples. It is shown that the interaction between the joint and link flexibilities causes significant changes in the dynamic behavior of the system. Also it is shown that in the present of link flexibility the tip points of the links oscillate undesirably which causes difficulties in control of flexible manipulators.

CHAPTER 5

DYNAMIC MODELING OF SPATIAL MANIPULATORS WITH FLEXIBLE LINKS AND JOINTS

5.1 Introduction

In this chapter, a redundant Lagrangian/finite element formulation is proposed to model the dynamics of lightweight spatial manipulators with both flexible links and joints. This modeling is an extension of the dynamic model developed for spatial manipulators with flexible links proposed by Farid and Lukasiewicz [105]. The links are assumed to be deformable due to bending and torsion. The elastic deformations of each link are expressed in its tangential (clamped free) local floating frame. The constraint equations representing kinematical relations among different coordinates due to connectivity of the links are added to the equations of motion of the system by using Lagrange multipliers. This leads to a mixed set of nonlinear ordinary differential equations and nonlinear algebraic equations with coordinates and Lagrange multipliers as unknown variables. The resulting system of differential algebraic equations (DAEs) is converted to a set of differential equations by substituting the constraints with their double time derivatives. These equations are solved numerically to predict the dynamic behavior of the system. The dynamic model derived here is free from the assumption of a nominal motion and takes into account not only the coupling effects between the rigid body motion and the elastic deformations of the links, but also the interaction between flexible links and actuated flexible joints.

5.2 Kinematics of the System

The manipulator system modeled in this chapter is a chain of flexible links connected by revolute actuated joints (figure 5.1). Each joint is flexible in the direction of the rotation of the connecting links. In addition to the base actuator which rotates the system about Z-axis, there is an actuator at each joint which rotates the next link about the axis of the rotor. The stator of each actuator k is fixed to the end of link k-1, while the stator of the base actuator is fixed to the ground. Each rotor k is connected to link k through a gear train and a flexible shaft which presents the joint flexibility.

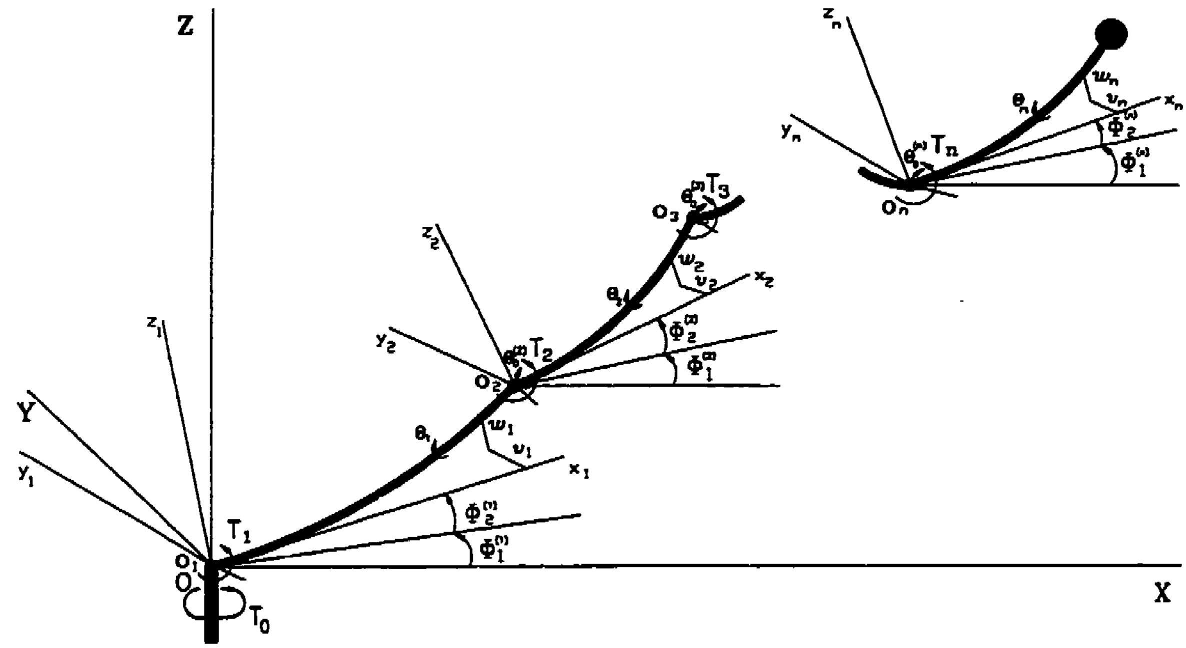

Figure 5.1 A spatial multi-link flexible manipulator system

5.2.1 Kinematic Modeling of Flexible Links

Each link is assumed to be deformable due to bending and torsion. The effects of axial and shear deformations are neglected. As shown in figures 5.1 and 5.2, elastic deformations of each link k are presented relative to a local floating frame o_k-$x_k y_k z_k$. This local frame is a clamped-free coordinate system whose x_k and y_k axes are tangent to link k at o_k and parallel to the horizontal plane (XY plane), respectively. $\Phi_1^{(k)}$ and $\Phi_2^{(k)}$ are two angles presenting the orientation of the x_k-axis of the local coordinate system in the inertial reference frame. $\Phi_1^{(k)}$ is the angle between the projection of the x_k-axis on the horizontal (XY) plane and the X-axis, while $\Phi_2^{(k)}$ is the angle between the x_k-axis and the Z-axis. v_k and w_k are y_k and z_k components of linear deformation of link k due to bending. $\Theta_0^{(k)}$ defines the rotation of link k at its base (o_k) about x_k-axis resulting from the absolute rotation of end point (o_k) of link k-1 about x_{k-1} axis, while Θ_k is rotational deformation of various sections of link k about x_k-axis relative to the cross section of link k at point o_k.

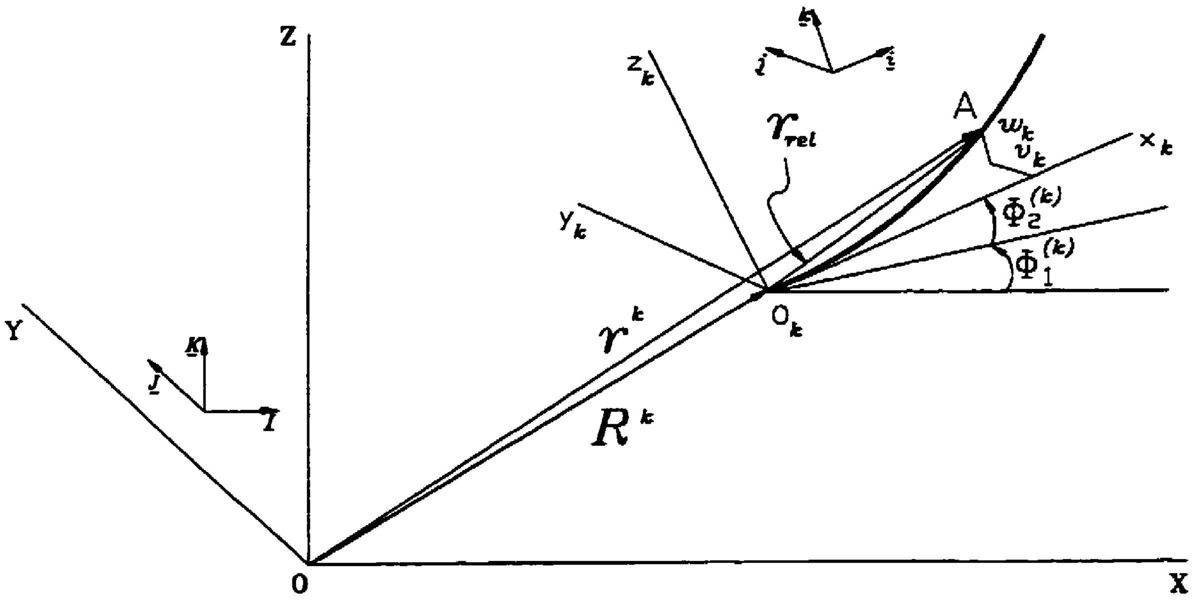

Figure 5.2 Absolute and relative position vectors of an arbitrary point A of link k

Referring to figure 5.2, the position vector of an arbitrary point A of link k on its elastic curve can be written in the following form:

$$r^k = R^k + r_{rel} \tag{5.1}$$

or

$$r^k = R_x^k \underline{I} + R_y^k \underline{J} + R_z^k \underline{K} + x_k \underline{i}_k + v_k \underline{j}_k + w_k \underline{k}_k \tag{5.2}$$

where $\mathbf{r}^k$, $\mathbf{R}^k$, and $\mathbf{r}_{rel}$ are the position vectors of point A in the global system, origin o_k in the global system, and point A in local coordinate system o_k-$x_k y_k z_k$. R_x^k, R_y^k, R_z^k are components of vector $\mathbf{R}^k$ along three axes of global coordinate system, and x_k, v_k, and w_k are x-coordinate and deflections in y_k and z_k-directions of point A in the local coordinate system, respectively. $\underline{\mathbf{I}}$, $\underline{\mathbf{J}}$, and $\underline{\mathbf{K}}$ are unit vectors along the coordinates of the global system, while $\underline{\mathbf{i}}_k$, $\underline{\mathbf{j}}_k$, and $\underline{\mathbf{k}}_k$ are unit vectors of the local system.

Local unit vectors $\underline{\mathbf{i}}_k$, $\underline{\mathbf{j}}_k$, and $\underline{\mathbf{k}}_k$ can be written in terms of $\underline{\mathbf{I}}$, $\underline{\mathbf{J}}$, and $\underline{\mathbf{K}}$ in the following forms:

$$\underline{i}_k = c_2^{(k)} c_1^{(k)} \underline{I} + c_2^{(k)} s_1^{(k)} \underline{J} + s_2^{(k)} \underline{K} \tag{5.3}$$

$$\underline{j}_k = -s_1^{(k)} \underline{I} + c_1^{(k)} \underline{J} \tag{5.4}$$

$$\underline{k}_k = -s_2^{(k)} c_1^{(k)} \underline{I} - s_2^{(k)} s_1^{(k)} \underline{J} + c_2^{(k)} \underline{K} \tag{5.5}$$

where $c_1^{(k)}=\cos(\Phi_1^{(k)})$, $s_1^{(k)}=\sin(\Phi_1^{(k)})$, $c_2^{(k)}=\cos(\Phi_2^{(k)})$, and $s_2^{(k)}=\sin(\Phi_2^{(k)})$. In order to reduce the length of the equations, unless it is necessary, superscript k will be kept only for components of R and angles Φ_1 and Φ_2, while other variables will be used without superscript or subscript.

By substituting local unit vectors $\underline{\mathbf{i}}_k$, $\underline{\mathbf{j}}_k$, and $\underline{\mathbf{k}}_k$ in terms of $\Phi_1^{(K)}$ and $\Phi_2^{(K)}$ and global unit vectors $\underline{\mathbf{I}}$, $\underline{\mathbf{J}}$, and $\underline{\mathbf{K}}$ from equations (5.3), (5.4), and (5.5) into equation (5.2) for $\mathbf{r}^k$, the velocity vector $\dot{\mathbf{r}}^k$ of each point of link k can be obtained as:

$$\begin{aligned}\dot{r}^k = & [\dot{R}_x^k - x(\dot{\Phi}_2^{(k)} s_2 c_1 + \dot{\Phi}_1^{(k)} c_2 s_1) - v\dot{\Phi}_1^{(k)} c_1 + w(-\dot{\Phi}_2^{(k)} c_2 c_1 + \dot{\Phi}_1^{(k)} s_2 s_1) - \dot{v} s_1 - \dot{w} s_2 c_1]\underline{I} \\ & + [\dot{R}_y^k - x(\dot{\Phi}_2^{(k)} s_2 s_1 - \dot{\Phi}_1^{(k)} c_2 c_1) - v\dot{\Phi}_1^{(k)} s_1 - w(-\dot{\Phi}_2^{(k)} c_2 s_1 + \dot{\Phi}_1^{(k)} s_2 c_1) + \dot{v} c_1 - \dot{w} s_2 s_1]\underline{J} \\ & + [\dot{R}_z^k + x\dot{\Phi}_2^{(k)} c_2 - w\dot{\Phi}_2^{(k)} s_2 + \dot{v} c_1 + \dot{w} c_2]\underline{K}\end{aligned} \tag{5.6}$$

The orientation of the tangent line to link k+1 at o_{k+1} presented by $\Phi_1^{(k+1)}$ and $\Phi_2^{(k+1)}$ (figure 5.3-b) is a function of the orientation ($\Phi_1^{(k)}$ and $\Phi_2^{(k)}$) and the elastic deformations of link k as well as angle $\gamma^{(k+1)}$ between tangent lines to links k and k+1 at point o_{k+1}. For small deformations, the angular deformation of link k at point o_{k+1} can be separated into three parts: v'_e, w'_e, and Θ_e (figure 5.3-a), where v'_e and $-w'_e$ respectively show the rotation angles of link k at point o_{k+1} about z_k-axis and y_k-axis, while Θ_e is the rotation of the end section of link k (at o_{k+1}) about x_k-axis.

Having unit vectors $\underline{i}_k$, $\underline{j}_k$, and $\underline{k}_k$ associated with o_k-$x_k y_k z_k$ coordinate system, we can find three unit vectors $\underline{i}'_k$, $\underline{j}'_k$, and $\underline{k}'_k$ at the end point (o_{k+1}) of link k by rotating subsequently each unit vector ($\underline{i}_k$, $\underline{j}_k$, and $\underline{k}_k$) an angle $-w'_e$ about y_k-axis, an angle v'_e about z_k-axis, and an angle Θ_e about x_k-axis. It is obvious that unit vector $\underline{i}'_k$ is tangent to link k at point o_{k+1}. Now let these three unit vectors ($\underline{i}'_k$, $\underline{j}'_k$, and $\underline{k}'_k$) rotate an angle $\gamma^{(k+1)}$, which is not necessarily small, about unit vector $\underline{j}'_k$ which is common normal of tangent lines to two links k and k+1 and also normal to the stator and rotor of the revolute actuator at joint o_{k+1}. As the result of these rotations (shown in figure 5.4), unit vector $\underline{i}_{k+1}$, which is along x_{k+1}-axis of link k+1 is found. This unit vector can be expressed in terms of its components along X, Y, and Z axes in the following form:

$$\underline{i}_{k+1} = l^{(k+1)}\underline{I} + m^{(k+1)}\underline{J} + n^{(k+1)}\underline{K} \tag{5.7}$$

in which $l^{(k+1)}$, $m^{(k+1)}$, and $n^{(k+1)}$ are functions of $\Phi_1^{(k)}$, $\Phi_2^{(k)}$, elastic rotations of link k at point o_{k+1}, and angle $\gamma^{(k+1)}$. Angles $\Phi_1^{(k+1)}$ and $\Phi_2^{(k+1)}$ can be found by the following simple equations:

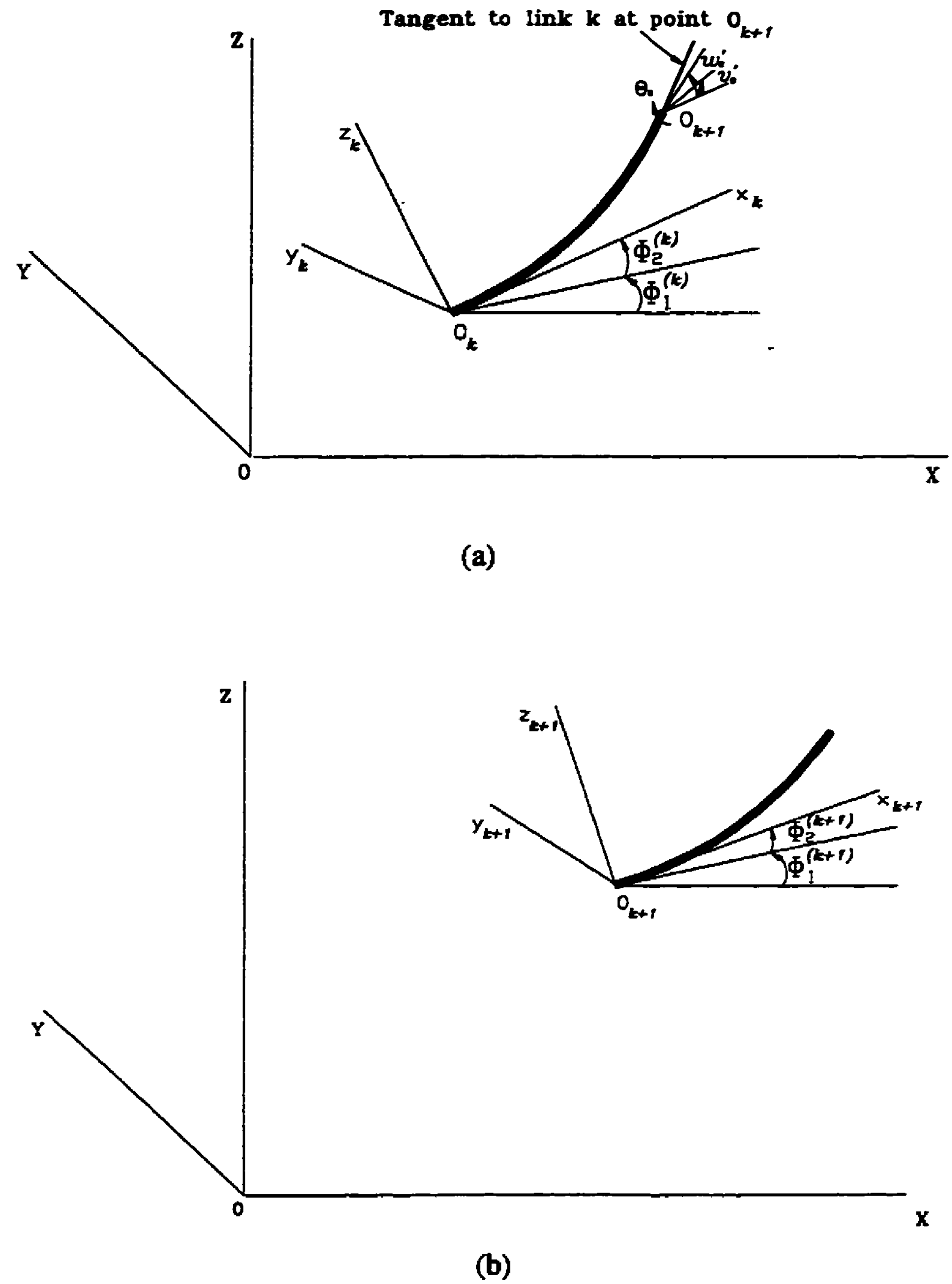

Figure 5.3 Angular deformations of link k at point o_{k+1} expressed in its local system and orientation of the tangent line to link k+1 at o_{k+1}

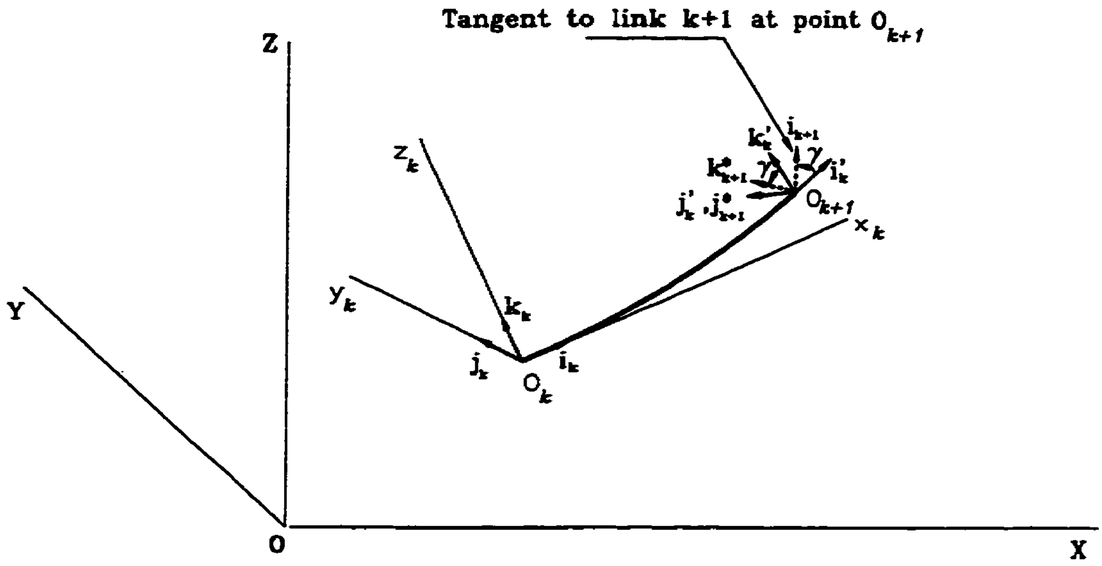

Figure 5.4 Representation of unit vector $\mathbf{i}_{k+1}$ resulting from various rotations of unit vectors $\mathbf{i}_k$, $\mathbf{j}_k$, and $\mathbf{k}_k$

$$\sin\Phi^{(k+1)} = n^{(k+1)} \tag{5.8}$$

$$\cos\Phi^{(k+1)} = \frac{l^{(k+1)}}{\sqrt{(l^{(k+1)})^2 + (m^{(k+1)})^2}} \tag{5.9}$$

$l^{(k+1)}$, $m^{(k+1)}$, and $n^{(k+1)}$ will be defined in the next section. These quantities are complicated nonlinear functions especially for multi-link manipulators. Therefore, it is better to consider $\Phi_1^{(k+1)}$ and $\Phi_2^{(k+1)}$ as additional variables and use equations (5.8) and (5.9) as two constraints (in addition to other constraints) for each joint o_{k+1}. There are five remaining constraints for each link. Three of them present the relation between coordinates of the position vectors of the origin of link k+1 and that of the link k. The forth one gives the angular rotation of the origin of the link k+1 about its x_k-axis in terms of that of the link k, rotational deformation of the end of the link k, and the angle $\gamma^{(k+1)}$ (between two vectors $\mathbf{i}'_k$ and $\mathbf{i}_{k+1}$). Finally the fifth one defines the relation between angle $\gamma^{(k+1)}$ and components of unit vectors $\mathbf{i}'_k$ and $\mathbf{i}_{k+1}$.

5.2.2 Kinematic Modeling of Flexible Joints

The arrangement of an actuated flexible joint is shown in figure 5.5. The rotations of the rotor and the link are presented by angles q_{k+1} and $\gamma^{(k+1)}$, respectively. q_{k+1} is the rotation angle of the rotor of actuator k+1 with respect to the line tangent to link k at $x^k=L_k$, while $\gamma^{(k+1)}$ represents the angle between tangent line of link k at $x^k=L_k$ and that of link k+1 at $x^{k+1}=0$. K_{k+1} is the drive shaft stiffness of the joint k+1, Γ_{k+1} is the gear ratio, and the difference $\gamma^{(k+1)}-\Gamma_{k+1}\, q_{k+1}$ shows the joint deflection. We assume that link k+1, joint k+1, and rotor k+1 all rotate about the same axis which can be an approximation for some arrangements of the gear train.

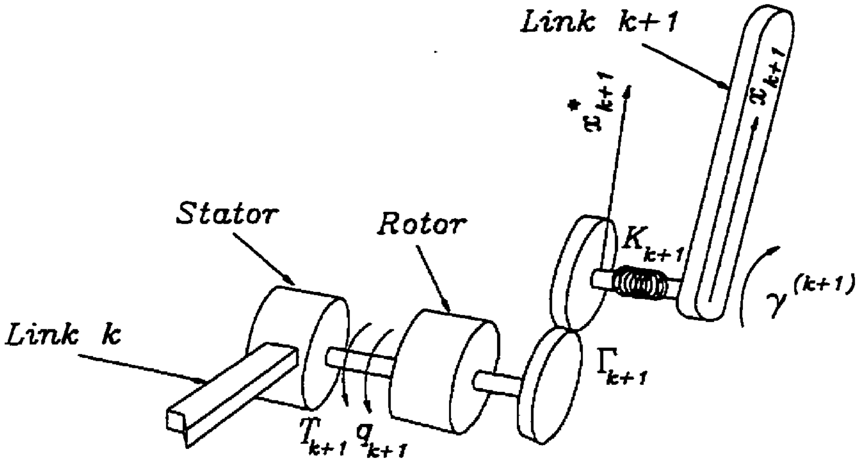

Figure 5.5 Model of the k+1th actuated flexible joint

As it can be seen in figure 5.5, axes x_{k+1}^* and x_{k+1} have different direction cosines due to the flexibility of joint k+1. We can introduce two angles $\Psi_1^{(k+1)}$ and $\Psi_2^{(k+1)}$ similar to angles $\Phi_1^{(k+1)}$ and $\Phi_2^{(k+1)}$ introduced in the previous section, to present the orientation of axis x_{k+1}^*. Two equations similar to equations (5.8) and (5.9) can be used to obtain angles $\Psi_1^{(k+1)}$ and $\Psi_2^{(k+1)}$ simply by substituting $l^{(k+1)}$, $m^{(k+1)}$, and $n^{(k+1)}$ respectively by $ls^{(k+1)}$, $ms^{(k+1)}$, and $ns^{(k+1)}$ as direction cosines of line x_{k+1}^*.

5.2.3 Rotation of a Vector about an Arbitrary Axis

As it was mentioned earlier, in order to find the orientation of the local x_{k+1} coordinate of link k+1, we should rotate the unit vectors $\mathbf{i}_k$, $\mathbf{j}_k$, and $\mathbf{k}_k$ of the local coordinate system of link k about various axes. Therefore, it is necessary to develop a rotation matrix which can generate the new orientation of any vector after rotating about any arbitrary axis. Without loss of generality we can consider that the axis of rotation passes through the origin of the vector.

Let **r** be the position vector of point Q and OC show the axis of rotation (figure 5.6). The angle between **r** and OC is β. We rotate the vector **r** an angle Θ about OC. It is shown in figure 5.6 that as the result of this rotation, the vector **r** (OQ) is transformed to the vector $\mathbf{r}^*$ (OQ*). The change of position vector **r** is defined as $\Delta\mathbf{r}$. The new vector $\mathbf{r}^*$

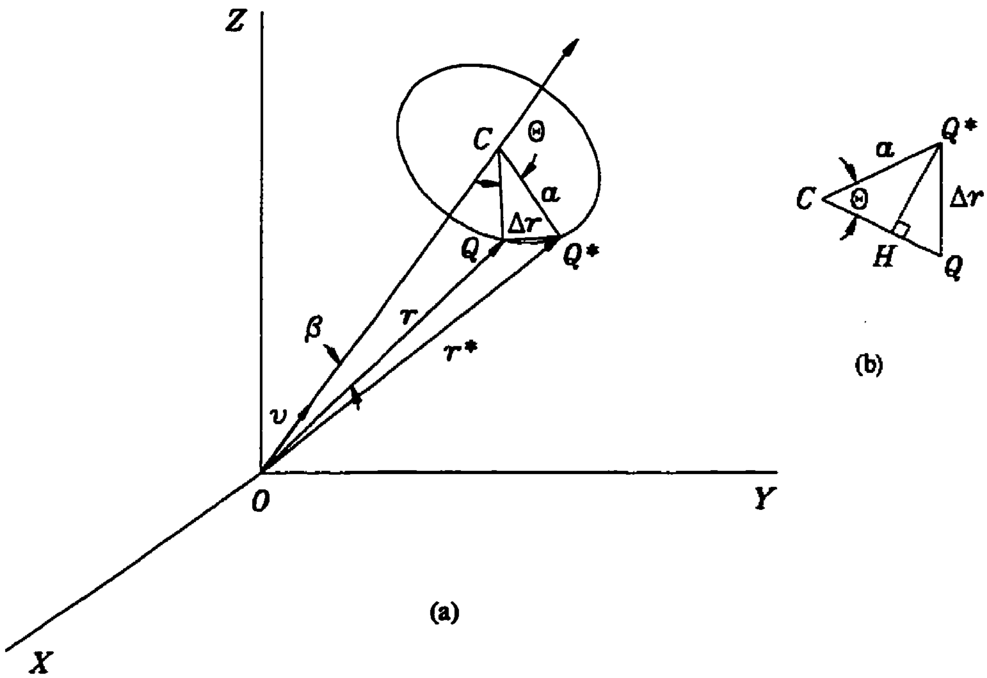

Figure 5.6 Rotation of vector r about axis OC

is

$$r^* = r + \Delta r \tag{5.10}$$

and the vector Δr can be written as:

$$\Delta r = QH + HQ^* \tag{5.11}$$

Since the vector **HQ*** is perpendicular to the plane OCQ, its direction can be found as **v x r**, where **v** is a unit vector along the axis of rotation OC. The magnitude of the vector **HQ*** is given by

$$|HQ^*| = a \ \sin\Theta \tag{5.12}$$

where a is the radius of the circle resulting from the rotation of the point Q about OC and from figure 5.6-a, it can be written as:

$$a = |r| \sin\beta \tag{5.13}$$

On the other hand, the magnitude of the vector QH can be found as:

$$|QH| = a(1 - \cos\Theta) = 2a \ \sin^2\frac{\Theta}{2} \tag{5.14}$$

Since the vector **QH** is perpendicular to both v and **HQ***, its direction is same as the unit vector $v \mathrm{x} \frac{v \mathrm{x} r}{a}$, thus

$$\begin{aligned} QH = |QH| \frac{v \mathrm{x} (v \mathrm{x} r)}{a} &= (2a \ \sin^2\frac{\Theta}{2}) \frac{v \mathrm{x} (v \mathrm{x} r)}{a} \\ &= 2 \ \sin^2\frac{\Theta}{2} [v \mathrm{x} (v \mathrm{x} r)] \end{aligned} \tag{5.15}$$

by substituting equations (5.12) and (5.15) into equation (5.11), we have

$$\Delta r = (v \times r)\sin\Theta + 2\,[v \times (v \times r)]\sin^2\frac{\Theta}{2} \tag{5.16}$$

and therefore;

$$r^* = r + \Delta r = r + (v \times r)\sin\Theta + 2\,[v \times (v \times r)]\sin^2\frac{\Theta}{2} \tag{5.17}$$

Moreover, we can use the identity

$$v \times r = \tilde{v}\, r = -\tilde{r}\, v \tag{5.18}$$

to write the equation (5.17) in the following form:

$$r^* = r + \tilde{v}\, r \sin\Theta + 2\,(\tilde{v})^2\, r \sin^2\frac{\Theta}{2} \tag{5.19}$$

where $\tilde{v}$ and $\tilde{r}$ are skew symmetric matrices given by

$$\tilde{v} = \begin{bmatrix} 0 & -v_z & v_y \\ v_z & 0 & -v_x \\ -v_y & v_x & 0 \end{bmatrix}, \qquad \tilde{r} = \begin{bmatrix} 0 & -r_z & r_y \\ r_z & 0 & -r_x \\ -r_y & r_x & 0 \end{bmatrix} \tag{5.20}$$

in which v_x, v_y, and v_z are the components of unit vector **v** and r_x, r_y, and r_z are the components of unit vector **r**.

Equation (5.19) can also be written in the following form:

$$r^* = [\, I + \tilde{v}\sin\Theta + 2\,(\tilde{v})^2 \sin^2\frac{\Theta}{2}\,]\, r = A r \tag{5.21}$$

where I is a 3 x 3 identity matrix and A is the 3 x 3 rotation matrix given by

$$A = [I + \tilde{v} \sin\Theta + 2\,(\tilde{v})^2 \sin^2\frac{\Theta}{2}] \tag{5.22}$$

which is expressed in terms of the angle of rotation (Θ) and the unit vector along the axis of rotation.

The orthogonality of the rotation matrix A can be proved in the following simple way. Since $\tilde{v}$ is a skew symmetric matrix ($\tilde{v}^T = -\tilde{v}$), $(\tilde{v})^2$ is a symmetric matrix and one can write

$$\begin{aligned} A^T A &= [I - \tilde{v}\sin\Theta + 2\,(\tilde{v})^2 \sin^2\frac{\Theta}{2}][I + \tilde{v}\sin\Theta + 2\,(\tilde{v})^2 \sin^2\frac{\Theta}{2}] \\ &= I + 4\sin^4\frac{\Theta}{2}\{(\tilde{v})^2 + (\tilde{v})^4\} \\ &= AA^T \end{aligned} \tag{5.23}$$

Also the following recurrence relations can be noted.

$$(\tilde{v})^{2n-1} = (-1)^{n-1}\,\tilde{v} \tag{5.24}$$

$$(\tilde{v})^{2n} = (-1)^{n-1}(\tilde{v})^2 \tag{5.25}$$

By utilizing these identities, equation (5.23) can be written as

$$A^T A = I \tag{5.26}$$

which proves the orthogonality of the rotation matrix.

In the case of small rotations, we can substitute $\sin\Theta$ by Θ and neglect the third term in equation (5.22) to yield an approximation of rotation matrix A as

$$A \approx I + \tilde{v}\Theta \tag{5.27}$$

5.2.4 Derivation of the Direction Cosines

As it was shown in figure 5.4, unit vectors $\underline{\mathbf{i}}'_k$, $\underline{\mathbf{j}}'_k$, and $\underline{\mathbf{k}}'_k$ at the end point (o_{k+1}) of link k can be found by rotating subsequently each unit vector ($\underline{\mathbf{i}}_k$, $\underline{\mathbf{j}}_k$, and $\underline{\mathbf{k}}_k$) an angle $-w'^{(k)}_e$ about y_k-axis, an angle $v'^{(k)}_e$ about z_k-axis, and an angle $\Theta^{(k)}_e$ about x_k-axis. By assuming that these elastic deformations are small, equation (5.27) can be used to find three rotation matrices A_y, A_z, and A_Θ in the following forms

$$A_y \approx \begin{bmatrix} 1 & 0 & -c_1 w'_e \\ 0 & 1 & -s_1 w'_e \\ c_1 w'_e & s_1 w'_e & 1 \end{bmatrix} \tag{5.28}$$

$$A_z \approx \begin{bmatrix} 1 & -c_2 v'_e & -s_2 s_1 v'_e \\ c_2 v'_e & 1 & s_2 c_1 v'_e \\ s_2 s_1 v'_e & -s_2 c_1 v' & 1 \end{bmatrix} \tag{5.29}$$

$$A_\Theta \approx \begin{bmatrix} 1 & -s_2 \Theta_e & c_2 s_1 \Theta_e \\ s_2 \Theta_e & 1 & -c_2 c_1 \Theta_e \\ -c_2 s_1 \Theta_e & c_2 c_1 \Theta_e & 1 \end{bmatrix} \tag{5.30}$$

in which $c_1=\cos(\Phi_1^{(k)})$, $s_1=\sin(\Phi_1^{(k)})$, $c_2=\cos(\Phi_2^{(k)})$, and $s_2=\sin(\Phi_2^{(k)})$.

Since the rotations are small, the order of rotations is not important and one rotation matrix can be obtained by multiplying the three different ones. After neglecting second order terms, we have

$$A_{yz\Theta} = A_y A_z A_\Theta \approx \begin{bmatrix} 1 & -c_2 v'_e - s_2 \Theta_e & -c_1 w'_e - s_2 s_1 v'_e + c_2 s_1 \Theta_e \\ c_2 v'_e + s_2 \Theta_e & 1 & -s_1 w'_e + s_2 c_1 v'_e - c_2 c_1 \Theta_e \\ c_1 w'_e + s_2 s_1 v'_e - c_2 s_1 \Theta_e & s_1 w'_e - s_2 c_1 v'_e + c_2 c_1 \Theta_e & 1 \end{bmatrix} \tag{5.31}$$

By multiplying unit vectors $\underline{i}_k$ and $\underline{j}_k$ by the rotation matrix $A_{yz\Theta}$ and neglecting higher order terms, $\underline{i}_k'$ and $\underline{j}_k'$ can be obtained in the following forms

$$\underline{i}_k' = A_{yz\Theta}\underline{i}_k = A_{yz\Theta}\begin{Bmatrix} c_2c_1 \\ c_2s_1 \\ s_2 \end{Bmatrix} = \begin{Bmatrix} c_2c_1 - s_1v'_e - s_2c_1w'_e \\ c_2s_1 + c_1v'_e - s_2s_1w'_e \\ s_2 + c_2w'_e \end{Bmatrix} \tag{5.32}$$

$$\underline{j}_k' = A_{yz\Theta}\underline{j}_k = A_{yz\Theta}\begin{Bmatrix} -s_1 \\ c_1 \\ 0 \end{Bmatrix} = \begin{Bmatrix} -s_1 - c_1(c_2v'_e + s_2\Theta_e) \\ c_1 - s_1(c_2v'_e + s_2\Theta_e) \\ -s_2v'_e + c_2\Theta_e) \end{Bmatrix} \tag{5.33}$$

Now we should rotate unit vector $\underline{i}_k'$ an angle $-\gamma^{(k+1)}$ about unit vector $\underline{j}_k'$ to reach to unit vector $\underline{i}_{k+1}$ tangent to the link k+1. Since $\gamma^{(k+1)}$ is not necessarily a small angle, we should use equation (5.22) to construct the proper rotation matrix A_γ.

$$A_\gamma = I - \tilde{v}_\gamma \sin\gamma^{(k+1)} + 2\,(\tilde{v}_\gamma)^2 \sin^2\frac{\gamma^{(k+1)}}{2} \tag{5.34}$$

since for this rotation the vector $v_\gamma = j'_k$, the associated skew symmetric matrix used in the above equation is

$$\tilde{v}_\gamma \approx \begin{bmatrix} 0 & s_2v'_e - c_2\Theta_e & c_1 - s_1(c_2v'_e + s_2\Theta_e) \\ -s_2v'_e + c_2\Theta_e & 0 & s_1 + c_1(c_2v'_e + s_2\Theta_e) \\ -c_1 + s_1(c_2v'_e + s_2\Theta_e) & -s_1 - c_1(c_2v'_e + s_2\Theta_e) & 0 \end{bmatrix} \tag{5.35}$$

By applying the rotation matrix A_γ to the vector $\underline{i}_k'$, we have

$$\underline{i}_{k+1} = \begin{Bmatrix} l_{k+1} \\ m_{k+1} \\ n_{k+1} \end{Bmatrix} = A_\gamma \underline{i}_k' = A_\gamma \begin{Bmatrix} c_2c_1 - s_1v'_e - s_2c_1w'_e \\ c_2s_1 + c_1v'_e - s_2s_1w'_e \\ s_2 + c_2w'_e \end{Bmatrix} \tag{5.36}$$

After substituting A_γ, various components of the unit vector $\mathbf{i}_{k+1}$ can be written in the following forms:

$$\begin{aligned} l_{k+1} &= (1-2c_1^2 \sin^2\frac{\gamma^{(k+1)}}{2})(c_2c_1 - s_1v'_e - s_2c_1w'_e) + 4c_2c_1^2s_1(s_2\Theta_e + c_2v'_e)\sin^2\frac{\gamma^{(k+1)}}{2} \\ &- 2c_1s_1(c_2s_1 + c_1v'_e - s_1s_2w'_e)\sin^2\frac{\gamma^{(k+1)}}{2} - c_1(s_2 + c_2w'_e)\sin\gamma^{(k+1)} \\ &+ c_2s_1[(-s_2v'_e + c_2\Theta_e)\sin\gamma^{(k+1)} - 2(c_1^2 - s_1^2)(c_2v'_e + s_2\Theta_e)\sin^2\frac{\gamma^{(k+1)}}{2}] \\ &+ s_2[s_1(c_2v'_e + s_2\Theta_e)\sin\gamma^{(k+1)} + 2s_1(s_2v'_e - c_2\Theta_e)\sin^2\frac{\gamma^{(k+1)}}{2}] \end{aligned} \tag{5.37}$$

$$\begin{aligned} m_{k+1} &= -2c_1s_1 \sin^2\frac{\gamma^{(k+1)}}{2}(c_2c_1 - s_1v'_e - s_2c_1w'_e) - 4c_1s_1^2c_2(c_2v'_e + s_2\Theta_e)\sin^2\frac{\gamma^{(k+1)}}{2} \\ &+ (1-2s_1^2 \sin^2\frac{\gamma^{(k+1)}}{2})(c_2s_1 + c_1v'_e - s_1s_2w'_e) - s_1(s_2 + c_2w'_e)\sin\gamma^{(k+1)} \\ &+ c_2c_1[(s_2v'_e - c_2\Theta_e)\sin\gamma^{(k+1)} - 2(c_1^2 - s_1^2)(c_2v'_e + s_2\Theta_e)\sin^2\frac{\gamma^{(k+1)}}{2}] \\ &+ s_2[-c_1(c_2v'_e + s_2\Theta_e)\sin\gamma^{(k+1)} + 2c_1(-s_2v'_e + c_2\Theta_e)\sin^2\frac{\gamma^{(k+1)}}{2}] \end{aligned} \tag{5.38}$$

$$n_{k+1} = -s_2w'_e \sin\gamma^{(k+1)} + (1-2\sin^2\frac{\gamma^{(k+1)}}{2})(s_2 + c_2w'_e) \tag{5.39}$$

5.3 Dynamic Modeling

The equations of motion of the flexible manipulator systems can be found by using standard Lagrangian approach. The proposed dynamic model contains dependent coordinates which are interrelated through holonomic constraint equations. Therefore, it is possible to use method of Lagrange multipliers to obtain the equations of motion. As it was shown in chapter 3, by using the formal way of dealing with constraints equation in the calculus of variations, we can obtain the following system of differential equations for a system with n degrees of freedom from which m degrees are redundant.

$$\frac{d}{dt}\left(\frac{\partial L}{\partial \dot{q}_i}\right)-\frac{\partial L}{\partial q_i}+\lambda^T C_{q_i}=Q_i, \qquad i=1,\ldots\ldots n \tag{5.40}$$

$$C_q \ddot{q}=Q_c \tag{5.41}$$

where L shows the Lagrangian of the system (L=KE-PE), λ is the vector of Lagrange multipliers, and ***Cq*** is the constraint Jacobian matrix (mXn) which shows the derivatives of the different constraints with respect to various variables. The system of differential equations (5.40, 5.41) can be solved numerically to predict the dynamic behavior of the manipulator system.

To obtain the equations of motion of a manipulator system by Lagrangian dynamics, first we need the kinetic and potential energies of its various components including the links, the actuators, and the payload. Since the number of degrees of freedom of each link is infinite due to its elastic deformations, we use the finite element method to approximate the real system with a system with finite degrees of freedom.

5.3.1 Kinetic and Potential Energies of the Links

Each link is divided into a number of elements. The link deflections are presented in terms of shape functions and nodal values of transverse deflections, slopes, and rotation angles. Hermite and Linear shape functions are used to approximate bending deflection and torsional deflection of the links, respectively. Each element e of link k has 17 degrees of freedom, namely, $\Phi_1^{(k)}$, $\Phi_2^{(k)}$, $\Psi_1^{(k)}$, $\Psi_2^{(k)}$, $\Theta_0^{(k)}$, q_k, and $\gamma^{(k)}$ as rigid degrees of freedom, v_{2e-1}, v_{2e}, v_{2e+1}, and v_{2i+2} as nodal transverse deflections and slopes in the y-direction, w_{2e-1}, w_{2e}, w_{2e+1}, and w_{2e+2} as nodal transverse deflections and slopes in the z-direction, and Θ_i, and Θ_{i+1} as nodal rotation angles about x-axis. The notations used for transverse deflections and slopes in y and z-directions are shown in figures 5.7-a, b and notations used for rotational deflection about x-axis are shown in figure 5.7-c.

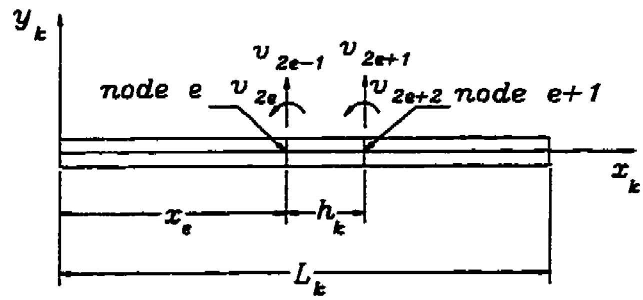

(a)

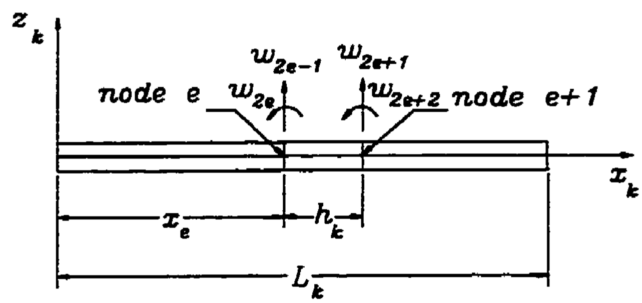

(b)

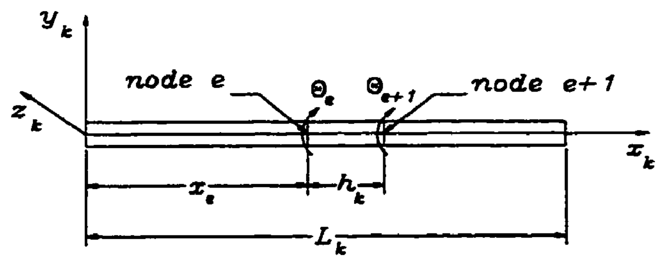

(c)

Figure 5.7 Nodal elastic deformations of each finite element of link k

Now kinetic and potential energies of each link k, presented by KEL^k and PEL^k, can be written as the summation of elemental kinetic and potential energies shown by KEE_e^k and PEE_e^k in the following forms:

$$KEL^k = \sum_{e=1}^{N_k} KEE_e^k = \sum_{e=1}^{N_k} [\frac{1}{2} \int_{x_e}^{x_{e+1}} \rho_k A_k \dot{r}.\dot{r}\, dx + \frac{1}{2} \int_{x_e}^{x_{e+1}} \rho_k J_k (\dot{\Theta}_0^{(k)} + \dot{\Theta} + \dot{\Phi}_1^{(k)} s_2)^2 dx] \quad (5.42)$$

$$\begin{aligned} PEL^k &= \sum_{e=1}^{N_k} PEE_e^k = \sum_{e=1}^{N_k} [\int_{x_e}^{x_{e+1}} \rho_k A_k g (R_z^k + x s_2 + w c_2) dx + \frac{1}{2} \int_{x_e}^{x_{e+1}} E_k I_z^k (\frac{\partial^2 v}{\partial x^2})^2 dx \\ &+ \frac{1}{2} \int_{x_e}^{x_{e+1}} E_k I_y^k (\frac{\partial^2 w}{\partial x^2})^2 dx + \frac{1}{2} \int_{x_e}^{x_{e+1}} G_k J_k (\frac{\partial \Theta}{\partial x})^2 dx] \end{aligned} \quad (5.43)$$

where N_k is the number of elements of link k and ρ_k, A_k, and J_k are the density, the cross sectional area, and the polar moment of inertia of link k at each point. E_k, G_k, I_y^k, and I_z^k are Young modulus of elasticity, shear modulus, and area moments of inertia about y and z axes, respectively. The notations: $c_1=\cos(\Phi_1^{(k)})$, $s_1=\sin(\Phi_1^{(k)})$, $c_2=\cos(\Phi_2^{(k)})$, and $s_2=\sin(\Phi_2^{(k)})$, are used to simplify the trigonometrical expressions in the above equations and also in the next parts of this chapter. The first term in the right side of equation (5.42) shows the kinetic energy resulting from the linear motion of each point, while the second term is due to the rigid and elastic angular rotations of the link about its x-axis. The first term of the potential energy shows the effect of gravity, while the second and third terms present the bending effects of the link about z and y axes, respectively. The last term presents strain energy due to torsional deformation of the link.

5.3.2 Kinetic and Potential Energies of the Actuators

The base actuator, whose stator is fixed to the ground, rotates the manipulator system about the global Z-axis. Its kinetic energy (KEA^{b}) and potential energy ($PEA^{(b)}$) can be written as:

$$KEA^{(b)} = \frac{1}{2} Ir_b \dot{q}_b^2 \tag{5.44}$$

$$PEA^{(b)} = \frac{1}{2} K_b (\Phi_1^{(1)} - \Gamma_b q_b)^2 \tag{5.45}$$

in which Ir_b, K_b, q_b, and Γ_b are the moment of inertia of the base rotor, the joint stiffness, the rotation angle of the base rotor, and the gear ratio of the base actuator, respectively.

The kinetic and potential energies of the first actuator, which rotates the firs link about its local y_1-axis, have the following forms:

$$KEA^{(1)} = \frac{1}{2} Isx_1 (\dot{\Phi}_1^{(1)})^2 + \frac{1}{2} Irz_1 (\dot{\Phi}_1^{(1)} \cos q_1)^2 + \frac{1}{2} Iry_1 \dot{q}_1^2 + + \frac{1}{2} Irx_1 (\dot{\Phi}_1^{(1)} \sin q_1)^2 \tag{5.46}$$

$$PEA^{(1)} = \frac{1}{2} K_1 (\Phi_2^{(1)} - \Gamma_1 q_1)^2 \tag{5.47}$$

where Isx_1, Isy_1, Isz_1, Irx_1, Iry_1, and Irz_1 are moment of inertia of the stator and rotor of the first actuator about different local axes. K_1 and Γ_1 present the stiffness and gear ratio of the joint, respectively.

Similarly the kinetic and potential energies of the k-th actuator (k=2,....,n) can be written in the following forms:

$$\begin{aligned} KEA^{(k)} &= \frac{1}{2} Isx_k (\dot{\Phi}_1^{(k-1)} s_2^{(k-1)} + \dot{\Theta}_e^{(k-1)} + \dot{\Theta}_0^{(k-1)})^2 + \frac{1}{2} Isy_k (\dot{\Phi}_2^{(k-1)} + \dot{w}_e^{(k-1)})^2 \\ &+ \frac{1}{2} Isz_k (\dot{\Phi}_1^{(k-1)} c_2^{(k-1)} + \dot{v}_e^{(k-1)})^2 + \frac{1}{2} Irx_k (\dot{\Psi}_1^{(k-1)} \sin \Psi_2^{(k-1)} + \dot{\Theta}_0^{(k)})^2 \\ &+ \frac{1}{2} Iry_k (\dot{\Psi}_2^{(k-1)})^2 + \frac{1}{2} Irz_k (\dot{\Psi}_1^{(k-1)} \cos \Psi_2^{(k-1)})^2 + \frac{1}{2} (mr_k + ms_k) \dot{\vec{R}}_k . \dot{\vec{R}}_k \end{aligned} \tag{5.48}$$

$$PEA^{(k)} = \frac{1}{2} K_k (\gamma^{(k)} - \Gamma_k q_k)^2 + (mr_k + ms_k) g R_z^{(k)} \tag{5.49}$$

where mr_k and ms_k are masses of the rotor and stator of the k-th actuator.

5.3.3 Virtual Work of the External and Damping Torques

There are 2n+2 nonconservative loads, namely n+1 actuator torques and n+1 damping torques resulting from friction of joints. The generalized forces due to the actuator torques and damping torques in the joints can be found by using the principle of virtual work. The total virtual work of these loads can be written as:

$$\delta W = (T_b - b_b \dot{q}_b)\delta q + \sum_{j=1}^{n} (T_j - b_j \dot{q}_j)\delta q_j \tag{5.50}$$

where b_b and b_j are viscous damping coefficients of the base and j-th joints, and T_b and T_j are torques applied by the base and j-th actuators. Using equation (5.50) the generalized forces required in the right hand side of the Lagrange's equations can be obtained.

5.3.4 Equations of Motion

Due to considering extra coordinates in describing the kinematics of the system, the manipulator is dynamically modeled in a redundant approach. By satisfying Lagrange equations and substituting the constraints with their double time derivatives, the following second order system of nonlinear differential equation can be obtained .

$$\begin{aligned} MS\,\{\ddot{q}\} + C_q^{\,T}\,\{\lambda\} &= \{Qv\} + \{Qe\} \\ C_q\,\{\ddot{q}\} &= \{Qc\} \end{aligned} \tag{5.51}$$

in which $\{q\}$ presents a vector consisting of all of the degrees of freedom of the system and $\{\lambda\}$ is the vector of Lagrange multipliers. $\{Qv\}$ is the load vector including the velocity terms due to Coriolis and centrifugal effects, and gravity terms. Also it includes $-KS\{q\}$ due to the elastic deformations and $-BS\{\dot{q}\}$ due to the joint dampings. $\{Qe\}$ is the vector of external loads and C_q and $\{Qc\}$ present the constraint Jacobean matrix and the vector consisting of nonlinear terms resulting from twice time differentiation of the constraints, respectively. ***MS*** and ***KS*** are system mass and stiffness matrices. These two system matrices and system vector $\{\boldsymbol{Qv}\}$ in equation (5.51) can be obtained in three steps. In the first step various matrices and vectors are built for finite elements of each link. Then they are assembled to find corresponding matrices and vectors for each link. And finally system matrices and vectors are formed by assembling those of various links and joints. Boundary conditions are used to eliminate non-changing degrees of freedom and to modify the elements of the link mass matrix and the load vector. These boundary effects are due to the clampedness of each link at its origin, the mass and moment of inertia of the stator and rotor of each revolute actuator, and the mass and moment inertia of the payload.

5.3.4.1 Derivation of Elemental Matrices and Vectors

To simplify the derivation of components of various elemental matrices and vectors of each link, they are partitioned into submatrices and subvectors in the following forms:

$$\boldsymbol{M}_e^k = \begin{bmatrix} [\boldsymbol{M}_{Se}^k]_{14X14} & [\boldsymbol{M}_{S\,Re}^k]_{14X3} \\ [\boldsymbol{M}_{RSe}^k]_{3X14} & [\boldsymbol{M}_{Re}^k]_{3X3} \end{bmatrix} \tag{5.52}$$

$$\boldsymbol{K}_e^k = \begin{bmatrix} [\boldsymbol{K}_{Se}^k]_{14X14} & [\boldsymbol{K}_{S\,Re}^k]_{14X3} \\ [\boldsymbol{K}_{RSe}^k]_{3X14} & [\boldsymbol{K}_{Re}^k]_{3X3} \end{bmatrix} \tag{5.53}$$

$$\boldsymbol{Qv}_e^k = \begin{Bmatrix} [\boldsymbol{Qv}_{Se}^k]_{14X1} \\ [\boldsymbol{Qv}_{Re}^k]_{3X1} \end{Bmatrix} \;, \boldsymbol{Qe}_e^k = \begin{Bmatrix} [\boldsymbol{Qe}_{Se}^k]_{14X1} \\ [\boldsymbol{Qe}_{Re}^k]_{3X1} \end{Bmatrix} \tag{5.54}$$

in which e and k, respectively, show the element and link numbers, and the size of each matrix and vector are shown on the right side of them. Matrices and vectors with subscript

Re refer to 3 degrees of freedom representing the linear motion of the origin of link k, while those with Se are associated with other 14 degrees of freedom of each element including $\Phi_1^{(k)}$, $\Phi_2^{(k)}$, $\Theta_0^{(k)}$, and $\gamma^{(k)}$ as rigid degrees of freedom, and v_{2e-1}, v_{2e}, v_{2e+1}, v_{2i+2}, w_{2e-1}, w_{2e}, w_{2e+1}, w_{2e+}, Θ_i, and Θ_{i+1} as nodal degrees of freedom due to the elastic deformation of the link. It is worth mentioning that due to the symmetry of the mass and stiffness matrices, $(\boldsymbol{M}_{RSe}^{k})^T=\boldsymbol{M}_{SRe}^{k}$ and $(\boldsymbol{K}_{RSe}^{k})^T=\boldsymbol{K}_{SRe}^{k}$. In addition $\boldsymbol{K}_{Re}^{k}$ and $\boldsymbol{K}_{SRe}^{k}$, in equation (5.53), are both zero matrices.

In order to find the components of the elemental mass and stiffness matrices and the load vector $\boldsymbol{Qv}$, we need to determine the kinetic and potential energies of each element. These energies can be written in the following decomposed forms:

$$KEE_e^k = KEE_{Re}^k + KEE_{Se}{}^k + KEE_{SRe}{}^k \tag{5.55}$$

$$PEE_e^k = PEE_{Re}^k + PEE_{Se}{}^k \tag{5.56}$$

KEE_{Re}^k is one part of the link kinetic energy due to the motion of the origin of the floating frame system. This part can be written as:

$$KEE_{Re}^k = \frac{1}{2} \int_{x_e}^{x_{e+1}} \rho_k A_k [(\dot{R}_x^k)^2 + (\dot{R}_y^k)^2 + (\dot{R}_z^k)^2] dx \tag{5.57}$$

while KEE_{Se}^k corresponds to the rigid and elastic degrees of freedom: $\Phi_1^{(k)}$, $\Phi_2^{(k)}$, $\Theta_0^{(k)}$, v, w, and Θ . KEE_{Se}^k can be written in the following form

$$\begin{aligned} KEE_{Se}^k = \frac{1}{2} \int_{x_e}^{x_{e+1}} & \rho_k A_k \{ x(-\dot{\Phi}_2^{(k)} s_2 c_1 - \dot{\Phi}_1^{(k)} c_2 s_1) - v\dot{\Phi}_1^{(k)} c_1 + w(-\dot{\Phi}_2^{(k)} c_2 c_1 + \dot{\Phi}_1^{(k)} s_2 s_1) - \dot{v} s_1 - \dot{w} s_2 c_1]^2 \\ & + [x(-\dot{\Phi}_2^{(k)} s_2 s_1 + \dot{\Phi}_1^{(k)} c_2 c_1) - v\dot{\Phi}_1^{(k)} s_1 - w(\dot{\Phi}_2^{(k)} c_2 s_1 + \dot{\Phi}_1^{(k)} s_2 c_1) + \dot{v} c_1 - \dot{w} s_2 s_1]^2 \\ & + [x\dot{\Phi}_2^{(k)} c_2 - w\dot{\Phi}_2^{(k)} s_2 + \dot{v} c_1 + \dot{w} c_2]^2 \} dx + \frac{1}{2} \int_{x_e}^{x_{e+1}} \rho_k J_k (x(\dot{\Theta}_0^{(k)} + \dot{\Theta} + \dot{\Phi}_1^{(k)} s_2)^2 dx \end{aligned} \tag{5.58}$$

KEE_{SRe}^k, given by equation (5.59), presents the kinetic energy resulting from interaction of the linear motion of the origin and the motion of the virtual single link.

$$
\begin{aligned}
KEE_{SR_e}^{k} = & \int_{x_e}^{x_{e+1}} \rho_k A_k \{ \dot{R}_x^{(k)} [x(-\dot{\Phi}_2^{(k)} s_2 c_1 - \dot{\Phi}_1^{(k)} c_2 s_1) - v\dot{\Phi}_1^{(k)} c_1 + w(-\dot{\Phi}_2^{(k)} c_2 c_1 + \dot{\Phi}_1^{(k)} s_2 s_1) - \dot{v} s_1 - \dot{w} s_2 c_1] \\
& + \dot{R}_y^{k} [x(-\dot{\Phi}_2^{(k)} s_2 s_1 + \dot{\Phi}_1^{(k)} c_2 c_1) - v\dot{\Phi}_1^{(k)} s_1 - w(\dot{\Phi}_2^{(k)} c_2 s_1 + \dot{\Phi}_1^{(k)} s_2 c_1) + \dot{v} c_1 - \dot{w} s_2 s_1] \\
& + \dot{R}_z^{k} [x\dot{\Phi}_2^{(k)} c_2 - w\dot{\Phi}_2^{(k)} s_2 + \dot{v} c_1 + \dot{w} c_2]\} dx
\end{aligned}
\tag{5.59}
$$

Similarly PEE_{Re}^{k} and PEE_{Se}^{k} can be written in the following forms:

$$
PEE_{Re}^{k} = \int_{x_e}^{x_{e+1}} \rho_k A_k g R_z^k dx \tag{5.60}
$$

$$
\begin{aligned}
PEE_{Se}^{k} = & \int_{x_e}^{x_{e+1}} \rho_k A_k g (x s_2 + w c_2) dx + \frac{1}{2} \int_{x_e}^{x_{e+1}} E_k I_z^k \left(\frac{\partial^2 v}{\partial x^2}\right)^2 dx \\
& + \frac{1}{2} \int_{x_e}^{x_{e+1}} E_k I_y^k \left(\frac{\partial^2 w}{\partial x^2}\right)^2 dx + \frac{1}{2} \int_{x_e}^{x_{e+1}} G_k J_k \left(\frac{\partial \Theta}{\partial x}\right)^2 dx]
\end{aligned}
\tag{5.61}
$$

Based on the Lagrangian approach the following expressions corresponding to rigid degrees of freedom $\Phi_1^{(k)}$ and $\Phi_2^{(k)}$, can be obtained.

$$
\begin{aligned}
\frac{d}{dt}\left(\frac{\partial KEE_{Se}^{k}}{\partial \dot{\Phi}_1^{(k)}}\right) - \frac{\partial KEE_{Se}^{k}}{\partial \Phi_1^{(k)}} = & [\int_{x_e}^{x_{e+1}} \rho_k A_k (x^2 c_2^2 - 2x c_2 s_2 w + v^2 + w^2 {s_2}^2) dx] \ddot{\Phi}_1^{(k)} \\
& + [\int_{x_e}^{x_{e+1}} \rho_k A_k (x v s_2 + v w c_2) dx] \ddot{\Phi}_2^{(k)} + \sum_{i=-1}^{2} [\int_{x_e}^{x_{e+1}} \rho_k A_k N_{i+2} (x c_2 - w s_2) dx] \ddot{v}_{2e+i} \\
& + \sum_{i=-1}^{2} [\int_{x_e}^{x_{e+1}} \rho_k A_k N_{i+2} v s_2 dx] \ddot{w}_{2e+i} + (s_2 \ddot{\Theta}_0^{(k)} + {s_2}^2 \ddot{\Phi}_1^{(k)}) \int_{x_e}^{x_{e+1}} \rho_k J_k dx \\
& + s_2 \int_{x_e}^{x_{e+1}} \rho_k J_k \left(\sum_{j=0}^{1} NL_{j+1} \ddot{\Theta}_{e+j}\right) dx + f_{v1}
\end{aligned}
\tag{5.62}
$$

where N_{i+2} and NL_{j+1} are Hermite and linear shape functions. f_{v1} presents quadratic velocity terms given by

$$
\begin{aligned}
f_{r1} = & \int_{x_e}^{x_{e+1}} \rho_k A_k \dot{\Phi}_1^{(k)} \dot{\Phi}_2^{(k)} [-2x^2 c_2 s_2 - 2xw(c_2{}^2 - s_2{}^2) + 2w^2 s_2 c_2] dx \\
& + \int_{x_e}^{x_{e+1}} \rho_k A_k (\dot{\Phi}_2^{(k)})^2 (x v c_2 - v w s_2) dx \\
& + \int_{x_e}^{x_{e+1}} \rho_k A_k (-x \dot{w} \dot{\Phi}_1^{(k)} c_2 s_2 + 2v\dot{v}\dot{\Phi}_1^{(k)} + 2v\dot{w} c_2 \dot{\Phi}_2^{(k)} - x\dot{w}\dot{\Phi}_2^{(k)} s_2 c_2 + 2w\dot{w}\dot{\Phi}_1^{(k)} s_2^2) dx \\
& + 2 s_2 c_2 \dot{\Phi}_1^{(k)} \dot{\Phi}_2^{(k)} \int_{x_e}^{x_{e+1}} \rho_k J_k dx
\end{aligned}
\tag{5.63}
$$

Similarly, we have

$$
\begin{aligned}
\frac{d}{dt}\left(\frac{\partial KEE_{Se}^k}{\partial \dot{\Phi}_2^{(k)}}\right) - \frac{\partial KEE_{Se}^k}{\partial \Phi_2^{(k)}} = & \left[\int_{x_e}^{x_{e+1}} \rho_k A_k (x v s_2 + v w c_2) dx \right] \ddot{\Phi}_1^{(k)} \\
& + \left[\int_{x_e}^{x_{e+1}} \rho_k A_k (x^2 + w^2) dx \right] \ddot{\Phi}_2^{(k)} + \sum_{i=-1}^{2} \left[\int_{x_e}^{x_{e+1}} \rho_k A_k x N_{i+2} dx \right] \ddot{w}_{2e+i} + f_{r2}
\end{aligned}
\tag{5.64}
$$

in which

$$
\begin{aligned}
f_{r2} = & \int_{x_e}^{x_{e+1}} \rho_k A_k (\dot{\Phi}_1^{(k)})^2 [x^2 c_2 s_2 + xw(c_2{}^2 - s_2{}^2) - w^2 s_2 c_2] dx \\
& + \int_{x_e}^{x_{e+1}} \rho_k A_k \dot{\Phi}_1^{(k)} (2x\dot{v} s_2 + 2\dot{v} w c_2) dx \\
& + \int_{x_e}^{x_{e+1}} \rho_k A_k \dot{\Phi}_2^{(k)} (2w\dot{w}) dx - \int_{x_e}^{x_{e+1}} \rho_k J_k c_2 \dot{\Phi}_1^{(k)} (\dot{\Theta}_0^{(k)} + \dot{\Theta} + \dot{\Phi}_1^{(k)} s_2) dx
\end{aligned}
\tag{5.65}
$$

Including nodal values of v, w, and Θ of each element e in two first terms of Lagrange equation, for each i=-1,0,1,2, we have

$$\frac{d}{dt}\left(\frac{\partial KEE_{Se}^{k}}{\partial \dot{v}_{2e+i}}\right)-\frac{\partial KEE_{Se}^{k}}{\partial v_{2e+i}}= \int_{x_e}^{x_{e+1}} \rho_k A_k N_{i+2}\left(\sum_{j=-1}^{2} N_{j+2}\ddot{v}_{2e-j}\right)dx$$
$$+\left[\int_{x_e}^{x_{e+1}} \rho_k A_k N_{i+2}(xc_2 - ws_2)dx\right]\ddot{\Phi}_1^{(k)}$$
$$+\sum_{i=-1}^{2}\left[\int_{x_e}^{x_{e+1}} \rho_k A_k N_{i+2}(-2xs_2\dot{\Phi}_1^{(k)}\dot{\Phi}_1^{(k)} - 2\dot{w}s_2\dot{\Phi}_1^{(k)} - 2wc_2\dot{\Phi}_1^{(k)}\dot{\Phi}_1^{(k)})dx\right] \tag{5.66}$$
$$-(\dot{\Phi}_1^{(k)})^2 \int_{x_e}^{x_{e+1}} \rho_k A_k N_{i+2}\left(\sum_{j=-1}^{2} N_{j+2}v_{2e+j}\right)dx$$

$$\frac{d}{dt}\left(\frac{\partial KEE_{Se}^{k}}{\partial \dot{w}_{2e+i}}\right)-\frac{\partial KEE_{Se}^{k}}{\partial w_{2e+i}}= \int_{x_e}^{x_{e+1}} \rho_k A_k N_{i+2}\left(\sum_{j=-1}^{2} N_{j+2}\ddot{w}_{2e-j}\right)dx$$
$$+\left[\int_{x_e}^{x_{e+1}} \rho_k A_k N_{i+2}vs_2\, dx\right]\ddot{\Phi}_1^{(k)} + \left[\int_{x_e}^{x_{e+1}} \rho_k A_k N_{i+2}x\, dx\right]\ddot{\Phi}_2^{(k)}$$
$$-\left[s_2^{\,2}(\dot{\Phi}_1^{(k)})^2 + (\dot{\Phi}_2^{(k)})^2\right] \int_{x_e}^{x_{e+1}} \rho_k A_k N_{i+2}\left(\sum_{j=-1}^{2} N_{j+2}w_{2e+j}\right)dx \tag{5.67}$$
$$+ \int_{x_e}^{x_{e+1}} \rho_k A_k N_{i+2}\left[xs_2c_2(\dot{\Phi}_1^{(k)})^2 + 2\dot{\Phi}_1^{(k)}s_2\left(\sum_{j=-1}^{2} N_{j+2}\dot{v}_{2e+j}\right)\right]dx$$

and for l=0,1

$$\frac{d}{dt}\left(\frac{\partial KEE_{Se}^{k}}{\partial \dot{\Theta}_{e+l}}\right)-\frac{\partial KEE_{Se}^{k}}{\partial \Theta_{e+l}}= \int_{x_e}^{x_{e+1}} \rho_k J_k NL_{l+1}\left[(\ddot{\Theta}_0^{(k)} + s_2^{\,2}\ddot{\Phi}_1^{(k)}) + 2s_2c_2\dot{\Phi}_1^{(k)}\dot{\Phi}_2^{(k)}\right]dx$$
$$+ \int_{x_e}^{x_{e+1}} \rho_k J_k NL_{l+1}\left(\sum_{j=0}^{1} NL_{j+1}\ddot{\Theta}_{e+j}\right)dx \tag{5.68}$$

where NL_{j+1} are linear shape functions.

We can also write the following expression corresponding to $\Theta_0^{(k)}$

$$\frac{d}{dt}\left(\frac{\partial KEE_{Se}^{k}}{\partial \dot{\Theta}_0^{(k)}}\right)-\frac{\partial KEE_{Se}^{k}}{\partial \Theta_0^{(k)}}= \int_{x_e}^{x_{e+1}} \rho_k J_k(\ddot{\Theta}_0^{(k)} + s_2^{\,2}\ddot{\Phi}_1^{(k)} + 2s_2c_2\dot{\Phi}_1^{(k)}\dot{\Phi}_2^{(k)})dx$$
$$+ \int_{x_e}^{x_{e+1}} \rho_k J_k\left(\sum_{j=0}^{1} NL_{j+1}\ddot{\Theta}_{e+j}\right)dx \tag{5.69}$$

By differentiation of the element potential energy PEE_{Se}^{k} with respect to various degrees of freedom, the following expressions are found.

$$\frac{\partial PEE_{Se}^{k}}{\partial \Phi_1^{(k)}} = 0 \tag{5.70}$$

$$\frac{\partial PEE_{Se}^{k}}{\partial \Phi_2^{(k)}} = \int_{x_e}^{x_{e+1}} \rho_k A_k g(xc_2 - ws_2)dx \tag{5.71}$$

$$\frac{\partial PEE_{Se}^{k}}{\partial v_{2e+i}} = \int_{x_e}^{x_{e+1}} E_k I_z^k N''_{i+2}(\sum_{j=-1}^{2} N''_{j+2} v_{2e+j})dx, \qquad i = -1,0,1,2 \tag{5.72}$$

$$\frac{\partial PEE_{Se}^{k}}{\partial w_{2e+i}} = \int_{x_e}^{x_{e+1}} E_k I_y^k N''_{i+2}(\sum_{j=-1}^{2} N''_{j+2} w_{2e+j})dx + \int_{x_e}^{x_{e+1}} \rho_k A_k g N_{i+2} c_2 dx, \qquad i = -1,0,1,2 \tag{5.73}$$

$$\frac{\partial PEE_{Se}^{k}}{\partial \Theta_{e+l}} = \int_{x_e}^{x_{e+1}} G_k J_k NL'_{l+1}(\sum_{j=0}^{1} NL_{j+1} \theta_{e+j})dx \tag{5.74}$$

in which (') and ('') denote the first derivative and the second derivative with respect to x, respectively.

Using the above expressions, we can construct the elemental mass and stiffness matrices and the load vector for each link.

5.3.4.1.1 Elemental Mass Matrix M_{Se}^{k}

Mass matrix of each element can be shown by the following 14X14 matrix which is partitioned into various submatrices:

$$M_{Se}^{k}=\begin{bmatrix} [M_R^e]_{2X2} & [M_{Rv}^e]_{2X4} & [M_{Rw}^e]_{2X4} & [M_{R\theta_0}^e]_{2X1} & [M_{R\theta}^e]_{2X2} & [0]_{2X1} \\ & [M_v^e]_{4X4} & [0]_{4X4} & [0]_{4X1} & [0]_{4X2} & [0]_{4X1} \\ & & [M_w^e]_{4X4} & [0]_{4X1} & [0]_{4X2} & [0]_{4X1} \\ & & & [M_{\theta_0}^e]_{1X1} & [M_{\theta_0\theta}^e]_{1X2} & [0]_{1X1} \\ & & & & [M_\theta^e]_{2X2} & [0]_{2X1} \\ \mathit{Symmetric} & & & & & [0]_{1X1} \end{bmatrix} \tag{5.75}$$

in which the elements of submatrix M_R^e associated with $\Phi_1^{(k)}$ and $\Phi_2^{(k)}$ are

$$M_R^e(1,1)=\int_{x_e}^{x_{e+1}}\rho_k A_k(x^2c_2^2-2xc_2s_2w+v^2+w^2{s_2}^2)dx \tag{5.76}$$

$$M_R^e(1,2)=M_R^e(2,1)=\int_{x_e}^{x_{e+1}}\rho_k A_k(xvs_2+vwc_2)dx \tag{5.77}$$

$$M_R^e(2,2)=\int_{x_e}^{x_{e+1}}\rho_k A_k(x^2+w^2)dx \tag{5.78}$$

The components of other sub-matrices, shown in equation (5.75), can be written as:

$$M_{Rv}^e(1,j)=\int_{x_e}^{x_{e+1}}\rho_k A_k N_j(xc_2-ws_2)dx \tag{5.79}$$

$$M_{Rv}^e(2,j)=0 \tag{5.80}$$

$$M_{Rw}^e(1,j)=\int_{x_e}^{x_{e+1}}\rho_k A_k N_j vs_2 dx \tag{5.81}$$

$$M_{Rw}^e(2,j)=\int_{x_e}^{x_{e+1}}\rho_k A_k N_j dx \tag{5.82}$$

in which j=1,2,3,4.

The elemental mass matrices regarding elastic degrees of freedom v, w, and Θ are classic bending and rotational mass matrices used in structural dynamics for beam elements.

$$M_v^e = M_w^e = \frac{\rho_k A_k h_k}{420}\begin{bmatrix} 156 & 22h_k & 54 & -13h_k \\ 22h_k & 4h_k^2 & 13h_k & -3h_k \\ 54 & 13h_k & 156 & -22h_k \\ -13h_k & -3h_k & -22h_k & 4h_k^2 \end{bmatrix} \tag{5.83}$$

$$M_\Theta^e = \frac{\rho_k J_k h_k}{6}\begin{bmatrix} 2 & 1 \\ 1 & 2 \end{bmatrix} \tag{5.84}$$

where h_k is the length of a uniform element e of link k.

The 1X1 and 1X2 mass matrices resulting from rigid rotation of the clamped end of link k are

$$M_{\Theta_0}^e = \int_{x_e}^{x_{e+1}} \rho_k J_k dx \tag{5.85}$$

$$M_{\Theta_0\Theta}^e(1,j) = \int_{x_e}^{x_{e+1}} \rho_k J_k NL_j dx, \qquad j=1,2 \tag{5.86}$$

N_j and NL_j in equations (5.79-82) and (5.86) are Hermite and linear shape functions.

It is worth mentioning that the last column and row of the elemental mass matrix are zero due to the fact that the rigid degree of freedom $\gamma^{(k)}$ is not an independent variable but it is a redundant degree of freedom. The aforementioned degree of freedom was defined as the angle between tangent lines to two links k and k+1 at their common point.

5.3.4.1.2 Elemental Stiffness Matrix K_{Se}^k

The stiffness matrix of each element (K_{Se}^k) can be divided into two parts Ke_{Se}^k

and $\mathbf{Kr}_{Se}{}^{k}$. $\mathbf{Ke}_{Se}{}^{k}$ is normal stiffness matrix due to elasticity of the link in bending and torsion. Stiffness matrix $\mathbf{Kr}_{Sf}{}^{e}$ is due to the centrifugal effects. The elements of this matrix are obtained by differentiating the link kinetic energy with respect to the nodal values of the elastic deflections. These two parts are shown as:

$$Ke_{Se}^{k}=\begin{bmatrix} [0]_{2X2} & [0]_{2X4} & [0]_{2X4} & [0]_{2X1} & [0]_{2X2} & [0]_{2X1} \\ & [K_v^e]_{4X4} & [0]_{4X4} & [0]_{4X1} & [0]_{4X2} & [0]_{4X1} \\ & & [K_w^e]_{4X4} & [0]_{4X1} & [0]_{4X2} & [0]_{4X1} \\ & & & [0]_{1X1} & [0]_{1X2} & [0]_{1X1} \\ & & & & [K_\theta^e]_{2X2} & [0]_{2X1} \\ Symmetric & & & & & [0]_{1X1} \end{bmatrix} \tag{5.87}$$

and

$$Kr_{Se}^{k}=\begin{bmatrix} [0]_{2X2} & [0]_{2X4} & [0]_{2X4} & [0]_{2X1} & [0]_{2X2} & [0]_{2X1} \\ & -(\dot{\Phi}_1^k)^2[M_v^e]_{4X4} & [0]_{4X4} & [0]_{4X1} & [0]_{4X2} & [0]_{4X1} \\ & & -[s_2{}^2(\dot{\Phi}_1^k)^2+(\dot{\Phi}_2^k)^2][M_w^e]_{4X4} & [0]_{4X1} & [0]_{4X2} & [0]_{4X1} \\ & & & [0]_{1X1} & [0]_{1X2} & [0]_{1X1} \\ & & & & [0]_{2X2} & [0]_{2X1} \\ Symmetric & & & & & [0]_{1X1} \end{bmatrix} \tag{5.88}$$

As equation (5.88) shows, $\mathbf{Kr}_{Sf}{}^{k}$ is nonlinear in terms of rigid degrees of freedom $\Phi_1{}^{(k)}$ and $\Phi_2{}^{(k)}$. Various submatrices in the equation (5.87) are

$$K_v^e=\frac{E_k I_z^k}{h_k^3}\begin{bmatrix} 12 & 6h_k & -12 & 6h_k \\ & 4h_k^2 & -6h_k & 2h_k^2 \\ & & 12 & -6h_k \\ Symmetric & & & 4h_k^2 \end{bmatrix} \tag{5.89}$$

$$K_w^e=\frac{I_y^k}{I_z^k}K_v^e \tag{5.90}$$

$$K_\theta^e=\frac{G_k J_k}{h_k}\begin{bmatrix} 1 & -1 \\ -1 & 1 \end{bmatrix} \tag{5.91}$$

5.3.4.1.3 Elemental Load Vector Qv_{Se}^k

The load vector for each element can be defined as:

$$Qv_{Se}^k = \left\{ \{f_R^e\}_{2X1} \quad \{f_v^e\}_{4X1} \quad \{f_w^e\}_{4X1} \quad \{f_{\Theta_0}^e\}_{1X1} \quad \{f_\Theta^e\}_{2X1} \quad \{0\}_{1X1} \right\}^T \tag{5.92}$$

in which

$$f_R^e(1,1) = -f_{v1} \tag{5.93}$$

$$f_R^e(2,1) = -f_{v2} - \int_{x_e}^{x_{e+1}} \rho_k A_k g(xc_2 - ws_2)dx \tag{5.94}$$

$$f_v^e(j) = 2 \int_{x_e}^{x_{e+1}} \rho_k A_k N_j (xs_2 \dot{\Phi}_1^{(k)} \dot{\Phi}_2^{(k)} + \dot{w} s_2 \dot{\Phi}_1^{(k)} + wc_2 \dot{\Phi}_1^{(k)} \dot{\Phi}_2^{(k)})dx, \quad j = 1,2,3,4 \tag{5.95}$$

$$f_w^e(j) = - \int_{x_e}^{x_{e+1}} \rho_k A_k N_j [2\dot{v} s_2 \dot{\Phi}_1^{(k)} + x(\dot{\Phi}_1^{(k)})^2 c_2 s_2 + gc_2]dx, \quad j = 1,2,3,4 \tag{5.96}$$

$$f_{\Theta_0}^e(1,1) = -2s_2 c_2 \dot{\Phi}_1^{(k)} \dot{\Phi}_2^{(k)} \int_{x_e}^{x_{e+1}} \rho_k J_k dx \tag{5.97}$$

$$f_\Theta^e(j,1) = -2s_2 c_2 \dot{\Phi}_1^{(k)} \dot{\Phi}_2^{(k)} \int_{x_e}^{x_{e+1}} \rho_k J_k NL_j dx, \qquad j = 1,2 \tag{5.98}$$

where f_{v1} and f_{v2} used in equations (5.93) and (5.94) were introduced in equations (5.63) and (5.65), respectively.

5.3.4.1.4 Elements of M_{Re}^k, Qv_{Re}^k, and M_{SRe}^k

In this section the submatrices and subvectors resulting from the movement of the origin of each link are found. Together with those found in the previous section, they can be used to construct the global matrices and vectors of each link. From the following expression of Lagrange equations, we have

$$\frac{d}{dt}\left(\frac{\partial KEE_{Re}^{k}}{\partial \dot{P}}\right)=\left(\int_{x_e}^{x_{e+1}} \rho_k A_k dx\right)\ddot{P} \tag{5.99}$$

in which P is chosen as one of R_x^k, R_y^k, and R_z^k. M_{Re}^k can be obtained in the following form:

$$M_{Re}^{k}=\begin{bmatrix} \int_{x_e}^{x_{e+1}} \rho_k A_k dx & 0 & 0 \\ 0 & \int_{x_e}^{x_{e+1}} \rho_k A_k dx & 0 \\ 0 & 0 & \int_{x_e}^{x_{e+1}} \rho_k A_k dx \end{bmatrix} \tag{5.100}$$

Also the load vector Qv_{Re}^k due to the gravity effect corresponding to motion of the origin of the link k can be obtained as:

$$Qv_{Re}^{k}=\begin{Bmatrix} 0 \\ 0 \\ -g\int_{x_e}^{x_{e+1}} \rho_k A_k dx \end{Bmatrix} \tag{5.101}$$

The remaining parts of link matrices and vectors are obtained by considering KEE_{RSe}^k in Lagrange equations.

$$\frac{d}{dt}\left(\frac{\partial KEE^k_{RSe}}{\partial \dot{R}^k_x}\right)-\frac{\partial KE^k_{RSe}}{\partial R^k_x}= \int_{x_e}^{x_{e+1}}\rho_k A_k [(-xc_2s_1-vc_1+ws_2s_1)\ddot{\Phi}_1^{(k)}$$
$$+(-xs_2c_1-wc_2c_1)\ddot{\Phi}_2^{(k)}-s_1\ddot{v}-s_2c_1\ddot{w})]dx \tag{5.102}$$
$$+\int_{x_e}^{x_{e+1}}\rho_k A_k [(\dot{\Phi}_1^{(k)})^2(-xc_2c_1+vs_1+ws_2c_1)+(\dot{\Phi}_2^{(k)})^2(-xc_2c_1+ws_2c_1)$$
$$+2\dot{\Phi}_1^{(k)}\dot{\Phi}_2^{(k)}(xs_2s_1+wc_2s_1)-2\dot{v}\dot{\Phi}_1^{(k)}c_1+2\dot{w}(-\dot{\Phi}_2^{(k)}c_2c_1+\dot{\Phi}_1^{(k)}s_2s_1)]dx$$

$$\frac{d}{dt}\left(\frac{\partial KEE^k_{REe}}{\partial \dot{R}^k_y}\right)-\frac{\partial KEE^k_{RSe}}{\partial R^k_y}= \int_{x_e}^{x_{e+1}}\rho_k A_k [(xc_2c_1-vs_1-ws_2c_1)\ddot{\Phi}_1^{(k)}$$
$$+(-xs_2s_1-wc_2s_1)\ddot{\Phi}_2^{(k)}+s_1\ddot{v}-s_2s_1\ddot{w})]dx \tag{5.103}$$
$$+\int_{x_e}^{x_{e+1}}\rho_k A_k [(\dot{\Phi}_1^{(k)})^2(-xc_2s_1-vc_1+ws_2s_1)+(\dot{\Phi}_2^{(k)})^2(-xc_2s_1+ws_2s_1)$$
$$-2\dot{\Phi}_1^{(k)}\dot{\Phi}_2^{(k)}(xs_2c_1+wc_2c_1)-2\dot{v}\dot{\Phi}_1^{(k)}s_1+2\dot{w}(-\dot{\Phi}_2^{(k)}c_2s_1-\dot{\Phi}_1^{(k)}s_2c_1)]dx$$

$$\frac{d}{dt}\left(\frac{\partial KEE^k_{RSe}}{\partial \dot{R}^k_z}\right)-\frac{\partial KE^k_{RSe}}{\partial R^k_z}= \int_{x_e}^{x_{e+1}}\rho_k A_k [(xc_2-ws_2)\ddot{\Phi}_2^{(k)}+c_2\ddot{w})]dx \tag{5.104}$$
$$+\int_{x_e}^{x_{e+1}}\rho_k A_k [(\dot{\Phi}_2^{(k)})^2(-xs_2-wc_2)-2\dot{w}\dot{\Phi}_2^{(k)}s_2]dx$$

$$\frac{d}{dt}\left(\frac{\partial KEE^k_{RSe}}{\partial \dot{\Phi}_1^{(k)}}\right)-\frac{\partial KEE^k_{RSe}}{\partial \Phi_1^{(k)}}= \int_{x_e}^{x_{e+1}}\rho_k A_k [(-xc_2s_1-vc_1+ws_2s_1)\ddot{R}^k_x \tag{5.105}$$
$$+(xc_2c_1-vs_1-ws_2c_1)\ddot{R}^k_y]dx$$

$$\frac{d}{dt}\left(\frac{\partial KEE^k_{RSe}}{\partial \dot{\Phi}_2^{(k)}}\right)-\frac{\partial KEE^k_{RSe}}{\partial \Phi_2^{(k)}}= \int_{x_e}^{x_{e+1}}\rho_k A_k [(-xs_2s_1-wc_2c_1)\ddot{R}^k_x \tag{5.106}$$
$$+(-xs_2s_1-wc_2s_1)\ddot{R}^k_y+(xc_2-ws_2)\ddot{R}^k_z]dx$$

The elements of mass matrix $M_{SRe}{}^k$ can be presented in the following forms:

$$M^k_{SRe}(1,1)= \int_{x_e}^{x_{e+1}}\rho_k A_k(-xc_2s_1-vc_1+ws_2s_1)dx \tag{5.107}$$

$$M^{k}_{SRe}(1,2) = \int_{x_e}^{x_{e+1}} \rho_k A_k (x c_2 c_1 - v s_1 - w s_2 c_1) dx \tag{5.108}$$

$$M^{k}_{SRe}(1,3) = 0 \tag{5.109}$$

$$M^{k}_{SRe}(2,1) = \int_{x_e}^{x_{e+1}} \rho_k A_k (-x s_2 c_1 - w c_2 c_1) dx \tag{5.110}$$

$$M^{k}_{SRe}(2,2) = \int_{x_e}^{x_{e+1}} \rho_k A_k (-x s_2 s_1 - w c_2 s_1) dx \tag{5.111}$$

$$M^{k}_{SRe}(2,3) = \int_{x_{e+1}}^{x_{e+1}} \rho_k A_k (x c_2 - w s_2) dx \tag{5.112}$$

The elements of 3X1 vector Qv_{Re}^{k} corresponding to coordinates: R_x^k, R_y^k, R_z^k are

$$\begin{aligned} Qv^{k}_{Re}(1) = - \int_{x_e}^{x_{e+1}} \rho_k A_k \Big[& (\dot{\Phi}_1^{(k)})^2 (-x c_2 c_1 + v s_1 + w s_2 c_1) + (\dot{\Phi}_2^{(k)})^2 (-x c_2 c_1 + w s_2 c_1) \\ & + 2\dot{\Phi}_1^{(k)} \dot{\Phi}_2^{(k)} (x s_2 s_1 + w c_2 s_1) - 2\dot{v}\dot{\Phi}_1^{(k)} c_1 + 2\dot{w}(-\dot{\Phi}_2^{(k)} c_2 c_1 + \dot{\Phi}_1^{(k)} s_2 s_1) \Big] dx \end{aligned} \tag{5.113}$$

$$\begin{aligned} Qv^{k}_{Re}(2) = - \int_{x_e}^{x_{e+1}} \rho_k A_k \Big[& (\dot{\Phi}_1^{(k)})^2 (-x c_2 s_1 - v c_1 + w s_2 s_1) + (\dot{\Phi}_2^{(k)})^2 (-x c_2 s_1 + w s_2 s_1) \\ & - 2\dot{\Phi}_1^{(k)} \dot{\Phi}_2^{(k)} (x s_2 c_1 + w c_2 c_1) - 2\dot{v}\dot{\Phi}_1^{(k)} s_1 + 2\dot{w}(-\dot{\Phi}_2^{(k)} c_2 s_1 - \dot{\Phi}_1^{(k)} s_2 c_1) \Big] dx \end{aligned} \tag{5.114}$$

$$Qv^{k}_{Re}(3) = - \int_{x_e}^{x_{e+1}} \rho_k A_k \Big[(\dot{\Phi}_2^{(k)})^2 (-x s_2 - w c_2) - 2\dot{w}\dot{\Phi}_2^{(k)} s_2 \Big] dx - \int_{x_e}^{x_{e+1}} \rho_k A_k g dx \tag{5.115}$$

For each element e for i=-1,0,1,2, we can write the following equations:

$$\frac{d}{dt}\left(\frac{\partial KEE^{k}_{RSe}}{\partial \dot{v}_{2e+i}}\right) - \frac{\partial KEE^{k}_{RSe}}{\partial v_{2e+i}} = (-s_1 \ddot{R}^{k}_{x} + c_1 \ddot{R}^{k}_{y}) \int_{x_e}^{x_{e+1}} \rho_k A_k N_{i+2} dx \tag{5.116}$$

$$\frac{d}{dt}\left(\frac{\partial KEE^{k}_{RSe}}{\partial \dot{w}_{2e+i}}\right) - \frac{\partial KEE^{k}_{RSe}}{\partial w_{2e+i}} = (-s_2 c_1 \ddot{R}^{k}_{x} - s_2 s_1 \ddot{R}^{k}_{y} + c_2 \ddot{R}^{k}_{z}) \int_{x_e}^{x_{e+1}} \rho_k A_k N_{i+2} dx \tag{5.117}$$

which can be used to obtain mass elements corresponding to nodal bending degrees of freedom v and w, respectively. Equations (5.118) to (5.122) give these elements for i=-1,0,1,2.

$$M^k_{S\,Re}(i+4,1) = -s_1 \int_{x_e}^{x_{e+1}} \rho_k A_k N_{i+2}\,dx \tag{5.118}$$

$$M^k_{S\,Re}(i+4,2) = c_1 \int_{x_e}^{x_{e+1}} \rho_k A_k N_{i+2}\,dx \tag{5.119}$$

$$M^k_{S\,Re}(i+7,1) = -s_2 c_1 \int_{x_e}^{x_{e+1}} \rho_k A_k N_{i+2}\,dx \tag{5.120}$$

$$M^k_{S\,Re}(i+7,2) = -s_2 s_1 \int_{x_e}^{x_{e+1}} \rho_k A_k N_{i+2}\,dx \tag{5.121}$$

$$M^k_{S\,Re}(i+7,3) = c_2 \int_{x_e}^{x_{e+1}} \rho_k A_k N_{i+2}\,dx \tag{5.122}$$

5.3.4.2 Link Matrices and Vectors

By assembling the elemental matrices and load vectors derived in the previous sections, the main parts of the link matrices and the load vectors can be found. Since the origin of each link is considered to be clamped in its local coordinate system, all of the elastic degrees of freedom at the first node of the first element of each link, namely, v_1, v_2, w_1, w_2, and Θ_1, are zero. Therefore, we can take into account this boundary conditions simply by eliminating corresponding rows of the link load vector and corresponding rows and columns of the link mass and stiffness matrices.

Each link k (k>1) has $10+5N_k$ degrees of freedom. They can be divided into two parts. $\Phi_1^{(k)}$, $\Phi_2^{(k)}$, $\Psi_1^{(k)}$, $\Psi_2^{(k)}$, $\Theta_0^{(k)}$, q_k, R_x^k, R_y^k, R_z^k, and $\gamma^{(k)}$ are 10 degrees of freedom which correspond to the rigid body motion of the link, while remaining $5N_k$ degrees of freedom correspond to the discretized bending deformations in the local y_k and z_k

directions and the discretized torsional deformation along the local x_k axis. It should be mentioned that variables $\Theta_0^{(k)}$, R_x^k, R_y^k, R_z^k, and $\gamma^{(k)}$ must not be taken into consideration for the first link. Without loss of generality, mass and stiffness matrices as well as load vector of each link can be partitioned in the following forms:

$$M_l^k = \begin{bmatrix} \left[M_{jj}^k\right]_{(3)X(3)} & \left[M_{jl}\right]_{(3)X(7+5N_k)} \\ \left[M_{lj}\right]_{(3+7N_k)X(3+5)} & \left[M_{ll}^k\right]_{(7+5N_k)X(7+5N_k)} \end{bmatrix} \tag{5.123}$$

$$K_l^k = \begin{bmatrix} \left[K_{jj}^k\right]_{(3)X(3)} & \left[K_{jl}\right]_{(3)X(7+5N_k)} \\ \left[K_{lj}\right]_{(3+7N_k)X(3+5)} & \left[K_{ll}^k\right]_{(7+5N_k)X(7+5N_k)} \end{bmatrix} \tag{5.124}$$

$$Qv_l^k = \begin{Bmatrix} \left\{Qv_{jj}^k\right\}_{(3)X(1)} \\ \left\{Qv_{ll}^k\right\}_{(3+7N_k)X(1)} \end{Bmatrix} \tag{5.125}$$

in which subscripts j and l are used to present the contribution of joint variables ($\Psi_1^{(k)}$, $\Psi_2^{(k)}$, and q_k) and link variables ($\Phi_1^{(k)}$, $\Phi_2^{(k)}$, $\Theta_0^{(k)}$, R_x^k, R_y^k, R_z^k, $\gamma^{(k)}$, $v^{(k)}$, $w^{(k)}$, and $\Theta^{(k)}$) in various parts of matrices and load vector.

Similar to the elemental matrices and load vectors, the link matrices ($\mathbf{M}_{ll}^{(k)}$, $\mathbf{K}_{ll}^{(k)}$) and vectors ($\mathbf{Qv}_{ll}^{(k)}$) can be partitioned into various matrices and vectors. For example, mass matrix $\mathbf{M}_{ll}^{(k)}$ of link k with N_k elements can be presented as follows

$$M_{ll}^k = \begin{bmatrix} \left[M_{Sl}^k\right]_{(3+5N_k)X(3+5N_k)} & \left[M_{SRl}^k\right]_{(3+5N_k)X3} & [0]_{(3+5N_k)X1} \\ & \left[M_{Rl}^k\right]_{3X3} & [0]_{3X1} \\ \textit{Symmetric} & & [0]_{1X1} \end{bmatrix} \tag{5.126}$$

in which $3+5N_k$ is the number of degrees of freedom: $\Phi_1^{(k)}$, $\Phi_2^{(k)}$, v_3 to v_{2N_k+2}, w_3 to w_{2N_k+2}, Θ_0^k and Θ_2 to Θ_{N_k+1}. All of the finite elements of link k have common degrees of freedom $\Phi_1^{(k)}$, $\Phi_2^{(k)}$, $\Theta_0^{(k)}$, R_x^k, R_y^k, R_z^k, and $\gamma^{(k)}$. The first three ones are associated with the submatrix $[M_{SI}^k]$, while the second three represent the linear motion of the origin of link k correspond to submatrix $[M_{RI}^k]$. The last one ($\gamma^{(k)}$) is associated with the last column of the mass matrix M_{II}^k. As it was mentioned earlier, all elements of that column are zero.

Matrix M_{SI}^k can be shown as

$$M_{SI}^k = \begin{bmatrix} [M_R^l]_{2X2} & [M_{Rv}^l]_{2X2N_k} & [M_{Rw}^l]_{2X2N_k} & [M_{R\Theta_0}^l]_{2X1} & [M_{R\Theta}^l]_{2XN_k} \\ & [M_v^l]_{2N_kX2N_k} & [0]_{2N_kX2N_k} & [0]_{4X1} & [0]_{4XN_k} \\ & & [M_w^l]_{2N_kX2N_k} & [0]_{4X1} & [0]_{4XN_k} \\ & & & [M_{\Theta0}^l]_{1X1} & [M_{\Theta_0\Theta}^l]_{1XN_k} \\ \mathit{Symmetric} & & & & [M_\Theta^l]_{N_kXN_k} \end{bmatrix} \tag{5.127}$$

Usual assemblage procedure is used to construct link matrices M_v^l, M_w^l, and M_θ^l from elemental matrices M_v^e, M_w^e, and M_θ^e. Application of boundary conditions corresponding to zero deflections, slopes, and rotation at the origin of x-axis of each link k, reduces the size of the matrices. For example the size of the matrix resulted from assemblage of matrices M_v^e is $(2+2N_k)X(2+2N_k)$, but after applying boundary conditions it is reduced to $2N_kX2N_k$ because at x=0, both the deflection (v) and the slope (v') are zero. In finding the first two rows (and columns) of link mass matrix the usual assemblage procedure is not applicable, this is why a special suitable approach is developed to assemble first two rows of the elemental mass matrices. The elements $M_R^k(1,1)$, $M_R^k(1,2)$, $M_R^k(2,2)$ of link matrix M_{SI}^k and the elements of link matrix M_{RI}^k can be found by the similar integrals given in equations (5.76-78) and (5-100), respectively, but by using $(0, L_k)$ instead of (x_e, x_{e+1}) as the bounds of integration. The remaining elements of the first and the second rows of the assembled matrix M_R^k and the elements of M_{SRI}^k can be obtained by assembling corresponding rows of elemental mass matrix in a columnwise manner.

Similarly $\mathbf{Ke}_{SI}{}^{k}$, $\mathbf{Kr}_{SI}{}^{k}$, and $\mathbf{Qv}_{SI}{}^{v}$ can be obtained by assembling and eliminating columns and rows corresponding to zero boundary conditions of elemental matrices $\mathbf{Ke}_{Se}{}^{k}$, $\mathbf{Kr}_{Se}{}^{k}$, and vector $\mathbf{Qv}_{Se}{}^{v}$ (equations 5.87, 5.88, and 5.92). The size of each link matrix ($\mathbf{M}_{ll}{}^{k}$ and $\mathbf{K}_{ll}{}^{k}$) and load vector ($\mathbf{Qv}_{ll}{}^{k}$) are $(3+5N_k)X(3+5N_k)$ and $(3+5N_k)X(1)$, respectively. After finding other parts of system matrices and load vector of each link k, the whole stiffness matrix $\mathbf{K}_{ll}{}^{k}$ and load vector $\mathbf{Qv}_{ll}{}^{k}$ of can be constructed.

The elements of matrices $\mathbf{M}_{jj}{}^{k}$, $\mathbf{M}_{jl}{}^{k}$, $\mathbf{K}_{jj}{}^{k}$, $\mathbf{K}_{jl}{}^{k}$ and load vector $\mathbf{Qv}_{jj}{}^{k}$ can be found by making use of different terms of Lagrange equation.

5.3.4.3 Modification of the Mass and Stiffness Matrices and the Load Vectors due to the Effects of Inertia and Stiffness of the Actuators

The kinetic and potential energies of various actuators were found in section 5.3.2. By using the following expression

$$\frac{d}{dt}\left(\frac{\partial KE_a^k}{\partial \dot{y}}\right)-\frac{\partial KE_a^k}{\partial y}+\frac{\partial PE_a^k}{\partial y} \tag{5.128}$$

the effect of mechanical properties of the actuators on the mass matrix and load vector of the whole system can be taken into account. In equation (5.128), $KE_a{}^{k}$ and $PE_a{}^{k}$ present kinetic and potential energies of the k-th actuator and y can be any of the coordinates of the system. Practically the effects of inertia and stiffness of various joints can be taken into account by modifying certain components of mass matrix $\mathbf{M}_{ll}{}^{k}$ and load vector $\mathbf{Qv}_{ll}{}^{k}$ as well as by obtaining the elements of matrices $\mathbf{M}_{jj}{}^{k}$, $\mathbf{M}_{jl}{}^{k}$, $\mathbf{K}_{jj}{}^{k}$, $\mathbf{K}_{jl}{}^{k}$ and those of load vector $\mathbf{Qv}_{jj}{}^{k}$. Since the procedure is similar to that presented in the previous sections, the details of the mathematical manipulations are not shown here.

It is worth mentioning that the effects of actuator torques will be taken into account in constructing external load vector of the manipulator system in section 5.3.2.4.

5.3.4.4 System Matrices and Load Vector

Having the mass matrix matrices, the stiffness matrices, and the load vectors of all of the links, we can create the system matrices and load vector in a straightforward manner. This can be done by assembling the matrices by simply placing them together diagonally. The resulting assembled vector consists of link load vectors which are placed together in a columnwise manner. These assemblages do not include any overlapping because each link has its own state variables. For example, the mass matrix **MS** and load vector **Qv** of the system can be constructed in the following way:

$$MS = \begin{bmatrix} M_l^1 & & & & \\ & M_l^2 & & & \\ & & \cdot & & \\ & & & M_l^k & \\ & & & & \cdot \\ & & & & & M_l^n \end{bmatrix}, \quad \mathbf{Qv} = \begin{Bmatrix} Qv_l^1 \\ Qv_l^2 \\ \cdot \\ Qv_l^k \\ \cdot \\ Qv_l^n \end{Bmatrix} \tag{5.129}$$

where $\mathbf{M}_l^k$ and $\mathbf{Qv}_l^k$ are the mass matrix and load vector of link k, respectively.

It is worthwhile noting that the dimensions of the matrices and load vector of the first link are (2+5N)X(2+5N) and (2+5N)X1, while those of other links are (10+5N)X(10+5N) and (10+5N)X1, respectively. This is due to the fact that the position vector of the origin of the local coordinate system of the first link is a zero vector.

5.3.4.5 Boundary Conditions due to the Payload

The boundary conditions due to the payload can be applied again by obtaining the expression of the left hand side of the Lagrange equation and then modifying the necessary components of the system mass matrix and the load vector. The kinetic and potential energies of the payload in terms of degrees of freedom of the system can be written as:

$$KE_p = \frac{1}{2} M_p \dot{r}_p . \dot{r}_p + \frac{1}{2} Ipz(c_2^{(n)} \dot{\Phi}_1^{(n)} + \dot{v}'_p)^2 + \frac{1}{2} Ipx(s_2^{(n)} \dot{\Phi}_1^{(n)} + \dot{\Theta}_p + \dot{\Theta}_0^{(n)})^2 \\ + \frac{1}{2} Ipy(\dot{\Phi}_2^{(n)} + \dot{w}'_p)^2 \tag{5.130}$$

$$PE_p = M_p g(R_z^n + L_n s_2^{(n)} + w_p c_2^{(n)}) \tag{5.131}$$

where M_p, Ipx, Ipy, and Ipz are payload mass and the moment of inertia of the payload about various axis of the local coordinate system of the last link. $\mathbf{r}_p$ is the absolute position vector of the payload, while w_p, v'_p, w'_p, and Θ_p are the w-deflection, the slope in the xz plane, the slope in the xy plane, and the torsional deflection of the end point of link n (the location of the payload).

5.3.4.6 Generalized Forces due to Actuator Torques

The generalized forces due to the actuator torques and damping torques in the joints can be found by using the virtual work of the nonconservative loads given by equation (5.50). As it was mentioned earlier, q_k is the angle between tangent to links k-1 and x_k^* axis at their common point o_k. Therefore, all of the effects of elastic deformations on the direction of actuator torques are taken into account automatically.

Using equation (5.50), the external load vector Qe can be constructed in the following way:

$$Qe(1) = T_b - b_b \dot{q}_b \tag{5.132}$$

$$Qe(2) = T_1 - b_1 \dot{q}_1 \tag{5.133}$$

$$
\begin{aligned}
& j \leftarrow 5+5N_1 \\
& \textbf{\textit{for}}\ \ i=2\ \ \textbf{\textit{to}}\ \ n \\
& \quad Qe(j)=T_i-b_j\dot{q}_j \\
& \quad j \leftarrow j+10+5N_i \\
& \textbf{\textit{end}}
\end{aligned}
\tag{5.134}
$$

The remaining components of the external load vector ***Qe*** are zero.

5.3.4.7 Constraints

As it was mentioned at the beginning of section (5.3.4), the following system of equations should be solved to predict the dynamic behavior of the deformable multibody systems.

$$
\begin{aligned}
& MS\ \{\ddot{q}\}+C_q^{\ T}\ \{\lambda\}=\{Qv\}+\{Qe\} \\
& C_q\ \{\ddot{q}\} \qquad\qquad\quad =\{Qc\}
\end{aligned}
\tag{5.51}
$$

This system includes the constraint equations. In the previous parts of this section, ***MS***, ***Qv***, and ***Qe*** were found for spatial flexible multi-link manipulators with flexible links and joints. Now the constraint equations are developed in order to find C_q and ***Qc***.

For each joint, except joint 1 whose linear position is fixed , ten constraint equations should be included. This is caused by introduction of ten redundant (or dependent) degrees of freedom at each joint i including: q_i, $\Psi_1^{(i)}$, $\Psi_2^{(i)}$, $\Phi_1^{(i)}$, $\Phi_2^{(i)}$, $\Theta_0^{(i)}$, R_x^i, R_y^i, R_z^i, and $\gamma^{(i)}$.

The following three equations present continuity of the global Cartesian coordinates at different joints. In other words, they show the relations between three components of position vectors of two successive joints i and i+1 for i=1,2,...,n-1.

$$
Cj^{(i+1)}(1): \quad R_x^{i+1}-R_x^i-(L_i c_2^{(i)} c_1^{(i)} - w_e^{(i)} s_2^{(i)} c_1^{(i)} - v_e^{(i)} s_1^{(i)})=0 \tag{5.135}
$$

$$Cj^{(i+1)}(2): \quad R_y^{i+1} - R_y^i - (L_i c_2^{(i)} s_1^{(i)} - w_e^{(i)} s_2^{(i)} s_1^{(i)} + v_e^{(i)} c_1^{(i)}) = 0 \quad (5.136)$$

$$Cj^{(i+1)}(3): \quad R_z^{i+1} - R_z^i - (L_i s_2^{(i)} + w_e^{(i)} c_2^{(i)}) = 0 \quad (5.137)$$

in which subscript e is used to identify the components of elastic deformations of link i at point o_{i+1}.

As it was shown is section (5.2), angles $\Phi_1^{(i+1)}$ and $\Phi_2^{(i+1)}$ can be found by using equations (5.8) and (5.9). These equations are presented here again in a different form.

$$Cj^{(i+1)}(4): \quad sin\Phi_2^{(i+1)} - n^{(i+1)} = 0 \quad (5.138)$$

$$Cj^{(i+1)}(5): \quad [(l^{(i+1)})^2 + (m^{(i+1)})^2]\ cos^2\Phi_1^{(i+1)} - (l^{(i+1)})^2 = 0 \quad (5.139)$$

The sixth constraint equation expresses the angular rotation of the origin of the link i+1 about its x_{i+1}-axis in terms of the angle $\gamma^{(i+1)}$ and the rigid and elastic rotation of the end of the link i about its x_i-axis.

$$Cj^{(i+1)}(6): \quad -\Theta_0^{(i+1)} + (\Theta_0^{(i)} + \Theta_e^{(i)})\underline{i}_i \cdot \underline{i}_{i+1} = 0 \quad (5.140)$$

where $\underline{i}_i$ and $\underline{i}_{i+1}$ are unit vectors along x_i and x_{i+1} axes, respectively.

The seventh constrain equation presents the cosine of angle $\gamma^{(i+1)}$ as dot product of two unit vectors $\underline{i}'_i$ and $\underline{i}_{i+1}$, which are tangent to links i and i+1 at their common point o_{i+1}.

$$Cj^{(i+1)}(7): \quad cos(\gamma^{(i+1)}) - \underline{i}_i' \cdot \underline{i}_{i+1} = 0 \quad (5.141)$$

Two constraint equations regarding the definition of angles $\Psi_1^{(i)}$ and $\Psi_2^{(i)}$ can be defined similar to the forth and fifth ones:

$$Cj^{(i+1)}(8): \quad sin\Psi_2^{(i+1)} - ns^{(i+1)} = 0 \quad (5.142)$$

$$Cj^{(i+1)}(9): \quad [(ls^{(i+1)})^2 + (ms^{(i+1)})^2]\ cos^2\Psi_1^{(i+1)} - (ls^{(i+1)})^2 = 0 \quad (5.143)$$

and finally the last constraint equation presents the cosine of angle q_{i+1} as dot product of two unit vectors $\underline{i}'_i$ and $\underline{i}_{i+1}^*$. As it was mentioned earlier, the first unit vector is tangent to the end of link i and the second one is along x_{k+1}^* axis shown in figure 5.4.

$$Cj^{(i+1)}(10): \quad cos(q_{i+1}) - \underline{i}_i' \cdot \underline{i}_{i+1}^* = 0 \tag{5.144}$$

To find Jacobian matrix C_q of the constraints, first we differentiate the constraints of each joint i+1 with respect to various variables to build submatrices $Cj_q^{(i+1)}$. Then by assembling these submatrices, C_q is found.

Vector Qc in equation (5.51) can be found by using following equation:

$$Qc = -[C_{tt} + (C_q \dot{q})_q \dot{q} + 2C_{qt} \dot{q}] \tag{5.145}$$

we can also find this vector by assembling subvectors, Qj_c obtained for various joints. Due to highly nonlinear and complex nature of the constraints, especially those which include unit vectors $\underline{i}'_i$ or $\underline{i}_{i+1}$, the details of derivation of C_q and Qc need many pages and patience. Therefore, interested readers are referred to the appendix for details.

It is worth mentioning that we should eliminate five columns of C_q corresponding to three components of position vector $\mathbf{R}^1$, zero $\Theta_0^{(1)}$, and zero $\gamma^{(1)}$, because the origin of the first link is attached to the origin of the inertial reference frame. Therefore, the size of non-square matrix C_q is 10(n-1)Xnv, where n and nv=n(10+5ΣN$_i$)-5 are the numbers of links and variables, respectively.

5.4 Numerical Solution

In this section a direct integration method is used to solve the problem shown by system of equations (5.51). There is a variety of direct integration methods available for solving transient problems such as finite difference, Wilson tetha, and Newmark methods. The algorithm used in this study, is one of the implicit type and chosen primarily because of its stability and accuracy under a wide range of element size and time step variations. It is based on linear acceleration scheme called Newmark type approximation.

Since many components of matrices $\boldsymbol{MS}$ and $\boldsymbol{C_q}$ and vectors $\boldsymbol{Qv}$, $\boldsymbol{Qe}$, and $\boldsymbol{Qc}$ in equation (5.51) are functions of various degrees of freedom and their time derivatives, the system of equations (5.51) can be written in the following form:

$$\begin{aligned} & MS(q_{i+1}^{(k)})\ddot{q}_{i+1}^{(k+1)} + C_q^{\,T}(q_{i+1}^{(k)})\lambda_{i+1}^{(k+1)} = Qv(q_{i+1}^{(k)},\dot{q}_{i+1}^{(k)}) + Qe(\dot{q}_{i+1}^{(k)}) \\ & C_q^{\,T}(q_{i+1}^{(k)})\ddot{q}_{i+1}^{(k+1)} = Qc(q_{i+1}^{(k)},\dot{q}_{i+1}^{(k)}) \end{aligned} \tag{5.146}$$

Due to the nonlinearities, the system must be solved iteratively at each time step. The iterative process can be performed as:

$$\begin{bmatrix} MS & C_q^T \\ C_q & 0 \end{bmatrix}_{i+1}^{(k)} \begin{Bmatrix} \ddot{q} \\ \lambda \end{Bmatrix}_{i+1}^{(k+1)} = \begin{Bmatrix} Qv + Qe \\ Qc \end{Bmatrix}_{i+1}^{(k)} \tag{5.147}$$

where subscript i+1 shows the time step number, while superscripts (k) and (k+1) present the iteration numbers at each time step. Since we need $\boldsymbol{q}$ and $\dot{\boldsymbol{q}}$ to evaluate $\boldsymbol{MS}$, $\boldsymbol{Cq}$, $\boldsymbol{Qv}$, and $\boldsymbol{Qc}$ at each iteration, it can be assumed that the acceleration varies linearly within each time interval. Therefore, the acceleration $\ddot{q}$ within each time interval Δt can be expressed by the equation:

$$\ddot{q}(t) = \ddot{q}_i + \frac{\ddot{q}_{i+1} - \ddot{q}_i}{\Delta t}(t - t_i) \tag{5.148}$$

where $\ddot{q}_i = \ddot{q}(t_i)$ and $\ddot{q}_{i+1} = \ddot{q}(t_{i+1})$. Now $\dot{q}(t)$ and $q(t)$ can be obtained by simple integration of equation (5.148),

$$\dot{q}(t) = \dot{q}_i + \ddot{q}_i(t - t_i) + \frac{\ddot{q}_{i+1} - \ddot{q}_i}{2\Delta t}(t - t_i)^2 \tag{5.149}$$

$$q(t) = q_i + \dot{q}_i(t - t_i) + \frac{1}{2}\ddot{q}_i(t - t_i)^2 + \frac{\ddot{q}_{i+1} - \ddot{q}_i}{6\Delta t}(t - t_i)^3 \tag{5.150}$$

Having q_i, $\dot{q}_i$, and $\ddot{q}_i$, we can describe q_{i+1} and $\dot{q}_{i+1}$ as functions of unknown acceleration $\ddot{q}_{i+1}$. Then by substituting the expressions for displacement and velocity vectors in the equation of motion of the system (5.147), the resulting system can be solved for unknown accelerations and Lagrange multipliers at the next time step till reaching the convergence.

5.4.1 Simulation Results

In this section some simulation results are presented in order to show the validity of the model and to illustrate the effects of link and joint flexibilities on the overall motion of the spatial flexible manipulator systems.

A three-link manipulator with the following physical parameters for its links, payload, rotors, and stators:

$$\begin{aligned}
&\rho_i A_i = 5 \quad kg/m, \quad \rho_i J_i = 0.05 \ kg.m, \ L_i = 1 \quad m \\
&Mp = 2 \quad kg, \quad Ipy = Ipz = 0.1 \quad kg.m^2, \ Ipx = 0.2 \quad kg.m^2 \\
&Ir_b = 0.05 \quad kg.m^2 \\
&Iry_i = Irz_i = 0.05 \quad kg.m^2, \ Irx_i = 0.1 \quad kg.m^2, \ mr_i = 0.2 \quad kg \\
&Isy_i = Isz_i = 0.05 \quad kg.m^2, \ Isx_i = 0.1 \quad kg.m^2, \ ms_i = 0.2 \quad kg \\
&\Gamma_b = 1, \quad \Gamma_i = 1 \\
&b_b = 0. \quad b_i = 0
\end{aligned} \tag{5.152}$$

has been considered (i=1,2,3). Different values for $E_iI_y^i$, $E_iI_z^i$, G_iJ_i, *and* K_i are used in various cases to show the effects of flexibility on the motion of the system.

Each link is divided into two elements. Therefore, the total number of degrees of freedom of the system (rigid and elastic degrees) is 54 in this examples, from which 20 degrees of freedom are redundant.

5.4.1.1 Validity of the Modeling

Very large values of $E_iI_y^i$, $E_iI_z^i$, G_iJ_i, and K_i are used to compare the results of the proposed model with those obtained from a modeling of a multi-link spatial manipulator with rigid links and joints. The initial position of the payload is chosen as: X_0=2 m, Y_0=1 m, and Z_0=0 m. The initial configuration of both rigid and flexible manipulators are found from proper inverse static algorithms. By considering constant torque T_b=250 N.m applied by the base actuator and constant torques T_1=T_2=T_3=300 N.m applied by other revolute

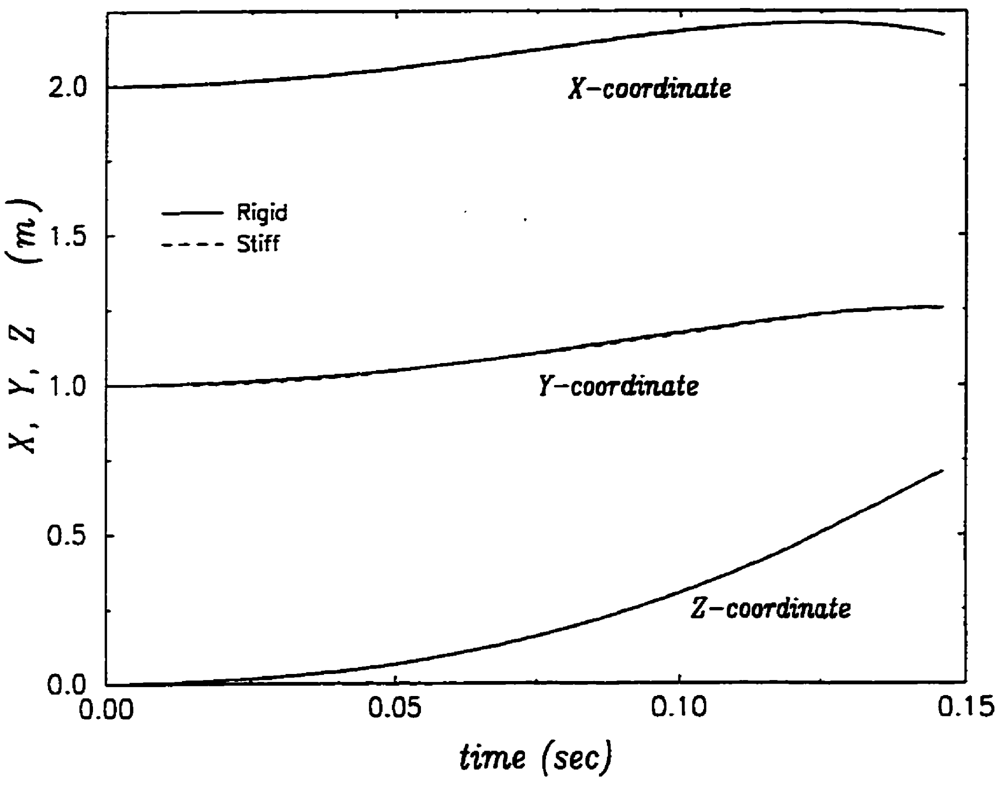

Figure 5.8 Comparison of the position of the payload of a three-link rigid manipulator with a similar flexible one with very stiff links and joints under the same loading

actuators, the motion of both systems are obtained within a finite period of time. Figure 5.8 shows X, Y, and Z coordinates of the payload of a rigid system and its counterpart stiff joints (K_i=1E6 N/rad) and links ($E_iI_y^i = E_iI_z^i = G_iJ_i$ =40000 N.m^2). As it can be seen, the response of the stiff system is completely in agreement with that of the rigid one. This shows the validity of the developed flexible model.

5.4.1.2 The Effect of Link and Joint Flexibilities on the Overall Motion of the System

In this part, the same external torques introduced in the previous section are applied to the manipulators with the same physical properties shown in equation (5.152), but different stiffness properties. The initial position of the payload in all of the cases is chosen X_0=2 m, Y_0=1 m, and Z_0=0 m. Figures 5.9, 5.10, and 5.11, respectively, show X, Y, and Z coordinates of the payload of seven similar manipulators with different joint flexibility and link flexibility in bending and torsion. G_i and E_i are related to each other in the form of $G_i = E_i/2(1+v_i)$, in which v_i is poison ratio. On the other hand, J_i can be found by $J_i=I_y^i+I_z^i$. Therefore, bending stiffnesses $E_iI_y^i$ and $E_iI_z^i$ and torsional stiffness G_iJ_i values have the same order of magnitude. However, different values are chosen in order to show the effect of bending and torsional flexibilities separately. As it can be seen, simultaneous presence of the flexural and torsional flexibilities of the links causes significant change in the dynamic behavior of the system. By comparing the end point coordinates of different manipulators with those of rigid one, we see that the effect of torsional flexibility of the links is much more significant than that of bending flexibility. On the other hand, figures 5.9, 5.10, and 5.11 reveal that the effect of joint flexibility is important when the links are flexible. In other words, the difference between dynamic behaviors of the flexible manipulator system and the rigid one becomes more significant when the joint flexibility is also taken into account. Therefore, the interaction among flexural, torsional, and joint flexibilities plays a big role in the dynamic behavior of the system.

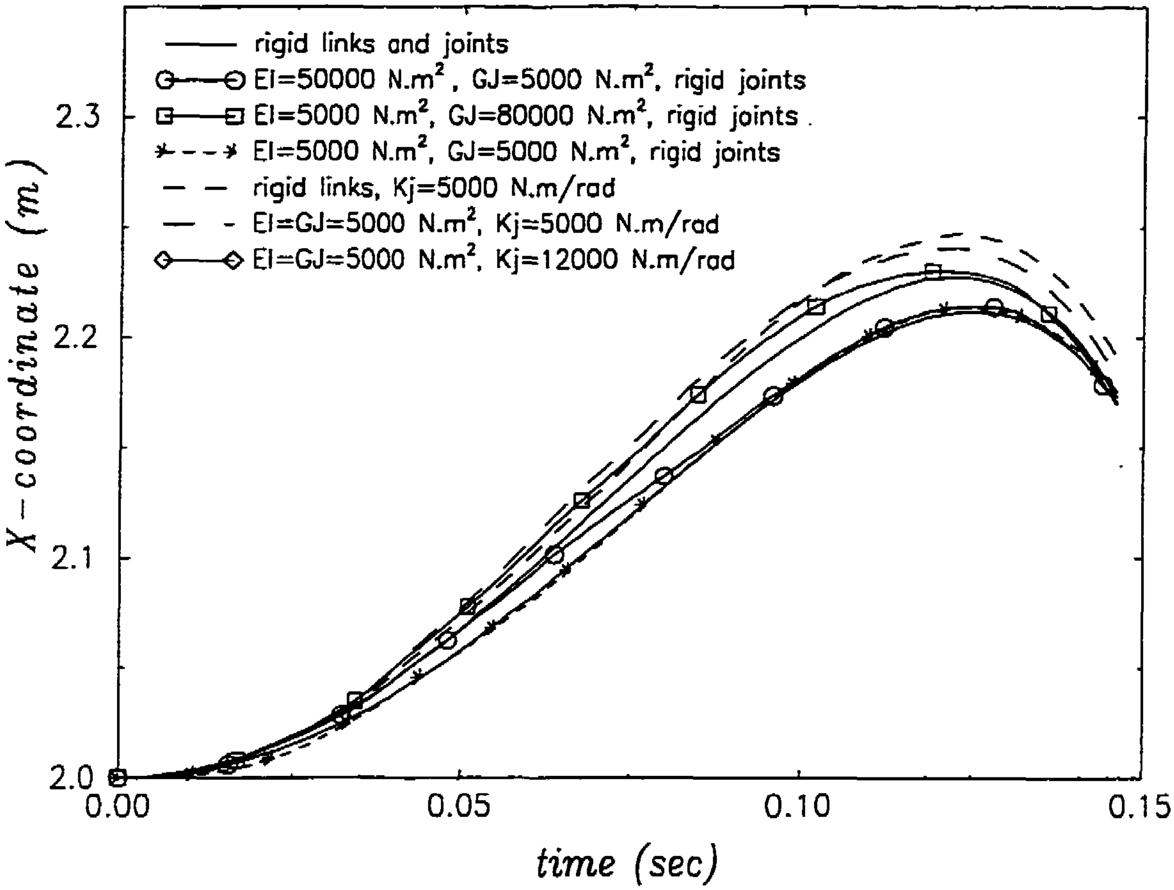

Figure 5.9 X -coordinates of the payload of various manipulators

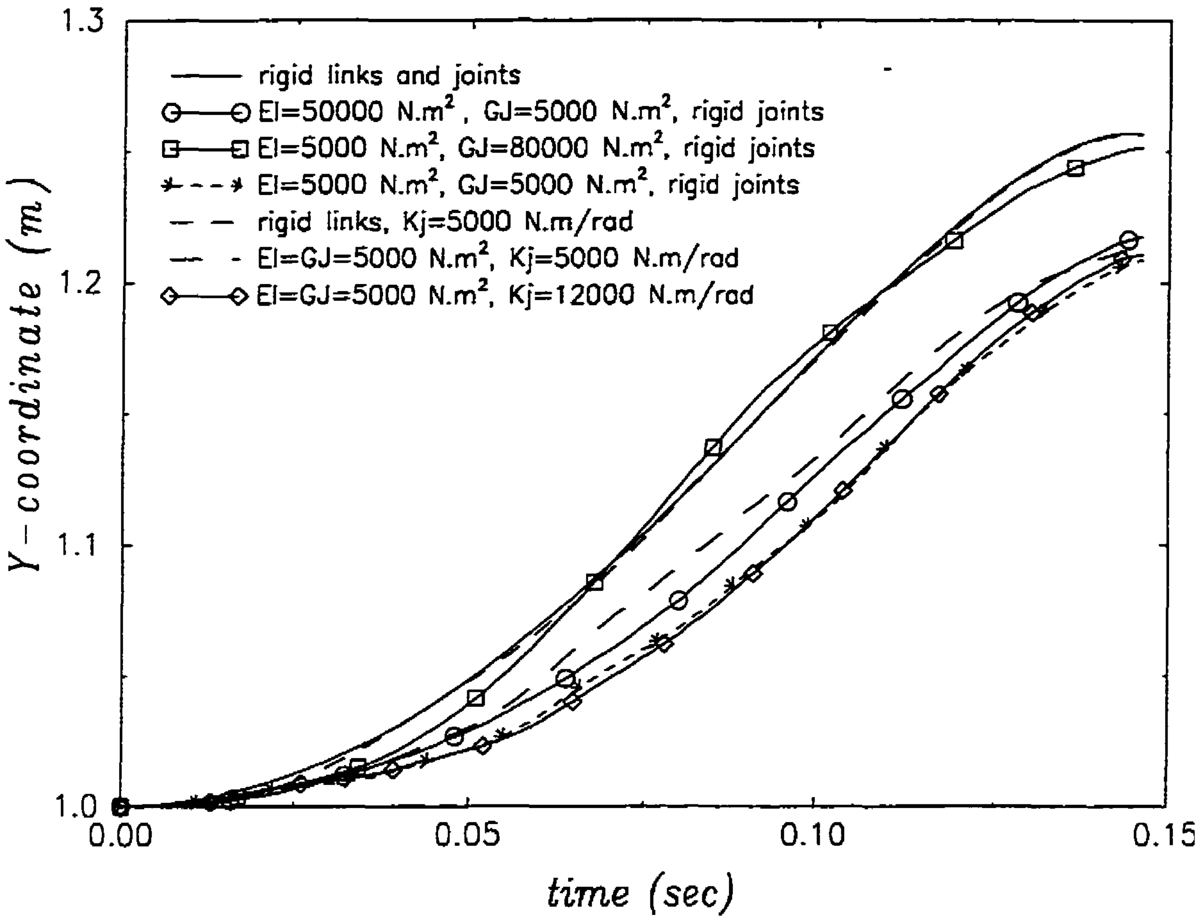

Figure 5.10 Y-coordinates of the payload of various manipulators

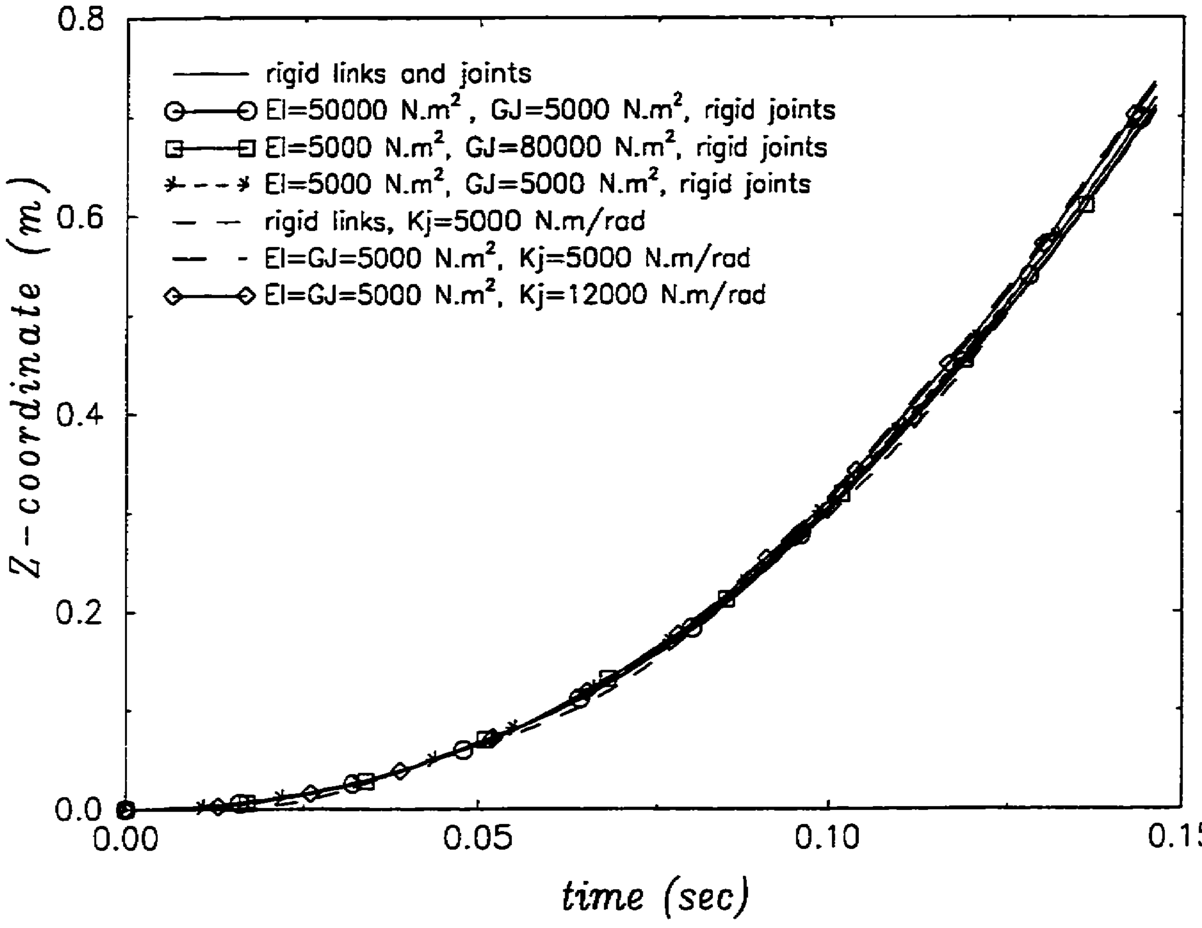

Figure 5.11 Z-coordinates of the payload of various manipulators

In a rigid manipulator, due to lack of elastic deformations, all of the links have the same Φ_1 angle, while in a flexible one each link i has its own $\Phi_1^{(i)}$ angle. Figure 5.12 presents the variation of angle Φ_1 for the rigid manipulator and the variation of angles $\Phi_1^{(i)}$ for flexible manipulators with $E_iI_y^i=E_iI_z^i=G_iJ_i=5000$ N.m^2 but different joint stiffnesses. Since the external torque T_b is applied to the first link, the difference among variations in angle $\Phi_1^{(1)}$, $\Phi_1^{(2)}$, and $\Phi_1^{(3)}$ reveals that each link responds in a delayed manner in comparison with the previous one. The reason for this phenomenon is the fact that elastic waves propagate with finite velocity.

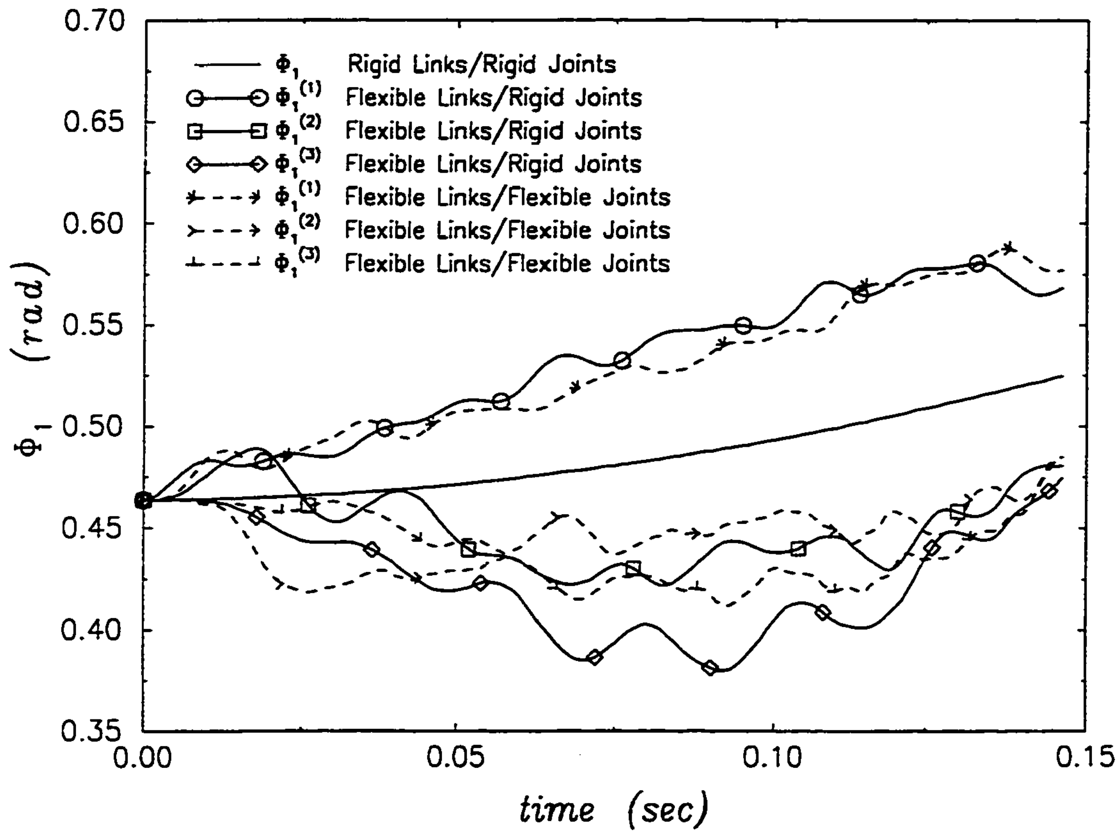

Figure 5.12 Variation of angles Φ_1 of various links of a rigid manipulator, a manipulator with flexible links ($E_iI_y^i=E_iI_z^i=G_iJ_i=5000$ N.m^2), and a manipulator with flexible links and joints ($E_iI_y^i=E_iI_z^i=G_iJ_i=5000$ N.m^2 and $K_i=5000$ N.m/rad)

Figure 5.13 presents the variation of the angles $\Phi_2^{(i)}$ of various links of both the flexible and rigid manipulators. In this figure, the difference between behavior of the rigid and flexible systems, due to link and joint flexibilities, can be also clearly seen.

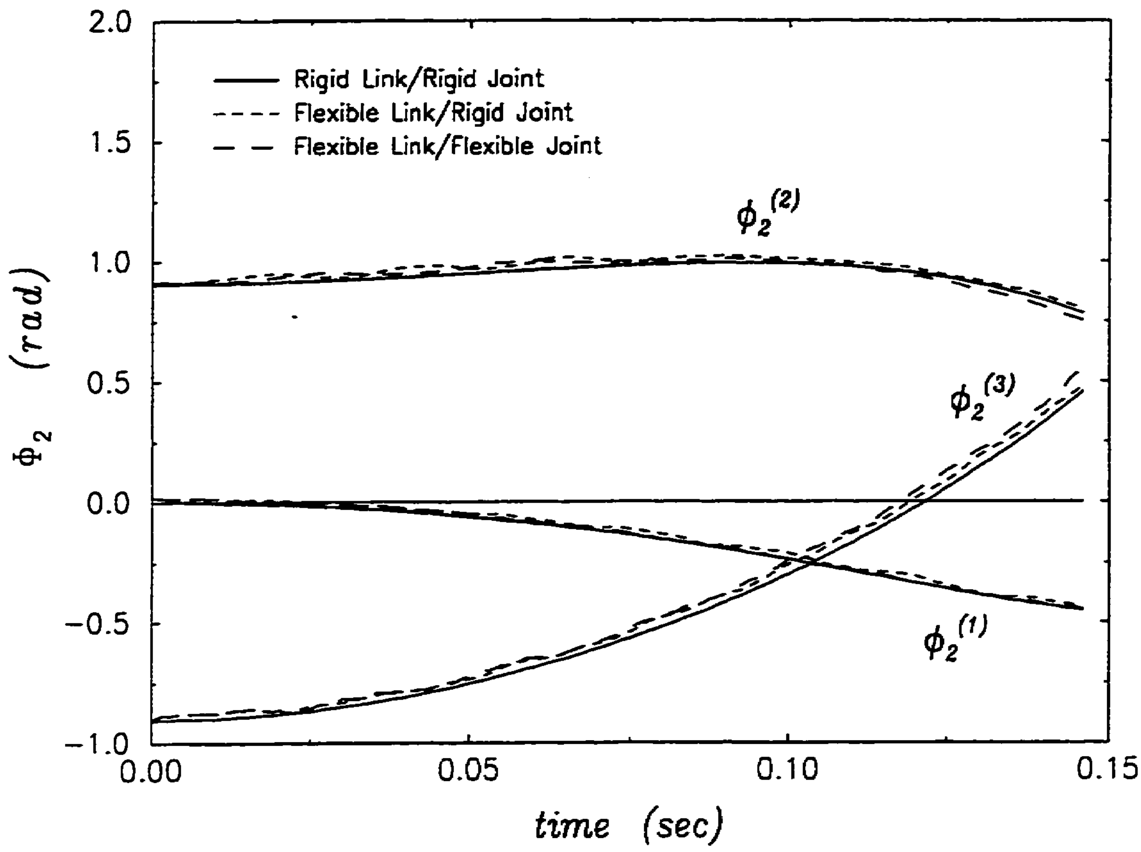

Figure 5.13 Variation of angles Φ_2 of various links of a rigid manipulator, a manipulator with flexible links ($E_iI_y^i = E_iI_z^i = G_iJ_i = 5000$ N.m^2), and a manipulator with flexible links and joints ($E_iI_y^i = E_iI_z^i = G_iJ_i = 5000$ N.m^2 and $K_i = 5000$ N.m/rad)

5.5 Summary and Conclusion

In this chapter an efficient finite element/Lagrangian approach was developed for dynamic modeling of lightweight multi-link spatial manipulators with flexible links and joints. The equations of motion of the system were derived by using Lagrange's equations. The constraint equations representing kinematical relations among different coordinates due to the connectivity of the links were added to the equations of motion of the system by using Lagrange multipliers. This leads to a mixed set of ordinary differential equations and nonlinear algebraic equations with coordinates and Lagrange multipliers as unknown variables. The resulting system of differential algebraic equations (DAEs) was converted to a set of differential equations by substituting the constraints with their double time derivatives, then the system was solved numerically to predict the dynamic behavior of the system. The proposed dynamic model is free from assumption of a nominal motion and takes into account the coupling effects among the rigid body motion of the system, the bending and torsional deflections of the links, and the flexibility of the joints. Due to these couplings as well as the time variation in the effective inertia of the system, the model is highly nonlinear and coupled.

The validity of the model is shown and the effect of link and joint flexibilities is illustrated by some case examples. It is shown that the torsional deflections have more significant effect than the bending deflections and joint deformations. Also it is shown that the effect of joint flexibility is significant when the links are flexible too. Figure 5.12 reveals that each link responds in a delayed manner in comparison with the previous one due the fact that elastic waves propagate with finite velocity. The last point is that the interaction among various flexibilities plays an important role in the dynamic behavior of the system.

CHAPTER 6

OPTIMAL CONTROL THROUGH OPTIMUM DESIGN THEORY

6.1 Introduction

Engineers are traditionally involved in designing systems for various applications. These systems should be efficient, versatile, unique, and economic. Usually engineering design is an iterative process involving modification of the system after examination of the results of the previous step. To design the best systems, we need analytical and numerical tools. Optimization theory, which is a branch of applied mathematics, can be viewed as means of systematizing the engineering design process. Using optimization theory, the design of each system can be formulated as an optimization problem in which a measure of performance of the system is maximized or minimized, while all constraints are satisfied. Optimization involves three steps: description of the system, adoption of a measure of performance, and selection of the system variables which yield optimum effectiveness.

A large number of optimization methods have been used to solve optimization problems over years. These techniques can be classified as direct or search methods and indirect or optimality criteria methods. Direct methods start at an arbitrary point and proceed stepwise towards the optimum point by successive improvement, while indirect methods are those which involve solving equations resulting from optimality conditions. Optimality conditions are the conditions a function must satisfy at its optimum point [106]. Since indirect methods find the roots of the equations representing the optimum point, they are very effective when they can be applied. However, due to complex and nonlinear nature of the objective functions and constraints in most of the engineering problems, these methods can be used only for simple cases. This is why indirect methods have not had a substantial growth, while direct methods have substantially grown due to their ease implementation.

Based on the physical structure of engineering problems, optimization problems can be classified as optimum design and optimal control problems. In an optimum design problem, the system and its elements, are designed to optimize an objective function such as weight and natural frequency. Then the system remains fixed for its whole life. But in an optimal control problem, the input to the system, which steers the system from a prescribed initial state to a desired final state, must be determined as a function of time so as to minimize or maximize some performance index such as time, path, and energy. Therefore, unlike the optimum design problems, optimal control problems are dynamic in nature.

6.2 Optimal Control Problems

Optimal control problems are defined by two different types of variables: the control variables and the state variables. The state variables describe the behavior of the system in any stage, while the control variables govern the evolution of the system from one stage to the next stage. In the optimal control problems, the optimization problem is to find a set of control variables to satisfy the given state equations, boundary conditions, and any constraints imposed on the state and/or control variables, while minimizing or maximizing a given performance index.

Methods available for the solution of the optimal control problems generally fall into two categories: direct and indirect methods. Indirect methods seek to solve the optimization problem by satisfying the necessary optimality conditions established from the calculus of variations. The resulting conditions generally provide multi-point boundary value problems in the form of variational problems. These problems are different from those of classical calculus of variations because of the appearance of two different types of variables; namely, state variables and control variables. Moreover, some equality constrains have the form of ordinary differential equations in such problems. These restrictions make these problems very difficult to solve and their analytical solutions exist only in exceptional simple cases.

Pontryagin [107] in 1962 derived a set of necessary conditions called Pontryagin minimum principle to minimize the functional:

$$P = \int_{t_A}^{t_B} L[x_j(t), u_l(t)]\, dt \tag{6.1}$$

subjected to the constraints in the form

$$\dot{x}_j = g_j(x_i(t), u_l(t), t) \qquad i, j = 1, 2, \ldots\ldots m \tag{6.2}$$

$$N_l \leq u_l(t) \leq M_l \qquad l = 1, 2, \ldots\ldots k \tag{6.3}$$

where x_j and u_l are state and control variables, respectively. The conditions were obtained by using Lagrange multipliers and a functional called Hamiltonian. However, pontryagin principle is very difficult to satisfy and in practice can be used only for linear problems.

A general analytical solution of optimal control problems is impossible due to nonlinearities and complexities in the state equations and the constraints. Therefore, numerical algorithms such as shooting methods [108,109] and quasi-linearization techniques [110,111] are used to solve such problems. It should be stated that, even in simple cases with only one control variable, the computation is likely to be extremely lengthy and time-consuming. Although, in the cases in which objective function, state equations, and constraints are linear, the process can be rather simple, the optimization of the dynamic systems such as flexible manipulators is usually so complex that the applicability of these numerical methods is quite doubtful.

Another option is to use the direct methods which transform the infinite-dimensional continuos problem into a finite-dimensional nonlinear problem. These methods require parameterization of the control and/or state time histories. Once the parameterization scheme is chosen, the problem can be formulated and solved by the well developed nonlinear programming algorithms used in optimum design.

6.3 Some Nonlinear Programming Techniques for Optimum Design Problems

Mathematical programming deals with the problem of optimizing an objective function in the presence of equality and inequality constraints. If any of the objective function and constraints is nonlinear, the problem is called a nonlinear programming problem. Since in most of the engineering problems, both the objective function and the constraints are nonlinear functions of design variable, nonlinear programming algorithms have found many applications in optimum design. In the following section, transformation techniques as the simplest and most important techniques of nonlinear programming will be discussed.

6.3.1 Transformation Techniques

One approach to solve a nonlinearly constrained problem is to construct an unconstrained objective function using transformation techniques. Optimum points of the original constrained problem can be found by solving the transformed problem using well developed unconstrained optimization algorithms. In the following sections three popular transformation techniques are reviewed.

6.3.1.1 Penalty Function Methods

In the constrained optimization, instead of applying constraints we can replace them by penalties whose magnitude depend on the degree of constraint violation. Because of the simplicity and effectiveness of these methods, they have been used widely in the constrained optimization in various fields. The penalties associated with the constraint violations have to be so high that the constraints can be only slightly violated. But there are numerical difficulties associated with imposing abrupt high penalties in numerical optimization. Thus a gradual approach, in which we start with small penalties and increase them gradually, is used in practice. Therefore, they transform the basic optimization with mixed equality and inequality constraints into alternative formulations such that numerical solutions are sought by solving a sequence of unconstrained optimization problems. This is why they are also called Sequential Unconstrained Minimization Techniques (SUMT) [112]. These methods are of great importance in solving real life problems. Penalty methods are classified as exterior and interior penalty function methods.

6.3.1.1.1 Exterior Penalty Functions

In this type of penalty functions the penalties are applied only in the exterior of the feasible domain. Consider the following basic problem:

Minimize $f(X)$ (6.4)

Subject to: $h_i(X)=0 \quad , \; i=1,\ldots..n_e$ (6.5)
$g_j(X)\le 0 \quad , \; j=1,\ldots.,n_g$

where **X** is the vector of design variables and n_e and n_g are number of equality and inequality constraints, respectively. This constraint minimization can be replaced

Minimize
$$\Phi(X,r_k)=f(X)+r_k\sum_{i=1}^{n_e}h_i^2(X)+r_k\sum_{j=1}^{n_g}<g_j(X)>^2 \tag{6.6}$$
$$r_j > r_{j-1} \quad \textbf{and} \quad r_j \to \infty$$

where $<g_j>=\max(0,g_j)$. The positive multiplier r_k controls the magnitude of the penalty terms. The minimization is started with a relatively small value of r_1, and then its value is gradually increased. As noted before, this is because of numerical difficulties due to ill-conditioning of penalty functions. This type of exterior penalty function method is the most common one. A typical example, which is finding the minimum of f(X) subject to $b-X\leq 0$, is shown graphically in figure 6.1 by constructing unconstrained objective function $\Phi(X,r)=f(X)+r\langle b-X\rangle^2$. As r increases, the minimum of Φ moves closer to the constraint boundary, but the curvature of Φ increases which leads to numerical difficulties. By using gradual approach, we can use the minimum obtained for smaller value of r as a starting point for the next step (with higher r) and; therefore, the ill-conditioning problem associated with the high curvature of Φ can be counterbalanced

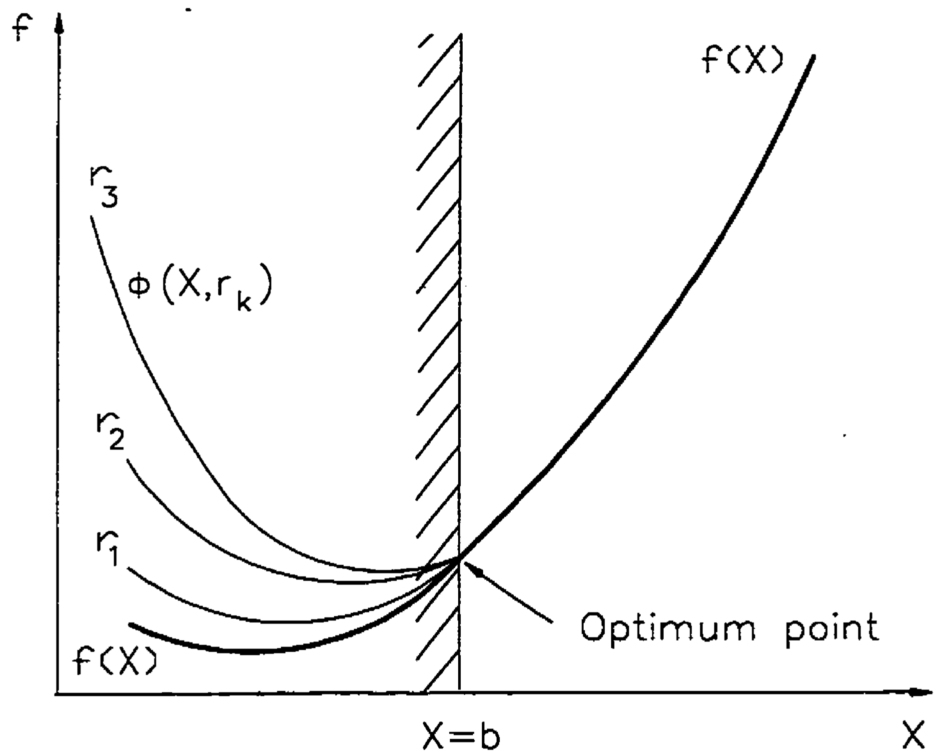

Figure 6.1 Illustration of exterior penalty function method

6.3.1.1.2 Interior Penalty Functions (Barrier Methods)

By using exterior penalty functions, the design typically moves in the infeasible domain. Therefore, if minimization is terminated before r becomes very large, the final result may be useless. We can define a penalty function that keeps the design in the feasible domain. The common form of interior penalty function for general problem expressed by equations (6.4) and (6.5) is

$$\text{Minimize} \qquad \Phi(X,r_k) = f(X) + \frac{1}{\sqrt{r_k}}\sum_{i=1}^{n_h} h_i^2(X) - r_k \sum_{j=1}^{n_g} \frac{1}{g_j(X)} \qquad (6.7)$$

$$r_k < r_{k-1} \quad , \quad r_k \to 0$$

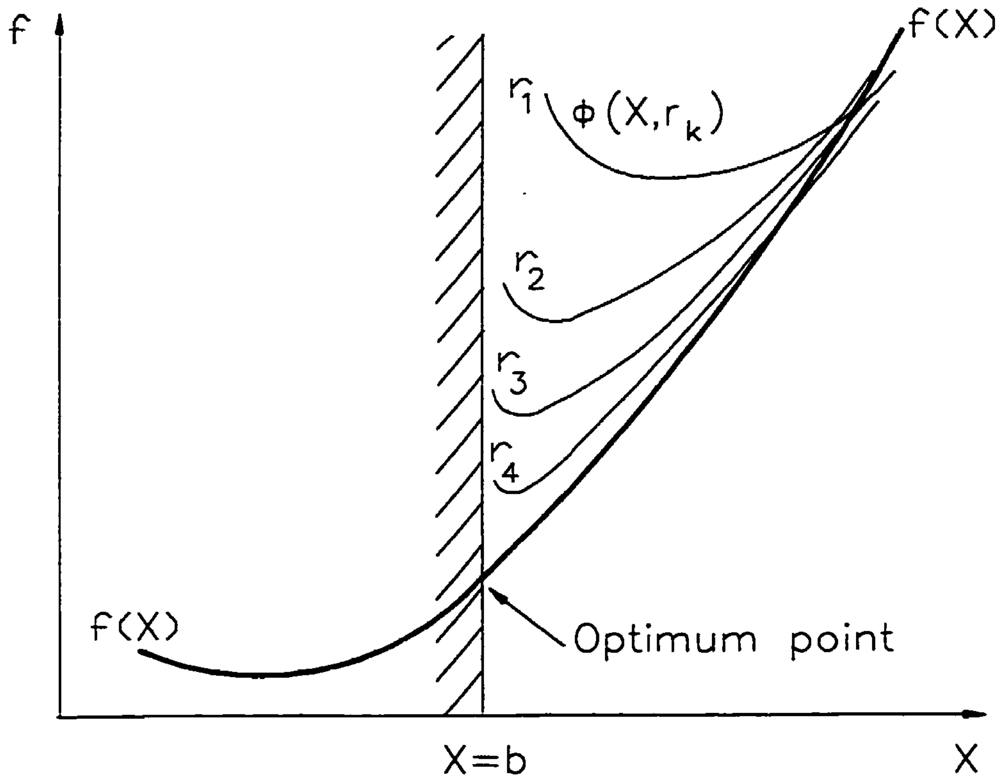

Figure 6.2 Illustration of interior penalty function method

in which $1/g_j(X)$ becomes infinity large at the boundary of the feasible domain which creates a barrier. Figure 6.2 shows the behavior of interior penalty function method applied to the simple example previously solved by exterior penalty functions.

6.3.1.2 Multiplier (Lagrange Augmented) Methods

The penalty function methods suffer from ill-conditioning. This difficulty may be avoided by using Multiplier methods which combine the use of Lagrange multipliers with exterior penalty functions. These methods, originally proposed in 1969 by Hestenes [113] and Powell [116], have been determined to be quite robust [115]. A review of the theory and computational procedures of multiplier methods was given by J.S. Arora et al [116]. When only Lagrange multipliers are employed the optimum point is a stationary point of the Lagrangian function and we have to check the Hessian matrix at that point to know whether or not it is a minimum. And when only penalty functions are employed, the optimum point, if it can be found in spite of ill-conditioning, is a minimum point. By using a combination of these methods we can get an unconstrained problem where the functions to be minimized do not suffer from ill-conditioning because there is no need to use the large values of penalty parameters which are required for external penalty function methods.

One of the common forms of Multiplier functions for the problem

Minimize $\quad f(X) \qquad (6.8)$

Subject to: $\quad h_i(X) = 0 \quad , \; i = 1,\ldots\ldots n_i \qquad (6.9)$

is

Minimize $$\Phi(X,\lambda,r) = f(X) + \sum_{i=1}^{n_i} \lambda_i h_i(X) + r\sum_{i=1}^{n_i} h_i^2(X) \qquad (6.10)$$

if $\lambda_i=0$, we have usual exterior penalty function, while for correct values of λ_i, we can get the correct minimum of the problem using any positive value of r.

These methods are based on estimating the Lagrange multipliers. When the estimated multipliers are good, it is possible to approach the minimum without using large values for r. They need to be only large enough so that Φ has a minimum rather than a stationary point. An estimate for Lagrange multipliers can be found using the stationary condition of Augmented Lagrangian in the following way:

$$\frac{\partial \Phi}{\partial x_i}=\frac{\partial f}{\partial x_i}+\sum_{j=1}^{n_e}(\lambda_j+2rh_j)\frac{\partial h_j}{\partial x_i}=0 \tag{6.11}$$

while for an optimal λ^* we have:

$$\frac{\partial f}{\partial x_i}+\sum_{j=1}^{n_e}\lambda^*\frac{\partial h_j}{\partial x_i}=0 \tag{6.12}$$

Then we expect that as $x \rightarrow x^*$, $\lambda_j + 2rh_j \rightarrow \lambda^*$, therefore

$$\lambda_j^*=\lambda_j+2rh_j \quad \text{or} \quad \lambda_j^{(k+1)}=\lambda_j^{(k)}+2r^{(k)}h_j^{(k)} \tag{6.13}$$

We can extend the Multiplier methods to deal with inequality constraints in several ways. Fletcher [117] suggested the following forms for the objective function:

$$\textbf{Minimize} \qquad \Phi(X,\mu,r)=f(X)+r\sum_{j=1}^{n_g}<g_j+\frac{\mu_j}{2r}>^2 \tag{6.14}$$

instead of

$$\textbf{Minimize} \qquad f(X) \tag{6.15}$$

$$\textbf{Subject to:} \qquad g_j(X)\leq 0 \quad , \ j=1,\dots,n_g \tag{6.16}$$

An estimated value for μ_j found by using optimality condition of the augmented objective function can be written in the form

$$\mu_j^{(k+1)} = < \mu_j^{(k)} + 2r^{(k)} g_j^{(k)} > \tag{6.17}$$

Therefore, for a general problem with both equality and inequality constraints, we can construct the following augmented Lagrangian function:

$$\textbf{Minimize} \qquad \begin{aligned} \Phi(X,\lambda^{(k)},\mu^{(k)},r^{(k)}) = f(X) + \sum_{i=1}^{n_e} (\lambda_j^{(k)} h_i + r^{(k)} h_i^2) \\ + r^{(k)} \sum_{j=1}^{n_g} < g_j + \frac{\mu_j^{(k)}}{2r^{(k)}} >^2 \end{aligned} \tag{6.18}$$

6.3.2 Unconstrained Minimization

By using transformation techniques the constrained minimization problems can be converted into unconstrained ones. Therefore, the selection of a suitable method for the unconstrained optimization is the most important part of the algorithm. The unconstrained optimization problems can be classified as one-dimensional (line search) problems and multidimensional problems. Most direct optimization algorithms have two phases, namely, search direction and step size determination subproblems. Therefore, even in the multi-dimensional problems it is necessary to use one-dimensional search techniques in finding the step size.

6.3.2.1 One-Dimensional Minimization

As it was mentioned earlier, after determining the search direction, the step length can be determined in a one-dimensional minimization problem. One of the simplest and most efficient algorithm called Quadratic curve fitting is used in this research.

A continuous, sufficiently smooth, and unimodal function on a given small interval of uncertainty can be approximated by a quadratic curve. To interpolate a function with quadratic curve, we need only to know the function value at three distinct points to determine the coefficients of the second-order polynomial. Then the minimum point of the approximating polynomial can be used as a good estimate of the exact minimum of the search function (figure 6.3). However, usually an iterative procedure is used to find a better approximation for minimum point of the original objective function.

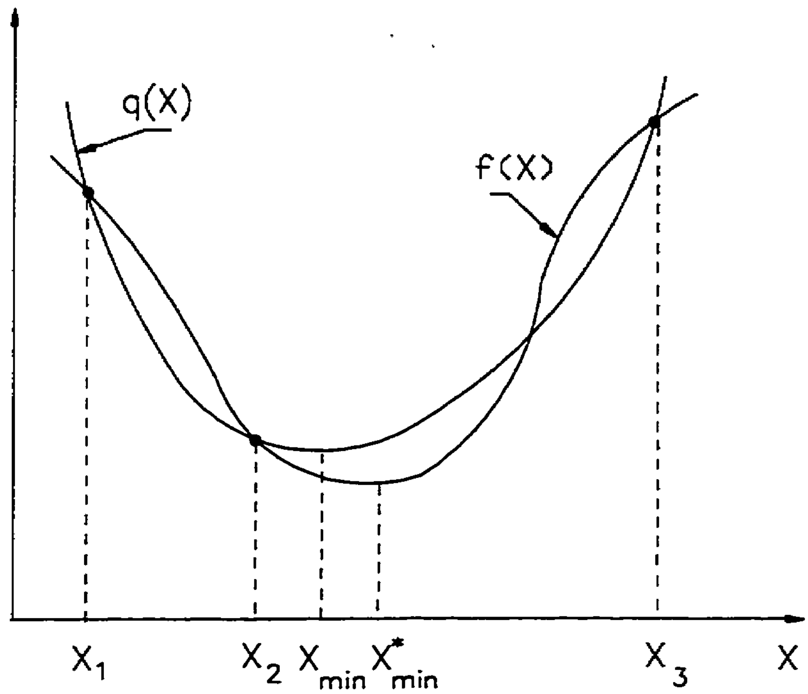

Figure 6.3 Minimization of a function f(X) by quadratic interpolation

6.3.2.2 Multi-Dimensional Minimization

In this section some direct search methods for unconstrained minimization are introduced and the methods which will be used in the next parts of the thesis will be described.

6.3.2.2.1 Zero Order Methods

Zero order methods use only function values for minimizing functions of several variables. These methods are usually reliable and easy to implement. Sequential simplex method, univariant methods, and pattern search methods including Hook and Jeeves method and Powell's method are examples of zero order search methods. Powell's method is the most powerful method among these methods.

New random based methods such as Genetic algorithm and simulated annealing method are also zero order methods. Genetic algorithms use techniques derived from biology and rely on the principle of Darwin's theory of survival of the fittest [118]. Simulated annealing algorithm was motivated by studies in statistical mechanics which deal with equilibrium of large number of atoms in solids and liquids at a given temperature [118]. These methods are the most efficient zero-order methods and can easily handle integer design variables or discretized variables. Moreover, by using these methods (especially Genetic algorithms), it is usually possible to reach the global optimum point, while all of the deterministic search methods can only find local optimum near the initial guess.

However, the main drawback of zero-order methods is that the location of the optimum point can not be found accurately.

6.3.2.2.2 First Order Methods

These methods use the gradient of the function as well as its value in finding the direction for function minimization. Steepest descent method is the oldest and simplest multi-dimensional first order method. In this method, iterations are made according to the following equation:

$$X^{k+1} = X^k - \lambda^k \nabla f(X^k) \tag{6.19}$$

where λ^k is the smallest positive value which locally minimizes f(**X**) along $-\nabla f(\mathbf{X}^k)$ starting from $\mathbf{X}^k$. The steepest descent directions at two consecutive steps are orthogonal to each other, that is, for all k

$$\nabla f(X^{k+1})\nabla f(X^k)=0 \tag{6.20}$$

This tends to slow down the convergence specially near the optimum point due to zigzagging moves. Another disadvantage of the steepest descent method is that each iteration is calculated independently of the others; that is, no information is stored and used which might accelerate convergence. Therefore, this method is not very efficient. Various attempts to accelerate convergence have been made in the literature. For example conjugate gradient methods, such as Fletcher-Reeves method, are very simple and effective modifications of the steepest descent method. The rationale for these methods is the minimum point can be found in n or fewer steps of a n-th order positive definite quadratic form. This desirable property is called quadratic convergence. The conjugate directions are not orthogonal to each other but tend to cut diagonally through the orthogonal steepest descent directions, this is why they improve the rate of convergence [106] of the steepest descent method. Although conjugate gradient methods are vastly superior to the steepest descent method, they are rather less efficient than quasi-Newton methods which are introduced in the following sections.

6.3.2.2.3 Second Order Methods

In addition to the function value and its first order derivative, the second order derivative can be used to represent the cost function more accurately. Therefore, it is possible to find a better direction of search which improves the rates of convergence.

6.3.2.2.3.1 Newton's Method

This method uses the Hessian of the cost function to determine the search direction. The basic idea is to use the second-order Taylor series expansion of the objective function about the current design point (**X**) as:

$$f(X+\Delta X)=f(X)+G^T\Delta X+\frac{1}{2}\Delta X^T H\,\Delta X \tag{6.21}$$

where **G** and **H** are gradient vector and Hessian matrix at design point **X**, respectively. They can be found in the following forms:

$$G=\nabla f(X), \qquad H=\nabla^2 f(X)=\left[\frac{\partial^2 f}{\partial x_i \partial x_j}\right] \tag{6.22}$$

Equation (6.21) provides a quadratic expression in terms of the increments of the design variables. Necessary conditions for minimization of this function give an explicit result for search direction in the design space as:

$$\frac{\partial f}{\partial(\Delta x)}=G+H\,\Delta x=0 \qquad \Rightarrow \qquad \Delta x=-H^{-1}G \tag{6.23}$$

Since in general the objective function is not a quadratic function, this process must be repeated to obtain the minimum point.

$$X_{i+1}=X_i-H^{-1}G \tag{6.24}$$

In each iteration, it is necessary to find Hessian matrix by finding n(n+1)/2 second order derivatives, therefore, a large number of computations is needed. Moreover, because the classical Newton's method uses unit step size, f(**X**+Δ**X**) may become grater than f(**X**) during the iterations. Therefore, there is no guarantee for convergence of the method.

6.3.2.2.3.2 Modified Newton's Method

A simple way to improve the Newton's method is to use step length parameter λ in finding new optimum point using

$$X_{i+1} = X_i + \lambda S^{(i)} \tag{6.25}$$

instead of equation (6.24). $\mathbf{S}^{(i)}$ is the search direction $(\mathbf{S}^{(i)} = -\mathbf{H}^{-1}\,\mathbf{G})$ and λ can be found by any one-dimensional minimization technique to minimize $f(\mathbf{X}^{(i)} + \lambda\ \mathbf{S}^{(i)})$. This approach, which is called modified Newton's method, not only increases the efficiency of the method, but also stabilizes it and guarantees the convergence to the local minimum (if **H** remains positive definite).

The drawback of Newton and modified Newton's methods is that a large number of calculations is required to find the Hessian matrix and it may become singular during iterations. Moreover, previous information is not used in the new iteration and the method dose not converge unless the Hessian matrix remains positive definite.

6.3.2.2.4 Variable Metric or Quasi-Newton Methods

The key to the success of Newton-type methods is the curvature information provided by the Hessian matrix. As mentioned earlier, although these methods have very good convergence properties, they suffer from some difficulties. This is why variable metric or quasi-Newton methods have been introduced in the literature as modifications of Newton's method. They are based on the idea of building up approximate curvature information without explicitly forming the Hessian matrix. Quasi-Newton methods require the computation of only first-derivatives to generate approximate Hessian which should remain positive definite at each iteration. These methods speed up the convergence by making use of the information obtained from previous iterations. Therefore, they are learning processes and have desired features of both the steepest descent and the Newton's methods. Although quasi-Newton methods are really first-order methods, because they use approximate second derivatives, they might be considered as pseudo second-order methods. Also they can be thought conjugate gradient methods [119].

In quasi-Newton methods, instead of Hessian matrix, an initial positive-definite matrix $\mathbf{H}_0$ (usually an identity matrix $\mathbf{I}$) is chosen. This matrix is subsequently updated by an update formula as

$$\boldsymbol{H}_{k+1} = \boldsymbol{H}_k + \boldsymbol{H}_k^* \tag{6.26}$$

where $\mathbf{H}_k^*$ is the update matrix. However, many update formulas are applied directly to the inverse Hessian ($\mathbf{B}_k=\mathbf{H}_{k-1}^{-1}$) in order to avoid the need for solution of a linear system of equations in each iteration. Then the updating formula for the inverse is also of the form

$$\boldsymbol{B}_{k+1} = \boldsymbol{B}_k + \boldsymbol{B}_k^* \tag{6.27}$$

Different quasi-Newton methods are distinguished by the choice for updating matrices. The desirable properties of the updating matrices are that only first derivative information is needed in updating and $\mathbf{H}_{k+1}$ remains positive definite during iterations. The second property guarantees that we always move in a downhill direction. Besides, approximate Hessian should converge to the true Hessian after successive updates.

Using the first-order Taylor series expansion of the gradient vector $\mathbf{G}$, we can write:

$$\boldsymbol{G}_{k+1} - \boldsymbol{G}_k = \boldsymbol{H}_k(\boldsymbol{X}_{k+1} - \boldsymbol{X}_k) \;\Rightarrow\; \Delta\boldsymbol{X}_k = \boldsymbol{H}_k^{-1}\Delta\boldsymbol{G}_k \tag{6.28}$$

In general approximate Hessian matrix does not satisfy this condition. Therefore, a good update should satisfy the requirement

$$\Delta\boldsymbol{X}_k = \boldsymbol{H}_{k+1}^{-1}\Delta\boldsymbol{G}_k = \boldsymbol{B}_{k+1}\Delta\boldsymbol{G}_k \tag{6.29}$$

which is called quasi-Newton condition. By substituting equation (6.27) into equation (6.29), we have

$$\Delta X_k = B_k \Delta G_k + B_k^* \Delta G_k \tag{6.30}$$

A general form of updating matrix is

$$B_k^* = a\, u\, u^T + b\, v\, v^T \tag{6.31}$$

where a and b are scalars and **u** and **v** are vectors. These scalars and vectors should be appropriately selected to satisfy equation (6.30) and the symmetry and positive-definiteness of $\mathbf{B}_{k+1}$.

Methods which take b=0 are using rank one updates, while resulting methods for b#0 are said to use rank two updates. Rank two updates are more flexible and are the most widely used schemes. Many rank one and two updates have been proposed in the literature, but we will limit ourselves only to two methods which are the most popular update formulas. They are rank two methods called DFP and BFGS methods.

6.3.2.2.4.1 DFP Method

This rank two quasi-Newton method initially was proposed by Davidon [120] and then Fletcher and Powell [121] modified it. This is why it is often called DFP method. This method is one on the most powerful methods for the minimization of a general function f(**X**).

By substituting equation (6.31) for B_k in equation (6.30), we have

$$\Delta X_k = B_k \Delta G_k + a\, u\, u^T \Delta G_k + b\, v\, v^T \Delta G_k \tag{6.32}$$

If we choose $u=\Delta X_k$, $v=B_k\Delta G_k$, and determine a and b such that $au^T\Delta G_k=1$ and $bv^T\Delta G_k=-1$, the resulting update formula is

$$B_{k+1}^{(DFP)} = B_k + \left[\frac{\Delta X\, \Delta X^T}{\Delta X^T\, \Delta G}\right]_k - \left[\frac{(B\, \Delta G)(B\, \Delta G)^T}{\Delta G^T B\, \Delta G}\right]_k \tag{6.33}$$

6.3.2.2.4.2 BFGS Method

In 1970, Broyden [122], Fletcher [123], Goldfarb [124], and Shanno [125], independently suggested another important rank two formula in the following form:

$$B_{k+1}^{(BFGS)} = B_k + \left[1 + \frac{\Delta G^T B\, \Delta G}{\Delta X^T\, \Delta G}\right]_k \left[\frac{\Delta X\, \Delta X^T}{\Delta X^T\, \Delta G}\right]_k - \left[\frac{\Delta X\, \Delta G^T B + B\, \Delta G\, \Delta X^T}{\Delta X^T\, \Delta G}\right]_k \tag{6.34}$$

This formula is known as BFGS formula.

Both DFP and BFGS methods have theoretical properties which guarantee the superlinear convergence rate and global convergence, under certain conditions [126]. The global convergence for DFP requires exact line searches, while inexact line searches will suffice for BFGS. This is why numerical experiments with BFSG algorithm [112] suggested that it is superior to other variable-metric algorithms including DFP method.

It is necessary to mention that quasi-Newton methods are considered as the most effective nonlinear optimization methods for solving general unconstrained problems. [126]. Because in quasi-Newton methods the approximate Hessian is forced to be positive-definite, a saddle point may be reached without any warning. Therefore, it is advisable to check if a descent direction can be found around the final point.

6.4 Optimal Control Using Nonlinear Programming Techniques

It is possible to transform some optimal control problems to the optimum design problems [127]. Then they can be formulated and solved by nonlinear programming algorithms which are well developed in optimum design theory.

In the next two chapters, direct methods will be used to solve trajectory control and time-optimal control of flexible manipulators. The proposed techniques, which are based on numerical optimization, find the joint torques required to move the end point from rest to rest along a specified path. In the trajectory problems the desired position of the payload is given versus time in the trajectory control problems, while in the time optimal control problems the path and the constraints on the joint torques are known. In the optimal control problems discussed in this work, the objective functions are obtained based on the method of least squares and the method of penalty functions. Hence the resulting objective functions are implicit functions of desired variables, BFSG method as a powerful quasi-Newton method is used to find the solution i.e. the minimum time (in time-optimal control problem) and the time history of the required joint torques.

6.5 Summary and Conclusion

Optimum design and optimal control problems and various methods to solve such problems were addressed in this chapter. A short review of nonlinear programming and numerical optimization techniques is presented. In the next two chapters, the aforementioned nonlinear programming techniques will used to solve the trajectory control and time-optimal control of flexible manipulator systems.

CHAPTER 7

TRAJECTORY CONTROL OF MULTI-LINK MANIPULATORS WITH FLEXIBLE LINKS AND JOINTS

7.1 Introduction

In the trajectory control problems, the desired position of the end point of the manipulator is given versus time. Therefore, the required joint torques or forces should be applied to move the end point along the given trajectory. This type of problem is one of the major open problems related to the flexible manipulators. Various feedback control strategies are proposed in the literature for suppressing vibration of the flexible-link manipulators [13,20]. But due to the non-collocated nature of the control system of flexible manipulators as well as the existence of high frequency components in the position commands, the feedback control may cause these systems unstable. To avoid this problem, many authors have recently proposed inverse dynamic methods. These methods simultaneously solve the equations of motion and the kinematic equations in order to determine the required joint torques or forces. But the main difficulty is that the numerical solution of the inverse dynamic problem of flexible manipulators normally diverges. This is not because of failure of the numerical analysis, but due to the nature of the problem which is non-causal.

This chapter first describes the noncausality of such systems and then presents a technique based on numerical optimization for solving the non-causal inverse dynamics of multi-link robot arms with flexible links and joints. This technique finds the joint torques required to move the end point of flexible manipulators through specified trajectories while avoiding tip oscillations. The proposed algorithm takes into account the non-causality of such a system via considering pre-actuation and post-actuation in the solution procedure.

7.2 Inverse Dynamics of Flexible Manipulators

Consider a two-link manipulator with both flexible links and flexible joints in Fig. 7.1. The purpose of the analysis is to find the required joint torques $T_1(t)$ and $T_2(t)$ to cause the desired motion of the payload, which is a rest to rest motion tracking a specified path $(x(t),y(t))_p$ from point A to point B in a given time interval t_f. The inverse dynamics of the flexible manipulator is redundant due to its flexibility. Therefore, a complete model consisting of the kinematic and dynamic equations of the system should be solved simultaneously.

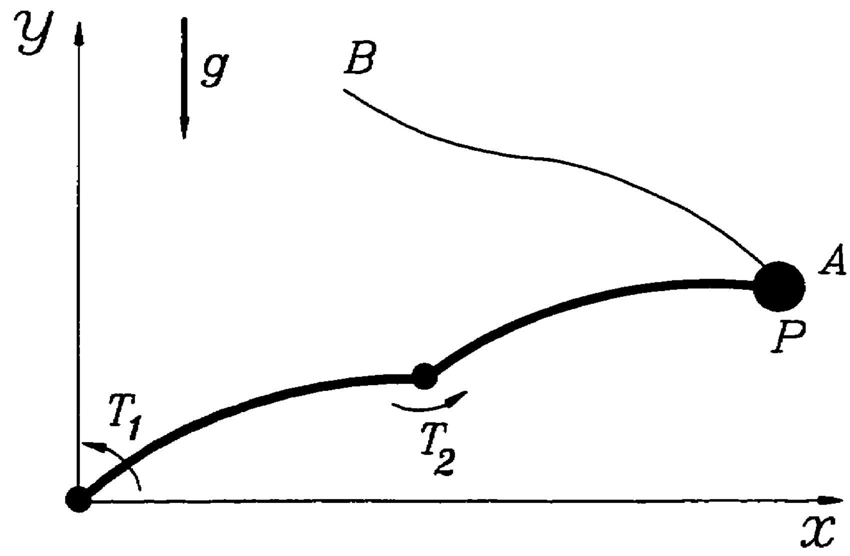

Figure 7.1 A two-link manipulator and its desired trajectory

Using the results of chapter 4, we can write the equation of the motion of the system in the following form:

$$\begin{bmatrix} MS_{mm} & MS_{mj}(\eta_j) & MS_{mf} \\ MS_{jm}(\eta_j) & MS_{jj}(\eta_j,\eta_f) & MS_{jf}(\eta_j,\eta_f) \\ MS_{fm} & MS_{fj}(\eta_j,\eta_f) & MS_{ff}(\eta_j,\eta_f) \end{bmatrix} \begin{Bmatrix} \ddot{\eta}_m \\ \ddot{\eta}_j \\ \ddot{\eta}_f \end{Bmatrix} + \begin{bmatrix} KS_{mm} & KS_{mj} & KS_{mf} \\ KS_{jm} & 0 & 0 \\ KS_{fm} & 0 & KS_{ff}(\dot{\eta}_f) \end{bmatrix} \begin{Bmatrix} \eta_m \\ \eta_j \\ \eta_f \end{Bmatrix} = \begin{Bmatrix} F_m(T_a) \\ F_j(\eta_j,\eta_f,\dot{\eta}_j,\dot{\eta}_f) \\ F_f(\eta_j,\eta_f,\dot{\eta}_j,\dot{\eta}_f) \end{Bmatrix} \tag{7.1}$$

where η_m, η_j, and η_f are the vectors of motor coordinates, joint coordinates, and elastic coordinates of the links. These variables all together present the degrees of freedom of the system. The desired trajectory or motion of the payload can be expressed by the following kinematic equation :

$$AU=h(t) \tag{7.2}$$

in which **A** is a non-square matrix, **U** is the state vector including all of the degrees of freedom of the system, and **h**(t) is a time dependent vector. After double differentiation of the kinematic equations with respect to time, the resulting system of second order differential equation can be shown in the following form.

$$\begin{gathered} MS(U)\ddot{U}+KS(U,\dot{U})U=fS(U,\dot{U})+\mu T_a \\ A\ddot{U}+B\dot{U}+CU=g(t) \end{gathered} \tag{7.3}$$

In the above equations, T_a presents the vector of unknown actuator torques and μ is a non-square matrix which maps the joint torque vector from a space whose dimension is equal to the number of joints to a vector with the dimension of all degrees of freedom of the system.

Because of the complexity of the system of equations (7.3), it should be solved numerically for unknown state variables (U) and control variables (T_a). But the numerical solution of this system of equations dose not normally converge. The divergence of the solution is not related to failure of the numerical approach, but the non-causal nature of the problem. This is due to this fact that the end point, for which the prescribed motion is specified, is connected to the application points of torques by deformable bodies. Thus, the joint torques should be applied from a negative time to a future time in order to control the position of the end-point according to the desired trajectory. Since standard causal time domain integration schemes are unstable in solving the inverse dynamics of flexible manipulators, it is necessary to develop proper non-causal schemes.

7.2.1 Classification of Inverse Dynamic Problems

For better understanding of the time-delayed behavior of the deformable bodies some terms will be introduced in this section and a simple example will be shown. Inverse dynamic problems can be classified as: causal systems, anticausal systems, and noncausal systems [87]:

<u>CAUSAL SYSTEM</u>: A system in which the output (impulse response) always occurs after an input (impulse) is given.

<u>ANTICAUSAL SYSTEM</u>: A system which has the output (backward impulse response) before an input (impulse) is given.

<u>NONCAUSAL SYSTEM</u>: A system which has the combined output of a causal system and an anticausal system.

Consider a single link flexible manipulator shown in figure 7.2 moving in the horizontal plane. We want to move the end-point from its initial position to a desired final position. At the beginning when we apply a torque to the hub, for a short time the payload doesn't move, while the link is deforming. Since torque, which is the output of the inverse

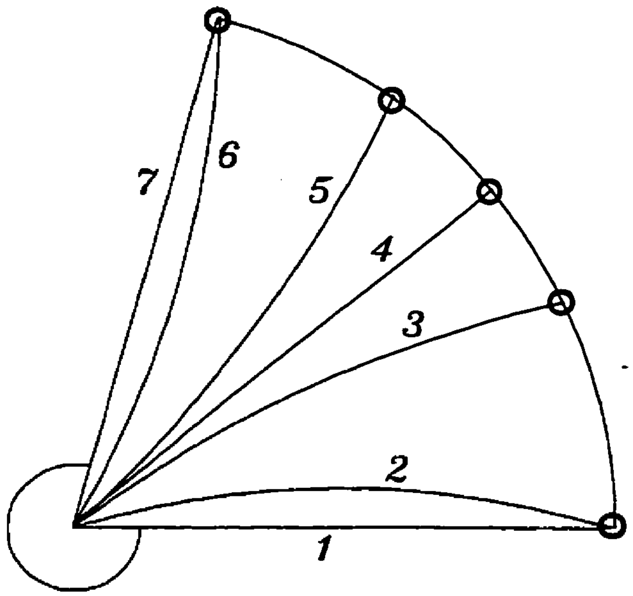

Figure 7.2. Point-to point motion of a single link flexible manipulator

dynamic problem, occurs before input, the system is anticausal at the beginning. At the end, to keep the payload at its desired position, we should apply a torque which only changes the curvature of the link. Thus, the system is causal at the final stage. Therefore, the inverse dynamics of the flexible manipulator is noncausal.

As it was mentioned in chapter 2, Kwon and Book [87] decoupled the inverse dynamics of a single flexible link manipulator into causal and anti-causal parts, then they solved these two parts forward and backward in time, respectively. This approach can be used only for linear systems in which the effects of gravity, Coriolis and centrifugal accelerations are neglected. Bayo [86] and Bayo and Moulin [89] proposed an iterative direct approach which finds the non-causal required torques by solving the inverse dynamics equations of flexible manipulators in the frequency [86] and time [89] domains. However, this approach is limited to manipulators with flexible links only and can not be used if joints are also flexible.

7.2.2 Time Delayed Response of a Single-Link Flexible Arm

As it was mentioned earlier, the inverse dynamics of flexible manipulators yields non-causal or time delayed joint torques with respect to the end-point motion. In this section, this phenomena is quantitatively shown for a single-link arm by using a simple Galerkin approach.

Consider a one-link flexible robot arm shown in figure 7.3. A clamped free floating coordinate system, which is fixed to the root of the link, is used to describe the elastic deformation of the link. The variables v(x,t) and φ(t) represent the deflection at point x along the arm and the arm angle, respectively. The displacement s(x,t) of any point on the arm is defined as

$$s(x,t) = x\varphi(t) + v(x,t) \tag{7.4}$$

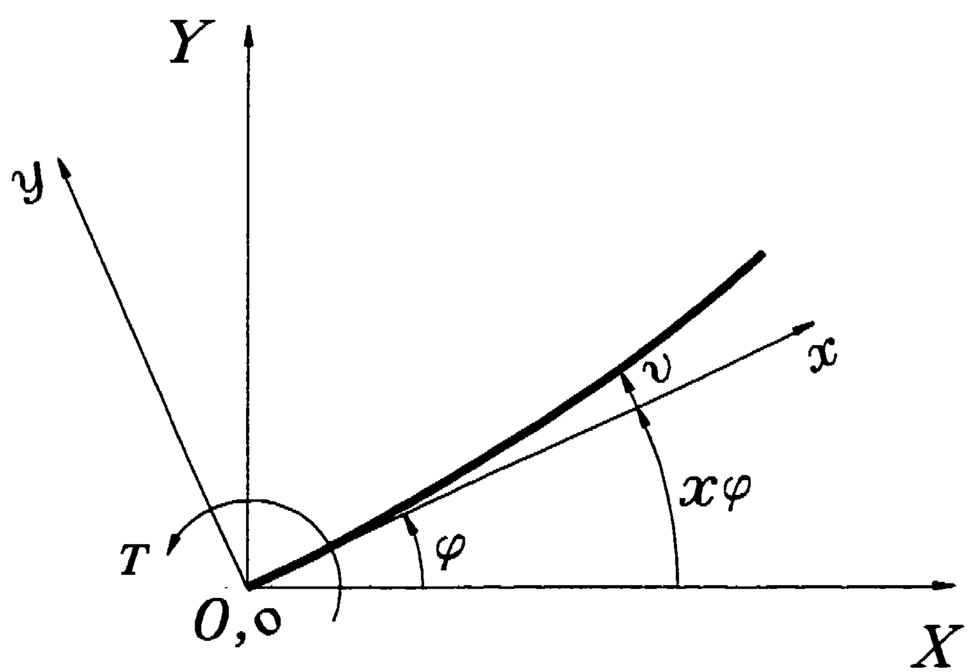

Figure 7.3. A single-link flexible arm moving in horizontal plane

from which the velocity and acceleration of the point can be simply found.

The beam deflection is defined by a forth order partial differential equation

$$EIv^{IV} + \rho A\ddot{s} = 0 \tag{7.5}$$

where EI is the flexural rigidity and ρA is the mass per unit length of the beam. The gravity effect is neglected and the motion is confined to a horizontal plane. After substituting s from equation (7.4) into equation (7.5) we have

$$EIv^{IV} + \rho A(\ddot{v} + x\ddot{\varphi}) = 0 \tag{7.6}$$

In addition to equation (7.6), we obtain the following constraint equation which expresses the overall balance of angular momentum of the system

$$(\int_0^L \rho Ax^2 dx)\ddot{\varphi} + \int_0^L \rho Ax\ddot{v}dx = T \tag{7.7}$$

where L is the length of the link.

To approximate the field equations (7.6) and (7.7), we use a Galerkin approach. In general, the variable v(x,t) can be assumed to be

$$v(x,t) = \sum_{i=1}^{n} a_i(t)N_i(x) \tag{7.8}$$

where $a_i(t)$ are time dependent generalized coordinates and $N_i(x)$ are shape functions which satisfy homogeneous boundary conditions. Using Galerkin approximation, equation (7.6) can be substituted by

$$\int_0^L [EIv^{iv} + \rho A(\ddot{v} + x\ddot{\varphi})]N_i(x)dx = 0, \qquad i = 1,\dots,n \tag{7.9}$$

For simplicity, we choose n=1 and $N_1(x)=x^2$; therefore, v(x,t) is assumed to be

$$v(x,t)=a(t)x^2 \tag{7.10}$$

By assuming constant ρA and EI, after using proper integrations by parts and applying the boundary conditions, we will have the following system of equations describing the dynamic behavior of the system

$$\frac{\rho AL^3}{3}\ddot{\varphi}+\frac{\rho AL^4}{4}\ddot{a}=T \tag{7.11-a}$$

$$\frac{\rho AL^4}{4}\ddot{\varphi}+\frac{\rho AL^5}{5}\ddot{a}+4(EI)L\,a=0 \tag{7.11-b}$$

If the end-point trajectory is given by $y_e=f(t)$, we want to obtain the required joint torque for this motion. The y-coordinate of the end-point of the flexible arm can be written as

$$y_e=L\sin\varphi+v_e\cos\varphi=L\sin\varphi+L^2a(t)\cos\varphi \tag{7.12}$$

where v_e, which is the elastic deflection of the end-point in the local coordinate system, is substituted from equation (7.10). Using equation (7.12), we can obtain a(t) in terms of y_e and φ in the following form

$$a(t)=\frac{1}{L^2\cos\varphi}(y_e-L\sin\varphi) \tag{7.13}$$

from which $\dot{a}(t)$ and $\ddot{a}(t)$ can be easily found. By substituting $a(t)$ and $\ddot{a}(t)$ in equation (7.11-b), we have the following differential equation in terms of only one unknown variable φ.

$$\begin{aligned}&\left[\frac{\rho AL^4}{4}+\frac{\rho AL^3}{5}\frac{y_e\sin\varphi}{\cos^2\varphi}\right]\ddot{\varphi}\\&+\frac{\rho AL^3}{5}\left\{\frac{(\ddot{y}_e+\dot{y}_e\dot{\varphi}^2)\cos^3\varphi+\dot{\varphi}\sin(2\varphi)[\dot{y}_e\cos\varphi+y_e\dot{\varphi}\sin\varphi-L\dot{\varphi}]}{\cos^4\varphi}\right\}\\&\qquad+4\frac{EI}{L\cos\varphi}(y_e-L\sin\varphi)=0\end{aligned} \tag{7.14}$$

This equation is highly nonlinear and can not be solved analytically. Fourth-order Runge-Kutta method is used to solve this equation numerically. Having φ, $\dot{\varphi}$, and $\ddot{\varphi}$, we can find $a(t)$, $\dot{a}(t)$ and $\ddot{a}(t)$ using equation (7.13). Then the required joint torque can be obtained from equation (7.11-a) by substituting known $\ddot{\varphi}(t)$ and $\ddot{a}(t)$.

Let consider the motion of the end point from initial time t=0 to final time $t=t_f$ to be described by

$$y_e(t) = y_0 + a_1 t^5 + a_2 t^6 + a_3 t^7 + a_4 t^8 + a_5 t^9 \tag{7.15}$$

where y_0 is the initial y-coordinate of the end-point and a_1 to a_5 are determined such that $y_e(t_f) = y_e$ and $\dot{y}_e(t_f) = \ddot{y}_e(t_f) = \dddot{y}_e(t_f) = y^{iv}{}_e(t_f) = 0$. This trajectory is shown in figure 7.4.

The required joint torque for a counterpart single-link rigid manipulator is also shown in figure 7.4. The initial position of the end point of the arm is considered to be ($x_e(0)=L$, $y_e(0)=0$) and subsequently the initial arm angle is zero ($\varphi(0)=0$). The rigid

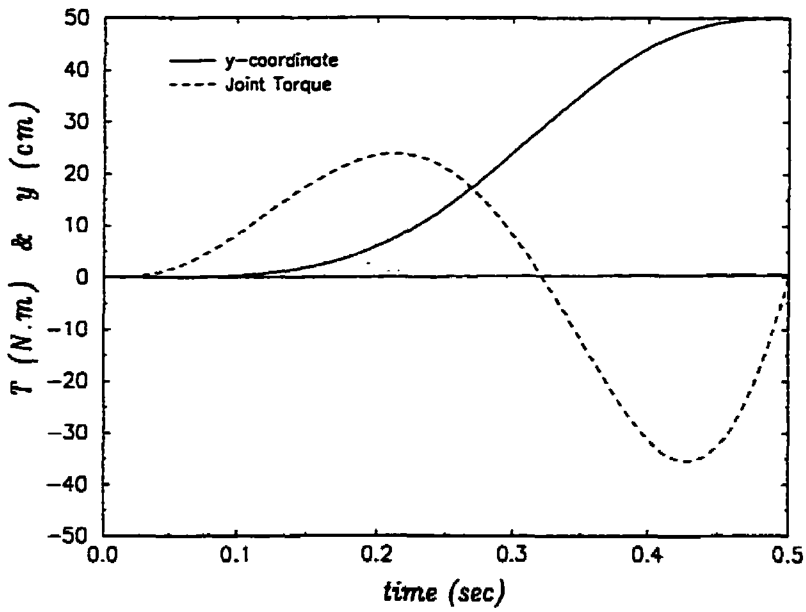

Figure 7.4. Joint torque and y-coordinate of the end-point of a single-link rigid arm

arm has the following physical properties: ρA=5 Kg/m and L=1 m. The required joint torque is accurately found from the following equations

$$\sin\varphi = \frac{y_e}{L} \tag{7.16-a}$$

$$\frac{\rho A L^3}{3}\ddot{\varphi} = T \tag{7.16-b}$$

Figure 7.5 shows the y-coordinate and the require joint torque T(t) for the flexible manipulator. Due to the divergence of the solution, only the first 0.072 second of the motion is illustrated in this figure. As it can be seen, at the beginning of the motion instead of positive torque (counter-clockwise) we should apply a negative torque in order to have the desired trajectory for the end-point. The value of the joint torque is rapidly increasing which causes the divergence of the solution.

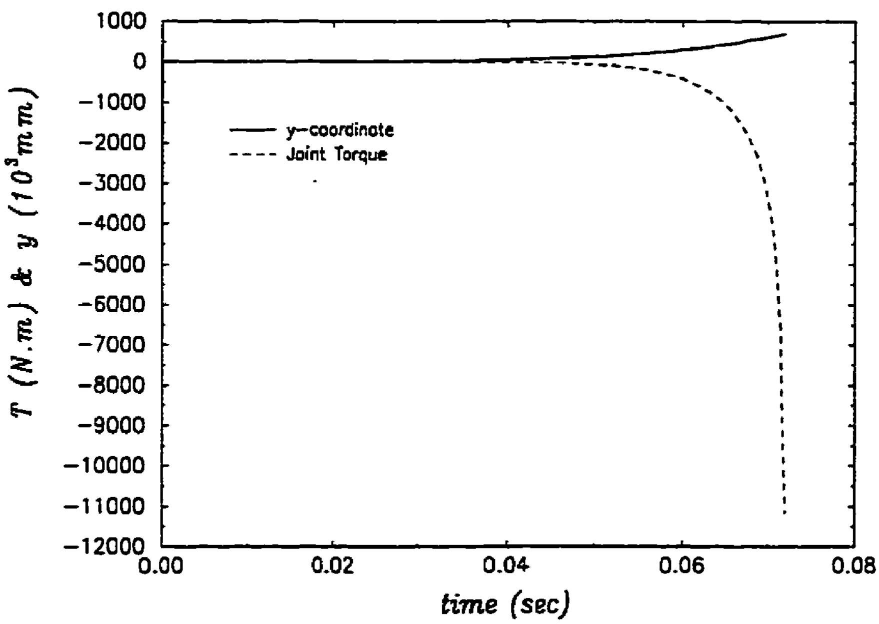

Figure 7.5. Joint torque and y-coordinate of the end-point of a single-link flexible arm

If we consider a known joint torque, we can solve equations (7.11-a) and (7.11-b) to find a(t) and φ(t). Then equation (7.12) can be used to obtain the path of the end-point of the arm. Figures 7.6 to 7.10 present the end-point y-coordinate of a single-link rigid arm and that of various single-link flexible arms with different link flexibilities (EI= 500, 1000, 2000, 10000, 50000 N.m^2). Constant torques (T=20 N, 100, 50 N.m) are considered as joint torques. The same physical properties and initial configuration introduced earlier are used in the aforementioned cases. As it can be seen, for each EI regardless of the magnitude of the applied torque, all of the curves (corresponding to the flexible arms) have a common point which shows zero y after movement of the end-point in the negative y-direction for a short time (Δt_d) at the beginning of the motion. It can be shown that there is a relation between this delayed time interval (Δt_d) for various cases and the corresponding flexural wave speed $c = \sqrt{EI/\rho A}$ [127] in the form

$$c\,\Delta t_d = 0.226 \tag{7.17}$$

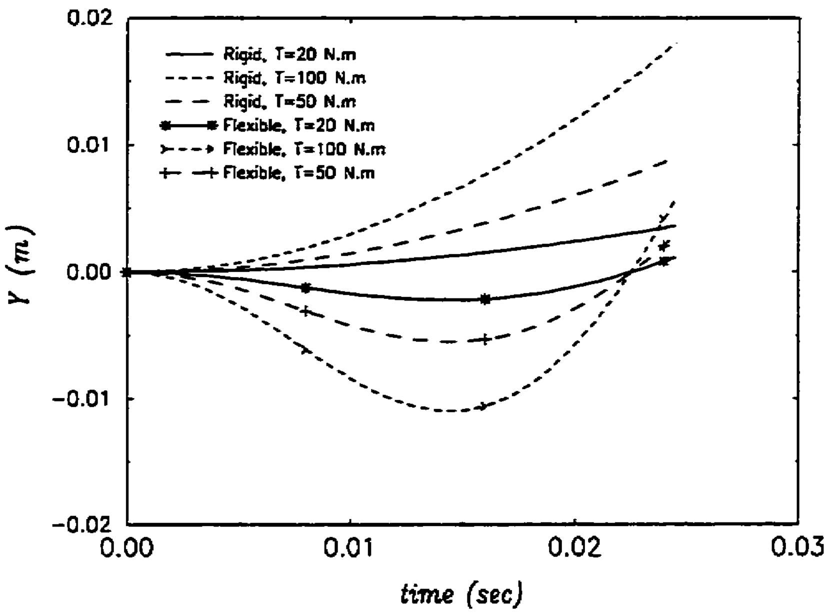

Figure 7.6. Y-coordinate of the end-point of a single flexible arm with EI=500 N.m^2

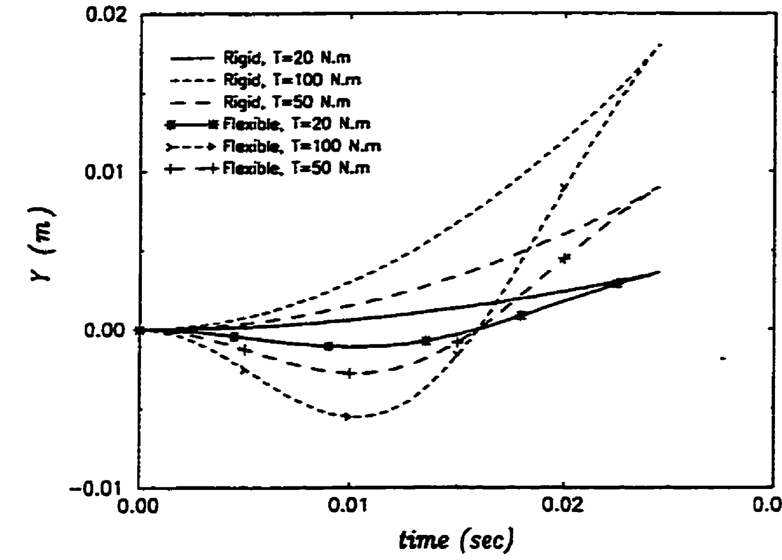

Figure 7.7. Y-coordinate of the end-point of a single flexible arm with EI=1000 N.m^2

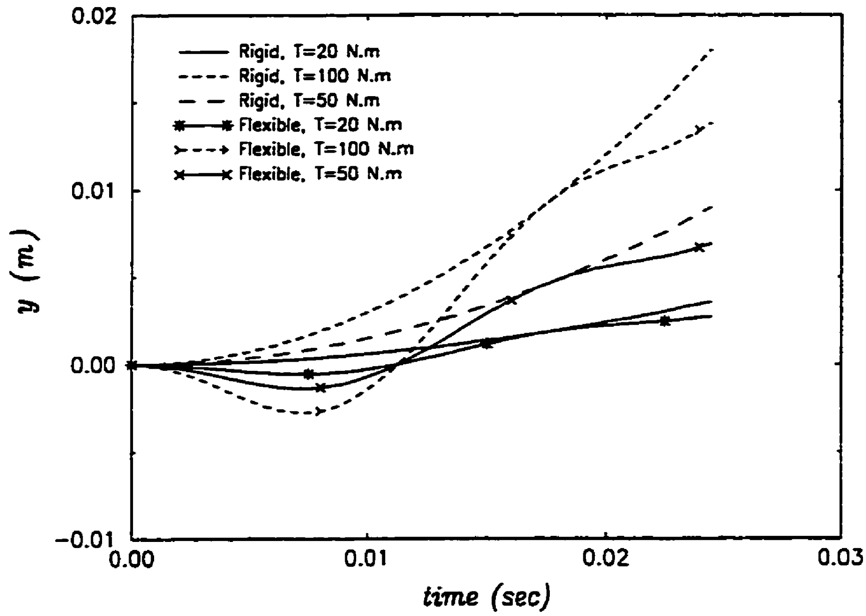

Figure 7.8. Y-coordinate of the end-point of a single flexible arm with EI=2000 N.m^2

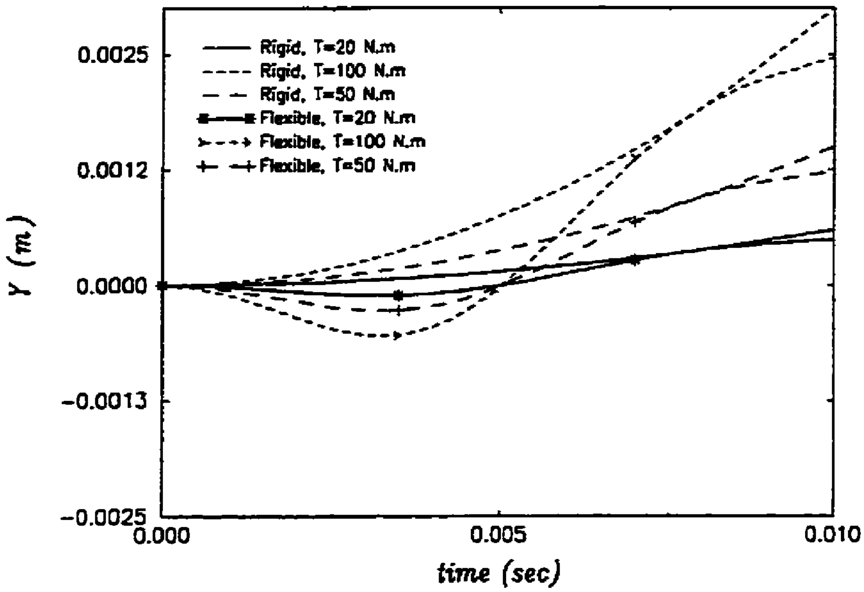

Figure 7.9. Y-coordinate of the end-point of a single flexible arm with EI=10000 N.m^2

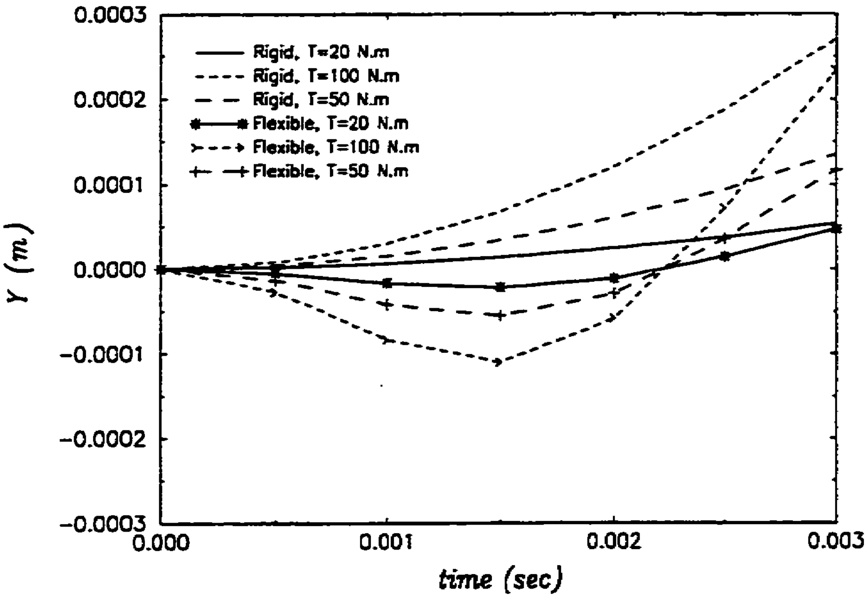

Figure 7.10. Y-coordinate of the end-point of a single flexible arm with EI=50000 N.m^2

Therefore, it can be concluded that the delayed response of the end-point of a flexible arm with respect to the joint torque is related to a characteristic of the flexible link associated with the finite speed of wave propagation.

7.3 Numerical Treatment of Non-Causality of Flexible Manipulators [129,130]

As it was mentioned earlier, due to the non-causality of the inverse dynamic problem, the actuator torques should be applied from a negative time to a future time in order to control the position of the end-point. Let t_1 and t_2 be defined as $c_1 t_f$ and $c_2 t_f$, respectively, where c_1 and c_2 are two constants. As it is shown in figure 7.11, the time duration of the motion of the system is considered $t_1+t_f+t_2$ instead of t_f. It is obvious that the correct values of t_1 and t_2 are required for pre-actuation and post-actuation times. Since these time intervals are not known in advance, two large enough numbers c_1 and c_2

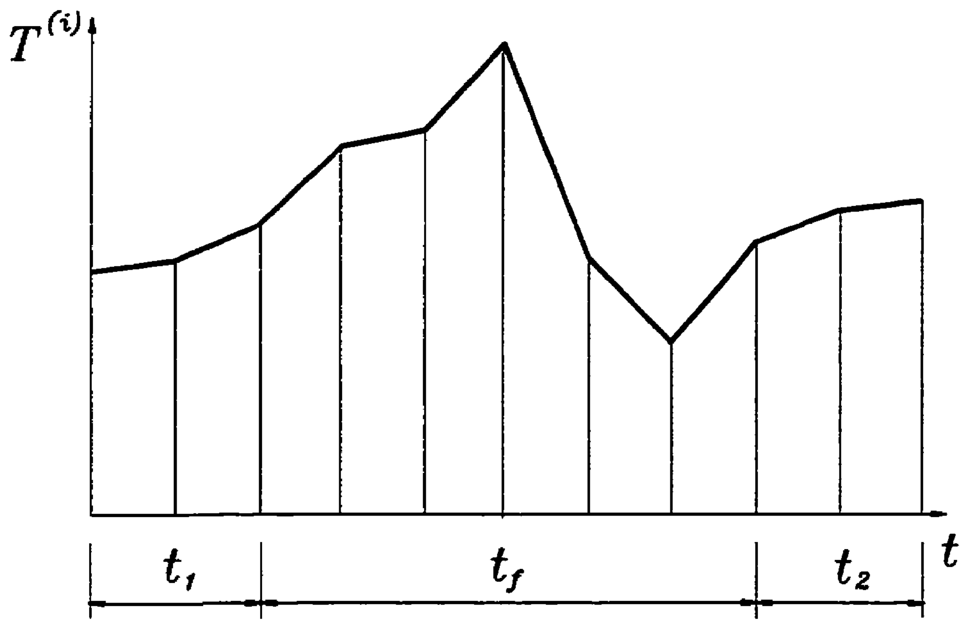

Figure 7.11. Extended time and torque discretization

can be selected such that the pre-actuation and post-actuation times can be captured.

7.4 Numerical Optimization Algorithm

The numerical optimization is used to solve the aforementioned inverse dynamic problem. A suitable parameterization of control torques $T_1(t)$ and $T_2(t)$ is necessary. $T_1(t)$ and $T_2(t)$ are represented by finite discrete numbers at specific times instead of continuos functions of time. Figure 7.11 shows a schematic diagram of torque discretization during the extended time $(t_1+t_f+t_2)$. Let NM be the number of intervals for torque discretization from $t=t_1$ to $t=t_1+t_f$ and $N_1=c_1\,NM$ and $N_2=c_2\,NM$ be the numbers of torque intervals for pre-actuation and post-actuation times, respectively. Therefore, T_1 and T_2 are approximated by two arrays each one with N_1+NM+N_2+1 components. Linear interpolation is used to compute the torque values between the given time-nodal values. Similarly the number of time steps in numerical integration of the equations of motion are chosen as $n_1=c_1nm$, nm, and $n_2=c_2nm$ within pre-actuation time interval t_1, main time interval t_f, and post-actuation interval t_2, respectively. Using the aforementioned parameterization of the control torques and considering the extended duration time of the motion due to the non-causality of the system, an objective function can be defined. This function is the summation of squares of tracking errors at integration time points from end of the pre-actuation time ($t= t_1$) to the end of the post-actuation time ($t=t_1+t_f+t_2$), can be defined as:

$$f(T_1,T_2)=K_1\sum_{i=n_1+1}^{n_1+nm+1}\{[x_i-\bar{x}_{i-n_1}]^2+[y_i-\bar{y}_{i-n_1}]^2\}+ \\ K_2\sum_{i=n_1+nm+2}^{n_1+nm+n_2+1}\{[x_i-\bar{x}_{nm+1}]^2+[y_i-\bar{y}_{nm+1}]^2\} \tag{7.18}$$

where $\mathbf{T}_1$ and $\mathbf{T}_2$ are the arrays of discretized joint torques as design variables, and K_1 and K_2 are two enough large numbers. x_i and y_i present the position of the payload at integration points between $t=t_1$ and $t=t_1+t_f+t_2$, while $\bar{x}_i$ and $\bar{y}_i$ show the desired position of the payload at integration points between $t=t_1$ and $t=t_1+t_f$. It is clear that the exact required joint torques which move the end-point through the specified trajectory make the objective function defined in equation (7.18) zero. The purpose is to minimize this objective function using an efficient optimization technique. The objective function is an implicit function of design variables and its analytical differentiation is not possible. Thus, an iterative search method together with numerical differentiation must be used. Having two arbitrary design vectors $\mathbf{T}_1$ and $\mathbf{T}_2$, we can numerically solve equation (7.1) by using Newmark method. Then the result can be used for the evaluation of the objective function. BFGS introduced in the previous chapter is used to solve the aforementioned unconstrained optimization problem.

7.5 Simulation Results

Consider a planar manipulator having two identical uniform links and two similar joints. Let the physical properties of its links be

$$\begin{aligned} L_1 &= L_2 = 1\ m \\ \rho_1 A_1 &= \rho_2 A_2 = 5\ \ kg\ /\ m \\ E_1 I_1 &= E_2 I_2 = 1500\ \ \ N.m^2 \end{aligned} \tag{7.19}$$

and the stiffness of the joints and the mass of the stators and rotors, respectively, have the following magnitudes

$$\begin{aligned} Kj_1 &= Kj_2 = 1000\, N\ /\ rad \\ ms_1 &= ms_2 = 0.2\ \ kg \\ mr_1 &= mr_2 = 0.2\ \ kg \end{aligned} \tag{7.20}$$

The gear ratio of each joint is considered to be 1. The mass of the payload is 5 Kg and its initial position (x_A, y_A) and final desired position (x_B, y_B) are assumed to be

$$\begin{aligned} x_A &= 1.8 \quad m, \;\; y_A = 0.2 \quad m \\ x_B &= 1.6 \quad m, \;\; y_B = 0.7 \quad m \end{aligned} \tag{7.21}$$

For trajectory control, the desired motion of the end-point within t_f=0.5 second is considered a straight line given by the following equations

$$x(t) = \frac{x_B - x_A}{t_f}\left(t - \frac{t_f}{2\pi}\sin\frac{2\pi t}{t_f}\right) + x_A \tag{7.22}$$

$$y(t) = \frac{y_B - y_A}{t_f}\left(t - \frac{t_f}{2\pi}\sin\frac{2\pi t}{t_f}\right) + y_A \tag{7.23}$$

The number of torque intervals within the main time interval t_f is chosen NM=10. By choosing c_1=c_2=0.2, the extended time is 0.7 second and the total number of the torque intervals becomes 14. Since two joint torques at t=0 can be found from the static equilibrium of the system, the number of design variables is 28. Computed joint torques needed to track the desired end-point trajectory are shown in figures 7.12 and 7.13. Also the corresponding rigid body torques are shown in the figures to illustrate the non-causal

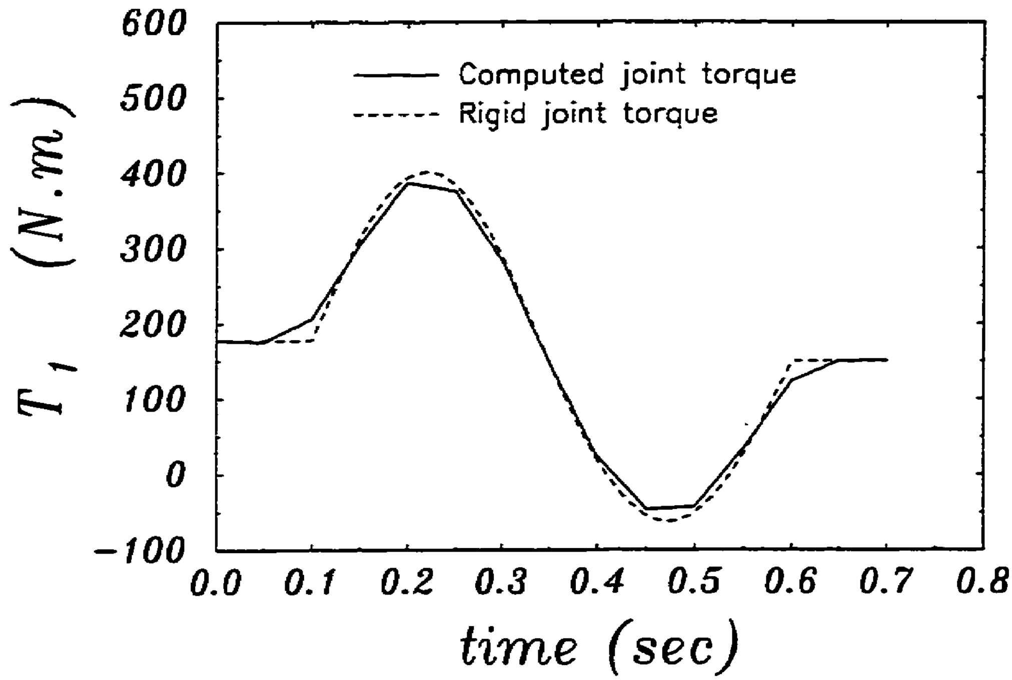

Figure 7.12. First joint torque (computed and rigid)

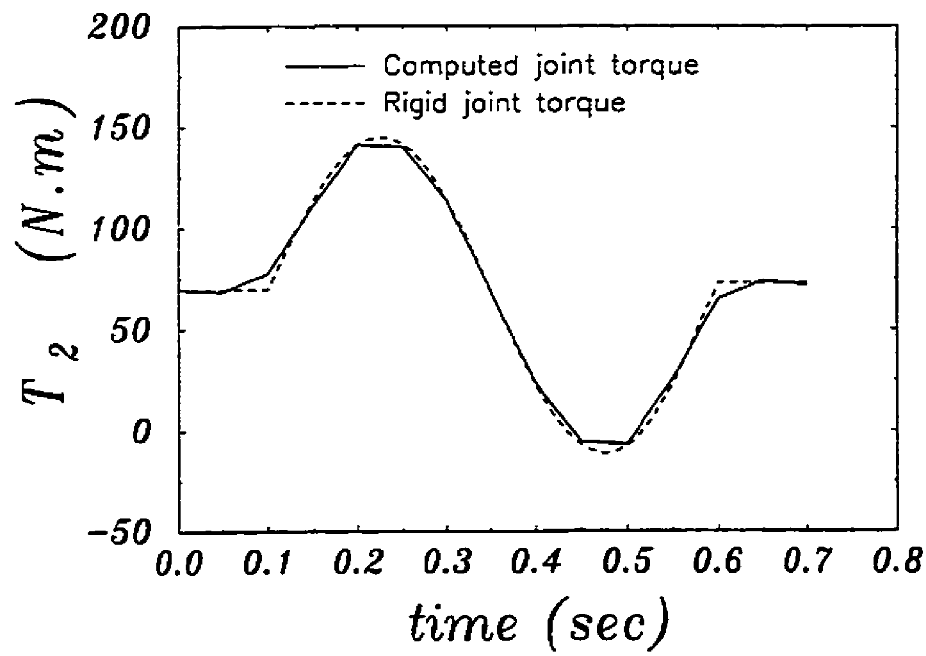

Figure 7.13. Second joint torque (computed and rigid)

nature of the problem. Figures 7.14 presents tracking errors for two cases of the loading, namely, the rigid body torques and the computed joint torques. The maximum tracking errors along x and y axes for rigid body torque case are 6.1 mm and 5 mm, while they are reduced to 0.1 mm and 0.268 mm for the computed joint torque case.

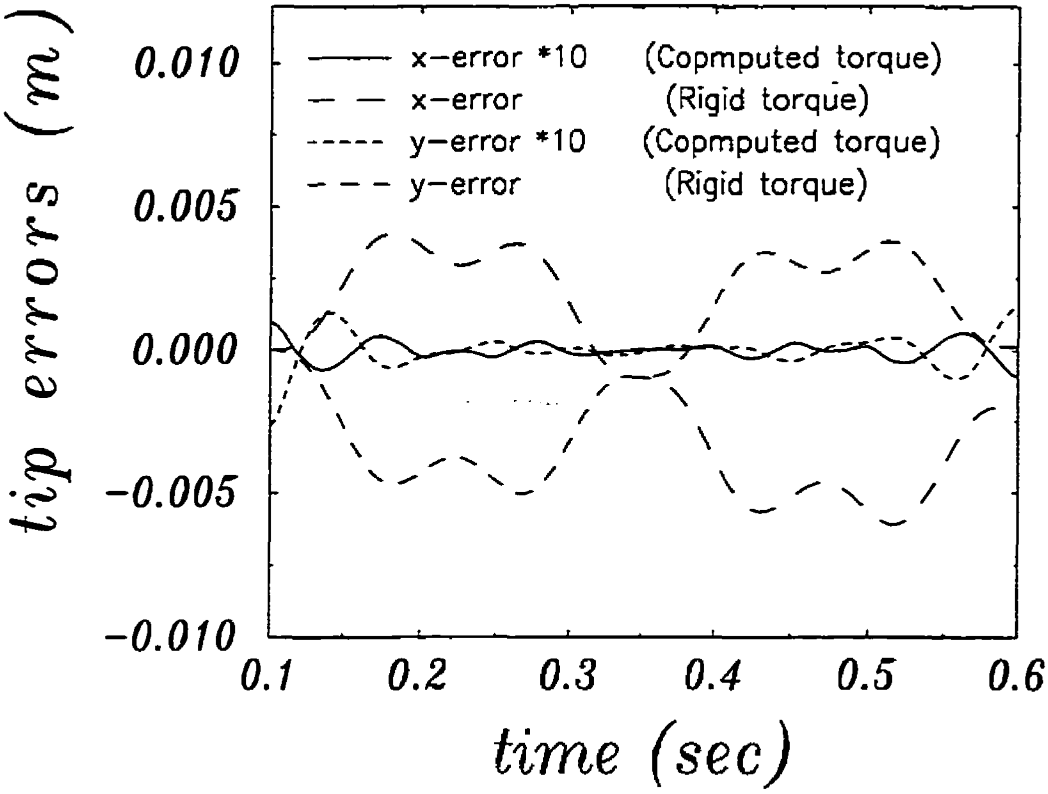

Figure 7.14. Tip errors along x and y axes

7.6 Summary and Conclusion

A technique based on numerical optimization is developed to find the joint torques required to move the end point of flexible manipulators through specified trajectories. The proposed approach takes into account the non-causality of such systems via considering pre-actuation and post-actuation in the solution procedure.

Results illustrate the non-causal nature of the inverse dynamics of flexible manipulators. It is shown that by applying the computed joint torques obtained from the proposed approach, the tracking errors are reduced significantly. The proposed technique is a complete and effective approach which can be used to find the input controls for the complicated flexible manipulators. The computed joint torques can be used as feedforward controls which minimize the work of the feedback controllers needed to compensate modeling errors.

CHAPTER 8

TIME OPTIMAL CONTROL OF MULTI-LINK FLEXIBLE MANIPULATORS ALONG SPECIFIED PATH

8.1 Introduction

This chapter deals with time optimal control of flexible manipulators. This subject is about controlling the position of the end-point of manipulators for a rest to rest motion in minimum time along a specified path, while actuator torques are not exceeding the limits due to physical capabilities of actuators or bending strengths of links. Although, many approaches have been developed in the literature for time-optimal control of rigid manipulators with and without path constraints, little work has been done in the area of time-optimal control of flexible manipulators.

The structure of the equations of motion of multi-link flexible manipulators is highly nonlinear and coupled and the nature of their inverse dynamics is non-causal. Therefore, the exact minimal time solution is not available at the present time. This chapter proposes a technique to find a near time-optimal control solution for a two-link flexible manipulator with torque and path constraints. Both links and joints are assumed to be flexible. The proposed technique is based on transforming the optimal control problem into an equivalent unconstrained optimum design problem using penalty function methods. Then BSFG method is used to find the solution i.e. the minimum time and the time history of the required joint torques. It is worth noting that this study takes into account the non-causality of the inverse dynamic system in describing the problem as an optimum design one.

8.2 Time-Optimal Control Problem

Consider a rest to rest motion of payload P (figure 8.1), which tracks a specified path $f(x_p,y_p)=0$ from point A to point B.

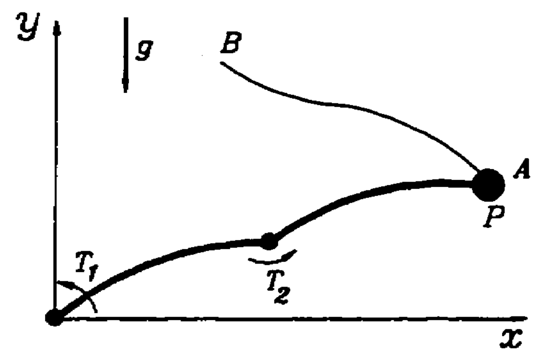

Figure 8.1 A two-link manipulator and its desired end path

The purpose is to find the bounded joint torques $T_1(t)$ and $T_2(t)$ which will cause this desired motion in minimum time. The bounds on the actuator torques are $T^{(1)}_{min}<T_1<T^{(1)}_{max}$ and $T^{(2)}_{min}<T_2<T^{(2)}_{max}$ due to physical capabilities of the actuators or bending strengths of the links.

The optimal control problem can be expressed as:

$$\text{minimize:} \quad t_f = \int_0^{t_f} dt \tag{8.1}$$

subject to:

$$M(U)\ddot{U} + K(U,\dot{U})U = F(U,\dot{U}) + \Omega T \tag{8.2-a}$$

$$f(x_p, y_p) = 0 \tag{8.2-b}$$

$$U(0) = U_0 \quad , \quad \dot{U}(0) = \bar{0} \tag{8.2-c}$$

$$x_p(t_f) = x_B,\ \dot{x}_p(t_f) = 0,\ \ddot{x}_p(t_f) = 0 \tag{8.2-d}$$

$$y_p(t_f) = y_B,\ \dot{y}_p(t_f) = 0,\ \ddot{y}_p(t_f) = 0 \tag{8.2-e}$$

$$T_{min}^{(i)} \le T_i \le T_{max}^{(i)} \qquad i = 1,2 \tag{8.2-f}$$

where U represents all of the degrees of freedom of the system, Ω is a non-square matrix which maps joint torques from a 2X1 vector to a vector whose size is equal to that of U, and x_p and y_p are coordinates of the payload which can be expressed as functions of some components of state variable vector U.

This two-point boundary value problem is a variational problem, but different from those in classical calculus of variation. Firstly, there are two different types of variables, namely, state variables U and control variables T. Secondly, some equality constraints have the form of nonlinear ordinary differential equations. These make the problem very difficult such that its exact solution does not exist at the present time.

8.2.1 Classical Approach to Solve Time Optimal Control Problems

As it was mentioned in chapter 6, Pontryagin minimum principle can be used as a mathematical tool to solve some optimal control problems.

Usually mechanical systems are assumed to be described by the following equations of motion

$$\dot{x}_j = f_j(x_i(t), u_l(t), t), \qquad i, j = 1,2,\ldots\ldots m \tag{8.3}$$

where m, x_j , and u_j are number of degrees of freedom of the system, state variables, and control variables, respectively. The system is assumed to be in the states $X(t_0)=X_0$ and

$X(t_f)=X_f$, respectively, at the time $t=t_0$ and at the final time $t=t_f$. In general, the mathematical model of a system include certain constraints on the control vector U in the form of

$$N_l \leq u_l(t) \leq M_l, \qquad l = 1,2,\ldots\ldots k \tag{8.4}$$

where k is the number of constrained controls.

The time-optimal control problem can now be stated as: Given the dynamical system described by its equations of the motion with initial state X_0, the terminal state X_f, and the constraints on the elements of the control vector U, find the admissible vector U which transforms the system from X_0 to X_f in the minimum time.

The minimum principle, which is based on using Lagrange multipliers in calculus of variations, furnishes locally the necessary conditions which an optimal control U(t) must satisfy. A Hamiltonian function, H, is defined as

$$H = 1 + \sum_{r=1}^{m} \lambda_j f_j(X,U,t) \tag{8.5}$$

where the functions $f_j(X,U,t)$ denote the right hand sides of equations (8.3). The variables λ_j are called the adjoint variables. Pontryagin minimum principle states the following conditions for the optimal solution:

a) controls $u_l(t)$ are piecewise continuous in the closed regions
b) adjoint variables $\lambda_1(t),\ldots\ldots\ \lambda_m(t)$, which are a set of continuous functions, must exist and satisfy the following equations:

$$\dot{\lambda}_i = -\frac{\partial H}{\partial x_i} = -\sum_{r=1}^{m} \lambda_r \frac{\partial f_r}{\partial x_i}, \qquad i = 1,..m \tag{8.6}$$

c) and make the Hamiltonian a minimum $M[l_j(t), x_j(t)]$ with respect to $u_l(t)$. This minimum has the following property:

$$M[\lambda_j(t), x_j(t)] = const \geq 0 \tag{8.7}$$

These conditions become simple for linear problems, in which the performance index and the constrains are linear. For example, in time minimization of a linear system with the following equality constraints (n first-order ordinary differential equation):

$$\dot{X} = AX + BU \tag{8.8}$$

If the eigenvalues of A are all real and $M_i \leq u_i \leq N_i$, then each control u_i is piecewise constant (Bang-Bang Control) and at most has n-1 switchings during a time optimal transition [131].

Recently, W. Szyszkowski and D. Youck [101] have used Ponryagin principle for time optimal control of single link manipulator moving in the horizontal plane. They derived the bang-bang control law for a flexible arm based on rigid body dynamics. Then they tried to improve it by examining its effectiveness through Finite Element analysis of the fully nonlinear dynamics of the flexible arm. However, as it was mentioned earlier, the governing equations of motion for multi-link flexible arms are highly nonlinear and coupled. Therefore, they can not be changed easily to the form of equations (8.3). Simply it means that Pontryagin minimum principle can not be easily used for time optimal control of such problems. Moreover, the constraint on the path of the end point is another factor which limits the use of minimum principle in time optimal problems of multi-link manipulators.

8.2.2 Optimum Design Theory instead of Optimal Control Theory

As it was mentioned earlier, it is possible to transform some optimal control problems to the optimum design problems. The purpose of this section is to solve time optimal control problems of manipulators with both flexible links and joints by using nonlinear programming instead of optimal control theory. In the following sub-section the suitable algorithms for doing this job are described.

8.2.2.1 Treatment of Non-Causality and Numerical Optimization Algorithm [130,132]

By using an approach similar to the approach presented in the previous chapter, we consider the non-causality of the inverse dynamics via defining two additional time intervals t_1 and t_2 as pre-actuation and post-actuation. The difference between the time optimal control problem and the trajectory problem is that the main time interval t_f is unknown in the first one, while t_f is given for the second one. In order to use numerical optimization, a suitable parameterization of control torques $T_1(t)$ and $T_2(t)$ is required. Since the joint torques have side limits, each joint torque i can be expressed by the following equations:

$$T_i(t)=\frac{1}{2}[(T^{(i)}{}_{max}+T^{(i)}{}_{min})+(T^{(i)}{}_{max}-T^{(i)}{}_{min})\sin\xi^{(i)}(t)], \quad i=1,2 \tag{8.9}$$

Therefore, the control inputs of the problem are transformed from bounded variables $T_1(t)$ and $T_2(t)$ to unbounded variables $\xi^{(1)}(t)$ and $\xi^{(2)}(t)$. In this study the free variables $\xi^{(1)}(t)$ and $\xi^{(2)}(t)$ are represented by finite discrete numbers at specific times instead of continuos functions of time. We consider NM intervals for torque discretization in the main time interval. Moreover, $N_1=c_1$ NM and $N_2=c_2$ NM are chosen to present the number of torque intervals in the pre-actuation and post-actuation times, respectively. Linear interpolation is used to compute torque values between the given time-nodal values. Also the number of time steps in three different parts of motion are defined exactly similar to the previous chapter. For the known extended time $(t_1+t_f+t_2)$ of the motion and known distribution of the joint torques, based on the aforementioned parameterization, equation of motion of the system can be solved numerically as an initial value problem. Then, we can define an objective function presented by equation (8.10), in which r_0 is a positive constant, r_1, r_2, r_3, and r_4 are large penalty coefficients. x_i and y_i are end-point coordinates at integration point i, while $\bar{y}(x_i)$ defines the y-coordinate obtained from the desired path equation.

$$
\begin{aligned}
f(t_f,\xi^{(1)},\xi^{(2)}) = {} & r_0 t_f + r_1[(x_{n_1+1}-x_A)^2+(y_{n_1+1}-y_A)^2] \\
& + r_2 \sum_{i=n_1+1}^{n_1+nm+1}[y_i-\bar{y}(x_i)]^2 + r_3 \sum_{i=n_1+nm+1}^{n_1+nm+n_2+1}[(x_i-x_B)^2+(y_i-y_B)^2] \\
& + r_4 \sum_{i=n_1+nm+1}^{n_1+nm+n_2+1}(\dot{\Phi}_{i,1}^2+\dot{\Phi}_{i,2}^2+\dot{\theta}_p^2)
\end{aligned}
\tag{8.10}
$$

The objective function in equation (8.10) is built using penalty function methods. The first term corresponds to the main time interval t_f. The second term is the penalty regarding the deviation of the coordinates of the payload from the given initial coordinates, while the third term defines the penalty due to the deviation of the path from the desired one. The payload should stay stationary at desired point B during the post-actuation time. The forth and fifth terms present penalties due to no satisfying this requirement. The constraints regarding payload acceleration are not taken into account.

In this way, the optimal control problem is transformed to an optimum design problem with $2(N_1+NM+N_2)+1$ design variables including main time interval t_f and discretized $\xi^{(1)}$ and $\xi^{(2)}$ values at N_1+NM+N_2 specific time points.

We use numerical differentiation to find its gradient vector, then BFGS method which required first derivatives to approximate Hessian matrix is used to find the optimum point of the objective function.

8.3 Simulation Results

This section presents some simulation results of the proposed algorithm applied to a planar manipulator which was used as an example in chapter 7. The initial and final positions of the payload are (x_A=1.8 m, y_A=0.2 m) and (x_B=1.6 m, y_B=0.7 m), respectively. The desired path of the payload is a straight line connecting these two points. Limits on the actuator joints are considered as: $T_{max}^{(1)}=-T_{min}^{(1)}=300$ N.m, $T_{max}^{(2)}=-T_{min}^{(2)}=120$ N.m

In this simulation the number of torque intervals within the main time interval t_f is chosen NM=10 and the post-actuation time is assumed to be $0.2t_f$ (c_2=0.2). c_1 is chosen 0 for no pre-actuation case and 0.2 for considering pre-actuation time, respectively. The joint torques needed to track the desired end-point trajectory for a counter-part manipulator with rigid links and joints are shown in figure 8.2-a. Figure 8.2-b shows the tip errors if these torques are applied to the flexible manipulator. Also the variations of joint velocities $\dot{\Phi}_1$ and $\dot{\Phi}_2$ and payload angular velocity $\dot{\theta}_P$ (in the second link coordinate system) are shown in figure 8.2-c. As it can be seen the maximum error is about 2.5 cm and the payload is not stationary at the end of the main time interval ($t=t_f$=0.4893 sec). The computed joint torques for the flexible manipulator without considering pre-actuation (c_1=0) are presented in figure 8.3-a. As it can be seen from figures 8.3-b 8.3-c after $t=t_f$ =04940 sec, the tip error and the payload velocities are very small but at the beginning of the motion the tip error has a considerable value (maximum error=3.5 mm). Figure 8.4-a shows optimal joint torques by considering pre-actuation time (c_1=0.2). From figures 8.4-b and 8.4-c, it is clear that not only the payload velocity is very close to zero after t=0.5658 sec (t_f=0.4850 sec), but also the maximum error during the motion is only about 0.4 mm.

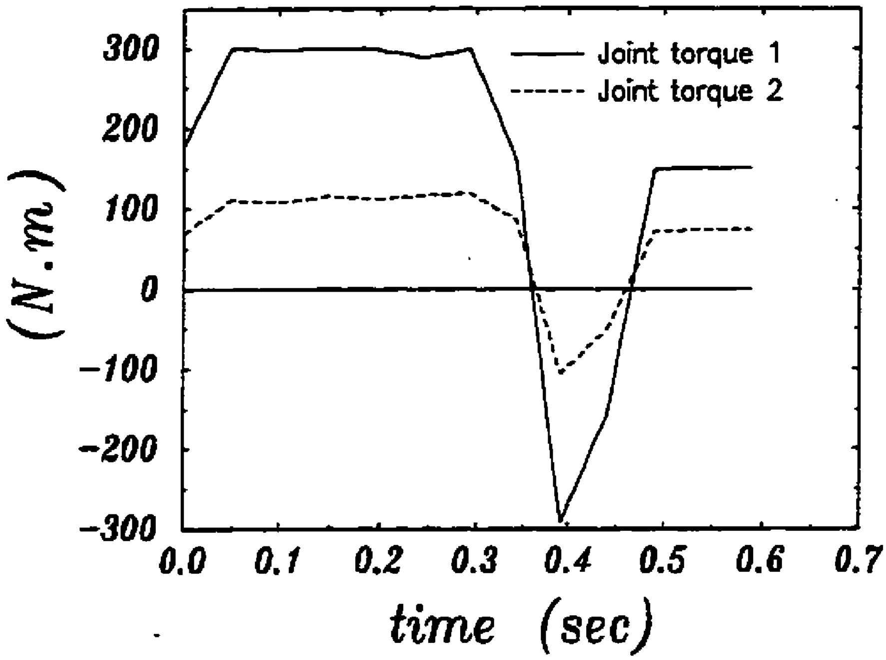

Figure 8.2-a Optimal joint torques for a rigid manipulator

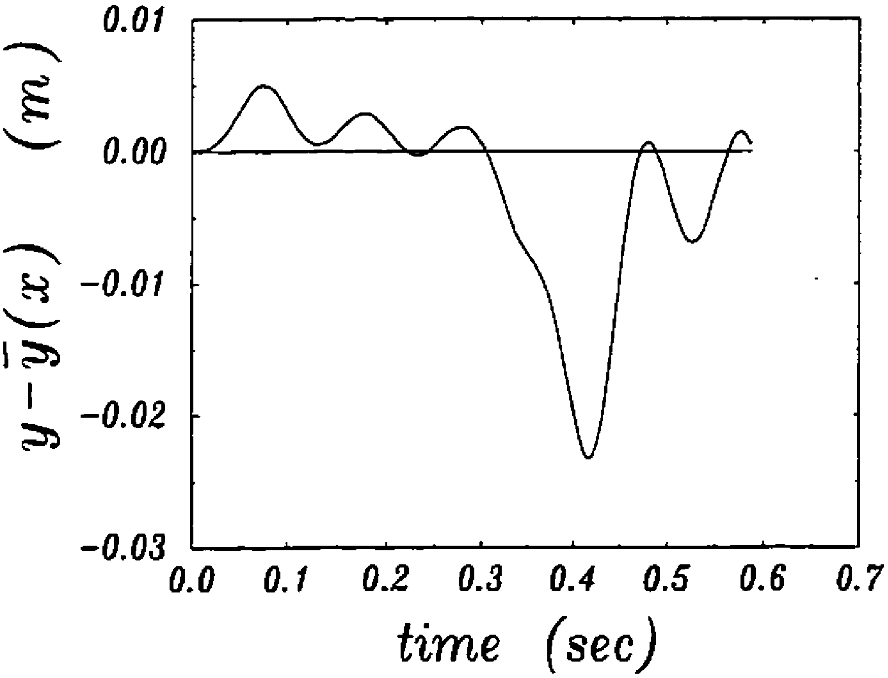

Figure 8.2-b Tip error when optimal rigid joint torques are applied to the flexible manipulator

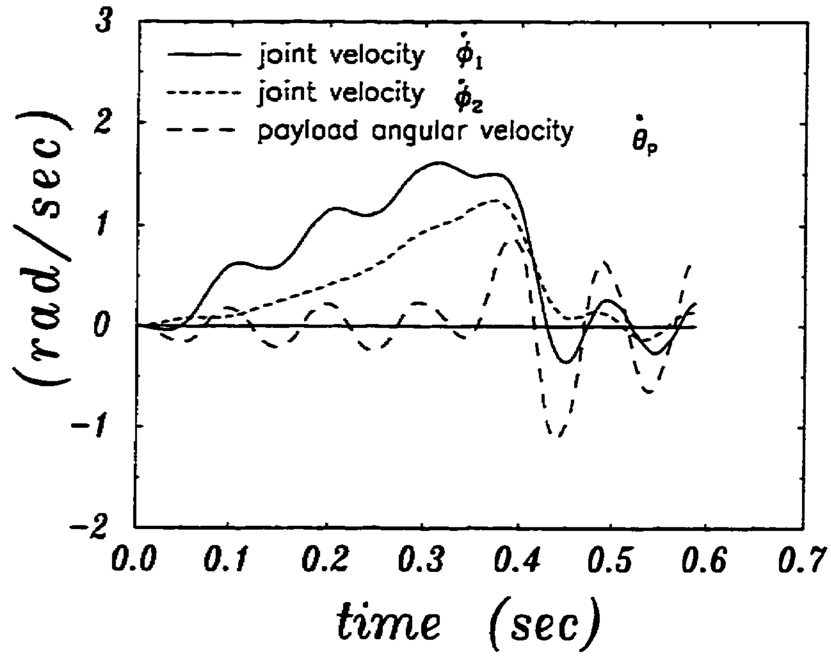

Figure 8.2-c Angular velocities when optimal rigid joint torques are applied to the flexible manipulator

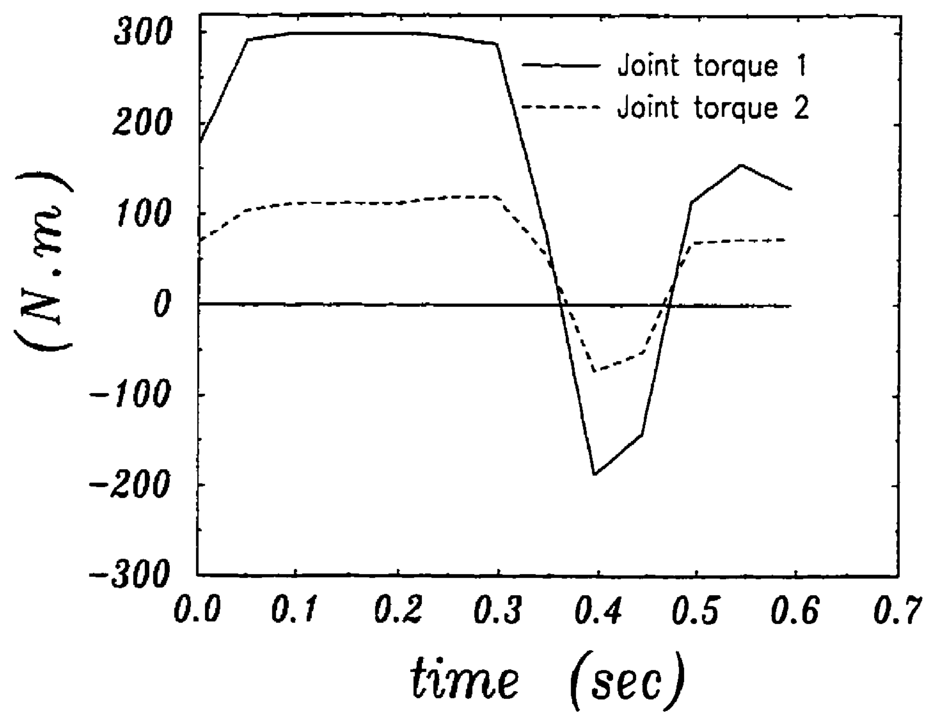

Figure 8.3-a Optimal joint torques without pre-actuation considering flexibility

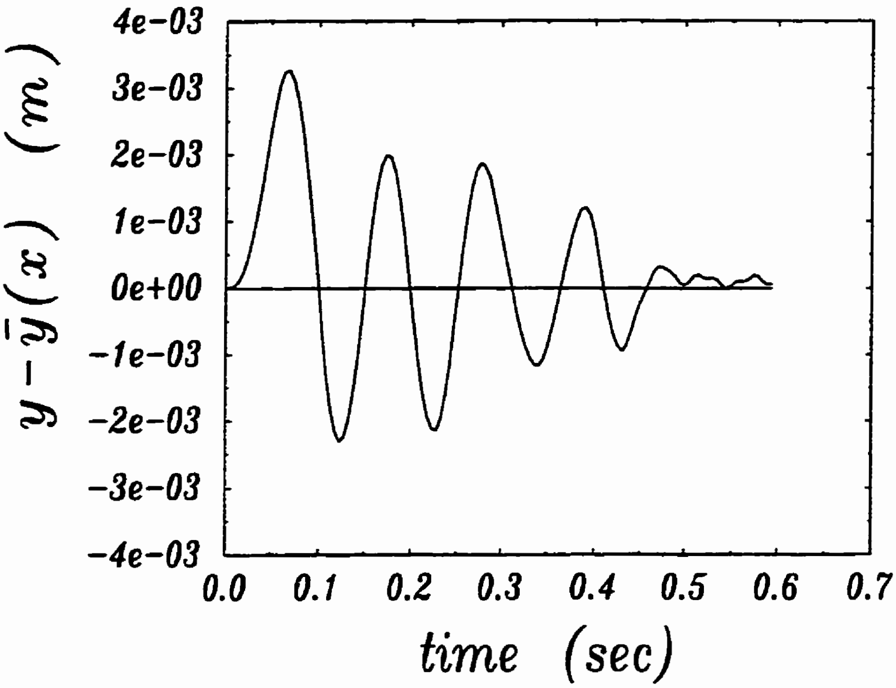

Figure 8.3-b Tip error in the case of optimal flexible joint torques without pre-actuation

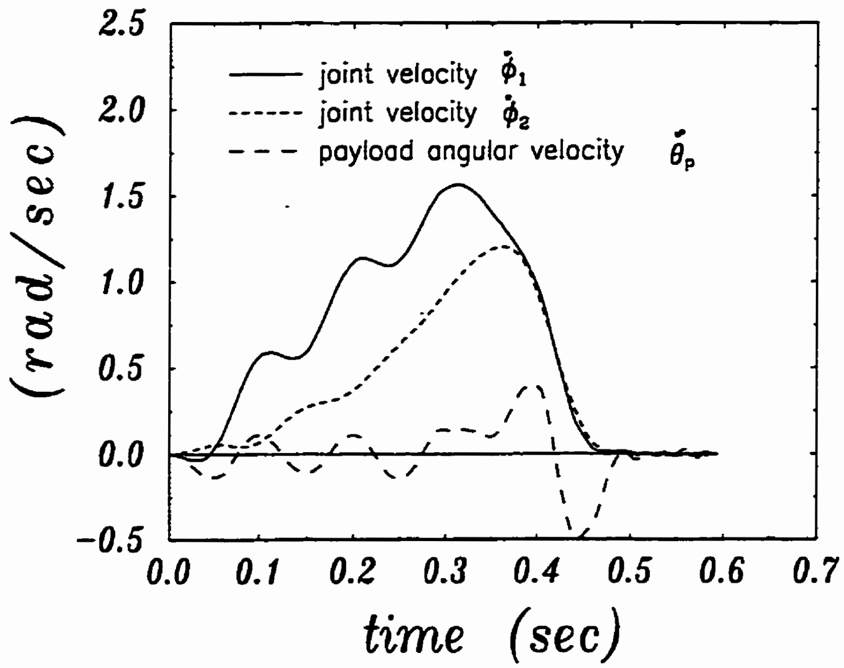

Figure 8.3-c Angular velocities in the case of optimal flexible joint torques without pre-actuation

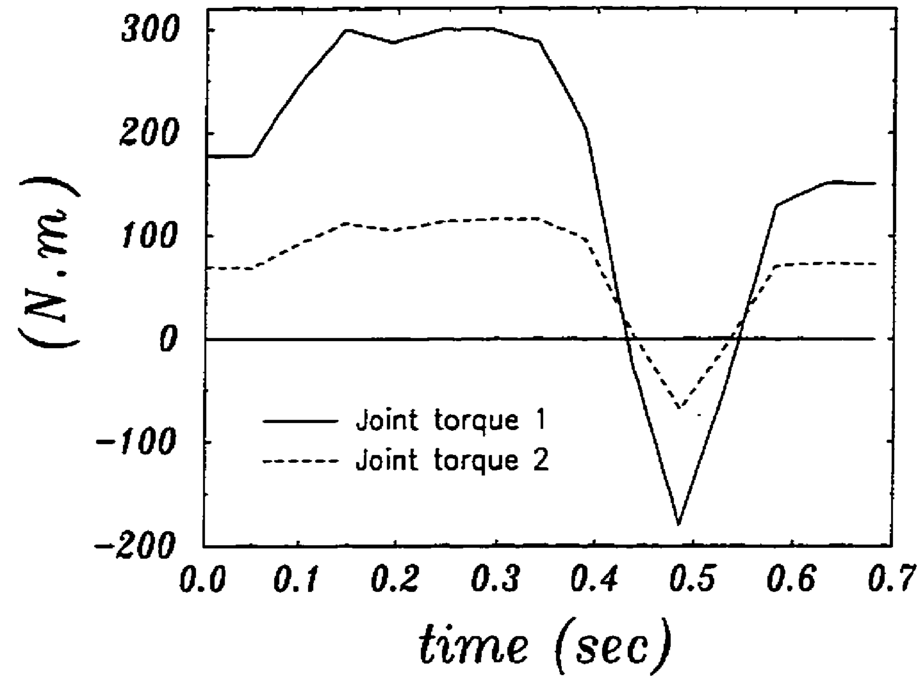

Figure 8.4-a Optimal joint torques with pre-actuation considering flexibility

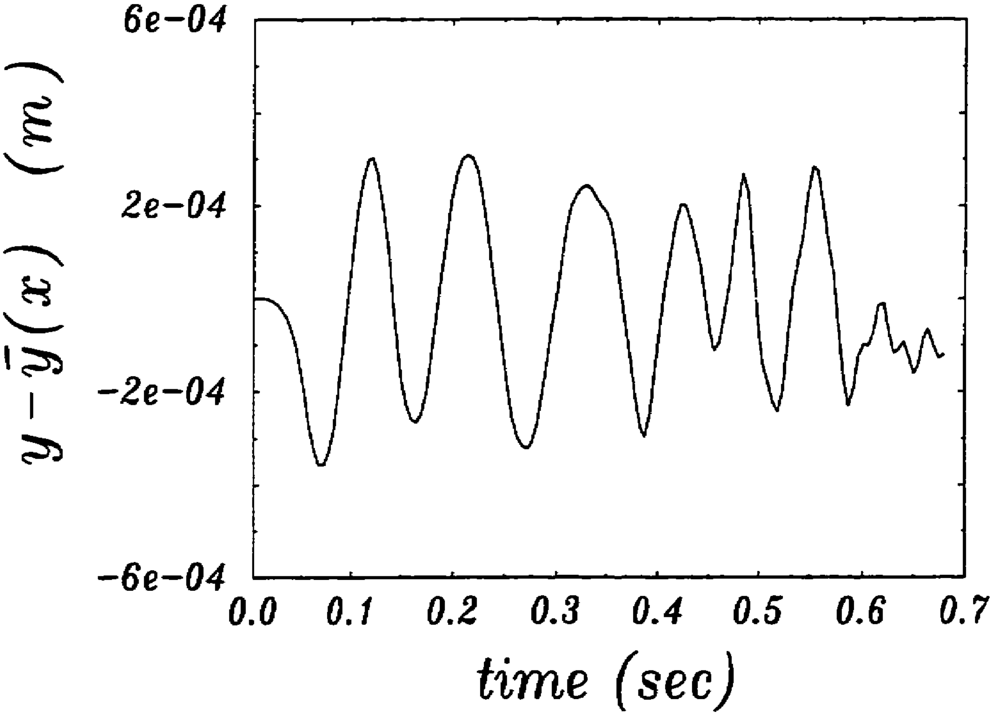

Figure 8.4-b Tip error in the case of optimal flexible joint torques with pre-actuation

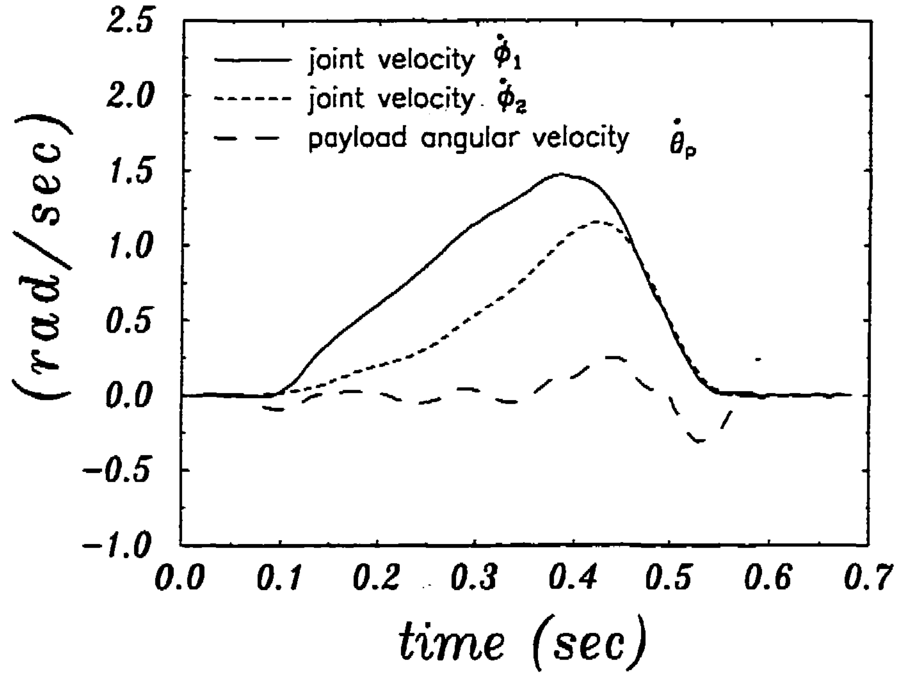

Figure 8.4-c Angular velocities in the case of optimal flexible joint torques with pre-actuation

8.4 Summary and Conclusion

In this chapter a technique based on numerical optimization is developed to find near time-optimal control solution of a two-link flexible manipulator with both torque and path constraints. Results show that by applying the computed joint torques without considering pre-actuation, the tip errors become very small and the payload is almost stationary at the end, but at the beginning of the motion the tip error has a considerable value. By applying pre-actuated computed joint torques, not only the payload velocity is very close to zero during post-actuation time, but also the maximum error is much smaller than previous case. Therefore, the simulation results present the effectiveness of the proposed approach which takes into account the non-causality of the system via considering pre-actuation and post-actuation. The computed joint torques can be used as feedforward controls to minimize the work of feedback controllers.

CHAPTER 9

CONCLUDING REMARKS

9.1 Summary

This dissertation presents development of dynamic modeling, trajectory control, and time-optimal control of multi-link flexible manipulators.

Two efficient finite element/Lagrangian approaches are used for dynamic modeling of flexible manipulators. In the first approach, the nonlinear and coupled equations of motion of multi-link planar manipulators with both flexible links and joints are derived using minimum number of coordinates by considering joint or relative coordinates. The dynamic model is free from assumption of nominal motion and takes into account not only the coupling effects between rigid body motion and elastic motion, but also the interaction between flexible links and actuated flexible joints. The validity of the model is shown and the effects of link and joint flexibilities are illustrated by some case examples. It is shown that the interaction between joint and link flexibilities has the most significant effect in the dynamic behavior of the system.

In the second approach, equations of motion of spatial multi-link manipulators with flexible links and joints are obtained. The constraint equations representing kinematical relations among different coordinates due to connectivity of the links are added to the equations of motion of the system by using Lagrange multipliers. This leads to a mixed set of nonlinear ordinary differential equations and nonlinear algebraic

9.2 Recommendations for Future Research

The following tasks and investigations can be suggested as extensions to the present work:

1. Experimental verification of the models. This is due to the fact that regardless of how precise the mathematical description is, a model should be tested experimentally.

2. Inclusion of various dampings in the dynamic models. Although, in the proposed modeling, viscous damping at the joints was included, other types of damping were neglected due to their complex nature. During the motion of a flexible manipulator, damping is present in various forms such as aerodynamic damping due to the air resistance, structural damping due to the internal losses of energy, and coulomb frictions at the joints due to the contact of various surfaces. To have a reliable and accurate model, the only way is to find various damping effects experimentally which is not a simple task.

3. Inclusion of the telescopic joints in addition to the revolute joints. In this work, all of the joints were assumed to be of revolute type.

4. Modification of the dynamic models in order to get rid of their limitations. The basic assumption used in the proposed dynamic modelings of flexible manipulators is small elastic deformations. Moreover, the dynamic model developed for spatial manipulators is limited to the manipulators whose tangents to various links do not become vertical during the motion.

5. Transferring the models onto more powerful computers and utilizing parallel processing capability in order to increase the computational speed.

BIBLIOGRAPHY

[1] Denavit, J., and Hertenburg, R. S., 1955, "A Kinematic Notation for Lower Pair Mechanisms Based on Matrices," ASME Journal of Applied Mechanics, Vol. 22, pp. 215-221.

[2] Uicker, J. J., Jr., 1969, "Dynamic Behavior of Spatial Linkages: Part I-Exact Equations of Motion," ASME Journal of Engineering for Industry, Vol. 91, No. 1, pp. 251-258.

[3] Paul, R. P., 1981, "Robot Manipulators: Mathematics, Programming, and Control," Cambridge, MIT Press.

[4] Greenwood, D., J., 1965, "Principles of Dynamics," Prantice-Hall Inc.

[5] Luh, J. Y. S, Walker, M. W., and Paul. R. P. C., S., 1980, " On-line Computational Scheme for Mechanical Manipulators," ASME Journal of Dynamic Systems, Measurements, and Control, Vol. 120, pp. 69-76.

[6] Asada, H., and Soltine, J. J. E., 1985, "Robot Analysis and Control," John Wiley and Sons.

[7] Hollerbach, J. M., 1980 , "A Recursive Lagrangian Formulation of Manipulator Dynamics and Comparative study of Dynamics Formulation Complexity," Transactions on System, Man, and Cybernetics, Vol. 10, pp. 730-736.

[8] Kane, T. R., and Levison, 1985, "Dynamics, Theory and Application," McGraw-Hill.

[9] Book, W. J., 1984, "Recursive Lagrangian Dynamics of Flexible Manipulator Arms," International Journal of Robotics Research, Vol. 3, pp. 87-101.

[10] Usoro, P. B., Nadira, R., and Mahil, S. S., 1986, "A Finite Element/Lagrangian Approach to Modeling Lightweight Flexible Manipulators," ASME Journal of Dynamic Systems, Measurements, and Control, Vol. 108, pp. 198-205.

[11] Shabana, A., 1989, "Dynamics of Multibody Systems," John Wiley and Sons.

[12] Turcic, D. A., and Midha, A., 1984, "Generalized Equations of Motion for the Dynamic Analysis of Elastic Mechanism Systems," ASME Journal of Dynamic Systems, Measurements, and Control, Vol. 106, pp. 243-248.

[13] Hasting, G. G., and Book, W. J., 1987, "A linear Dynamic Model for Flexible Robot Manipulators," IEEE Control Systems Magazine, Vol. 7, No. 1, pp. 61-67.

[14] Naganathan, G., and Soni, A. H., 1988, "Nonlinear Modeling of kinematic and Flexibility Effects in Manipulator Design," ASME Journal of Mechanisms, Transmission and Automation in Design, Vol. 110, pp. 243-254.

[15] Biswas, K. S., and Klafter, R. D., 1988, "Dynamic Modeling and Optimal Control of Flexible Robot Manipulators," Proceedings of IEEE International Conference on Robotics and Automation, Vol. 1, pp. 15-20.

[16] Benati, M., and Morro, A., 1994, "Formulation of Equations of Motion for a Chain of Flexible Links Using Hamilton's Principle," ASME Journal of Dynamic Systems, Measurements, and Control, Vol. 116, pp. 81-88.

[17] Canavin, J. R., and Likins, P. W., 1977, "Floating Reference Frames for Flexible Spacecrafts," Journal of Spacecraft, Vol. 14, No. 12, pp. 724-732.

[18] Hasting, G. G., and Book, W. J., 1985, "Experiments in the Optimal Control of a Flexible Manipulators," Proceedings of American Control Conference, pp. 828-729.

[19] Wang, D., and Vidyasagar, M., 1986, "Modeling and Control of Flexible Beam Using the Stable Factorization," Proceedings of ASME Winter Annual Meeting, Robotics: Theory and Application, pp. 31-37.

[20] Cannon, R. H., and Schmitz, E., 1984, "Initial Experiments on End-Point Control of a Flexible One- Link Robot," International Journal of Robotics Research, Vol. 3, pp. 49-54.

[21] Asada, H., and Ma, Z.-D., and Tokumaru, H., 1990, "Inverse Dynamics of Flexible Robot Arms: Modeling and Computation for Trajectory Control," ASME Journal of Dynamic Systems, Measurements, and Control, Vol. 112, pp. 177-185.

[22] Simo, J. C., and Vu-Quoc, L., 1986, "On the Dynamics of Flexible Beams Under Large Overall Motions-The Plane case: Part I," ASME Journal of Dynamic Systems, Measurements, and Control, Vol. 53, pp. 849-854.

[23] Yang, Z., and Sadler, J. P., 1990, "Large-Displacement Finite Element Analysis of Flexible Linkages," ASME Journal of Mechanical Design, Vol. 112, pp. 175-182.

[24] Jonker, B., 1989, "A finite Element Dynamic Analysis of Spatial Mechanisms with Flexible Links," Computer Methods in Applied Mechanics and Engineering, Vol. 76, pp. 17-40.

[25] Crisfield, M. A., 1990, "A Consistent Co-rotational Formulation for Non-linear, Three-dimensional, Beam-elements," Computer Methods in Applied Mechanics and Engineering, Vol. 81, pp. 131-150.

[26] Hsiao, K. M., and Jang, J. Y., 1991, "Dynamic Analysis of Planar Flexible Mechanisms by Co-rotational Formulation," Computer Methods in Applied Mechanics and Engineering, Vol. 87, pp. 1-14.

[27] Reissner, E., 1972, "On a One Dimensional Large-Displacement, Finite Strain Beam Theory," Studies in Applied Mathematics, Vol. 52, pp. 87-95.

[28] Song, J. O., and Haug, E. J., 1980, "Dynamic Analysis of Planar Flexible Mechanisms," Computer Methods in Applied Mechanics and Engineering, Vol. 24, pp. 359-381

[29] Avello, A., and Garcia de Jalon, J., 1991, "Dynamics of Flexible Multibody Systems Using Cartesian Co-ordinates and Large Displacement Theory," Computer Methods in Applied Mechanics and Engineering, Vol. 32, pp. 1543-1563.

[30] Nagarajan, S., and Turcic, D. A., 1990, "Lagrangian Formulation of the Equations of Motion for Elastic Mechanisms with Mutual Dependence Between Rigid Body and Elastic Motions, Part I: Element Level Equations," ASME Journal of Dynamic Systems, Measurements, and Control, Vol. 112, pp. 203-214.

[31] Mirro, J., 1972, "Automatic Feedback Control of a Vibrating Beam," Master's Thesis, Massachusetts Institute of Technology, Department of Mechanical Engineering, Cambridge, Massachusetts.

[32] Book, W. J., 1973, " Study of Design and Control of Remote Manipulators. Part II: Vibration Considerations in Manipulator Design," NAS8-28055 Cambridge, Massachusetts, MIT, Department of Mechanical Engineering.

[33] Book, W. J., Maizz-Neto, O., and Whitney, D. E., 1975, "Feedback Control of Two beam, Two Joint Systems with Distributed Flexibility," ASME Journal of Dynamic Systems, Measurements, and Control, Vol. 97, pp. 424-431.

[34] Sadler, J. P., and Sandor, G. N., 1973, "A Lumped Approach to Vibration and Stress Analysis of Elastic Linkages," AMSE Journal of Engineering for Industry, Vol. 95, pp. 549-557.

[35] Sadler, J. P., 1975, "On the Analytical Lumped-Mass Model of an Elastic Four-Bar Mechanism," AMSE Journal of Engineering for Industry, Vol. 97, No. 2, pp. 561-565.

[36] Book, W. J., 1979, "Analysis of Massless Elastic Chains with Servo Controlled Joints," ASME Journal of Dynamic Systems, Measurements, and Control, Vol. 101, pp. 187-192.

[37] Meirovitch, L., 1967, "Analytical Methods in Vibrations," Macmillan.

[38] Judd, D., and Falkenburge, 1985, " Dynamics of Nonrigid Articulated Robot Linkages," IEEE Transactions on Automatic Control, Vol. 30, pp. 499-502.

[39] Singh, S. N., and Schy, A. A., 1986, "Control of Elastic Robotic Systems by Nonlinear Inversion and Modal Damping," ASME Journal of Dynamic Systems, Measurements, and Control, Vol. 108, pp. 180-189.

[40] Yuan, B. S., Book, W. J., and Huggins, J. D., 1993, "Dynamics of Flexible Manipulator Arms: Alternative Derivation, Verification, and Characteristics for Control," ASME Journal of Dynamic Systems, Measurements, and Control, Vol. 115, pp. 394-404.

[41] Singh, R. P., VanderVoort, R. J., and Likins, P. W., 1984, "Dynamics of Flexible Bodies in Tree Topology- A Computer Oriented Approach," AIAA paper 84-1024, pp. 327-337.

[42] Abduljabbar, Z., ElMadany, M. M., and Al-Dokheil, H. D., 1993, "Controller Design of a One-Link Flexible Robot Arm," Computers and Structures, Vol. 49, No. 1, pp. 117-126.

[43] Benati, M., and Morro, A., 1988, "Dynamics of Chain of Flexible Links", Journal of Dynamic Systems, Measurement, and Control , Vol. 110, pp. 411-415.

[44] King, J. O., Gourishankar, V. G., and Rink, R. E., 1987, "Lagrangian Dynamics of Flexible Manipulators Using Angular Velocities Instead of Transformation Matrices," IEEE Transaction on Systems, Man, and Cybernetics, Vol. 17, pp. 1059-1068.

[45] Li, C-J., and Sankar, T. S., 1993, "Systematic Methods for Efficient Modeling and Dynamics Computation of Flexible Robot Manipulator," IEEE Transaction on Systems, Man, and Cybernetics, Vol. 23, pp. 77-95.

[46] Neubauer, A. H., Jr., Cohen, J. R., and Hall, A. S., Jr., 1966, " An Analytical Study of the Dynamics of an Elastic Linkage," AMSE Journal of Engineering for Industry, Vol. 88, pp. 311-317.

[55] Midha, A., Erdman, A. G., and Frohrib, D. A., 1978, "Finite Element Approach to Mathematical Modeling of High Speed Elastic Linkages", Mechanism and Machine Theory, Vol. 13, pp. 603-618.

[56] Bahgat, B. M., and Willmert, K. D., 1976, "Finite Element Vibrational Analysis of Planar Mechanisms," Mechanism and Machine Theory, Vol. 11, pp. 47-71.

[57] Khan, M. R., and Willmert, K. D., 1981, "Finite Element Quasi-Static Deformation Analysis of Planar Mechanisms with External Loads Using Static Condensation," ASME paper 81-DET-104., pp. 1-8

[58] Sunada, W., and Dubowsky, S., 1981, "The Application if Finite Element Methods to the Dynamic Analysis of Flexible Spatial and Co-Planar Linkage Systems," ASME Journal of Mechanical Design, Vol. 103, pp. 643-651.

[59] Nath, P. K., and Ghosh, A., 1980, " Kineto-Elastodynamic Analysis of Mechanism by Finite Element Method," Mechanism and Machine Theory, Vol. 15, pp. 179-197.

[60] Nath, P. K., and Ghosh, A., 1980, " Steady State Response of Mechanisms with Elastic Links by Finite Element Methods," Mechanism and Machine Theory, Vol. 15, pp. 199-211.

[61] Kalra, P., and Sharan, A. M., 1991, "Accurate Modeling of Flexible Manipulators Using Finite Element Analysis," Mechanism and Machine Theory, Vol. 26, pp. 299-313.

[62] Spong, M. W., 1987, "Modeling and Control of Elastic Joint Robots" ASME Journal of Dynamic Systems, Measurements, and Control, Vol. 109, pp. 310-319.

[63] Good, M. C., Sweet, L. W., and Strobel, K. L., 1985, "Dynamic Models for Control System Design of Integrated Robot and Drive Systems," ASME Journal of Dynamic Systems, Measurements, and Control, Vol. 107, pp. 53-59.

[64] Soni, A. H., and Dado, M. H. F., 1987, "Dynamic Response Analysis of 2-R Robot with Flexible Joints," IEEE International Conference on Robotics and Automation, pp. 479-483.

[65] Readman, M. C., and Belanger, P. R., 1992, "Stabilization of the Fast Modes of a Flexible-Joint Robot", The International Journal of Robotics Research, Vol. 11, No. 2, pp. 123-134.

[66] Gebler, B., 1987, "Feed-Forward Control Strategy for an Industrial Robot with Elastic Links and Joints," Proceedings of IEEE International Conference on Robotics and Automation, pp. 923-928.

[67] Jonker, B., 1990, "A Finite Element Dynamic Analysis of Flexible Manipulators," The International Journal of Robotics Research, Vol. 9, No. 4, pp. 59-74.

[68] Huang, S-J., and Wang, T-Y,. 1991, "Structural Dynamics Analysis of Spatial Robots with Finite Element Approach," Computers and Structures, Vol. 46, pp. 703-716.

[69] Yang, G. B., and Donath, M., 1988, "Dynamic Model of a one-Link Robot Manipulator with both Structural and Joint Flexibility," Proceedings of IEEE International Conference on Robotics and Automation, Vol. 1, pp. 476-481.

[70] Yang, J-H., and Fu, L-C., 1993, "Analysis and Control for Manipulators with Both Joint and Link Flexibility," Proceedings of IEEE International Conference on Robotics and Automation, pp. 984-989.

[71] Gogate, S., and Lin, Y-J., 1993, "Formulation and Control of Robots with Link and Joint Flexibility," Robotica, Vol. 11, pp. 273-282.

[72] Xi, F., Fenton, R. G., and Tabarrok, B., 1994, "Coupling Effects in a Manipulator With Both a Flexible Link and Joint," ASME Journal of Dynamic Systems, Measurement, and Control, Vol. 116, pp. 827-831.

[73] Lieh, J., 1994, "Dynamic Modeling of a Slider-Crank Mechanism with Coupler and Joint Flexibility," Mechanism and Machine Theory, Vol. 29, pp. 139-147.

[74] Sakawa, I. Y., 1985, "Feedback Control of Second Order Evolution Equations with Unbounded Observation,", International Journal of Control, Vol. 41, pp. 713-731.

[75] Siciliano, B., Prasad, J. V. R., and Calise, A. J., 1992, "Output Feedback Two-Time Scale Control of Multilink Flexible Arms," ASME Journal of Dynamic Systems, Measurement, and Control, Vol. 114, pp. 70-77.

[76] Siciliano, B., and Book, W. J., 1988, "A Singular Perturbation Approach to Control of Lightweight Flexible Manipulator," International Journal of Robotis Research, Vol. 7, No. 4. pp. 79-90.

[77] Khorrami, B., and Ozguner , 1988, "Singular Perturbation Analysis of a Distributed Parameter Model of Flexible Manipulators," Proceedings of American Control Conference, pp. 1704-1709.

[78] Sakawa, Y., Matsuno, F., and Fukushimo, S., 1985, "Modeling and Feedback Control of a Flexible Arm," Journal of Robotic Systems, Vol. 2, pp. 453-472.

[79] Shchuka, A, and Goldenberg, A. A., 1989, "Tip Control of a Single-Link Flexible Arm Using a Feedforward Technique," Mechanism and Machine Theory, Vol. 24, pp. 439-455.

[80] Pfeiffer, F., 1988, "A Feedforward Decoupling Concept for the Control of Elastic Robots," Journal of Robotic Systems, Vol. 6, No. 6, pp. 406-416.

[81] De Luca, A., Lucibello, P., and Ulivi, G., 1989, "Inverse Techniques for Trajectory Control of Flexible Robot Arms," Journal of Robotic Systems, Vol. 6, No. 6, pp. 325-344.

[82] De Luca, A., Lanari, L., Lucibello, P., Panzieri, S., and Ulivi, G., 1990, "Control Experiments on a Two-Link Robot with a Flexible Forearm," Proceedings of IEEE Conference on Decision and Control, Vol. 2, pp. 520-527.

[83] Wang, S. H., Hsia, T. C., and Wiederrich, J. L., 1986, "Open-Loop Control of a Flexible Robot Manipulator," International Journal of Robotics and Automation, Vol. 1, No. 2, pp. 54-57.

[84] Idler, S. K., 1995, "Open-Loop Flexibility Control in Multibody Systems Dynamics," Mechanism and Machine Theory, Vol. 30, pp. 861-869.

[85] Xi, F., 1995, "Trajectory Tracking of a Spatial Flexible Link Manipulator Using an Inverse Dynamics Method," Mechanism and Machine Theory, Vol. 30, pp. 1113-1126.

[86] Bayo, E., 1987, "A Finite Element Approach to Control the End-Point Motion of a Single-Link Flexible Robot," Journal of Robotic Systems, Vol. 4, pp. 63-75.

[87] Kwon, D-S., and Book, W. J., 1994, "A Time-Domain Inverse Dynamic Tracking Control of a Single-Link Flexible Manipulator," ASME Journal of Dynamic Systems, Measurement, and Control, Vol. 116, pp. 193-200.

[88] Moulin, H. and Bayo, E., 1991, "On the Accuracy of End-Point Trajectory Tracking for Flexible Arms by Noncausal Inverse Dynamic Solutions," ASME Journal of Dynamic Systems, Measurement, and Control, Vol. 113, pp. 321-324.

[89] Bayo. E., and Moulin, H., 1989, "An Efficient Computation of the Inverse Dynamics of Flexible Manipulators in the Time-Domain," Proceedings of IEEE International Conference on Robotics and Automation, pp. 710-715.

[90] Ledesma, R., and Bayo, E., 1992, "A Non-Recursive Lagrangian Solution of the Non-Causal Inverse Dynamics of Flexible Multibody Systems: The Planar Case," International Journal for Numerical Methods in Engineering, Vol. 36, pp. 2725-2741.

[91] Ledesma, R., and Bayo, E., 1994, "A Lagrangian Approach of the Non-Causal Inverse Dynamics of Flexible Multibody Systems: The Three-Dimensional Case," International Journal for Numerical Methods in Engineering, Vol. 37, pp. 3343-3361.

[92] Kahn, M.E., and Roth, B., 1971, "The Near-Time-Minimum Control of Open-Loop Articulated Kinematic Chains," ASME Journal of Dynamic Systems, Measurement, and Control, Vol. 93, pp. 164- 171.

[93] Luh, J. Y. S., and Lin, C. S., 1981, "Optimum Path Planing for Mechanical Manipulators," ASME Journal of Dynamic Systems, Measurement, and Control, Vol. 102, pp. 142- 151.

[94] Lin, C. S., Chang, P.-R., and Luh, J. Y. S., 1983, "Formulation and Optimization of Cubic Polynomial Trajectories for Industrial Robots," IEEE Transactions on Automatic Control, Vol. 28, pp. 1066-1073.

[95] Sahar, G., and Hollerbach, J. M., 1986, "Planning of Minimum-Time Trajectories for Robot Arms," The International Journal of Robotics Research, Vol. 5, No. 3, pp. 91-100.

[96] Niv, M., and Auslander, D. M., 1984, " Optimal Control of a Robot with Obstacles," Proceedings of American Control Conference, Vol. 1, pp. 280-287.

[97] Shiller, Z., and Dubowsky, S., 1985, "On Time Optimal Control of Robot Manipulator with Actuator and End-Effector Constraints," Proceedings of IEEE International Conference on Robotics and Automation, pp. 614-628.

[98] Bobrow, J. E., Dubowsky, S., and Gibson, J. S., 1985, "Time-Optimal Control of Robotic Manipulators Along Specified Paths," The International Journal of Robotics Research, Vol. 4, No. 3, pp. 3-17.

[99] Pao, L. Y.. and Franklin, G. F. , 1990, "Time-Optimal Control of Flexible Structures," Proceedings of IEEE Conference on Decision and Control, Vol. 5, pp. 2580-2581.

[100] Hecht, N.K., and Junkins, J. L., 1991, "Time-Optimal Reference Maneuvers for a Flexible Arm," Proceedings of AIAA Guidance, Navigation and Control Conference, pp. 1592-1598.

[101] Szyszkowski, W., and Youck, D., 1993, "Optimal Control of a Flexible Manipulator," Computers and Structures, Vol. 47, No. 4, pp. 801-813.

[102] Eisler, G. R., Robinett, R. D., Segalman, D. J., and Feddema, J. D., 1993, "Approximate Optimal Trajectories for Flexible-Link Manipulator Slewing Using Recursive Quadratic Programming," ASME Journal of Dynamic Systems, Measurement, and Control, Vol. 115, pp. 405-410.

[103] Hwang, S.-T., and Eltimsahy, A., 1994, "Simulation Studies for Effect of Link Flexibility on a Near-Minimum-Time Controller for Planar Flexible Manipulator," IASTED Control and Computers, Vol. 22, No. 2, pp. 42-50.

[104] Hildebrand, F. B., 1965, "Methods of Applied Mathematics," Pretice-Hall, New Jersy.

[105] Farid, M., and Lukasiewicz, S. A., 1997, "Dynamic Modeling of Spatial Flexible Manipulators," Computational Methods and Experimental Measurments, Vol. 3, pp. 255-264.

[106] Arora, J. S., 1989, "Introduction to Optimum Design," Wiley.

[107] Pontryagin, L. S., 1962, "The Mathematical Theory of Optimal Control Processes", Interscience Publishers, New York.

[108] Roberts, S. M., and Shipman, J. S., 1971, "Multipoint Solution of a Two-Point Boundary Value Problems," Journal of Optimization Theory and Applications, Vol. 7, pp. 301-318.

[109] Roberts, S. M., and Shipman, J. S., 1972, "Two-Point Boundary Value Problems: Shooting Methods," American Elsevier Publishing Company Inc, New York.

[110] Bryson, A. E., and Ho, Y.-C, 1975, "Applied Optimal Control," Hemisphere Publishing, New York.

[111] Menon, P. K. A., and Lehman, L. L., 1986, "A Parallel Quasi-Linearization Algorithm for Air Vehicle Trajectory Optimization," Journal of Guidance, Vol. 9, pp. 119-121.

[112] Fiacco, A. V., and McCormick, G. P, 1968, "Nonlinear Programming: Sequential Unconstrained Minimization Techniques," Wiley, New York.

[113] Hestenes, M. R., 1969, "Multiplier and Gradient Methods," Journal of Optimization Theory and Application, Vol. 4, pp. 303-320.

[114] Powell, M. J. D., 1969, "A Method for Nonlinear Constraints in Minimization Problems," in R. Fletcher (ed.) Optimization Academic Press, New York.

[115] Bertsekas, D.P., 1976, "Multiplier Methods: A Survey", Automatica, Vol. 12, pp. 133-145.

[116] Arora, J. S., Chahande, A. I., and Paeng, J. K., 1991, "Multiplier Methods for Engineering Optimization", Int. Journal for Numerical Methods in Engineering, Vol. 32, pp. 1485-1525.

[117] Fletcher, R., 1980, "Practical Methods of Optimization Vol. 2: Constrained," Wiley, Chichester.

[118] Haftka, R.T. and Gurdal, Z., 1992, "Elements of Structural Optimization", Kluwer Academic Publishers.

[119] Rao, S. S, 1984, "Optimization: theory and application", Wiley.

[120] Davidon, W. C., 1959, "Variable Metric Method for Minimization," U.S. Atomic Energy Commission Research and Development Report No. ANL-5990, Argonne National

Laboratories.

[121] Fletcher, R., and Powell, M. J. D., 1963, "A Rapidly Convergent Descent Method for Minimization," Computer Journal, Vol. 6, pp. 163-168.

[122] Broyden, C. G., 1970, "The Convergence of a Class of Double Rank Minimization Algorithms: Parts I and II," Journal of the Institute of Mathematics and its Applications., Vol. 6, pp. 76-90 and 222-231.

[123] Fletcher, R., 1970, "A New Approach to Variable Metric Algorithms," Computer Journal, Vol. 13, pp. 317-322.

[124] Goldfarb, D., 1970, "A Family of Variable Metric Methods Derived by Variational Means," Mathematics of Computations, Vol. 24, pp. 23-26.

[125] Shanno, D. F., 1970, "Conditioning of Quasi-Newton Methods for Function Minimization," Mathematics of Computations, Vol. 24, pp. 647-656.

[126] Papalambros, P., and Wilde, D. J., 1988, "Principles of Optimum Design, Modeling and Computation," Cambridge University Press.

[127] Dimarogonas, A. D., and Haddad, S., 1992, " Vibration For Engineers," Prentice-Hall.

[128] Farid, M., and Lukasiewicz, S. A., 1996, "Time Optimal Control of Flexible Structures Using Multiplier (Lagrange Augmented) Method," Fourth Annual Mechanical Engineering Conference of ISME and Second International Mechanical Engineering Conference, Shiraz, Iran, Vol. 4, pp. 1033-1040.

[129] Farid, M., and Lukasiewicz, S. A., 1996, "On Trajectory Control of Mult-Link Robots with Flexible Links and Joints," Proceedings of IEEE Canadian Conference on Electrical and Computer Engineering, Vol. 2, pp. 513-516.

[130] Farid, M., and Lukasiewicz, S. A., 1997, "Optimal control of Multi-Link Manipulators with both Flexible Links and Joints," Submitted to the International Journal of Robotics and Automation (IASTED).

[131] Ian, M., 1969, "Introduction to Optimal Control," Wiley.

[132] Farid, M., and Lukasiewicz, S. A., 1996, "Optimal Control of a Two-Link Flexible Manipulator Along Specified Path," Proceedings of ASME International Mechanical Engineering Congress and Exposition, Atlanta, Vol. 52, pp. 535-540.

APPENDIX

DERIVATION OF ELEMENTS OF CONSTRAIN JACOBEAN MATRIX C_q AND VECTOR Qc

As it was mentioned in chapter 5, due to introducing redundant variables at each joints i (i>1), ten constraint equations are needed to represent the continuity of the manipulator system. These constraints were shown by the following equations for each joint i=2,...,n.

$Cj^{(i)}(1)$: $$R_x^i - R_x^{i-1} - (L_{i-1}c_2^{(i-1)}c_1^{(i)} - w_e^{(i)}s_2^{(i-1)}c_1^{(i-1)} - v_e^{(i-1)}s_1^{(i-1)}) = 0 \tag{A.1}$$

$Cj^{(i)}(2)$: $$R_y^i - R_y^{i-1} - (L_{i-1}c_2^{(i-1)}s_1^{(i)} - w_e^{(i-1)}s_2^{(i-1)}s_1^{(i-1)} + v_e^{(i-1)}c_1^{(i-1)}) = 0 \tag{A.2}$$

$Cj^{(i)}(3)$: $$R_z^i - R_z^{i-1} - (L_{i-1}s_2^{(i-1)} + w_e^{(i-1)}c_2^{(i-1)}) = 0 \tag{A.3}$$

$Cj^{(i)}(4)$: $$sin\Phi_2{}^{(i)} = n^{(i)} \tag{A.4}$$

$Cj^{(i)}(5)$: $$[(l^{(i)})^2 + (m^{(i)})^2]\ cos^2\Phi_1^{(i)} - (l^{(i)})^2 = 0 \tag{A.5}$$

$Cj^{(i)}(6)$: $$-\Theta_0^i + (\Theta_0^{i-1} + \Theta_e^{i-1})\underline{i}_{i-1}.\underline{i}_i = 0 \tag{A.6}$$

$Cj^{(i)}(7)$: $$cos(\gamma^{(i)}) - \underline{i}_{i-1}{}'.\underline{i}_i = 0 \tag{A.7}$$

$Cj^{(i)}(8)$: $$sin\Psi_2{}^{(i)} = ns^{(i)} \tag{A.8}$$

$Cj^{(i)}(9)$: $$[(ls^{(i)})^2 + (ms^{(i)})^2]\ cos^2\Psi_1^{(i)} - (ls^{(i)})^2 = 0 \tag{A.9}$$

$Cj^{(i)}(10)$: $$cos(q_i) - \underline{i}_{i-1}{}'.\underline{i}_i{}^* = 0 \tag{A.10}$$

To find Jacobean matrix C_q of the constraints, first we differentiate the constraints of each joint i with respect to various variables to build submatrices $Cj^{(i)}{}_q$. Then by assembling these submatrices, C_q is found.

For each joint i, the non-zero components of submatrix $Cj^{(i)}{}_q$ are:

$$Cj^{(i)}{}_q(j,5+2N_i-1)=\frac{\partial(Cj^{(i)}(j))}{\partial v_e^{(i)}},\quad j=1,2,3 \tag{A.11}$$

$$Cj^{(i)}{}_q(j,5+4N_i-1)=\frac{\partial(Cj^{(i)}(j))}{\partial w_e^{(i)}},\quad j=1,2,3 \tag{A.12}$$

$$Cj^{(i)}{}_q(1,7+5N_i)=\frac{\partial(Cj^{(i)}(1))}{\partial R_x^i} \tag{A.13}$$

$$Cj^{(i)}{}_q(1,10+5N_i+7+5N_{i+1})=\frac{\partial(Cj^{(i)}(1))}{\partial R_x^{i+1}} \tag{A.14}$$

$$Cj^{(i)}{}_q(2,8+5N_i)=\frac{\partial(Cj^{(i)}(2))}{\partial R_y^i} \tag{A.15}$$

$$Cj^{(i)}{}_q(2,10+5N_i+8+5N_{i+1})=\frac{\partial(Cj^{(i)}(2))}{\partial R_y^{i+1}} \tag{A.16}$$

$$Cj^{(i)}{}_q(3,9+5N_i)=\frac{\partial(Cj^{(i)}(3))}{\partial R_z^i} \tag{A.17}$$

$$Cj^{(i)}{}_q(3,10+5N_i+9+5N_{i+1})=\frac{\partial(Cj^{(i)}(3))}{\partial R_z^{i+1}} \tag{A.18}$$

$$Cj^{(i)}{}_q(j,4)=\frac{\partial(Cj^{(i)}(j))}{\partial \phi_1^{(i)}},\quad j=1,\ldots,10 \tag{A.19}$$

$$Cj^{(i)}{}_q(j,5)=\frac{\partial(Cj^{(i)}(j))}{\partial\phi_2^{(i)}},\quad j=1,\ldots,10 \tag{A.20}$$

$$Cj^{(i)}{}_q(5,5+2N_i)=\frac{\partial(Cj^{(i)}(5))}{\partial v_e'^{(i)}},\quad j=1,\ldots,10 \tag{A.21}$$

$$Cj^{(i)}{}_q(j,5+4N_i)=\frac{\partial(Cj^{(i)}(j))}{\partial w_e'^{(i)}},\quad j=1,\ldots,10 \tag{A.22}$$

$$Cj^{(i)}{}_q(j,6+5N_i)=\frac{\partial(Cj^{(i)}(j))}{\partial\Theta_e^{(i)}}=1,\quad j=1,\ldots,10 \tag{A.23}$$

$$Cj^{(i)}{}_q(j,10+5N_i+10+5N_{i+1})=\frac{\partial(Cj^{(i)}(j))}{\partial\gamma^{(i+1)}},\quad j=1,\ldots,7 \tag{A.24}$$

$$Cj^{(i)}{}_q(4,10+5N_i+5)=\frac{\partial(Cj^{(i)}(4))}{\partial\phi_2^{(i+1)}} \tag{A.25}$$

$$Cj^{(i)}{}_q(5,10+5N_i+4)=\frac{\partial(Cj^{(i)}(5))}{\partial\phi_1^{(i+1)}} \tag{A.26}$$

$$Cj^{(i)}{}_q(6,5+4N_i+1)=\frac{\partial(Cj^{(i)}(6))}{\partial\Theta_0^{(i)}} \tag{A.27}$$

$$Cj^{(i)}{}_q(6,10+5N_i+6+5N_{i+1})=\frac{\partial(Cj^{(i)}(6))}{\partial\Theta_0^{(i+1)}} \tag{A.28}$$

$$Cj^{(i)}{}_q(j,10+5N_i+1)=\frac{\partial(Cj^{(i)}(j))}{\partial q_{i+1}},\quad j=8,9,10 \tag{A.29}$$

$$Cj^{(i)}{}_q(8,10+5N_i+3)=\frac{\partial(Cj^{(i)}(8))}{\partial\Psi_2^{(i+1)}} \tag{A.30}$$

Vector Qc in equation (5.51) can be found by using following equation found in chapter 3.

$$Qc = -[C_{tt} + (C_q \dot{q})_q \dot{q} + 2C_{qt}\dot{q}] \tag{5.146}$$

Since the constrains are not explicitly functions of time, equation (5.146) can be simplified as

$$Qc = -(C_q \dot{q})_q \dot{q} \tag{A.31}$$

Vector Qc can be found by assembling subvectors, Qj_c obtained for various joints.

TEST TARGET (QA-3)

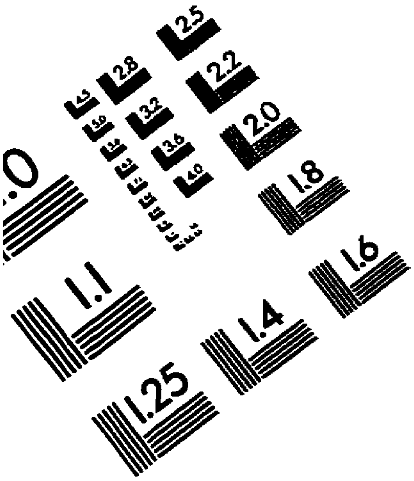

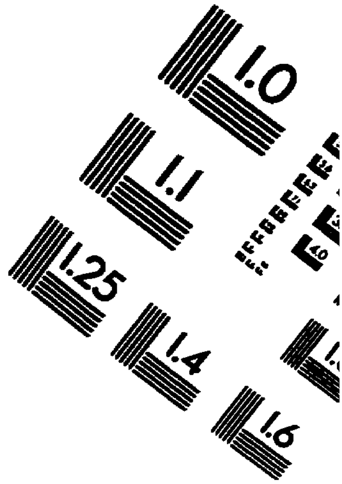

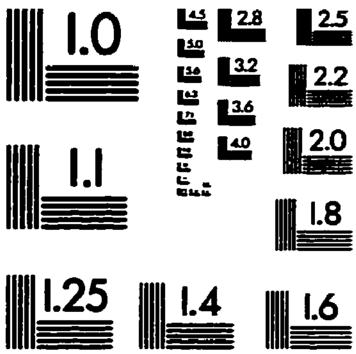

150mm

6"

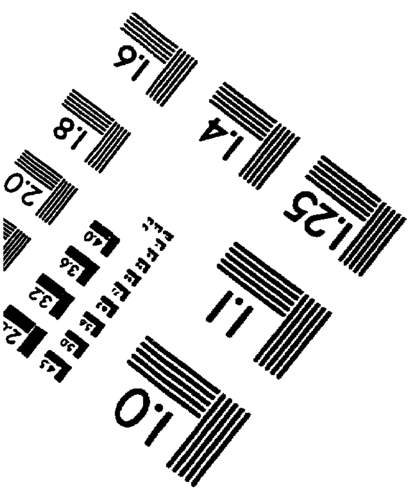

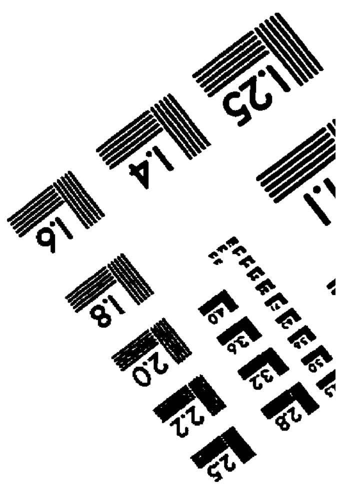

APPLIED IMAGE, Inc
1653 East Main Street
Rochester, NY 14609 USA
Phone: 716/482-0300
Fax: 716/288-5989